

**Synthetic Studies of Heterocyclic and Bioactive Agents**

by

**Taber S. Maskrey**

B.A. Chemistry, University of North Carolina at Wilmington, 2014

Submitted to the Graduate Faculty of the  
Dietrich School of Arts and Sciences in partial fulfillment  
of the requirements for the degree of  
Doctor of Philosophy

University of Pittsburgh

2021

UNIVERSITY OF PITTSBURGH

DIETRICH SCHOOL OF ARTS AND SCIENCES

This dissertation was presented

by

**Taber S. Maskrey**

It was defended on

March 17, 2021

and approved by

Dr. Kazunori Koide, Professor, Department of Chemistry

Dr. Peng Liu, Associate Professor, Department of Chemistry

Dr. Hülya Bayir, Professor, Critical Care Medicine, Environmental and Occupational Health

Thesis Advisor: Dr. Peter Wipf, Distinguished University Professor, Department of Chemistry

Copyright © by Taber S. Maskrey

2021

# **Synthetic Studies of Heterocyclic and Bioactive Agents**

Taber S. Maskrey, PhD

University of Pittsburgh, 2021

This dissertation describes a novel one-pot preparation of bicyclic heterocycles and improved synthetic procedures for the production of compounds possessing established biological activity. A five-component condensation reaction was discovered that follows a mechanistic sequence starting with a Biginelli reaction and ending in a Diels-Alder reaction to form a new class of bicyclic heterocycles. New protocols were developed to synthesize the bioactive compounds Gefitinib and analogs of JP4-039. The FDA approved EGFR inhibitor Gefitinib was synthesized on a pilot-plant scale using a more efficient synthetic sequence and fewer hazardous reagents. A shorter synthetic sequence to ferroptosis inhibitors, JP4-039 and related analogs, was developed with a key vinylogous Mannich reaction utilizing an oxazolidinone auxiliary. The biological activity of new ferroptosis inhibitors was used to generate a structure-activity relationship (SAR) hypothesis.



## Table of Contents

List of Tables .....	vii
List of Figures.....	viii
List of Schemes.....	xii
List of Equations .....	xv
List of Abbreviations .....	xvi
Preface.....	xix
1.0 Five-Component Biginelli-Diels-Alder Cascade Reaction .....	1
1.1 Introduction .....	1
1.1.1 The Biginelli Reaction.....	1
1.1.2 The Diels-Alder Reaction .....	5
1.1.3 Multi-Component Reactions .....	7
1.2 Results and Discussion .....	9
1.3 Conclusions .....	16
1.4 Experimental Procedures .....	17
2.0 A Pilot-Plant Synthesis of Gefitinib.....	25
2.1 Introduction .....	25
2.1.1 Background and Early Syntheses .....	25
2.1.2 Synthesis of Gefitinib from 2,4-Dichloroquinazoline.....	28
2.2 Results and Discussion .....	30
2.3 Conclusions .....	37
2.4 Experimental Procedures .....	38

<b>3.0 Synthesis of JP4-039 Analogs Through a Vinylogous Mannich Reaction and Their</b>	
<b>In Vitro Activity as Ferroptosis Inhibitors .....</b>	<b>44</b>
<b>3.1 Introduction .....</b>	<b>44</b>
<b>3.1.1 Mitochondria Targeting Nitroxides and Their Therapeutic Indications .....</b>	<b>44</b>
<b>3.1.2 Ferroptosis, an Iron-Mediated Cell Death Pathway .....</b>	<b>52</b>
<b>3.1.3 SAR In Vitro Assay and JP4-039 Zones for Modification .....</b>	<b>61</b>
<b>3.1.4 The Vinylogous Mannich Reaction .....</b>	<b>64</b>
<b>3.1.5 Oxazolidinone Auxiliaries in (Vinylogous) Mannich Reactions .....</b>	<b>71</b>
<b>3.2 Results and Discussion .....</b>	<b>77</b>
<b>3.2.1 Synthesis of JP4-039 Through a Vinylogous Mannich Reaction with a</b>	
<b>Pyrazole Auxiliary.....</b>	<b>77</b>
<b>3.2.2 Vinylogous Mannich Reaction with an Oxazolidinone Auxiliary .....</b>	<b>85</b>
<b>3.2.3 Synthesis of JP4-039 Analogs.....</b>	<b>104</b>
<b>3.2.4 Activity of JP4-039 Analogs in an Erastin-Induced Ferroptosis Assay .....</b>	<b>114</b>
<b>3.3 Conclusions .....</b>	<b>121</b>
<b>3.4 Experimental Procedures .....</b>	<b>122</b>
<b>4.0 Appendix A .....</b>	<b>175</b>
<b>5.0 Bibliography .....</b>	<b>205</b>

## List of Tables

Table 1-1 Investigation of reaction time, concentration, equivalents, and catalyst with formaldehyde, <i>N,N</i> -dimethylurea, and ethyl acetoacetate .....	12
Table 1-2 Reaction scope with formaldehyde, <i>N,N'</i> -dimethyl(thio)urea (X=O,S), and alkyl ( <i>R</i> <sup>1</sup> ) acetoacetates .....	13
Table 2-1 Pilot-plant optimizations of step 1 – S <sub>N</sub> Ar reaction .....	34
Table 2-2 Pilot-plant optimizations of step 2 – Demethylation reaction.....	35
Table 2-3 Pilot-plant optimizations of step 3 – Alkylation reaction.....	36
Table 2-4 Pilot-plant optimizations of step 4 – Dechlorination reaction .....	37
Table 3-1 Vinylogous Mannich reaction optimizaitons with ( <i>S</i> )-DTBM-SEGPHOS.....	81
Table 3-2 Photochemical isomerization substrates and conditions.....	83
Table 3-3 Synthesis of oxazolidinone derivatives.....	86
Table 3-4 Oxazolidinone auxiliary screen in the vinylogous Mannich reaction .....	88
Table 3-5 Base screen for the vinylogous Mannich reaction between 3-28 and 3-17 .....	90
Table 3-6 Analysis of stereochemical outcome with phenyl imine .....	96
Table 3-7 Analysis of stereochemical outcome with furan imine .....	98
Table 3-8 Analysis of stereochemical outcome with fluorophenyl imine.....	99
Table 3-9 Activity of analogs in erastin induced CellTiter-Glo® ferroptosis assay .....	119

## List of Figures

Figure 1-1 Biginelli reaction possible mechanistic routes .....	2
Figure 1-2 DHPMs targeting HSP70 synthesized through Biginelli reactions.....	4
Figure 1-3 Lewis acid coordination in N-acylimines and $\beta$ -keto ester .....	5
Figure 1-4 Overman and Kappe preparation of atypical Biginelli reaction products.....	5
Figure 1-5 Literature precedence and synthetic plans .....	10
Figure 1-6 Attempted five-component condensation with a cyclic 1,3-diketone.....	13
Figure 2-1 Drugs approved to treat NSCLC with EGFR mutations .....	26
Figure 2-2 2-L Jacketed reactor design .....	32
Figure 2-3 Proposed oxidation side product.....	36
Figure 3-1 Structure of gramicidin S .....	44
Figure 3-2 ( <i>E</i> )-alkene is an isostere of an amide .....	45
Figure 3-3 Structures of TEMPO and TEMPOL .....	45
Figure 3-4 Structure of natural and dietary antioxidants.....	46
Figure 3-5 A) TEMPO catalytic cycle B) Proposed nitroxide catalytic cycle to quench peroxy radicals.....	47
Figure 3-6 Structure of JP4-039 .....	49
Figure 3-7 Uncontrolled cell death can drive tumor evolution.....	51
Figure 3-8 Comparison of apoptosis, necroptosis, and ferroptosis .....	53
Figure 3-9 Phospholipid peroxidation cycle .....	54
Figure 3-10 Mechanisms to regulate iron in the cell.....	56
Figure 3-11 Mechanisms to regulate lipid peroxidation and ferroptosis in the cell .....	58

Figure 3-12 Two ferroptosis inducers, erastin and RSL3 .....	59
Figure 3-13 A) Iron chelators DFOA and 2,2'-bipyridine B) Antioxidants Fer-1, Lip-1, and phenothiazine #51.....	60
Figure 3-14 JP4-039 bis-nitroxide anlaog .....	61
Figure 3-15 SAR zones of JP4-039 .....	63
Figure 3-16 Oxazolidinone derived chiral propanoates .....	72
Figure 3-17 Oxazolidinone auxiliaries are the gold standard in chiral auxiliaries .....	73
Figure 3-18 Double asymmetric reaction to form product with new stereogenic center .....	75
Figure 3-19 Analysis of matched/mismatched product outcome in a conjugate addition reaction.....	76
Figure 3-20 Retrosynthetic analysis of JP4-039 .....	78
Figure 3-21 Experimental designs for determining the outcome of a double asymmetric synthesis methodology .....	92
Figure 3-22 A) Proposed cyclic transition state and B) Proposed open transition state ....	101
Figure 3-23 Scigress modeled cyclic transition state with ( <i>R</i> )-auxiliary and ( <i>S</i> )-ligand leading to A) ( <i>R,R</i> )-major product and B) ( <i>S,R</i> )-minor product .....	103
Figure 3-24 Scigress modeled open transition state with ( <i>R</i> )-auxiliary and ( <i>S</i> )-ligand leading to A) ( <i>R,R</i> )-major product and B) ( <i>S,R</i> )-minor product .....	103
Figure 3-25 Activity and logP comparison of JP4-039 and ( <i>R</i> )-3-44.....	115
Figure 3-26 Activity and logP comparison of ( <i>R</i> )-3-44, ( <i>R</i> )-3-47 and ( <i>S</i> )-3-47 .....	115
Figure 3-27 Activity and logP comparison of ( <i>R</i> )-3-47 and ( <i>R</i> )-3-53.....	116
Figure 3-28 Activity and logP comparison of ( <i>S</i> )-3-47 and ( <i>S</i> )-3-49 .....	117
Figure 3-29 Activity and logP comparison of ( <i>R</i> )-3-56 and ( <i>R</i> )-3-58.....	118

Figure 3-30 Activity and logP comparison of (S)-992-38 and (S)-3-60 and (S)-3-61 .....	118
Figure 4-1 Representative five-component condensation product <sup>1</sup> H spectra (1-6B) .....	176
Figure 4-2 Structural confirmation of five-component condensation product by NOE analysis of 1-10 .....	177
Figure 4-3 <sup>1</sup> H NMR spectra of Gefitinib (2-5) synthesized on pilot-plant scale.....	178
Figure 4-4 <sup>1</sup> H NMR spectra of vinylogous Mannich product (R,R)-3-39 .....	179
Figure 4-5 <sup>13</sup> C NMR spectra of vinylogous Mannich product (R,R)-3-39 .....	180
Figure 4-6 <sup>1</sup> H NMR spectra of vinylogous Mannich product (R)-3-39 .....	181
Figure 4-7 <sup>13</sup> C NMR spectra of vinylogous Mannich product (R)-3-39 .....	182
Figure 4-8 <sup>1</sup> H NMR spectra of ester (R)-3-54 .....	183
Figure 4-9 <sup>13</sup> C NMR spectra of ester (R)-3-54 .....	184
Figure 4-10 <sup>1</sup> H NMR spectra of bis-alkylated ester (R)-3-55 .....	185
Figure 4-11 <sup>13</sup> C NMR spectra of bis-alkylated ester (R)-3-55 .....	186
Figure 4-12 <sup>19</sup> F NMR spectra of bis-alkylated ester (R)-3-55 .....	187
Figure 4-13 <sup>1</sup> H NMR spectra of nitroxide analog (R)-3-44 .....	188
Figure 4-14 <sup>13</sup> C NMR spectra of nitroxide analog (R)-3-44 .....	189
Figure 4-15 <sup>19</sup> F NMR spectra of nitroxide analog (R)-3-44 .....	190
Figure 4-16 <sup>1</sup> H NMR spectra of nitroxide analog (R)-3-47 .....	191
Figure 4-17 <sup>13</sup> C NMR spectra of nitroxide analog (R)-3-47 .....	192
Figure 4-18 <sup>19</sup> F NMR spectra of nitroxide analog (R)-3-47 .....	193
Figure 4-19 <sup>1</sup> H NMR spectra of nitroxide analog (R)-3-53 .....	194
Figure 4-20 <sup>13</sup> C NMR spectra of nitroxide analog (R)-3-53 .....	195
Figure 4-21 <sup>19</sup> F NMR spectra of nitroxide analog (R)-3-53 .....	196

Figure 4-22 $^1\text{H}$ NMR spectra of nitroxide analog ( <i>S</i> )-3-56.....	197
Figure 4-23 $^{13}\text{C}$ NMR spectra of nitroxide analog ( <i>S</i> )-3-56.....	198
Figure 4-24 $^{19}\text{F}$ NMR spectra of nitroxide analog ( <i>S</i> )-3-56.....	199
Figure 4-25 $^1\text{H}$ NMR spectra of nitroxide analog ( <i>R</i> )-3-58 .....	200
Figure 4-26 $^{13}\text{C}$ NMR spectra of nitroxide analog ( <i>R</i> )-3-58 .....	201
Figure 4-27 $^{19}\text{F}$ NMR spectra of nitroxide analog ( <i>R</i> )-3-58.....	202
Figure 4-28 $^1\text{H}$ NMR spectra of nitroxide analog ( <i>S</i> )-3-60.....	203
Figure 4-29 $^{19}\text{F}$ NMR spectra of nitroxide analog ( <i>S</i> )-3-60 .....	204

## List of Schemes

<b>Scheme 1-1 Pietro Biginelli's initial multi-component reaction .....</b>	<b>1</b>
<b>Scheme 1-2 Acid catalayzed Biginelli reaction.....</b>	<b>3</b>
<b>Scheme 1-3 Diels-Alder reaction mechanism and product .....</b>	<b>6</b>
<b>Scheme 1-4 Sharma et al. Diels-Adler reaction with Biginelli dienophile .....</b>	<b>7</b>
<b>Scheme 1-5 Whitwood et al. five-component condensation formation of piperidines.....</b>	<b>8</b>
<b>Scheme 1-6 Mirkhani et al. five-component condensation to form phenylacetamides .....</b>	<b>8</b>
<b>Scheme 1-7 Hasaninejad et al. five-component condensation to form pyrazoline-containing Schiff bases .....</b>	<b>8</b>
<b>Scheme 1-8 Hasaninejad et al. seven-component condensation to form diasepines .....</b>	<b>9</b>
<b>Scheme 1-9 Ugi seven-component condensation reaction and proposed route.....</b>	<b>9</b>
<b>Scheme 1-10 Five-component condensation reaction. For conditions see Table 1-1 .....</b>	<b>11</b>
<b>Scheme 1-11 Stepwise conversions of intermediate DHPM (Biginelli) products in a hetero Diels-Alder reaction .....</b>	<b>14</b>
<b>Scheme 1-12 Retro Diels-Alder reaction under Krapcho dealkylation conditions.....</b>	<b>14</b>
<b>Scheme 1-13 Proposed mechanism of five-component condensation.....</b>	<b>15</b>
<b>Scheme 2-1 AstraZeneca synthesis of Gefitinib .....</b>	<b>27</b>
<b>Scheme 2-2 Reddy et al. synthesis of Gefitinib.....</b>	<b>27</b>
<b>Scheme 2-3 Suh et al. synthesis of Gefitinib .....</b>	<b>28</b>
<b>Scheme 2-4 A 2,4-dichloroquinazoline as a new starting material for Gefitinib preparation .....</b>	<b>30</b>
<b>Scheme 3-1 Synthesis of XJB-5-131 .....</b>	<b>48</b>



Scheme 3-2 Synthesis of JP4-039 through a hydrozirconation/transmetalation reaction ...	50
Scheme 3-3 The Fenton reaction .....	55
Scheme 3-4 Proposed vinylogous Mannich reaction towards JP4-039.....	64
Scheme 3-5 A) Three-component Mannich reaction and B) Two-component Mannich reaction.....	65
Scheme 3-6 Acyclic, indirect vinylogous Mannich reaction.....	66
Scheme 3-7 Martin et al. vinylogous Mannich reaction .....	66
Scheme 3-8 Hoveyda et al. Ag(I) catalyzed indirect vinylogous Mannich reaction.....	67
Scheme 3-9 Chen et al. direct vinylogous Mannich reaction .....	68
Scheme 3-10 Schneider et al. acyclic vinylogous Mannich reaction.....	68
Scheme 3-11 Schneider et al. vinylogous Mannich reaction of form amides .....	69
Scheme 3-12 Yin et al. vinylogous and bisvinylogous Mannich reaction of $\beta,\gamma$ -unsaturated amides.....	70
Scheme 3-13 Praveen et al. Mannich reaction with chiral phenyl-substituted oxazolidinone .....	73
Scheme 3-14 Olivo et al. Mannich reaction with chiral thiazolidine auxiliary .....	74
Scheme 3-15 Feng et al. Mannich reaction with achiral unsubstituted oxazolidinone.....	74
Scheme 3-16 Synthesis of sulfones 3-15 and 3-16.....	78
Scheme 3-17 Synthesis of aryl- or alkyl-substituted Boc-protect imines .....	79
Scheme 3-18 Vinylogous Mannich reaction with pyrazole auxiliary to form JP4-039 backbone .....	80
Scheme 3-19 Proposed photochemical isomerization mechanism.....	82

Scheme 3-20 Coupling of vinylogous Mannich product to 4-AT and isomerization/oxidation to JP4-039 .....	84
Scheme 3-21 <i>N</i> -Methylmorpholine mediated synthesis of $\beta,\gamma$ -unsaturated oxazolidinone..	87
Scheme 3-22 Single asymmetric synthesis reactions controlled by chiral ligand.....	93
Scheme 3-23 Determination of absolute configuration of ( <i>R</i> )-3-34 .....	94
Scheme 3-24 LDA mediated deconjugation reaction.....	105
Scheme 3-25 Synthesis of analog ( <i>R</i> )-3-44 .....	106
Scheme 3-26 Attempted deconjugative alkylation reaction with oxazolidinone auxiliary.	107
Scheme 3-27 Ytterbium triflate catalyzed oxazolidinone cleavage .....	108
Scheme 3-28 Deconjugative alkylation reaction with methyl ester 3-45.....	108
Scheme 3-29 Synthesis of analogs ( <i>S</i> )- and ( <i>R</i> )-3-47 .....	109
Scheme 3-30 Synthesis of analog ( <i>S</i> )-3-49 .....	110
Scheme 3-31 Synthesis of analog ( <i>R</i> )-3-53 .....	111
Scheme 3-32 Synthesis of analogs ( <i>S</i> )- and ( <i>R</i> )-3-56 .....	112
Scheme 3-33 Synthesis of analog ( <i>R</i> )-3-58 .....	113
Scheme 3-34 Synthesis of analogs ( <i>S</i> )-3-60 and ( <i>S</i> )-3-61 .....	114
Scheme 3-35 Synthetic scheme proceeding through a vinylogous Mannich reaction and deconjugative alkylation towards JP4-039 analogs .....	122

## List of Equations

Equation 3-1 .....	124
Equation 3-2 .....	124

## List of Abbreviations

AIFM2. ....	apoptosis-inducing factor mitochondria-associated 2
API. ....	active pharmaceutical ingredient
4-AT. ....	4-amino-tempo
ATP. ....	adenosine triphosphate
Bn. ....	benzyl
Boc. ....	<i>tert</i> -butyloxycarbonyl
CL. ....	cardiolipin
[Cu(CH <sub>3</sub> CN) <sub>4</sub> ]PF <sub>6</sub> . ....	tetrakis(acetonitrile)copper(I) hexafluorophosphate
CRO. ....	contract research organization
DABCO. ....	1,4-diazabicyclo[2.2.2]octane
DBU. ....	1,8-diazabicyclo[5.4.0]undec-7-ene
DCM. ....	dichloromethane
DFOA. ....	deferoxamine
DHPM. ....	dihydropyrimidinone
DIPEA. ....	<i>N,N</i> -diisopropylethylamine
DMAP. ....	4-dimethylaminopyridine
DMF. ....	<i>N,N</i> -dimethylformamide
DMP. ....	Dess-Martin Periodinane
DMPU. ....	<i>N,N'</i> -dimethylpropyleneurea
DMSO. ....	dimethylsulfoxide
dr. ....	diastereomeric ratio
EC <sub>50</sub> . ....	half maximal effective concentration
EC <sub>80</sub> . ....	.80% effective concentration
EDC. ....	1-ethyl-3-(3-dimethylaminopropyl)carbodiimide
ee. ....	enantiomeric excess
EGFR. ....	epidermal growth factor receptor
equiv. ....	equivalent(s)

er. .... enantiomeric ratio  
 ESI. .... electrospray ionization  
 Et<sub>3</sub>N. .... triethylamine  
 EtOAc. .... ethyl acetate  
 FDA. .... Food and Drug Administration  
 Fer-1. .... ferrostatin-1  
 Fesulphos ligand. .... (R<sub>FC</sub>)-2-(*tert*-Butylsulfenyl)-1-[bis(1naphthyl)phosphino]ferrocene  
 FSP1. .... ferroptosis-suppressor protein 1  
 GSH. .... glutathione  
 GPX4. .... glutathione peroxidase 4  
 HOBt. .... hydroxybenzotriazole  
 HMPA. .... hexamethylphosphoramide  
 HPLC. .... high performance liquid chromatography  
 HRMS. .... high resolution mass spectroscopy  
 HSPB1. .... heat shock protein beat-1  
 IAP. .... inhibitor of apoptosis proteins  
 IBA. .... indolizidine based alkaloids  
 IL. .... ionic liquid  
 IR. .... infrared spectroscopy  
 LCMS. .... liquid chromatography mass spectroscopy  
 LDA. .... lithium diisopropylamide  
 LIP-1. .... liproxstatin-1  
 LogP. .... partition coefficient  
 LOX. .... lipoxygenases  
 MCR. .... multi-component reaction  
 MeOH. .... methanol  
 MLKL. .... mixed lineage kinase domain like  
 MOMP. .... mitochondrial outer membrane permeabilization  
 MW. .... molecular weight  
 NCOA4. .... nuclear receptor coactivator 4  
 NMM. .... *N*-methylmorpholine

NMR. .... nuclear magnetic resonance  
 NOE. .... nuclear Overhauser enhancement  
 NSCLC. .... non-small cell lung cancer  
 OMM. .... outer mitochondria membrane  
 OXPHOS. .... oxidative phosphorylation  
 POR. .... cytochrome P450 oxidoreductase  
 PMP. .... *p*-methoxyphenyl ether  
 PUFAs. .... polyunsaturated fatty acids  
 RIPK. .... receptor-interacting protein kinase  
 rt. .... room temperature  
 (*R*)-DTBM-SEGPPOS ..... CAS #566940-03-2  
 rac-BINAP. .... CAS #98327-87-8  
 ROS. .... reactive oxygen species  
 (*S*)-BINOL. .... CAS #18531-99-2  
 (*S*)-DTBM-SEGPPOS ..... CAS #210169-40-7  
 SAR. .... structure activity relationship  
 SFC. .... super critical fluid chromatography  
 SM. .... starting material  
 SNAr. .... nucleophilic aromatic substitution  
 TANIAPHOS. .... CAS #10030012-96-1  
 TBDPS. .... *tert*-butyldiphenylsilyl  
 TBME. .... *tert*-butylmethylether  
 TBS. .... *tert*-butyldimethylsilyl  
 TFA. .... trifluoroacetic acid  
 THF. .... tetrahydrofuran  
 TLC. .... thin layer chromatography

## Preface

I would like to first thank my advisor, Professor Peter Wipf, for always encouraging me to achieve more and for providing me with the opportunities to do so. Professor Wipf has created a group environment where I am always learning, able to ask questions, and have access to state of the art resources. His work ethic is second to none and something I aspire to. I would also like to thank Professor Kazunori Koide, Professor Peng Liu, and Professor Hülya Bayir for being members of my committee.

I am thankful for all of my coworkers who have contributed to a stimulating and enjoyable environment. In particular I would like to thank Mary Liang and Desirae Crocker. Without their help and expertise, things would not operate as smoothly as they do in the lab. I would also like to thank several of my colleagues, Dr. Marina Kovaliov, Dr. James Johnson, Dr. Manwika Charaschanya, and Dr. Matt LaPorte who I have worked in close proximity with over the years and were great sources of knowledge.

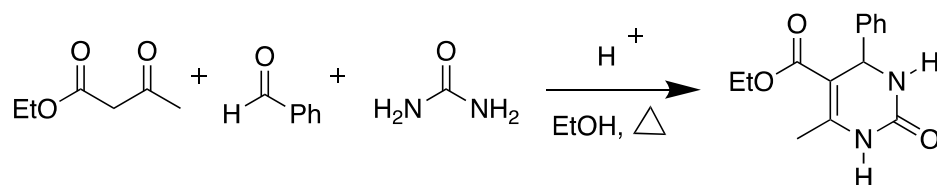
Lastly, I would like to thank my husband, Josh, for his unconditional support and encouragement as I pursued my Ph.D.; we are a team through everything. Additionally, I would like to thank my parents for all they sacrificed to put both my brother and I in the best positions to succeed growing up.

## 1.0 Five-Component Biginelli-Diels-Alder Cascade Reaction

### 1.1 Introduction

#### 1.1.1 The Biginelli Reaction

The Biginelli reaction was discovered by Pietro Biginelli in 1891.<sup>1</sup> It is a one-pot multi-component reaction (MCR) that generates dihydropyrimidinones (DHPMs) from an acid catalyzed reaction of a  $\beta$ -keto ester, aldehyde, and urea in a protic solvent. Biginelli's earliest example was with ethyl acetoacetate, benzaldehyde, and urea (Scheme 1-1).



**Scheme 1-1** Pietro Biginelli's initial multi-component reaction<sup>1</sup>

With three components in the reaction, there are three possible mechanisms. All three mechanisms involve protonated intermediates that lead to the formation of the DHPM (Figure 1-1). The iminium route (Figure 1-1 A) begins with condensation between the aldehyde and urea. Following the loss of water, the iminium intermediate acts as an electrophile for the enol tautomer of the  $\beta$ -keto ester. The ketone carbonyl of the resulting intermediate undergoes an intramolecular condensation with the  $NH_2$  of the urea to generate the cyclized DHPM product (Scheme 1-2).<sup>2</sup> The enamine route (Figure 1-1 B) was hypothesized to begin with a condensation between the urea and  $\beta$ -keto ester to form an enamine intermediate which subsequently reacts with the aldehyde.<sup>3</sup> The Knoevenagel route (Figure 1-1 C) was based on the initial reaction between the aldehyde and  $\beta$ -keto ester to form a carbenium intermediate that then reacts with the urea.<sup>4</sup> C. Oliver Kappe first elucidated that the iminium route (Figure 1-1 A) was the most probable mechanistic route through



a combination of  $^1\text{H}$  and  $^{13}\text{C}$  NMR spectroscopy and trapping reactions.<sup>5</sup> Puripat et al. provided the most conclusive evidence of the iminium intermediate pathway through the use of artificial force induced reaction (AFIR) method and DFT calculations.<sup>6</sup> They calculated the energy barrier for the rate determining step in each pathway and determined that C-N bond formation during the cyclization step in the iminium route (Figure 1-1 A) had the lowest overall energy barrier, 21.5 kcal/mol, compared to 31.2 kcal/mol for the cyclization step in the enamine route (Figure 1-1 B) and 28.0 kcal/mol for the rate limiting condensation step between the aldehyde and  $\beta$ -keto ester in the Knoevenagel route (Figure 1-1 C). The most energetically favorable route is the most likely to occur.

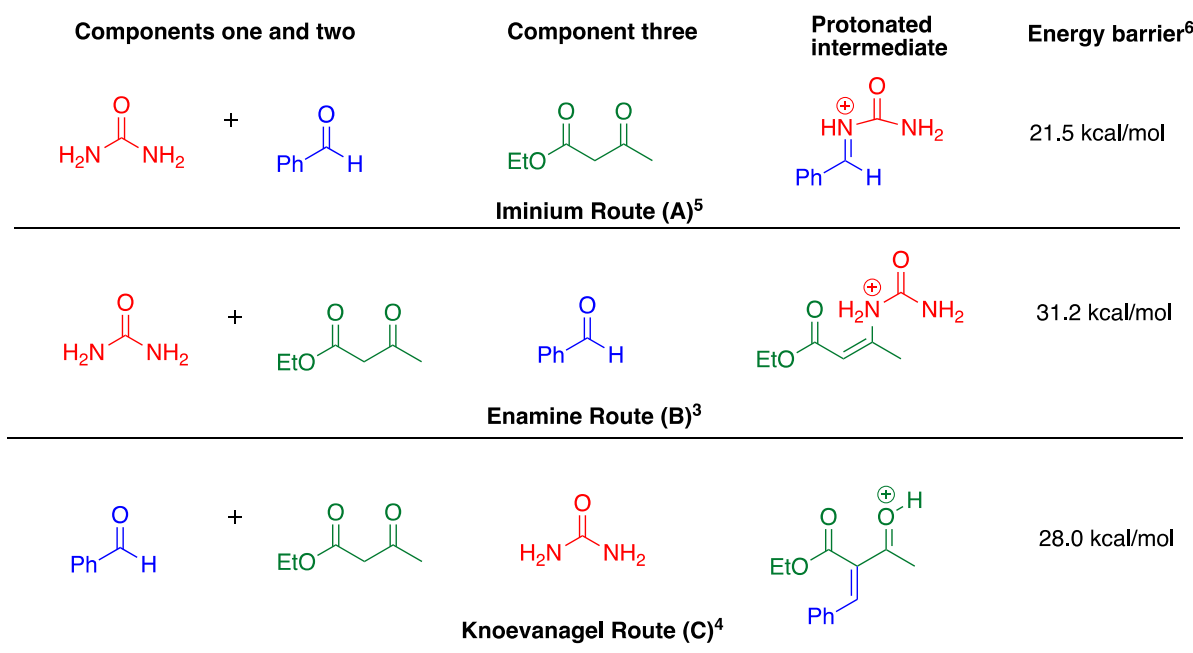
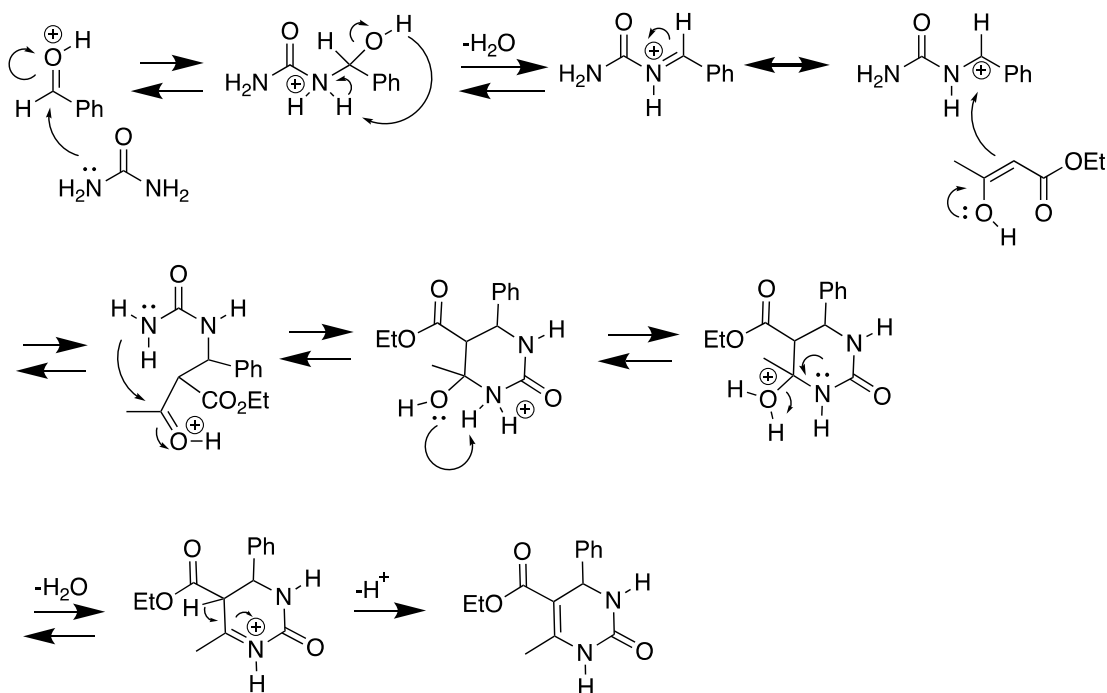


**Figure 1-1 Biginelli reaction possible mechanistic routes**



**Scheme 1-2 Acid catalyzed Biginelli reaction<sup>2</sup>**

The synthetic utility of the Biginelli reaction did not garner much interest for almost 100 years. However, beginning in the 1980s, the MCR became more prominent as it provided easy access to biologically active heterocycles and even marine natural products.<sup>7-8</sup> DHPMs have been shown to have neuroprotective, antiparasitic, antiviral, antitumor, anti-inflammatory, and anticancer activities.<sup>9</sup> Specifically, they have been shown to be potent A<sub>2B</sub> receptor antagonists<sup>10</sup> and antihypertensive agents.<sup>11</sup> One of the most studied DHPMs is Monastrol which was found to disrupt mitosis in 1999.<sup>12-13</sup> Several potent analogs with increased anticancer potency have been synthesized since.<sup>14</sup> Nifedipine is a drug approved by the Food and Drug Administration (FDA) to treat severe high blood pressure in pregnancy that is structurally related to a Biginelli DHPM. New, more potent, analogs of Nifedipine with superior half-lives have been synthesized through Biginelli reactions. These compounds have been useful tools in the further development of structure activity relationships (SAR).<sup>15-16</sup>

The synthesis of a structurally diverse library of pharmacologically active compounds is an attractive possibility with this three-component reaction. There are many readily available aldehydes, (thio)ureas, and  $\beta$ -keto esters that can be purchased or synthesized in one step. With three aldehydes, three ureas, and three esters, 27 unique compounds can be synthesized. If the

number of each component increases to five, then 125 unique compounds can be made. Following this strategy, we have developed a library of over 100 compounds that act as biologically active antagonists and agonists against heat shock protein70 (HSP70) such as MAL3-101, MAL1-271, and BBQU015254 (Figure 1-2).<sup>17-18</sup>

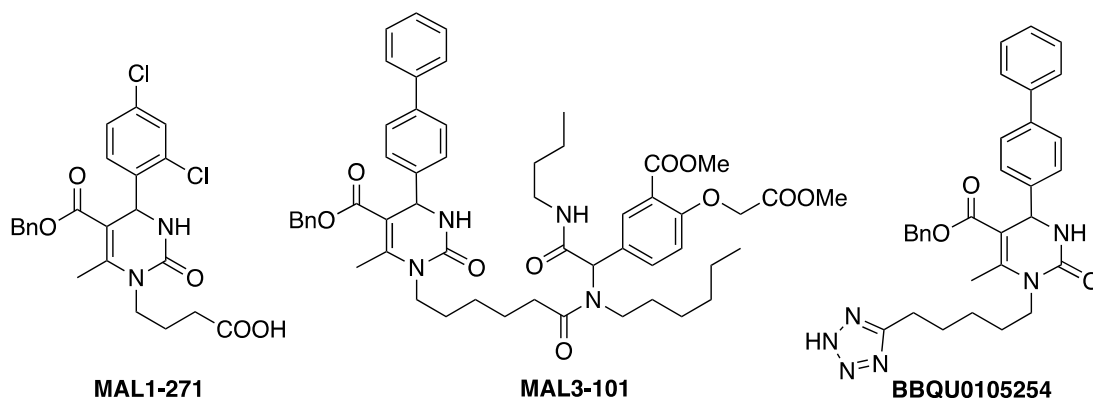


**Figure 1-2 DHPMs targeting HSP70 synthesized through Biginelli reactions**

As more complex molecules were targeted, new synthetic methods were required. The standard strong acid conditions limited functional group compatibility on the various components and also resulted in lower yields. In place of the typical strong Brønsted acid catalyst, hydrochloric acid (HCl), various Lewis acid catalysts including  $\text{InCl}_3$ <sup>19</sup>,  $\text{FeCl}_3$ <sup>20</sup>,  $\text{BF}_3 \cdot \text{OEt}_2$ <sup>21</sup>,  $\text{ZnCl}_2$ <sup>22</sup>,  $\text{GaCl}_3$ <sup>23</sup>, and  $\text{InBr}_3$ <sup>24</sup> have been used successfully. The Lewis acid catalysts are believed to coordinate to the urea oxygen or nitrogen in the iminium route (A) and stabilize the *N*-acyliminium ions. Lewis acids are also hypothesized to interact with the  $\beta$ -keto ester (Figure 1-3).<sup>21, 25</sup> A number of ionic liquids have also been used as catalysts to both increase the rate of reaction and provide a “green chemistry” alternative.<sup>26</sup> Another catalyst variation includes the use of organocatalysts to impart enantioselectivity in the DHPM synthesis.<sup>27</sup> More recently, new techniques have been employed to enhance the scope of the reaction and also improve isolation and purification. In our group, we have utilized highly fluorinated substrates that can easily be isolated from organic solvents through liquid-liquid extractions, thus streamlining the synthesis of a large library of diverse DHPMs.<sup>28</sup> We have also employed a resin-linked GABA urea in a solid phase protocol that is readily cleaved with trifluoroacetic acid to streamline purification.<sup>17</sup>

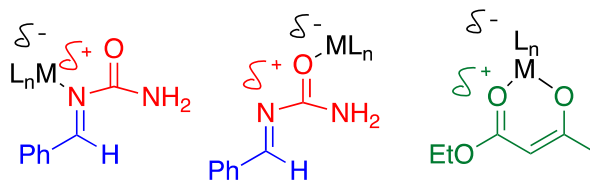


**Figure 1-3** Lewis acid coordination in N-acylimines and  $\beta$ -keto ester

While Biginelli reaction conditions typically furnish 3,4-dihydropyrimidinones, there are several examples of conditions that lead to alternative products (Figure 1-4). Overman utilized a tethered aldehyde and urea to synthesize hexahydropyrrolo[1,2-c]pyrimidines.<sup>29</sup> Kappe and coworkers demonstrated the use of precondensed enones, derived from a Knoevenagel condensation of the aldehyde and carbonyl, with thioureas to form a library of 1,3-thiazines, an isomer of thio-Biginelli compounds.<sup>30</sup>

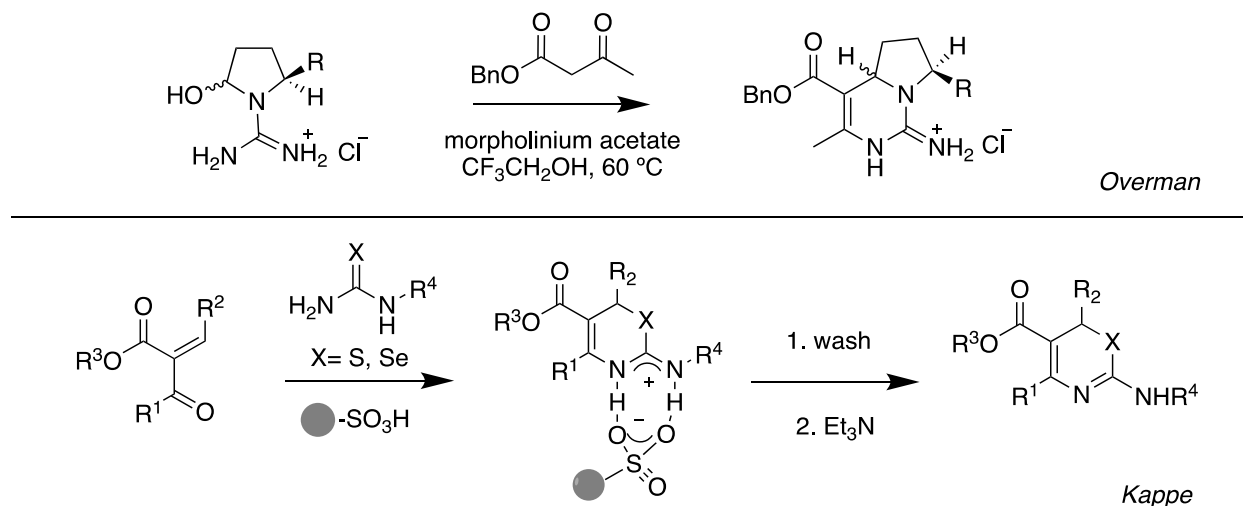
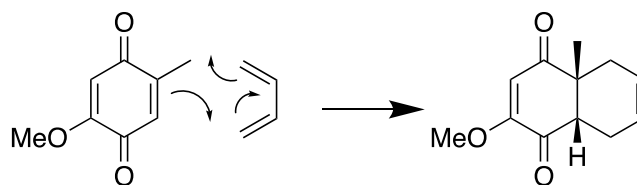


**Figure 1-4** Overman<sup>29</sup> and Kappe<sup>30</sup> preparation of atypical Biginelli reaction products

### 1.1.2 The Diels-Alder Reaction

The Diels-Alder reaction was first described by Otto Diels and Kurt Alder in 1928; an accomplishment for which they would be awarded the Nobel Prize in Chemistry in 1950.<sup>31</sup> It is a [4+2] cycloaddition between a conjugated diene and an alkene (dienophile) (Scheme 1-3). The

Diels-Alder reaction is a particularly useful reaction as it provides control over regio- and stereochemical properties through a six-member transition state. It can occur inter- or intramolecularly and through various hetero  $\pi$ -systems to form functionalized heterocycles.

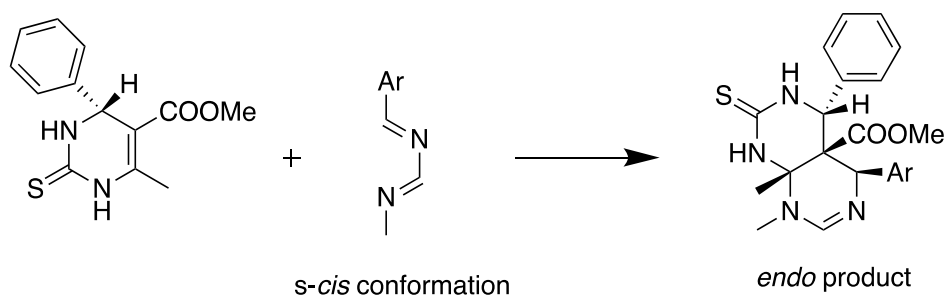


**Scheme 1-3 Diels-Alder reaction mechanism and product**

Many rules have been established for determining the reactivity, regio-, and stereochemical selectivity in the reaction: 1. cycloaddition is most facile when the *s-cis* conformation is favored in the diene; 2. in normal-electron-demand Diels-Alder reactions, reactivity increases when the diene is electron rich and the dienophile is electron poor; 3. in inverse-electron-demand Diels-Alder reactions, electron withdrawing groups on the diene promote reactivity; 4. the stereochemistry of the diene and dienophile is retained in the product; 5. the ortho-para directive rule for regioselectivity is controlled by frontier molecular orbital (FMO) theory;<sup>32-34</sup> and 6. the Alder endo rule governs stereoselectivity.<sup>35</sup>

Based on the amount of control intrinsic to the reaction, it has been utilized as a key step in multiple natural product total syntheses, including cortisone and cholesterol by R.B. Woodward<sup>36</sup>, prostaglandins F2 $\alpha$  and E2 by E.J. Corey<sup>37</sup>, and racemic reserpine by Stephen F. Martin.<sup>38</sup>

The Biginelli DHPM can function as a tetrasubstituted dienophile in the Diels-Alder reaction albeit with low expected reactivity. Accordingly, publications on this topic are rare. Sharma and coworkers demonstrated the reaction of the Biginelli heterocycle with *N*-arylidine-*N'*-methylformamidines and *N*-arylidine guanidine in a hetero Diels-Alder reaction but few other examples are readily available.<sup>39</sup>

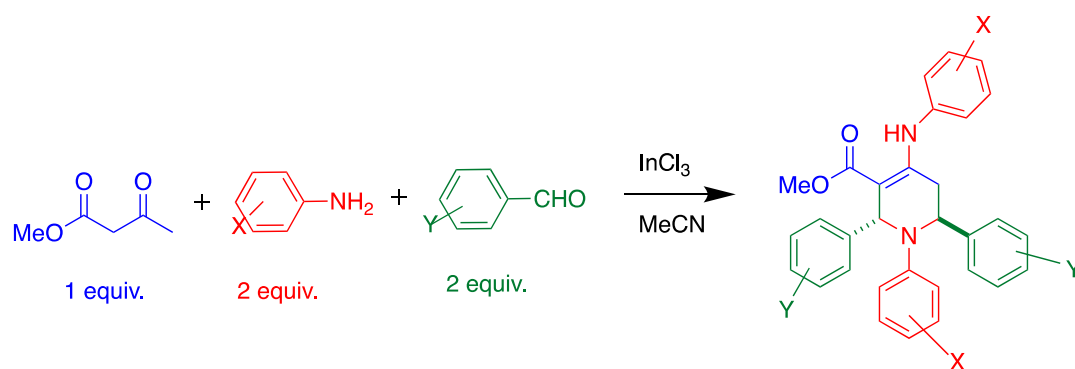


**Scheme 1-4 Sharma et al. Diels-Adler reaction with Biginelli dienophile<sup>39</sup>**

### 1.1.3 Multi-Component Reactions

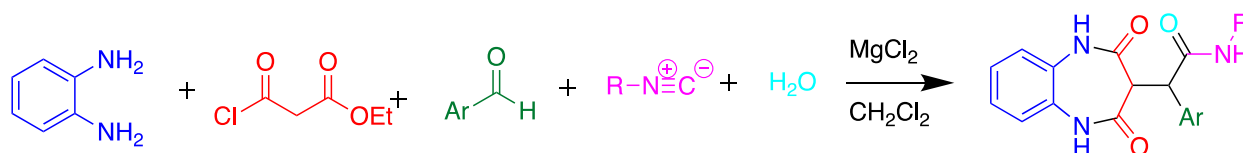
MCRs are convergent reactions in which three or more starting materials react to form a product and most, if not all, atoms are incorporated into the product structure. In addition to the Biginelli reaction, there are many examples of named three-component MCRs including: Mannich reaction,<sup>40</sup> Hantzsch Dihydropyridine (Pyridine) synthesis,<sup>41</sup> Bucherer-Bergs reaction,<sup>42</sup> Strecker amino-acid synthesis,<sup>43</sup> Gewald reaction,<sup>44</sup> Passerini reaction,<sup>45</sup> Grieco condensation reaction,<sup>46</sup> and Petasis reaction.<sup>47</sup> There have been fewer four-component MCRs reported, the most well-known of which is the Ugi reaction.<sup>48</sup> Other four-component condensation reactions involve slight variations in the Ugi protocol, such as replacing the carboxylic acid with Meldrum's acid.<sup>49</sup> Ghashang et. al recently reported a new four-component condensation synthesis of  $\beta$ -amido ketones with an aldehyde, enolizable ketone, acetyl chloride, and acetonitrile or benzonitrile in the presence of ferric hydrogensulfate as a catalyst.<sup>50</sup>

Even less has been published on five-component condensation reactions. Whitwood et al. disclosed an economic synthesis of highly functionalized piperidines from methyl acetoacetate, two equivalents of an aniline and two equivalents of an aromatic aldehyde (Scheme 1-5). The reaction is hypothesized to proceed through a Knoevenagel-like condensation between the imine and enamine intermediate followed by a subsequent aza-Diels Alder cyclization or a tandem Mannich-Michael reaction.<sup>51</sup>



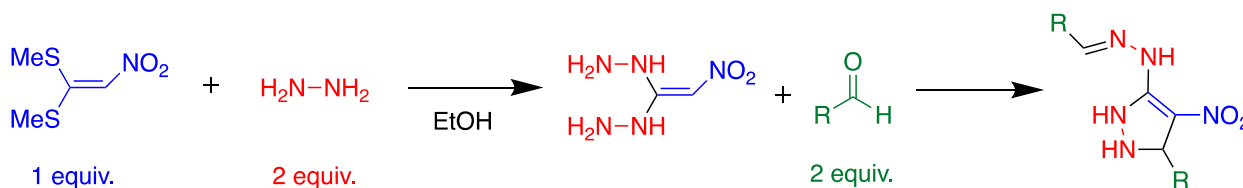
**Scheme 1-5 Whitwood et al. five-component condensation formation of piperidines<sup>51</sup>**

Mirkhani et. al described a five-component synthesis of phenylacetamides catalyzed by magnesium chloride.<sup>52</sup> The reaction components include an aromatic diamine, ethyl malonyl chloride, an aromatic aldehyde, isocyanide, and water (Scheme 1-6). The reaction was tolerant of limited substitutions on the aldehyde and isocyanide components.

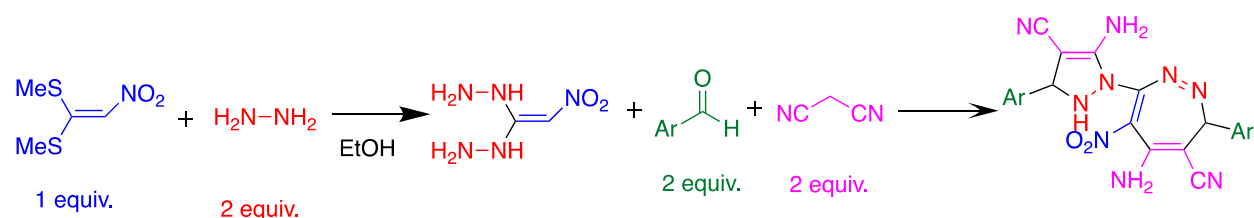


**Scheme 1-6 Mirkhani et al. five-component condensation to form phenylacetamides<sup>52</sup>**

Hasaninejad et al. described a *pseudo* five-component synthesis of pyrazoline-containing Schiff bases, from 1,1-bis(methylthio)-2-nitroethylene (BMTNE), two equivalents of hydrazine, and two equivalents of aldehyde at room temperature (Scheme 1-7).<sup>53</sup> The group further demonstrated a *pseudo* seven-component synthesis to form highly functionalized diazepines through the addition of two equivalents of malonitrile (Scheme 1-8).<sup>54</sup>

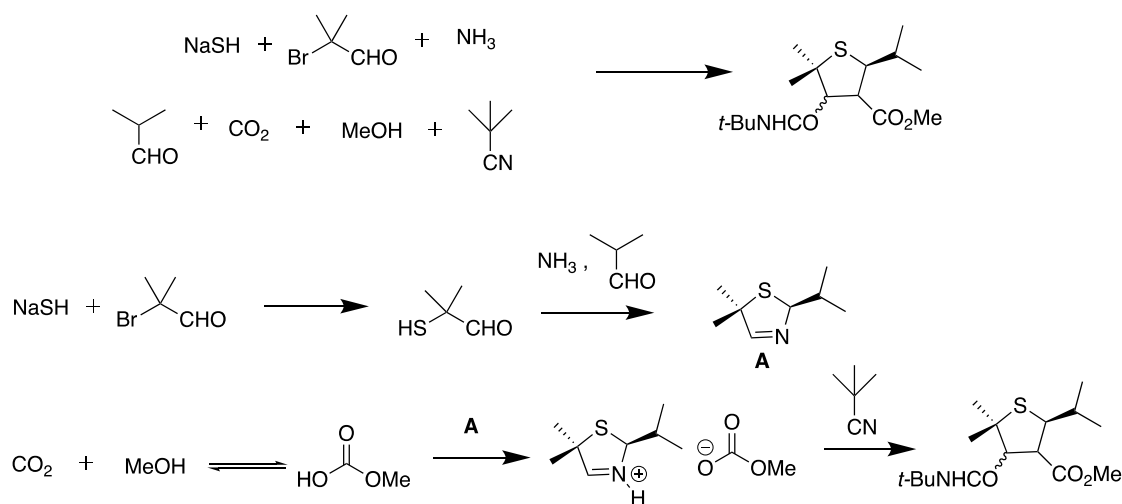


**Scheme 1-7 Hasaninejad et al. five-component condensation to form pyrazoline-containing Schiff bases<sup>53</sup>**



**Scheme 1-8** Hasaninejad et al. seven-component condensation to form diasepines<sup>54</sup>

In 1993, Ugi disclosed a seven-component condensation reaction that occurred through a combination of an Asinger condensation and an Ugi-type four-component condensation reaction (Scheme 1-9).<sup>55-56</sup>



**Scheme 1-9** Ugi seven-component condensation reaction and proposed route<sup>55</sup>

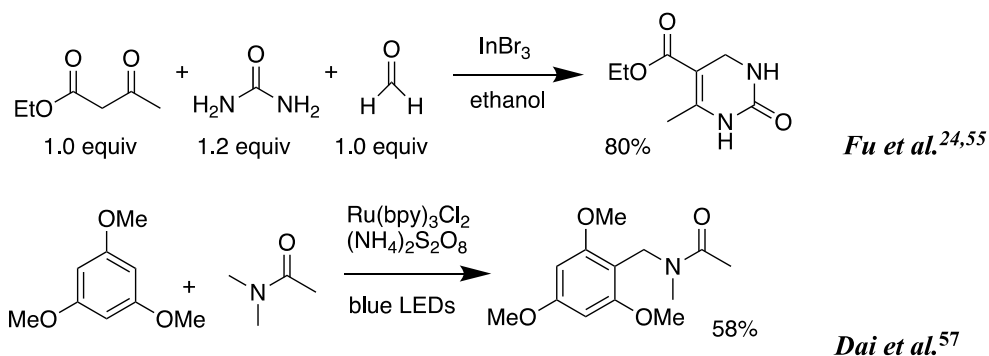
## 1.2 Results and Discussion<sup>57</sup>

While working to advance the scope of our DHPM library, we noted the use of 10% indium(III) bromide (InBr3) as a catalyst at reflux in ethanol for 7 h to produce a variety of DHPMs.<sup>24, 58</sup> Particularly attractive was that these conditions gave good yields even with formaldehyde as a reaction component. Many other protocols catalyzed by Brønsted acids were not suitable with the unsubstituted aldehyde. Singh et al. demonstrated that 1,3-oxazinane could

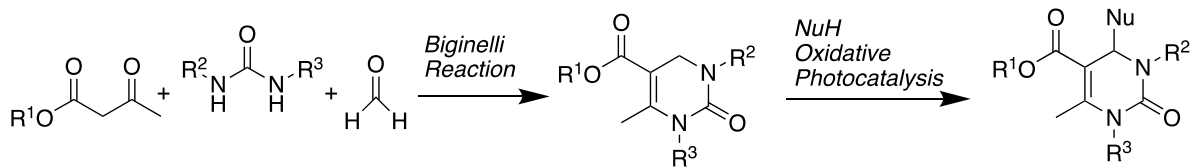


be used as a formaldehyde substitute,<sup>59</sup> but few methods actually utilized the highly reactive unsubstituted aldehyde. Initially, we hoped to be able to introduce substituents at the 4-position of the DHPM ring through an oxidative photochemical reaction related to the previously reported Friedel-Crafts amidoalkylation with the visible light catalyst, Ru(bpy)<sub>3</sub>Cl<sub>2</sub>.<sup>60</sup> However, we found that InBr<sub>3</sub> conditions promoted a new five-component condensation with formaldehyde, and decided to first investigate the scope of this process (Figure 1-5).

#### PRIOR WORK



#### PROPOSED WORK



#### THIS WORK

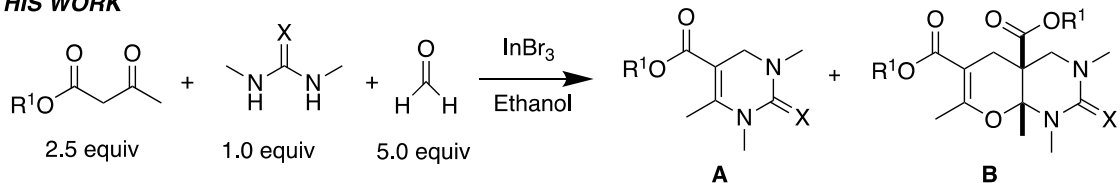
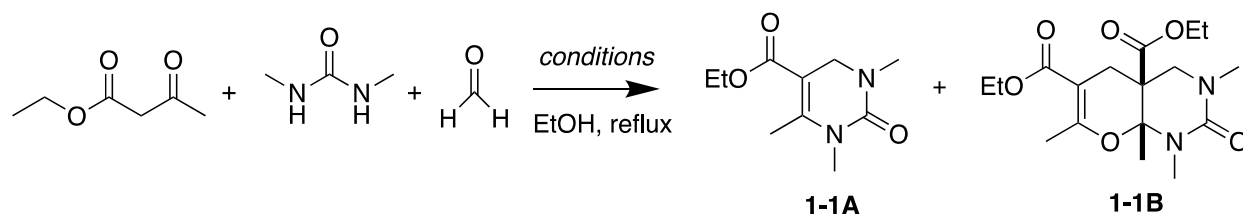


**Figure 1-5 Literature precedence and synthetic plans**

The originally reported InBr<sub>3</sub> reaction conditions utilized an excess of urea and equal equivalents of  $\beta$ -keto ester and aldehyde. For our initial test reactions, we chose *N,N'*-dimethylurea as the limiting reagent. The reaction of *N,N'*-dimethylurea, 1.8 equiv of ethyl acetoacetate as the  $\beta$ -keto ester, and 3 equiv of formaldehyde in 95% ethanol at reflux for 7 h yielded not only the expected DHPM product **1-1A** but also a higher molecular weight product that we did not anticipate (Scheme 1-10). Through NMR and NOE analyses, we were able to assign its fused

bicyclic structure as **1-1B**. We hypothesized that this secondary product occurred through a five-component condensation reaction, and an *in situ* formal hetero Diels-Alder reaction of the expected DHPM Biginelli intermediate, which was in agreement with the product structure.



**Scheme 1-10** Five-component condensation reaction. For conditions see Table 1-1

We subsequently explored a range of reaction conditions in an attempt to improve overall yield and selectivity. For these optimizations, we used our original reaction components *N,N'*-dimethylurea, ethyl acetoacetate, and formaldehyde (Table 1-1). The traditional Brønsted acid catalyst, HCl, gave no conversion with formaldehyde (entry 2). We experimented with other Lewis acids (entries 3-6) to catalyze the reaction but saw no conversion with FeCl<sub>3</sub> or ZnCl<sub>2</sub>. Conversion was modest with both InCl<sub>3</sub> and AlCl<sub>3</sub>. Increasing the proportions of the β-keto ester and the aldehyde to 2.5 and 5 equiv, respectively, improved the yield of both products **1-1A** and **1-1B** (entry 7). However, increasing or decreasing the reactant concentration (entries 8 and 9) did not improve the overall yield. Doubling the reaction time to 14.5 h also did not increase the conversion to product **1-1B** (entry 10 vs entry 7). After a shortened reaction time of 2.0 h, only product **1-1A** was isolated in 28% yield (entry 11). Accordingly, entry 7 represented our optimized conditions: 1 equiv of urea, 2.5 equiv of β-keto ester, 5.0 equiv of aldehyde, and 0.1 equiv of InBr<sub>3</sub> at reflux conditions in ethanol (0.2 M) for 7 h provided 45% of DHPM **1-1A** and 48% of pyranopyrimidinone **1-1B**.

**Table 1-1 Investigation of reaction time, concentration, equivalents, and catalyst with formaldehyde, *N,N*-dimethylurea, and ethyl acetoacetate**

Entry <sup>a</sup>	Urea (equiv)	Ester (equiv)	Aldehyde (equiv)	Catalyst (equiv)	Time (h)	Concentration (M)	1-1A [% Yield] <sup>b</sup>	1-1B [% Yield] <sup>b</sup>
1	1	1.8	3	InBr <sub>3</sub> (0.1)	7	0.2	10	26
2	1	1.8	3	HCl (1.0)	7	0.5	0	0
3	1	1.8	3	InCl <sub>3</sub> (0.1)	7	0.3	23	25
4	1	1.8	3	AlCl <sub>3</sub> (0.1)	7	0.3	3	14
5	1	1.8	3	FeCl <sub>3</sub> (0.2)	7	0.2	0	0
6	1	1.8	3	ZnCl <sub>2</sub> (0.2)	7	0.3	0	0
7	1	2.5	5	InBr <sub>3</sub> (0.1)	7	0.2	45	48
8	1	2.5	5	InBr <sub>3</sub> (0.1)	7	1.0	55	37
9	1	2.5	5	InBr <sub>3</sub> (0.1)	7	0.05	38	27
10	1	2.5	5	InBr <sub>3</sub> (0.1)	14.5	0.2	41	36
11	1	2.5	5	InBr <sub>3</sub> (0.1)	2	0.2	28	0

<sup>a</sup>Conditions: EtOH, reflux

<sup>b</sup>Isolated yield

We then used these optimized conditions to further explore the scope of the reaction (Table 1-2). Formaldehyde was used as the aldehyde component in all reactions since preliminary trials with other aldehydes and ketones were not successful in producing any fused bicycles **B**. We also used symmetrical ureas exclusively to avoid possible regioisomers (exploratory reactions confirmed a lack of regioselectivity with unsymmetrical ureas; for example, while 1-methylurea and 1-(4-methoxyphenyl)-3-methylurea provided both the Biginelli DHPM and the Diels-Alder products, we were unable to separate the regioisomers formed in approximately 1:1 ratio). Curiously, the reaction with the *N,N'*-dimethylthiourea stopped at the Biginelli product **1-2A**, which was isolated in 61% yield (entry 2). Methyl acetoacetate with thiourea (entry 3) also gave similar results, but product **1-3A** was formed in lower yield, likely due to *trans*-esterification with ethanol. Utilizing benzyl acetoacetate, we were able to isolate both Biginelli (**1-4A**, **1-5A**) and five-component condensation products (**1-4B**, **1-5B**) in good overall yields with the urea and thiourea derivatives (entries 4 and 5). However, the yield of the five-component condensation Diels-Alder product **1-4B** was considerably higher with the urea derivative than the pyranopyrimidinethione **1-5B** resulting from the thiourea. With allyl acetoacetate and *N,N'*-dimethylurea, we were able to isolate the five-component condensation product **1-6B**, but not the

corresponding Biginelli intermediate, as it proved unstable. We also attempted to replace the traditional  $\beta$ -keto ester with 5,5-dimethyl-1,3-cyclohexanedione (dimedone) to probe the feasibility of adding an additional ring in the hetero Diels-Alder reaction (Figure 1-6). Unfortunately, with both *N,N'*-dimethylurea and its thiourea equivalent, we were only able to isolate Biginelli products **1-7A** and **1-8A**, in significantly lower yields than for the  $\beta$ -keto ester conversions.

**Table 1-2 Reaction scope with formaldehyde, *N,N'*-dimethyl(thio)urea (X=O,S), and alkyl ( $R^1$ ) acetoacetates<sup>a</sup>**

No.	$R^1$	X	A [% Yield] <sup>b</sup>	B [% Yield] <sup>b</sup>
1-1	Ethyl	O	45	48
1-2	Ethyl	S	61	0
1-3	Methyl	S	31	0
1-4	Benzyl	O	12	73
1-5	Benzyl	S	61	32
1-6	Allyl	O	0	21

<sup>a</sup>Conditions: formaldehyde (5 equiv), *N,N'*-dimethyl(thio)urea (1.0 equiv), alkyl ( $R^1$ ) acetoacetate (2.5 equiv), InBr<sub>3</sub>(0.1 equiv), EtOH (0.2 M), reflux.

<sup>b</sup>Isolated yield

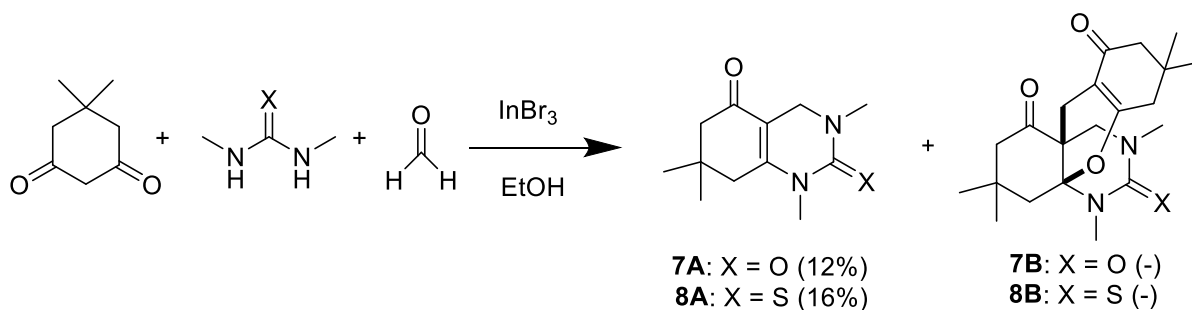
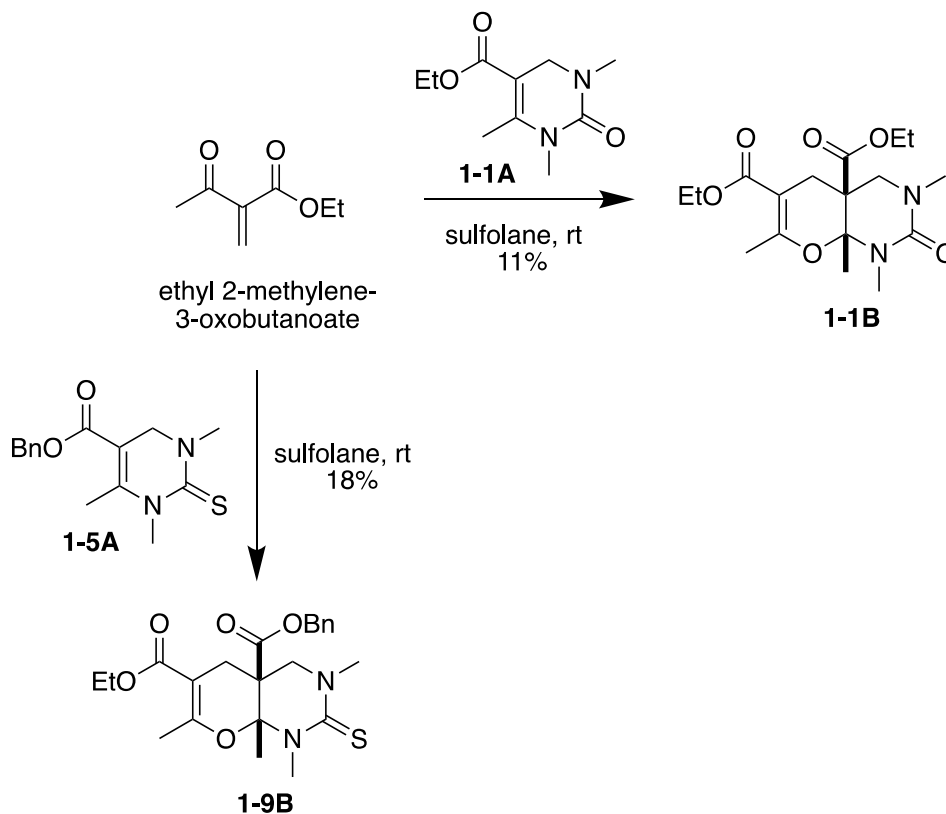


**Figure 1-6 Attempted five-component condensation with a cyclic 1,3-diketone**

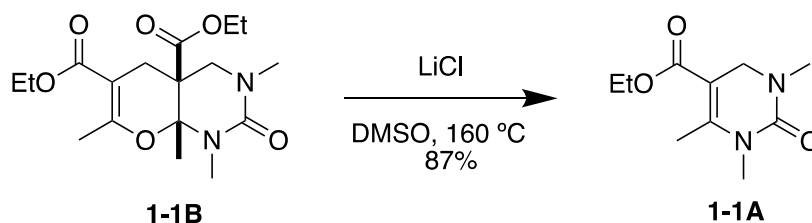
To confirm our hypothesis that the five-component condensation product formed through a hetero Diels-Alder reaction with the DHPM (Biginelli) intermediate, we reacted Biginelli product **1-1A** with ethyl 2-methylene-3-oxobutanoate (Figure Scheme 1-11). After stirring in sulfolane at room temperature for 18 hours, we isolated the corresponding hetero Diels-Alder

Product, **1-1B**, in 11% yield. We were also able to repeat this conversion with the Biginelli intermediate **1-5A** to form the hetero Diels-Alder product **1-9B**.

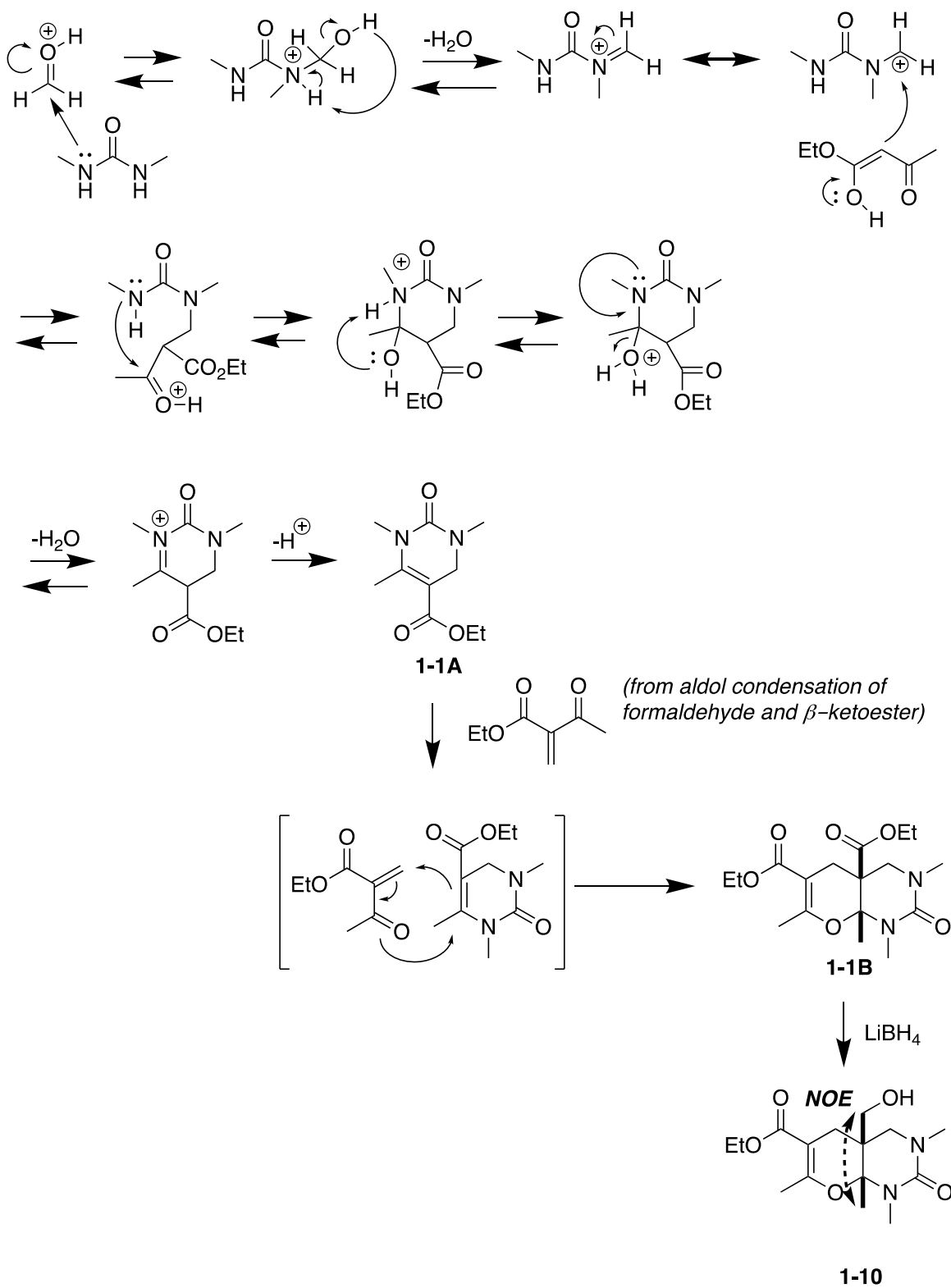


Scheme 1-11 Stepwise conversions of intermediate DHPM (Biginelli) products in a hetero Diels-Alder reaction

Interestingly, when the five-component condensation product **1-1B** was subjected to Krapcho dealkylation conditions with LiCl in DMSO, we isolated the DHPM product, **1-1A**, in 87% yield, presumably through a retro Diels-Alder reaction (Scheme 1-12) <sup>61</sup>.



Scheme 1-12 Retro Diels-Alder reaction under Krapcho dealkylation conditions



**Scheme 1-13 Proposed mechanism of five-component condensation**

Scheme 1-13 illustrates our proposed mechanism for the five-component condensation reaction. In the presence of a Lewis acid, condensation of the urea with the aldehyde and subsequent loss of water generates a sufficiently reactive electrophile for attack by the  $\beta$ -keto ester, which then undergoes cyclization to give **1-1A**. The excess  $\beta$ -keto ester and formaldehyde react to form a methylene group at the  $\alpha$ -position, and this electrophile then undergoes a hetero Diels-Alder reaction with the intermediate DHPM **1-1A** to provide the fused heterocyclic **1-1B** a single stereoisomer. It should be noted that the hetero Diels-Alder reaction may occur via a step-wise addition reaction as many inverse-electron-demand Diels-Alder reactions occur via a step-wise mechanism opposed to a concerted mechanism.<sup>32</sup> The condensation product resulting from the  $\beta$ -keto ester and formaldehyde is able to adopt the *s-cis* conformation as the diene. We determined the configuration of the methyl group to be *cis* to the ester at the two quaternary ring fusion atoms by converting the ester to the primary alcohol **1-10** with LiBH<sub>4</sub>, and then using a NOE analysis to confirm that the methyl group protons showed a >10% percent double resonance enhancement with the newly formed CH<sub>2</sub> protons.

### 1.3 Conclusions

We have discovered and optimized experimental conditions for a novel one pot, five-component condensation reaction with a  $\beta$ -keto ester, urea, and formaldehyde. The reaction appears to proceed through an intermediate DHPM (Biginelli) product. The DHPM then reacts with the condensation product of the  $\beta$ -keto ester and formaldehyde through a formal hetero Diels-Alder reaction. While the scope of this new process is still limited to formaldehyde and symmetrical *N,N'*-dialkylated ureas, it provides easy access to bicyclic ring systems that were previously inaccessible through a single transformation. Going forward, nucleophilic additions at the 4-position of the Biginelli product can be investigated. Functionalities not compatible with the traditional Biginelli reaction can be introduced this way to expand a DHPM library. Additionally, the five-component condensation products should be tested for activity in HSP70 and other heat shock protein models. The bicyclic heterocycle represents a unique functionality that has not yet been tested.

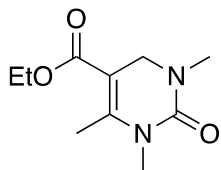
## 1.4 Experimental Procedures

**General.** All reagents were obtained commercially unless otherwise noted. All glassware was dried in an oven at 140 °C for 2 h prior to use. Reactions were monitored by TLC analysis (EMD Millipore pre-coated silica gel 60 F254 plates, 250 µm layer thickness) and visualization was accomplished with a 254 nm UV light or staining with a PMA solution (5 g of phosphomolybdic acid in 100 mL of 95% EtOH), p-anisaldehyde solution (2.5 mL of p-anisaldehyde, 2 mL of AcOH, and 3.5 mL of conc. H<sub>2</sub>SO<sub>4</sub> in 100 mL of 95% EtOH), or a KMnO<sub>4</sub> solution (1.5 g of KMnO<sub>4</sub> and 1.5 g of K<sub>2</sub>CO<sub>3</sub> in 100 mL of a 0.1% NaOH solution). Some purification by chromatography was performed using a SiO<sub>2</sub> Büchi flash chromatography system. <sup>1</sup>H/<sup>13</sup>C NMR spectra were recorded on either a Bruker Avance 300/75 MHz, Bruker Avance 400/100 MHz, Bruker Avance 500/135 MHz, or Bruker Avance 600/150 MHz instruments. Chemical shifts were reported in parts per million with the residual solvent peak used as the internal standard (<sup>1</sup>H/<sup>13</sup>C: CDCl<sub>3</sub>, 7.26, 77.0 ppm; CD<sub>3</sub>OD, 3.31, 49.3 ppm; DMSO, 2.50, 39.5 ppm). Chemical shifts were tabulated as follows: chemical shift, multiplicity (s = singlet, d = doublet, t = triplet, q = quarter, dd = doublet of doublet, dt = doublet of triplet, dq = doublet of quartet, m = multiplet, brd = broad, app = apparent), coupling constants, and integration. All 1D NMR spectra were processed using Bruker Topspin NMR. IR spectra were obtained on an Identity IR-ATR spectrometer. Melting points (uncorrected) were determined using a Mel-Temp instrument. HRMS data were obtained on a Thermo Scientific Exactive HRMS coupled to a Thermo Scientific Accela HPLC system using a 2.1 x 50 mm 3.5 µm Waters XTerra C18 column eluting with MeCN/H<sub>2</sub>O containing 0.1% formic acid.

**General five-component condensation reaction procedure.** Representative procedure for **ethyl 1,3,6-trimethyl-2-oxo-1,2,3,4-tetrahydropyrimidine-5-carboxylate (1-1A)** and **diethyl (4aSR,8aRS)-1,3,7,8a-tetramethyl-2-oxo-1,3,4,8a-tetrahydro-2H-pyrano[2,3-d]pyrimidine-4a,6(5H)-dicarboxylate (1-1B)**. A solution of ethyl acetoacetate (1.21 mL, 9.43 mmol, 2.5 equiv), paraformaldehyde (0.478 g, 15.3 mmol, 5 equiv), and N,N'-dimethylurea (0.456 g, 5.07 mmol, 1 equiv) in 95% ethanol (25 mL) was stirred at room temperature for 10 min. Indium(III) bromide (0.180 g, 0.507 mmol, 0.1 equiv) was added and the reaction mixture was heated under reflux for 7 h, cooled to room temperature, filtered through basic Al<sub>2</sub>O<sub>3</sub> (EtOAc) and concentrated under reduced pressure. The residue was purified by chromatography on SiO<sub>2</sub> (3:1 to 1:3,

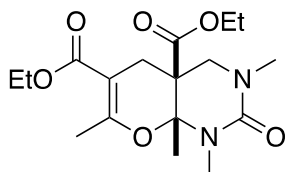


hexanes:EtOAc) to afford **1-1A** (0.481 g, 2.26 mmol, 45%) as a light-yellow wax and **1-1B** (0.855 g, 2.41 mmol, 48%) as a yellow oil. This procedure was followed for all products in Table 1-2 and Figure 1-6, and spectral properties are presented below.



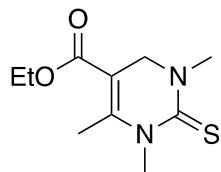
**1-1A**      **Ethyl 1,3,6-trimethyl-2-oxo-1,2,3,4-tetrahydropyrimidine-5-carboxylate (1-1A).**

IR (ATR, neat) 2981, 2908, 1673, 1623, 1414, 1262, 1204, 1077, 1027, 749  $\text{cm}^{-1}$ ;  $^1\text{H}$  NMR (400 MHz,  $\text{CD}_3\text{OD}$ )  $\delta$  4.16 (q,  $J = 7.1$  Hz, 2H), 4.01 (d,  $J = 1.1$  Hz, 2H), 3.17 (s, 3H), 2.92 (s, 3H), 2.46 (t,  $J = 1.3$  Hz, 3H), 1.28 (t,  $J = 7.1$  Hz, 3H);  $^{13}\text{C}$  NMR (100 MHz,  $\text{CD}_3\text{OD}$ )  $\delta$  165.9, 154.8, 150.8, 98.3, 59.8, 48.5, 34.2, 29.8, 14.8, 13.2; HRMS (HESI)  $m/z$  calcd for  $\text{C}_{10}\text{H}_{17}\text{N}_2\text{O}_3$   $[\text{M}+\text{H}]^+$  213.1234, found 213.1234.



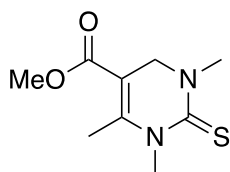
**1-1B**      **Diethyl (4aSR,8aRS)-1,3,7,8a-tetramethyl-2-oxo-1,3,4,8a-tetrahydro-2H-pyrano[2,3-d]pyrimidine-4a,6(5H)-dicarboxylate (1-1B).**

IR (ATR, neat) 2988, 2932, 1705, 1629, 1498, 1443, 1344, 1234, 1087, 1042, 984, 870, 844, 753  $\text{cm}^{-1}$ ;  $^1\text{H}$  NMR (400 MHz,  $\text{CD}_3\text{OD}$ )  $\delta$  4.22-4.14 (m, 4 H), 3.53 (d,  $J = 12.7$  Hz, 1H), 3.30 (d,  $J = 12.7$  Hz, 1H), 2.95 (s, 3H), 2.92 (s, 3H), 2.69 (dq,  $J = 17.8, 1.7$  Hz, 1H), 2.45 (dq,  $J = 17.8, 1.6$  Hz, 1H), 2.24 (t,  $J = 1.6$  Hz, 3H), 1.61 (s, 3H), 1.28 (t,  $J = 7.2$  Hz, 3H), 1.25 (t,  $J = 7.2$  Hz, 3H);  $^{13}\text{C}$  NMR (100 MHz,  $\text{CD}_3\text{OD}$ )  $\delta$  170.6, 167.2, 160.2, 154.9, 99.8, 87.8, 61.4, 59.9, 49.3, 44.0, 34.9, 27.6, 27.5, 19.5, 18.5, 13.5, 13.1; HRMS (HESI)  $m/z$  calcd for  $\text{C}_{17}\text{H}_{27}\text{N}_6\text{O}_2$   $[\text{M}+\text{H}]^+$  355.1864, found 355.1862.



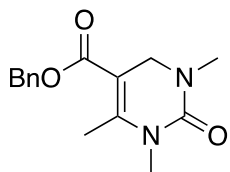
**1-2A Ethyl 1,3,6-trimethyl-2-thioxo-1,2,3,4-tetrahydropyrimidine-5-carboxylate**

**(1-2A).** IR (ATR, neat) 2978, 1670, 1636, 1525, 1443, 1357, 1267, 1208, 1169, 1141, 1088, 1016  $\text{cm}^{-1}$ ;  $^1\text{H}$  NMR (400 MHz,  $\text{CDCl}_3$ )  $\delta$  4.20 (q,  $J = 7.1$  Hz, 2H), 4.06 (q,  $J = 1.0$  Hz, 2H), 3.55 (s, 3H), 3.42 (s, 3H), 2.45 (t,  $J = 1.0$  Hz, 3H), 1.30 (t,  $J = 7.1$  Hz, 3H);  $^{13}\text{C}$  NMR (100 MHz,  $\text{CDCl}_3$ )  $\delta$  180.8, 165.3, 149.2, 101.3, 60.5, 47.9, 42.9, 37.9, 16.2, 14.3; HRMS (HESI)  $m/z$  calcd for  $\text{C}_{10}\text{H}_{17}\text{N}_2\text{O}_2\text{S}$   $[\text{M}+\text{H}]^+$  229.1005, found 229.1004.



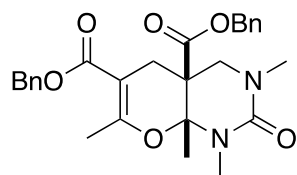
**1-3A Methyl 1,3,6-trimethyl-2-thioxo-1,2,3,4-tetrahydropyrimidine-5-carboxylate**

**(1-3A).** IR (ATR, neat) 2930, 2829, 1698, 1619, 1516, 1460, 1426, 1366, 1317, 1261, 1169, 1091, 991, 803, 765  $\text{cm}^{-1}$ ;  $^1\text{H}$ -NMR (400 MHz,  $\text{CDCl}_3$ )  $\delta$  4.09 (s, 2H), 3.77 (s, 3H), 3.58 (s, 3H), 3.45 (s, 3H), 2.48 (s, 3H);  $^{13}\text{C}$  NMR (100 MHz,  $\text{CDCl}_3$ )  $\delta$  180.8, 165.7, 149.6, 101.0, 51.6, 47.9, 42.9, 37.9, 16.3; HRMS (HESI)  $m/z$  calcd for  $\text{C}_9\text{H}_{15}\text{N}_2\text{O}_2\text{S}$   $[\text{M}+\text{H}]^+$  215.0849, found 215.0848.



**1-4A Benzyl 1,3,6-trimethyl-2-oxo-1,2,3,4-tetrahydropyrimidine-5-carboxylate**

**(1-4A).** IR (ATR) 2933, 1663, 1554, 1486, 1450, 1193, 1128, 1077, 1027, 692  $\text{cm}^{-1}$ ;  $^1\text{H}$ -NMR (300 MHz,  $\text{CD}_3\text{OD}$ )  $\delta$  7.37-7.34 (m, 5H), 5.17 (s, 2H), 4.04 (bd,  $J = 1.2$  Hz, 2H), 3.17 (s, 3H), 2.91 (s, 3H), 2.47 (t,  $J = 1.2$  Hz, 3H);  $^{13}\text{C}$  NMR (75 MHz,  $\text{CDCl}_3$ )  $\delta$  180.8, 165.0, 149.9, 136.0, 128.6, 128.3, 128.1, 101.8, 66.3, 47.9, 42.9, 37.9, 16.4; HRMS (HESI)  $m/z$  calcd for  $\text{C}_{15}\text{H}_{19}\text{N}_2\text{O}_3$   $[\text{M}+\text{H}]^+$  275.1390, found 275.1388.

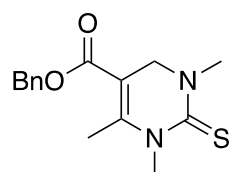


**1-4B**

**Dibenzyl**

**(4aSR,8aRS)-1,3,7,8a-tetramethyl-2-oxo-1,3,4,8a-**

**tetrahydro-2H-pyrano[2,3-d]pyrimidine-4a,6(5H)-dicarboxylate (1-4B).** IR (ATR, neat) 2937, 2882, 1713, 1629, 1506, 1448, 1379, 1348, 1232, 1077, 982, 884, 757  $\text{cm}^{-1}$ ;  $^1\text{H}$  NMR (300 MHz,  $\text{CD}_3\text{OD}$ )  $\delta$  7.35-7.32 (m, 10H), 5.17 (d,  $J = 16.4$  Hz, 2H), 5.15 (s, 2H), 3.54 (d,  $J = 12.9$  Hz, 1H), 3.27 (d,  $J = 12.9$  Hz, 1H), 2.90 (s, 3H), 2.84 (s, 3H), 2.73 (dq,  $J = 17.8, 1.6$  Hz, 1H), 2.48 (dq,  $J = 17.8, 1.6$  Hz, 1H), 2.20 (t,  $J = 1.6$  Hz, 3H), 1.54 (s, 3H);  $^{13}\text{C}$  NMR (100 MHz,  $\text{CDCl}_3$ )  $\delta$  170.6, 167.0, 161.2, 154.1, 136.2, 135.0, 128.6, 128.5 (2C), 128.1 (2C), 128.0, 99.6, 87.6, 67.3, 66.0, 49.7, 44.1, 35.7, 28.1, 27.8, 20.7, 19.7; HRMS (HESI)  $m/z$  calcd for  $\text{C}_{27}\text{H}_{31}\text{N}_2\text{O}_6$   $[\text{M}+\text{H}]^+$  479.2177, found 479.2176.

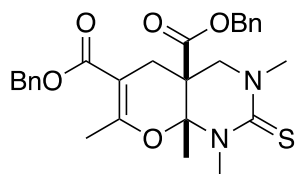


**1-5A**

**Benzyl**

**1,3,6-trimethyl-2-thioxo-1,2,3,4-tetrahydropyrimidine-5-**

**carboxylate (1-5A).** IR (ATR, neat) 2934, 1713, 1629, 1450, 1359, 1254, 1215, 1163, 1094, 1066, 1029, 734  $\text{cm}^{-1}$ ;  $^1\text{H}$ -NMR (600 MHz,  $\text{CDCl}_3$ )  $\delta$  7.39-7.32 (m, 5H), 5.19 (s, 2H), 4.08 (d,  $J = 1.0$  Hz, 2H), 3.55 (s, 3H), 3.41 (s, 3H), 2.47 (d,  $J = 1.0$  Hz, 3H);  $^{13}\text{C}$  NMR (150 MHz,  $\text{CDCl}_3$ )  $\delta$  180.8, 165.0, 149.9, 136.0, 128.6, 128.30, 128.17, 100.9, 66.3, 47.9, 43.0, 38.0, 16.4; HRMS (HESI)  $m/z$  calcd for  $\text{C}_{15}\text{H}_{19}\text{N}_2\text{O}_2\text{S}$   $[\text{M}+\text{H}]^+$  291.1162, found 291.1160.



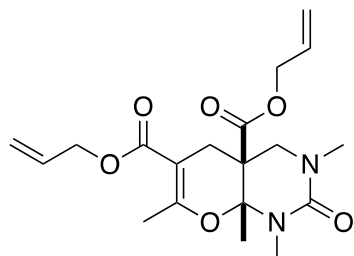
**1-5B**

**Dibenzyl**

**(4aSR,8aRS)-1,3,7,8a-tetramethyl-2-thioxo-1,3,4,8a-**

**tetrahydro-2H-pyrano[2,3-d]pyrimidine-4a,6(5H)-dicarboxylate (1-5B).** IR (ATR, neat) 2934, 1713, 1629, 1450, 1340, 1232, 1215, 1077, 1003, 995, 734, 695  $\text{cm}^{-1}$ ;  $^1\text{H}$  NMR (300 MHz,  $\text{CDCl}_3$ )  $\delta$  7.35-7.32 (m, 10H), 5.19-5.08 (m, 4 H), 3.79 (d,  $J = 13.6$  Hz, 1H), 3.39 (s, 3H), 3.34 (s, 3H), 3.31

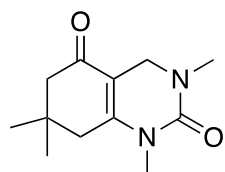
(d,  $J = 13.5$  Hz, 1H), 2.63 (dd,  $J = 17.8, 1.5$  Hz, 1H), 2.36 (dd,  $J = 17.8, 1.5$  Hz, 1H), 2.23 (t,  $J = 1.5$  Hz, 3H), 1.51 (s, 3H);  $^{13}\text{C}$  NMR (100 MHz,  $\text{CD}_3\text{OD}$ )  $\delta$  178.3, 169.0, 166.8, 160.1, 136.4, 135.4, 128.3, 128.2 (2C), 128.1 (2C), 128.0, 127.9 (2C), 127.8, 101.1, 86.5, 68.0, 67.1, 65.7, 51.5, 43.1, 42.7, 34.1, 26.0, 20.2, 18.1, 13.9; HRMS (HESI)  $m/z$  calcd for  $\text{C}_{27}\text{H}_{31}\text{N}_2\text{O}_5\text{S}$   $[\text{M}+\text{H}]^+$  495.1948, found 495.1945.



**1-6B**

**Diallyl(4aSR,8aRS)-1,3,7,8a-tetramethyl-2-oxo-1,3,4,8a-**

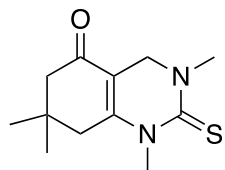
**tetrahydro-2H-pyrano[2,3-d]pyrimidine-4a,6(5H)- dicarboxylate (1-6B).** IR (ATR, neat) 2934, 1728, 1709, 1646, 1500, 1445, 1410, 1345, 1234, 1214, 1102, 1082, 1040, 987, 882, 754  $\text{cm}^{-1}$ ;  $^1\text{H}$  NMR (400 MHz,  $\text{DMSO}-d_6$ )  $\delta$  6.00–5.84 (m, 2H), 5.32–5.21 (m, 4H), 4.61 (dd,  $J = 16.0, 4.0$  Hz, 4H), 3.51 (d,  $J = 12.4$  Hz, 1H), 3.22 (d,  $J = 12.4$  Hz, 1H), 2.80 (s, 3H), 2.68 (s, 3H), 2.66 (d,  $J = 17.6$  Hz, 1H), 2.40 (d,  $J = 17.6$  Hz, 1H), 2.20 (s, 3H), 1.52 (s, 3H);  $^{13}\text{C}$  NMR (100 MHz,  $\text{DMSO}-d_6$ )  $\delta$  170.5, 166.6, 160.6, 153.8, 133.5, 132.5, 118.1, 118.0, 99.9, 88.1, 65.8, 64.7, 49.3, 44.2, 35.7, 28.3, 27.7, 20.7, 19.7; HRMS (HESI)  $m/z$  calcd for  $\text{C}_{19}\text{H}_{27}\text{N}_2\text{O}_6$   $[\text{M}+\text{H}]^+$  379.1864, found 379.1862.



**1-7A**

**1,3,7,7-Tetramethyl-4,6,7,8-tetrahydroquinazoline-2,5(1H,3H)-dione (1-**

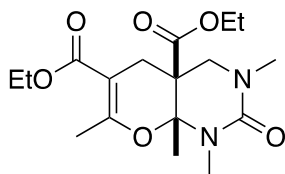
**7A).** IR (ATR, neat) 2960, 2890, 1722, 1620, 1574, 1438, 1381, 1268, 1224, 1127, 1080, 1007  $\text{cm}^{-1}$ ;  $^1\text{H}$  NMR (400 MHz,  $\text{CDCl}_3$ )  $\delta$  4.04 (s, 2H), 3.20 (s, 3H), 2.98 (s, 3H), 2.39 (s, 2H), 2.24 (s, 2H), 1.11 (s, 6H);  $^{13}\text{C}$  NMR (100 MHz,  $\text{CDCl}_3$ )  $\delta$  194.3, 153.5, 153.2, 105.6, 49.2, 45.6, 40.2, 35.8, 32.8, 30.4, 28.6; HRMS (HESI)  $m/z$  calcd for  $\text{C}_{12}\text{H}_{19}\text{N}_2\text{O}_2$   $[\text{M}+\text{H}]^+$  223.1441, found 223.1440.



**1-8A**      **1,3,7,7-Tetramethyl-2-thioxo-2,3,4,6,7,8-hexahydroquinazolin-5(1H)-one**

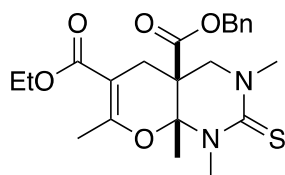
**(1-8A).** IR (ATR, neat) 2950, 2922, 2869, 1724, 1629, 1450, 1262, 1215, 1128, 1064, 982  $\text{cm}^{-1}$ ;  $^1\text{H}$  NMR (400 MHz,  $\text{CDCl}_3$ )  $\delta$  4.12 (s, 2H), 3.60 (s, 3H), 3.44 (s, 3H), 2.43 (s, 2H), 2.26 (s, 2H), 1.11 (s, 6H);  $^{13}\text{C}$  NMR (100 MHz,  $\text{CDCl}_3$ )  $\delta$  194.6, 180.1, 151.0, 107.4, 49.3, 45.8, 43.8, 40.6, 37.4, 33.1, 28.6; HRMS (HESI)  $m/z$  calcd for  $\text{C}_{12}\text{H}_{19}\text{N}_2\text{OS}$   $[\text{M}+\text{H}]^+$  239.1213, found 239.1211.

**Diels-Alder reaction of DHPM intermediate to form five-component condensation product.**



**1-1B**      **Diethyl (4aSR,8aRS)-1,3,7,8a-tetramethyl-2-oxo-1,3,4,8a-tetrahydro-**

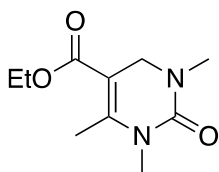
**2H-pyrano[2,3-d]pyrimidine-4a,6(5H)-dicarboxylate (1-1B).** Ethyl 1,3,6-trimethyl-2-oxo-1,2,3,4-tetrahydropyrimidine-5-carboxylate (**1-1A**, 0.096 g, 0.45 mmol) was added to ethyl 2-methylene-3-oxobutanoate containing residual sulfolane (0.244 g, 1.72 mmol). The reaction mixture was stirred at room temperature for 18 h and then concentrated under reduced pressure. The residue was purified by chromatography on  $\text{SiO}_2$  with gradient elution (4:1 to 1:1, hexanes:EtOAc) to afford **1-1B** (0.0682 g, 0.192 mmol, 11%) as a yellow oil that was spectroscopically identical to **1-1B** previously obtained in the one-pot Biginelli-Diels-Alder reaction.



**1-9B**

**4a-Benzyl 6-ethyl (4a*SR*,8a*RS*)-1,3,7,8a-tetramethyl-2-thioxo-1,3,4,8a-tetrahydro-2*H*-pyrano[2,3-*d*]pyrimidine-4a,6(5*H*)-dicarboxylate (1-9B).** Benzyl 1,3,6-trimethyl-2-thioxo-1,2,3,4-tetrahydropyrimidine-5-carboxylate (**1-5A**, 0.043 g, 0.15 mmol) was added to ethyl 2-methylene-3-oxobutanoate containing residual sulfolane (0.021 g, 0.15 mmol). The mixture was stirred at room temperature for 18 h. Another 5 equiv of ethyl 2-methylene-3-oxobutanoate containing residual sulfolane (0.105 g, 0.738 mmol) was added and the reaction mixture was stirred at room temperature for an additional 48 h. The mixture was concentrated under reduced pressure and the resulting residue was purified by chromatography on SiO<sub>2</sub> (4:1 to 2:1, hexanes:EtOAc) to afford **1-9B** (0.0113 g, 0.0261 mmol, 18%) as a yellow oil: IR (ATR, neat) 2975, 2934, 1705, 1644, 1525, 1450, 1340, 1232, 1077, 734, 701 cm<sup>-1</sup>; <sup>1</sup>H NMR (400 MHz, CDCl<sub>3</sub>) δ 7.34-7.25 (m, 5H), 5.13 (d, *J* = 12.0 Hz, 2H), 4.19-4.08 (m, 2H), 3.78 (d, *J* = 13.6 Hz, 1H), 3.38 (s, 3H), 3.32-3.28 (m, 4H), 2.60-2.55 (m, 1H), 2.35-2.29 (m, 1H), 2.20 (t, *J* = 1.6 Hz, 3H), 1.48 (s, 3H), 1.27-1.23 (m, 3H); <sup>13</sup>C NMR (100 MHz, CDCl<sub>3</sub>): δ 178.5, 170.0, 166.9, 159.6, 134.9, 128.7, 128.6, 128.1, 101.3, 86.1, 67.6, 61.7, 60.3, 52.2, 43.9, 43.1, 34.9, 21.5, 19.2, 14.3, 14.0; HRMS (HESI) *m/z* calcd for C<sub>22</sub>H<sub>29</sub>N<sub>2</sub>O<sub>5</sub>S [M+H]<sup>+</sup> 433.1792, found 433.1788.

#### Conversion of five-component condensation product to DHPM under Krapcho conditions.

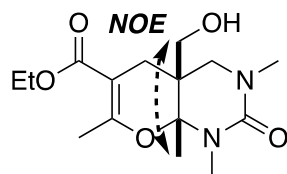


**1-1A**

**Ethyl 1,3,6-trimethyl-2-oxo-1,2,3,4-tetrahydropyrimidine-5-carboxylate (1-1A).** A mixture of diethyl (4a*SR*,8a*RS*)-1,3,7,8a-tetramethyl-2-oxo-1,3,4,8a-tetrahydro-2*H*-pyrano[2,3-*d*]pyrimidine-4a,6(5*H*)-dicarboxylate (**1-1B**, 0.050 g, 0.14 mmol), LiCl (0.016 g, 0.37 mmol), DMSO (2 mL), and water (4 drops) was heated at 160 °C and the reaction was monitored by TLC analysis (2:1, hexanes:EtOAc). After 4 h, the reaction mixture was cooled to room temperature and extracted with EtOAc. The organic layer was dried (MgSO<sub>4</sub>), filtered,

and concentrated to yield ethyl 1,3,6-trimethyl-2-oxo-1,2,3,4-tetrahydropyrimidine-5-carboxylate (**1-1A**, 0.026 g, 0.12 mmol, 87%) as a light-yellow oil that was spectroscopically identical to **1-1A** previously obtained in the one-pot Biginelli-Diels-Alder reaction.

#### Structural confirmation by conversion to alcohol.



**1-10**

**Ethyl (4aRS,8aRS)-4a-(hydroxymethyl)-1,3,7,8a-tetramethyl-2-oxo-**

**1,3,4,4a,5,8a-hexahydro-2H-pyrano[2,3-*d*]pyrimidine-6-carboxylate (1-10).** A mixture of 4 M LiBH<sub>4</sub> in THF (0.16 mL, 0.63 mmol) and diethyl (4aSR,8aRS)-1,3,7,8a-tetramethyl-2-oxo-1,3,4,8a-tetrahydro-2H-pyrano[2,3-*d*]pyrimidine-4a,6(5H)-dicarboxylate (**1-1B**, 150 mg, 0.42 mmol) in Et<sub>2</sub>O (2.1 mL) was heated at 35 °C for 3 h. The reaction was monitored by TLC analysis (1:2, hexanes:EtOAc). After 3 h, the reaction mixture was quenched with 1 M HCl with ice-cooling. The solution was diluted with water and extracted with CH<sub>2</sub>Cl<sub>2</sub> (3x5mL). The organic layer was dried (MgSO<sub>4</sub>), filtered, and concentrated under reduced pressure to yield **1-10** (0.0794 g, 0.254 mmol, 60%) as white solid: Mp 114.8 - 116.9 °C; IR (ATR, neat) 3367, 2924, 1702, 1622, 1507, 1445, 1407, 1378, 1347, 1291, 1250, 1159, 1110, 985, 885, 839, 754 cm<sup>-1</sup>; <sup>1</sup>H NMR (400 MHz, DMSO) δ 5.01 (t, *J* = 5.4 Hz, 1H), 4.08 (q, *J* = 7.2 Hz, 2H), 3.42 (dd, *J* = 10.8, 5.2 Hz, 1H), 3.27 (dd, *J* = 10.8, 5.2 Hz, 1H), 3.12 (d, *J* = 12.0 Hz, 1H), 2.94 (d, *J* = 12.0 Hz, 1H), 2.81 (s, 3H), 2.80 (s, 3H), 2.32 (brd d, *J* = 16.4 Hz, 1H), 2.15 (s, 3H), 2.13 (brd d, *J* = 16.4 Hz, 1H), 1.37 (s, 3H), 1.21 (t, *J* = 7.2 Hz, 3H); <sup>13</sup>C NMR (100 MHz, DMSO) δ 167.6, 159.9, 154.3, 100.0, 89.9, 62.1, 59.9, 48.7, 37.6, 35.9, 28.1, 27.1, 19.8, 19.7, 14.8; HRMS (HESI) *m/z* calcd for C<sub>15</sub>H<sub>25</sub>N<sub>2</sub>O<sub>5</sub> [M+H]<sup>+</sup> 313.1758, found 313.1759.

## 2.0 A Pilot-Plant Synthesis of Gefitinib

### 2.1 Introduction

#### 2.1.1 Background and Early Syntheses

Gefitinib (Iressa®) is a small molecule tyrosine kinase inhibitor (TKI) of the epidermal growth factor receptor (EGFR) originally developed by AstraZeneca.<sup>62</sup> The drug was approved in 2015 by the Food and Drug Administration (FDA) as a first-line treatment for metastatic non-small cell lung cancer (NSCLC) with EGFR mutations, specifically exon 19 deletion or exon 21 substitution mutation.<sup>63</sup> Gefitinib was actually the first EGFR-TKI approved by the FDA for NSCLC in 2003 but, at the time, the specific target patient population was not known so the compound was recommended as a third-line treatment only after chemotherapy failure. It is taken orally, once-daily, as a 250 mg tablet.<sup>64</sup> In 2017 the market share was estimated at \$136 million in the European Union (EU). Gefitinib came off patent in the EU in 2019 and Sandoz, a division of Novartis, and Lotus Chemicals, a division of Alvogen, both received approval for their generic versions in 13 EU countries. Currently, no “therapeutically equivalent” version of Gefitinib is available in the United States.

Worldwide, lung cancer is the most prevalent fatal cancer for both men and women. In NSCLC, mutation of the EGFR tyrosine kinase domain destabilizes the kinase conformation and affects downstream signaling pathways.<sup>65</sup> These disruptions stimulate cancer cell proliferation and inhibit apoptosis. Gefitinib reversibly binds to the ATP-site of the EGFR kinase domain to inhibit autophosphorylation and signal transduction thus stopping the growth and spread of tumors.<sup>66</sup>

Four molecules have been approved for treatment of NSCLC with EGFR mutations (Figure 2-1). A quinazoline makes up the core structure of Gefitinib, Erlotinib, and Afatinib. Osimertinib, possessing a pyrimidine and 1-methylindole, was also produced by AstraZeneca specifically to target a T790M mutation.<sup>67</sup>



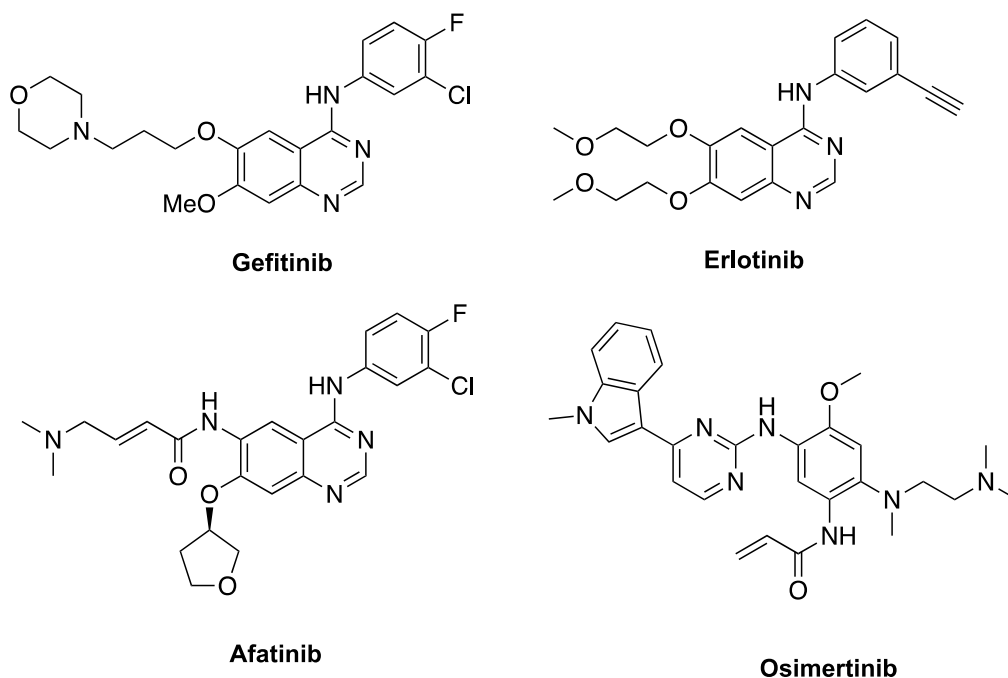
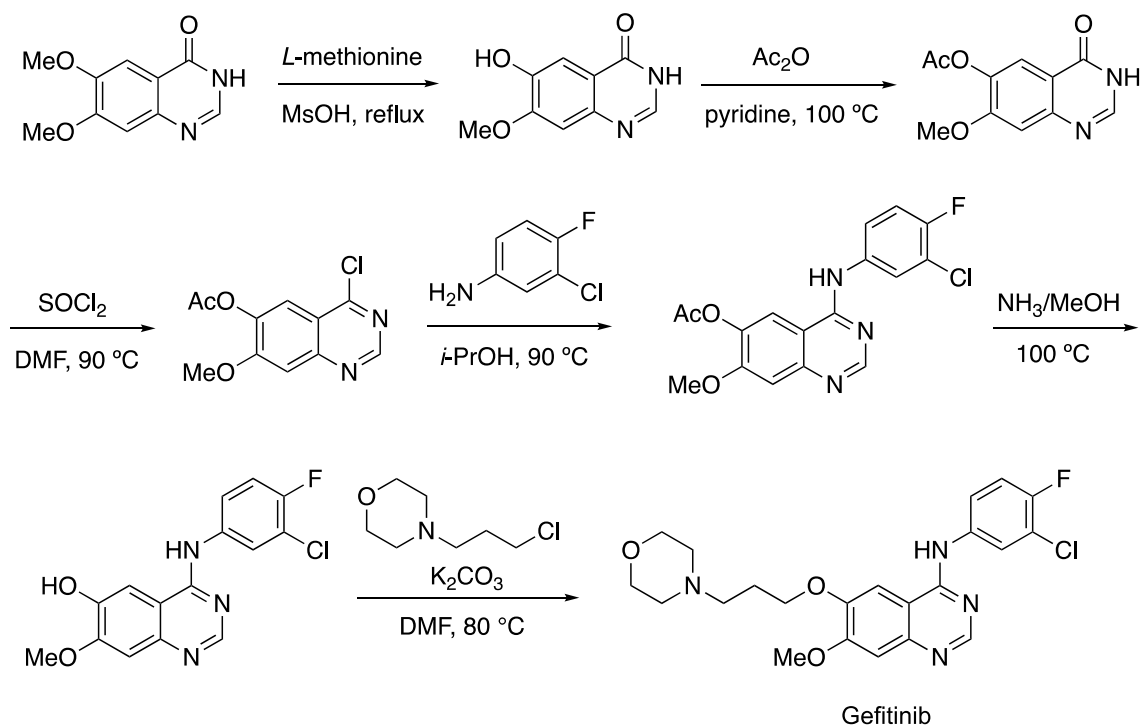


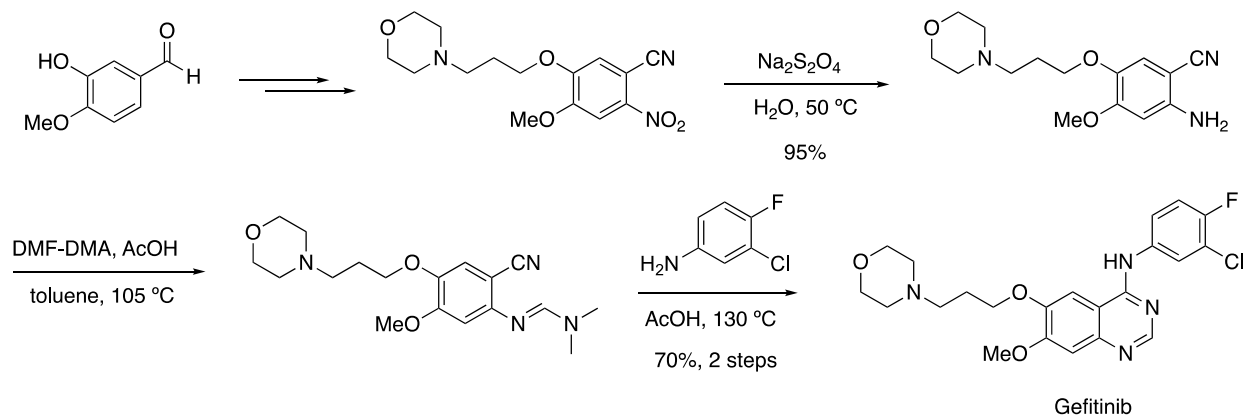
**Figure 2-1 Drugs approved to treat NSCLC with EGFR mutations**

Several syntheses of Gefitinib have been described in the literature. AstraZeneca's original synthesis began with the demethylation of 6,7-dimethoxyquinazoline-4-one with *L*-methionine and methanesulfonic acid, followed by acetylation, halogenation, aniline S<sub>N</sub>Ar, deacetylation, and *O*-alkylation (Scheme 2-1).<sup>68</sup> This six-step synthesis (10% overall yield) required chromatographic purifications and utilized hazardous reagents, such as thionyl chloride, which reacts violently with water to produce toxic sulfur dioxide and also contaminates the air very quickly upon evaporation at 20 °C.



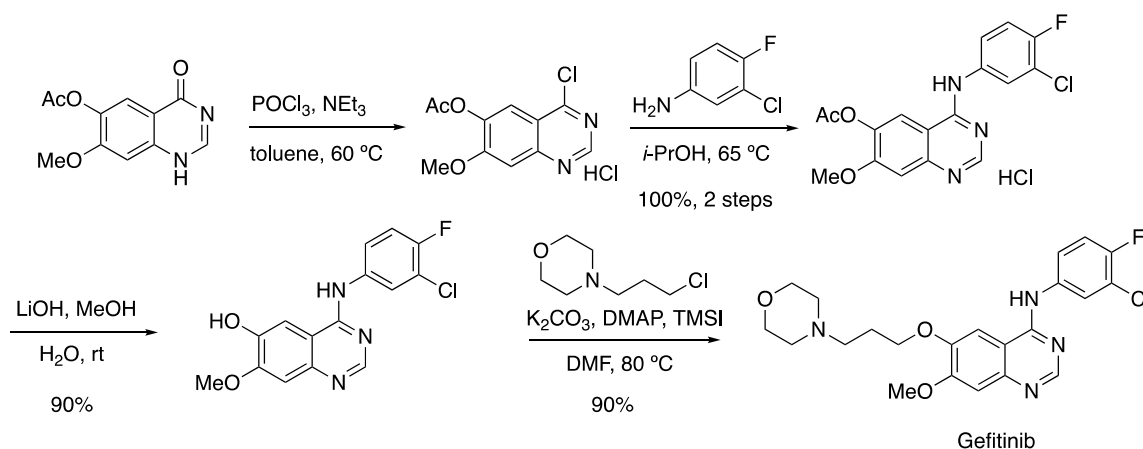
**Scheme 2-1 AstraZeneca synthesis of Gefitinib<sup>68</sup>**

In 2007, Reddy et al. reported a synthesis of Gefitinib from isovanillin (Scheme 2-2).<sup>69</sup> The nitro group in the isovanillin-derived intermediate was reduced with sodium dithionite, followed by treatment with dimethylformamide-dimethylacetal (DMF-DMA) and amination with 3-chloro-4-fluoroaniline to yield the API. No chromatography was required, but high reaction temperatures were needed and DMF was used in large quantities in the seven-step synthesis.



**Scheme 2-2 Reddy et al. synthesis of Gefitinib<sup>69</sup>**

More recently, Suh et al. disclosed a variant of the AstraZeneca synthesis utilizing a transient protective group strategy (Scheme 2-3).<sup>70</sup> An acetylated quinazoline core was subjected to a chlorination with POCl<sub>3</sub>, substitution with 3-chloro-4-fluoroaniline, and deprotection with LiOH, which set the stage for alkylation with 4-(3-chloropropyl)morpholine utilizing TMSI to transiently protect the aniline nitrogen. While high yielding, this synthetic route required hazardous TMSI and a more elaborate starting material. It also utilized phosphoryl chloride, which reacts violently with water to produce toxic gases and is highly corrosive.



**Scheme 2-3 Suh et al. synthesis of Gefitinib<sup>70</sup>**

At this time we were contacted by a pharmaceutical company interested in a novel synthesis of Gefitinib that could eventually be translated to a process-plant. For the synthesis we envisioned a new route to Gefitinib with fewer than five steps from inexpensive starting materials that would avoid hazardous reagents and chromatographic separations and keep reaction temperatures in the 0-60 °C range. Such a process would be commercially relevant and potentially attractive for pharmaceutical manufacturing.

### 2.1.2 Synthesis of Gefitinib from 2,4-Dichloroquinazoline<sup>71-72</sup>

We chose the commercially available 2,4-dichloro-6,7-dimethoxyquinazoline (**2-1**) as the starting material (Scheme 2-4). To the best of our knowledge, a synthesis of Gefitinib or related analogs that utilizes a 2,4-dichloroquinazoline as a starting material or advanced intermediate is

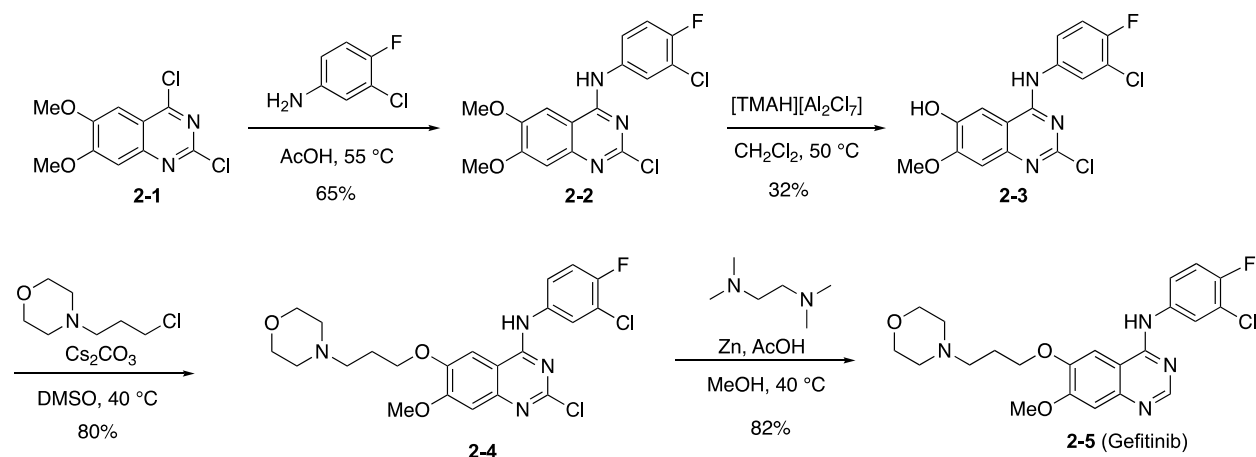
unprecedented. Dichloroquinazoline **2-1** was reacted with 3-chloro-4-fluoroaniline in 20.4 equiv of acetic acid at 55 °C for 2 h to yield the coupling product **2-2** after extraction and filtration with EtOAc. Under these conditions, we were able to exclusively isolate the desired 4-position aminated product **2-2** in 65% yield on a 5 g scale. Based on the large volumes of EtOAc and 2 M NaOH required for extraction, we were not able to run a single batch of this reaction on a scale larger than 5 g. Efficient stirring was also a concern with the standard glassware that was readily available.

The ensuing selective demethylation of **2-2** proved challenging and a variety of conditions were attempted to try and improve the ratio of demethylated isomers while not compromising the overall yield. It was important that, no matter the crude ratio, we would be able to obtain phenol **2-3** in high selectivity through crystallization. Eventually we came across a protocol for the cleavage of methyl esters through ionic liquid (IL) reagents.<sup>73-74</sup> Our IL was synthesized *in situ* from aluminum trichloride and trimethylammonium hydrochloride in dichloromethane and was directly used for the demethylation step in a one-pot protocol. With intermediate **2-2**, we found that treatment with [TMAH][Al<sub>2</sub>Cl<sub>7</sub>] at 50 °C for 2 h provided a 1.1-1.3 to 1 ratio of mono-demethylated regioisomers, but that a favorable ratio of >95:5 of the desired product could readily be obtained in 30-35% yield without chromatography after crystallization of the concentrated reaction mixture from hot methanol. While not required for the next step, a second crystallization increased the regioisomeric purity to >99%. Once again, we were limited to a 5 g scale with this reaction due to stirring problems with the glassware at hand and also the large volumes of 2 M HCl required during the workup.

For the alkylation of **2-3** we found that 4-(3-chloropropyl)morpholine in the presence of cesium carbonate in DMSO at 40 °C for 2.5 h provided ether **2-4** in 80% yield after filtration and crystallization in hot methanol. While this was a more concentrated reaction requiring less solvent, we were limited to a 1 g scale on this reaction based on the preceding steps scale limitations and overall yields.

The final dehalogenation step also took considerable optimization but we eventually found that 15 equiv of zinc dust, 10 equiv of *N,N,N',N'*-tetramethylethylenediamine (TMEDA) in a mixture of MeOH and AcOH provided exclusively the desired dehalogenation of **2-4**. After stirring the reaction mixture at 40 °C for 24 h, 15 equiv of 2-mercaptonicotinic acid was added to assist in the removal of excess zinc and zinc salts.<sup>75</sup> Ultimately, we were able to crystallize the product with

hot MeOH to provide Gefitinib (**2-5**) as colorless crystals in 82% yield with >99% purity by LCMS analysis on a 1 g scale (Scheme 2-4).



**Scheme 2-4 A 2,4-dichloroquinazoline as a new starting material for Gefitinib preparation**<sup>71-72</sup>

## 2.2 Results and Discussion

With the route established, we wanted to explore the feasibility of performing the sequence on a scale that would be more applicable to an industrial setting. The concept of a pilot-plant was described by Frank Vilbrant in *Industrial & Engineering Chemistry* in 1945.<sup>76</sup> A pilot-plant serves to translate a concept into a commercially feasible, practical working plan. Chemists devising a future process route may readily avoid hazardous reagents and solvents but they fail to consider numerous important variables including: 1. just how endothermic or exothermic a reaction will be on scale and how to control the temperature; 2. how an amorphous reaction mixture is best mixed; and 3. if an extraction is really feasible based on the amount and identity of solvent required. A pilot-plant is intermediary between the benchtop and a process-plant. One of the key aspects of a pilot-plant is that it is flexible and that chemists operating in the pilot-plant can quickly make changes based on real time observations and challenges. This is what we set out to do with our benchtop Gefitinib synthesis; to not only run the reaction sequence on a larger scale but to think critically and problem solve during each individual step.

For our pilot-plant scale synthesis we first considered our choice of reaction vessel. Most steps in the reaction sequence are performed at a relatively high concentration, particularly step 1 at 1.8 M and step 3 at 0.6 M. However, the large volumes of solvents required for work-up and extraction made the sequence difficult to execute in most standard glassware. With conventional glassware we were successful with the SNAr reaction and demethylation reaction on only a 5 g scale and the alkylation and final dehalogenation on 1 g scale. When a larger scale was attempted, particularly in step 1, we experienced a dramatic reduction in yields and in most cases were unable to isolate clean product. We hypothesized that two reasons for this were the inability to consistently and efficiently heat and cool reaction mixtures and also limitations with stirring. We addressed both of these concerns by purchasing a jacketed 2-L reactor (Figure 2-2). The reactor was compatible with a dual recirculating heater/chiller with a temperature range of -20 °C to 100 °C. The recirculating heater/chiller allowed better maintenance of temperature on larger scales both during the actual reaction and during the often exothermic work-up protocols. Additionally, with the jacketed reactor an overhead stirrer capable of reaching 1000 rpm could be utilized. With high speeds and the proper blade, efficient stirring was possible on >10 g scales. The reactor also had multiple ports for an addition funnel, N<sub>2</sub> stream, and internal temperature probe.

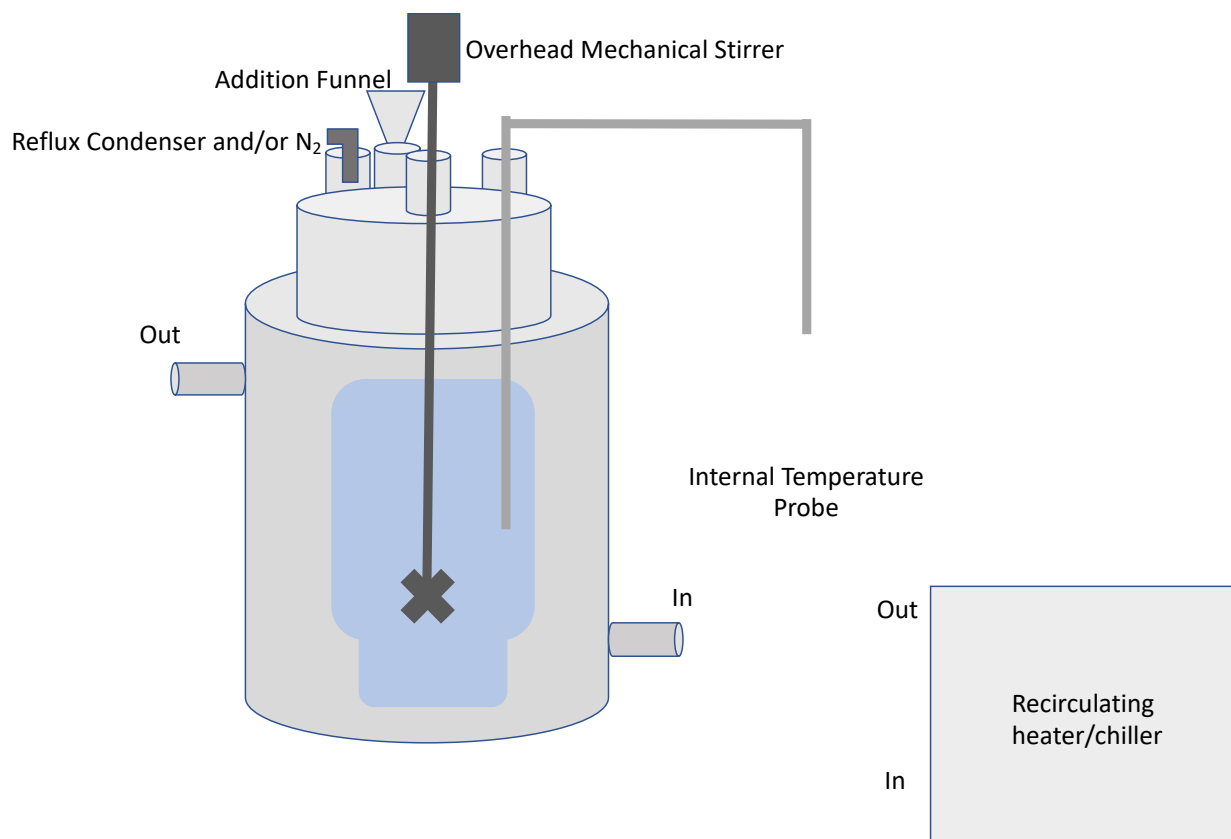


**Figure 2-2 2-L Jacketed reactor design**

First, we turned our attention to the SNAr reaction. We had repeated success carrying out this reaction on a 5 g scale; however, when we attempted to scale up the reaction to 10 g we experienced many problems. The profile of this reaction is unique. If quinazoline **2-1** is too soluble in the volume of acetic acid, there are many side products. If quinazoline **2-1** is not soluble enough, mixing is insufficient and there is no reaction. Through screening, we determined that the reaction worked best at a 1.8 M concentration in acetic acid. At this concentration the reaction mixture is very viscous and stirs for ~30 min before solidifying. During the remaining 1.5 h of reaction time, pockets of unreacted starting material are seemingly consumed. Initially, when scaling this reaction from 5 g to 10 g, sufficient mixing was never achieved; the presence of starting material and side products made purification difficult.

We believed that the 2-L jacketed reactor with specialized overhead stirrer capable of reaching 1000 rpm would allow us to scale this reaction beyond 5 g. We decided to perform the reaction on a 75 g scale as this would allow a sufficient volume of acetic acid (332 mL) for

mechanical stirring. Gratifyingly, at 315 rpm we observed homogenous mixing for the first 30 min. After 30 min, there was partial solidification but some mixing (30 rpm) was maintained. The paddle shape of the stirring rod was important for this; it pulled the mixture in instead of pushing the reaction mixture out towards the edges of the reactor, something that was not possible when performing the reaction in standard glassware. After 2 h, the reaction appeared much more uniform compared to previous trials.

With the goal of demonstrating that this reaction could be performed on a process scale, we made modifications to the work up procedure that would reduce solvent volumes and thus required process reactor sizes. Previously, the product was extracted in a separatory funnel with EtOAc (0.5 L) and 2 M NaOH (275 mL). If this procedure was applied to a 75 g reaction, 7.5 L of EtOAc and 4.1 L of 2 M NaOH would be required. These volumes coupled with the use of a separatory funnel were not practical on this scale. Accordingly, we decided to carry out the extraction in the reactor and switch to dichloromethane and 6 M NaOH for the extraction solvents. After cooling to 0 °C, CH<sub>2</sub>Cl<sub>2</sub> (300 mL) and 6 M NaOH (800 mL) were added and the resulting mixture was stirred vigorously (400 rpm). Based on density, the top (aqueous) layer was siphoned off and the process was repeated with additional 2 M NaOH (200 mL). After the extraction was complete, the organic layer was transferred to a fritted funnel, the filter cake collected, and the solids recrystallized from methanol (500 mL). With this protocol, **2-2** was successfully obtained in 87% yield (91 g, 247 mmol) as a ca. 90% pure colorless solid with a similar purity profile to the 5 g scale reactions.

Throughout the reaction sequence, the first step was a major obstacle. We had a difficult time generating sufficient material to optimize the subsequent steps. The scale limitations of the first step decreased the attractiveness of the route for manufacturing companies. With the 2-L jacketed reactor and protocol modifications, we were able to increase the yield to 87% while reducing overall solvent use to: CH<sub>2</sub>Cl<sub>2</sub> (500 mL), 6 M NaOH (800 mL), 2 M NaOH (200 mL), MeOH (600 mL) on a 75 g scale (Table 2-1).



**Table 2-1 Pilot-plant optimizations of step 1 – SNAr reaction**

	5-g Reaction	75-g Reaction
Reaction Vessel	Round bottom flask	2-L jacketed reactor
Stirring Method	Magnetic stirring	Overhead stirring (315 rpm)
Heating Mechanism	Ceramic heating block	Recirculating heater/chiller
Cooling Mechanism	Ice bath	Recirculating heater/chiller
Extraction Vessel	Separatory funnel	2-L jacketed reactor
Extraction Solvent	EtOAc and 2 M NaOH	CH <sub>2</sub> Cl <sub>2</sub> and 6 M NaOH

With the success obtained with the 2-L jacketed reactor in the first step, we decided to also try the second, demethylation step in the reactor. Like the first step, the demethylation step was previously limited to a 5 g scale. The most important aspect of this reaction is the work up. The demethylation is catalyzed by the ionic liquid [TMAH][Al<sub>2</sub>Cl<sub>7</sub>]. The work up procedure functions to break up the aluminum complexes. If the particle size is too large, crystallization of the desired phenol regioisomer in high selectivity is difficult. On a 5 g scale, 2 M HCl (200 mL) was added at a controlled rate to break up the complexes. However, this addition was very exothermic and in standard glassware it was difficult to sufficiently cool the resulting suspension and ensure that the internal temperature did not rise above 20 °C.

We initially targeted an 18 g reaction in the reactor. The ionic liquid [TMAH][Al<sub>2</sub>Cl<sub>7</sub>] was synthesized directly in the 2-L jacketed reactor. The dual recirculating heater/chiller allowed for the addition of aluminum chloride and trimethylammonium chloride at 0 °C and then warming to rt once addition was complete. After 2 h, intermediate **3-2** was added through one of the three addition ports at the top of the reactor. These addition ports allowed for the reaction to be kept under N<sub>2</sub>, use of a reflux condenser as needed, and also use of an addition funnel when required. Once the reaction was complete, the dual recirculating heater/chiller enabled efficient cooling of the reactor from 50 °C to 0 °C. An internal thermometer indicated that the recirculating chiller was effective in maintaining the desired temperature. The 18 g reaction required 900 mL of 2 M HCl. Vigorous stirring (410 rpm) was maintained and 2 M HCl was added through an addition funnel, initially dropwise. The recirculating chiller maintained complete control of the exothermic addition; the temperature did not rise above 10 °C during the addition. Once the pH was <1, the

mixture was transferred to a fritted funnel and the filter cake was collected, concentrated by rotary evaporation, and crystallized from methanol two times to provide the desired isomer **2-3** in 43% yield (7.65 g, 20.5 mmol) with ~95% purity (Table 2-2).

The demethylation, step 2 of the reaction, proved to be the lowest yielding step of the sequence. In our experience, it was important to carry on intermediate **2-3** with high purity (<10% undesired phenol isomer) in order to have success in the alkylation and dechlorination steps. With the 2-L jacketed reactor, we were able to efficiently heat/cool the reaction mixture while more than tripling our scale and increase the yield to ~40% while maintaining the overall purity of intermediate **2-3**.

**Table 2-2 Pilot-plant optimizations of step 2 – Demethylation reaction**

	5-g Reaction	18.4-g Reaction
Reaction Vessel	Round bottom flask	2-L jacketed reactor
Stirring Method	Mechanical stirring	Overhead stirring (310 rpm)
Heating Mechanism	Ceramic heating block	Recirculating heater/chiller
Cooling Mechanism	Ice bath	Recirculating heater/chiller
Extraction Vessel	Separatory funnel	2-L jacketed reactor

With the material obtained from step 2 in the 2-L jacketed reactor, we attempted the alkylation step on larger scale. Our major limitations in this step had been a lack of material, thus the largest successful scale this reaction was performed was a 1 g scale. Step 3 is relatively concentrated (0.6 M), so on a 4.4 g scale, the 2-L reactor was not required. Intermediate **2-3** (4.38 g), cesium carbonate (8.14 g), and 4-(3-chloropropyl)morpholine (2.12 mL) were dissolved in DMSO (35 mL) in a 250 mL round bottom flask. Minimum changes were made from the 1 g scale work-up protocol as the volume of the extraction solvents was <650 mL; a 1-L separatory funnel could be used. After extraction, concentration, and crystallization in MeOH, intermediate **2-4** was obtained in 37% yield (2.18 g, 4.53 mmol) (Table 2-3).

This yield was significantly lower than the 80% yield obtained on a 1 g scale. There was still room for optimization on this step. We hypothesized that there was oxidation of phenol **2-3** which, when stirred in MeOH, resulted in the loss of the quinazoline Cl and subsequent attack by methanol to form the methyl isourea at the 2-position (Figure 2-3). This could be avoided by

running the reaction under an N<sub>2</sub> atmosphere. Accordingly, we repeated the reaction on a 1.8 g theoretical yield scale and kept the mixture under an N<sub>2</sub> atmosphere until work-up/extraction. We also used degassed solvents during the extraction. With these modifications, **2-4** was obtained in 70% yield. It was evident that the N<sub>2</sub> atmosphere was critical as the reaction remained a light brown color and did not turn black like the previous trial.

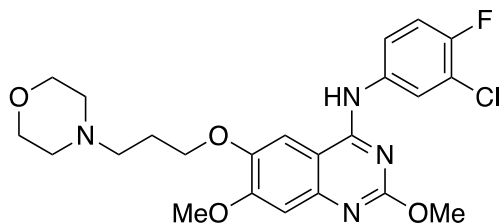


**Figure 2-3 Proposed oxidation side product**

**Table 2-3 Pilot-plant optimizations of step 3 – Alkylation reaction**

	1-g Reaction	4.3-g Reaction
Reaction Vessel	Round bottom flask	Round bottom flask
Stirring Method	Conventional stirring	Conventional stirring
Heating Mechanism	Ceramic heating block	Ceramic heating block
Extraction Vessel	Separatory funnel (500 mL)	Separatory funnel (1 L)

Finally, we attempted to double our scale for the final, dechlorination step of the sequence. The dechlorination step was the step we had the least experience with, so we were interested to see how scalable it was. In scaling from 1 g to 2 g, we altered the ratios of zinc dust and 2-mercaptonicotinic acid used. We did not believe the full 15 equiv of zinc dust and 2-mercaptonicotinic acid were required for the reaction and that using less of these reagents, particularly zinc dust, would make this step more amenable to a process scale. Accordingly, to intermediate **2-4**, zinc dust (10 equiv), TMEDA (10 equiv), and acetic acid (20 equiv) were added and after stirring for 24 h at 40 °C, 2-mercaptonicotinic acid (5 equiv) was added to help complex and remove the zinc. After extraction, concentration, and crystallization from methanol, **2-5** (Gefitinib) was obtained in 75% yield (1.51 g, 3.38 mmol) (Table 2-4).

On a 2 g scale, we successfully reduced the amount of zinc dust and 2-mercaptionicotinic acid used while maintaining the >70% yield and high purity of the final API **2-5**.

**Table 2-4 Pilot-plant optimizations of step 4 – Dechlorination reaction**

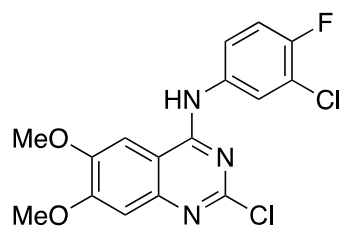
	1-g Reaction	2.2-g Reaction
Reaction Vessel	Round bottom flask	Round bottom flask
Stirring Method	Conventional stirring	Conventional stirring
Heating Mechanism	Ceramic heating block	Ceramic heating block
Zinc equivalents	15	10
2-Mercaptionicotinic acid equivalents	15	5

## 2.3 Conclusions

We have successfully demonstrated that our Gefitinib synthesis route can be carried out on a pilot-plant scale. With the use of a 2-L jacketed reactor, recirculating heater/chiller, overhead mechanical stirrer capable of spin speeds up to 1000 rpm, and modifications to extraction solvents and volumes and reagent equivalents, we were able to conduct all reaction steps on a larger scale: SNAr reaction - 75 g, demethylation reaction – 18 g, alkylation reaction – 4.3 g, dechlorination reaction – 2.2 g. In the future, the alkylation step should be carried out on a >4 g scale, under an inert N<sub>2</sub> atmosphere, to confirm our hypothesis for the formation of oxidation side products. Once the yield is improved on this step, the final dechlorination reaction can be carried out on a >5 g scale.

## 2.4 Experimental Procedures

**General.** All reagents and solvents were used as received unless otherwise specified. CH<sub>2</sub>Cl<sub>2</sub> was distilled over CaH<sub>2</sub>. Reactions were monitored by TLC analysis (pre-coated silica gel 60 F254 plates, 250  $\mu$ m layer thickness) and visualization was accomplished with a 254/280 nm UV light and/or by staining with KMnO<sub>4</sub> solution (1.5 g KMnO<sub>4</sub> and 1.5 g K<sub>2</sub>CO<sub>3</sub> in 100 mL of a 0.1% NaOH solution), a ninhydrin solution (2 g ninhydrin in 100 mL EtOH), a PMA solution (5 g phosphomolybdic acid in 100 mL EtOH), or a *p*-anisaldehyde solution (2.5 mL *p*-anisaldehyde, 2 mL AcOH and 3.5 mL conc. H<sub>2</sub>SO<sub>4</sub> in 100 mL EtOH). Melting points were determined on a Mel-Temp II capillary melting point apparatus fitted with a Fluke 51 II digital thermometer. Infrared spectra were recorded on a Perkin Elmer Spectrum 100 FTIR spectrometer. NMR spectra were recorded on a Bruker Avance 400 MHz instrument. Chemical shifts were reported in parts per million (ppm) and referenced to residual solvent. <sup>1</sup>H NMR spectra are tabulated as follows: chemical shift, multiplicity (br = broad, s = singlet, d = doublet, t = triplet, q = quartet, m = multiplet, brd s = broad singlet, dd = doublet of doublets, app t = apparent triplet), coupling constant(s), number of protons. <sup>13</sup>C NMR spectra were obtained using a proton-decoupled pulse sequence and are tabulated by observed peak. <sup>19</sup>F NMR spectra were obtained using a proton-decoupled pulse sequence. HRMS data were obtained on a Thermo Scientific Exactive Orbitrap LC-MS (ESI positive ion mode) coupled to a Thermo Scientific Accela HPLC system using a 2.5  $\mu$ M Waters XBridge C18 column (2.1 x 50 mm; 10 min gradient elution with MeCN/H<sub>2</sub>O/ MeOH containing 0.1% formic acid at a flow rate of 500  $\mu$ L/min from 3:92:5 at 0-0.5 min to 93:2:5 at 4.0 min, back to 3:92:5 from 6.0 to 7.5 min). Where applicable, both an internal and external thermometer were utilized to maintain accurate temperature control.



**2-2**

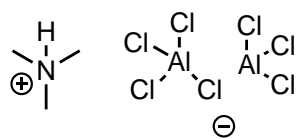
**2-Chloro-N-(3-chloro-4-fluorophenyl)-6,7-dimethoxyquinazolin-4-**

**amine (2-2).** In a jacketed 2-L reactor, a vigorously mechanically stirred (315 rpm), pale pink, homogeneous solution of 3-chloro-4-fluoroaniline (46.4 g, 312 mmol, 1.1 equiv) in acetic acid (332 mL, 5787 mmol, 20.4 equiv) was treated at 45 °C with neat 2,4-dichloro-6,7-dimethoxyquinazoline (75.0 g, 283 mmol) in three portions. The temperature was monitored with an internal digital thermometer probe. After the addition was complete (1 min), the resulting mixture was warmed to 55 °C for a total of 2 h. The pink solution turned golden yellow and viscous and solids precipitated after about 15 min. After 30 min, the stirring speed was decreased (30 rpm). TLC analysis (5% MeOH:CH<sub>2</sub>Cl<sub>2</sub>; product R<sub>f</sub>=0.2) after 2 h showed that the aniline and quinazoline starting materials were consumed and the product had formed. The heterogeneous pinkish brown reaction slurry was cooled to 0 °C, diluted with CH<sub>2</sub>Cl<sub>2</sub> (300 mL), and 6 M NaOH (800 mL) was added over 1 h (5 mL/min for the first 150 mL and 15 mL/min afterwards) under vigorous stirring (215-400 rpm). The aqueous layer (top, pH 14) was siphoned off, additional 2 M NaOH (200 mL) was added to the organic layer (pH 7 before addition of 2 M NaOH). The biphasic mixture was stirred vigorously (400 rpm) to generate a slurry with small particle size. The aqueous layer (top) was siphoned off again, and the organic layer was transferred onto the top of a fritted funnel. Liquids were filtered off under aspirator vacuum. The filter cake was washed with CH<sub>2</sub>Cl<sub>2</sub> (200 mL) and dried under reduced pressure to yield a first batch of product (133 g) that was mostly brown but retained some pink clumps. <sup>19</sup>F NMR indicated >85% product (ratio of product to side products, 10:1:1.5).

The combined aqueous layers can be back-extracted with CH<sub>2</sub>Cl<sub>2</sub> (2 x 200 mL). The resulting organic layers were combined, dried (Na<sub>2</sub>SO<sub>4</sub>), filtered, and concentrated to yield a light brown residue (25.2 g). This residue was dissolved in MeOH (45 mL) and allowed to precipitate at rt for 3 h. The precipitate was filtered, washed with MeOH (30 mL), and concentrated under reduced pressure to provide additional product (6.6 g).

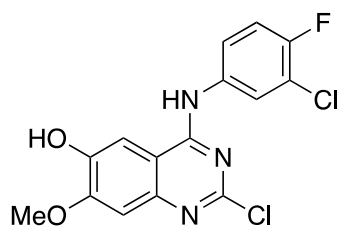
The combined solids (139 g) were dissolved in MeOH (500 mL) and vigorously magnetically stirred at reflux for 30 min. The suspension was allowed to cool at rt for 3 h and

transferred to a fritted funnel. The filter cake was washed with cold (0 °C) MeOH (3 x 30 mL), and dried under reduced pressure to provide **2-2** (91 g, 247 mmol, 87%) as a ca. 90% pure colorless solid ( $^{19}\text{F}$  NMR indicated a product to side products ratio of 20:1:2) that was used for step 2 without further purification: TLC 5% MeOH/ $\text{CH}_2\text{Cl}_2$   $R_f$ =0.2; Mp 271.5-273.9 °C; IR (ATR, neat) 3392, 1664, 1624, 1608, 1572, 1497, 1430, 1137, 1207, 1144, 997, 963, 845, 795, 695;  $^1\text{H}$  NMR (DMSO- $d_6$ , 400 MHz)  $\delta$  9.92 (s, 1H), 8.01 (dd,  $J$  = 6.8, 2.4 Hz, 1 H), 7.83 (s, 1 H), 7.77-7.73 (m, 1 H), 7.50 (app t,  $J$  = 8.8, Hz, 1 H), 71.9 (s, 1 H), 3.95 (s, 3 H), 3.93 (s, 3 H);  $^{13}\text{C}$  NMR (DMSO- $d_6$ , 400 MHz)  $\delta$  158.2, 155.6, 154.4, 149.6, 148.7, 136.3, 124.7, 123.5, 123.4, 117.3, 117.1, 107.6, 107.2, 102.5, 56.8, 56.5;  $^{19}\text{F}$  NMR (376 MHz, DMSO- $d_6$ )  $\delta$  -121.9; HRMS (LCMS ESI+)  $m/z$  calcd for  $\text{C}_{16}\text{H}_{13}\text{Cl}_2\text{FN}_3\text{O}_2$  [M+H] 368.0363, found 368.0364.



**[TMAH][Al<sub>2</sub>Cl<sub>7</sub>]**. A suspension of aluminum chloride (51.6 g, 383 mmol)

in  $\text{CH}_2\text{Cl}_2$  (500 mL) was cooled to 0 °C for 10 min in a 2-L reactor and then treated with trimethylammonium chloride (18.7 g, 192 mmol) under  $\text{N}_2$  atmosphere. Upon addition of trimethylammonium chloride, the reaction mixture changed from a yellow to a golden-brown color. After addition was complete, the reaction mixture was warmed to 23 °C and allowed to stir via mechanical stirring at 72 rpm for 2 h. This mixture (69.4 g in 500 mL  $\text{CH}_2\text{Cl}_2$ ) was used in the subsequent reaction without further purification or concentration.



**2-3**

**2-Chloro-4-((3-chloro-4-fluorophenyl)amino)-7-**

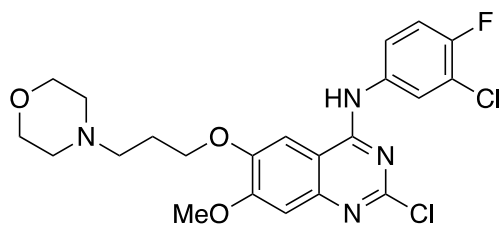
**methoxyquinazolin-6-ol (2-3)**. In a jacketed 2-L reactor, a suspension of 2-chloro-N-(3-chloro-4-fluorophenyl)-6,7-dimethoxyquinazolin-4-amine (18.4 g, 50.0 mmol) in  $\text{CH}_2\text{Cl}_2$  (100 mL) was added in 6 portions to a freshly prepared solution of the ionic liquid [TMAH][Al<sub>2</sub>Cl<sub>7</sub>] (69.4 g, 191 mmol, 3.8 equiv, in 500 mL  $\text{CH}_2\text{Cl}_2$ ) under  $\text{N}_2$  atmosphere. Additional  $\text{CH}_2\text{Cl}_2$  (25 mL) was used

as a wash. The golden yellow-brown reaction mixture was mechanically stirred (250 rpm) and heated for 2.5 h at 50 °C. After 2.5 h, the suspension was cooled to 0 °C (over 0.5 h), and 2M HCl (~900 mL) was added through an addition funnel at the top of the reactor, drop-wise for the first 125 mL, and subsequently at a rate of 20.0 mL/min over 40 min while the rapidly forming suspension was stirred vigorously (410 rpm). The internal temperature of the solution was maintained below 10 °C. After complete addition of 2M HCl, the resulting mixture was transferred to a fritted funnel (5 L) with filter paper and the solid/filter cake was collected. The collected filter cake was washed with water (200 mL) and briefly dried by vacuum filtration to give ~350 g of a viscous residue which was transferred into a round bottom flask and concentrated by rotary evaporation until a slurry of 90 g was obtained. This residue was then suspended in hot MeOH (450 mL), heated to reflux for 30 min, and allowed to cool and precipitate for 12 h; 4 h while stirring was maintained and 8 h once stirring was stopped. The sticky solid was collected by filtration, washed with MeOH (250 mL), and suspended in hot methanol (500 mL), and allowed to precipitate for 20 h. The solid was collected by filtration, washed with MeOH (60 mL), and dried in vacuo (0.5 Torr, 20 °C) to provide a first batch of product (5.85 g).

The filtrate was concentrated, suspended in hot MeOH (150 mL), heated to reflux for 30 min, and allowed to cool and precipitate for 5 h while stirring was maintained. The solid was collected by filtration, washed with MeOH (40 mL), and dried in vacuo (0.5 Torr, 20 °C) to provide a second batch of product (1.8 g).

Total, **2-3** (7.65 g, 20.5 mmol, 43%) was obtained as a >95% pure off-white solid: TLC (5% MeOH:CH<sub>2</sub>Cl<sub>2</sub>) R<sub>f</sub>= 0.4; Mp 348.2-349.6 °C; IR (ATR, neat) 2941, 1631, 1541, 1499, 1458, 1337, 1303, 1262, 1226, 1080, 1062, 1009, 864, 826, 743, 694; <sup>1</sup>H NMR (400 MHz, DMSO-*d*<sub>6</sub>) δ 9.86 (s, 1 H), 8.09 (dd, *J* = 6.8, 2.8 Hz, 1 H), 7.80-7.76 (m, 2 H), 7.46 (appt t, *J* = 9.2 Hz, 1 H), 7.20 (s, 1 H), 3.97 (s, 3 H); <sup>13</sup>C NMR (400 MHz, DMSO-*d*<sub>6</sub>) δ 158.1, 155.2, 153.6, 152.8, 147.5, 136.6, 124.2, 123.0, 119.4, 119.2, 117.2, 117.0, 108.3, 106.3, 56.6; <sup>19</sup>F NMR (376 MHz, DMSO-*d*<sub>6</sub>) δ -122.3; HRMS (LCMS ESI+) *m/z* calcd for C<sub>15</sub>H<sub>11</sub>Cl<sub>2</sub>FN<sub>3</sub>O<sub>2</sub> [M+H] 354.0207, found 354.0208.

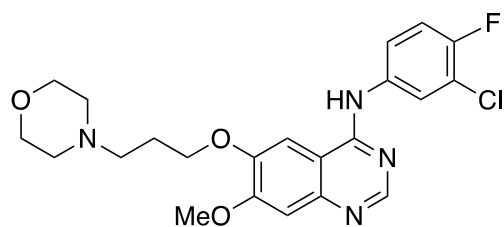




**2-4**

**2-Chloro-N-(3-chloro-4-fluorophenyl)-7-methoxy-6-(3-**

**morpholinopropoxy)-quinazolin-4-amine (2-4).** A solution of 2-chloro-4-((3-chloro-4-fluorophenyl)amino)-7-methoxy-quinazolin-6-ol (4.38 g, 12.4 mmol), 4-(3-chloropropyl)morpholine (2.12 mL, 13.6 mmol), and cesium carbonate (8.14 g, 24.7 mmol) in DMSO (35 mL) was stirred at 40 °C and monitored by TLC (2% MeOH/CH<sub>2</sub>Cl<sub>2</sub>; starting material R<sub>f</sub>=0.3; product R<sub>f</sub>=0.2). After 3 h, the mixture was cooled to rt, diluted with EtOAc (350 mL) and water (100 mL), and extracted. The organic layer was washed with sat. NaHCO<sub>3</sub> (2 x 85 mL), 1M LiCl (25 mL) and 2M NaOH (25 mL). The aqueous layer (pH 12) was then back-extracted with EtOAc (2 x 175 mL) and the combined organic layers were dried (Na<sub>2</sub>SO<sub>4</sub>, 55 g), filtered, rinsed with EtOAc (100 mL) and concentrated. The crude residue (7.3 g) was heated at reflux in MeOH (70 mL) for 10 min and then allowed to precipitate at rt for 5 h. The solids were collected by filtration, washed with MeOH (35 mL), and dried in vacuo (0.5 Torr, 20 °C) to afford **2-4** (2.18 g, 4.53 mmol, 37%) as a colorless solid: TLC (2% MeOH:CH<sub>2</sub>Cl<sub>2</sub>) R<sub>f</sub>= 0.2; Mp 216.2-218.9 °C; IR (ATR, neat) 3329, 2946, 2812, 1623, 1579, 1494, 1431, 1290, 1256, 1221, 1149, 1110, 1057, 1014, 961, 853, 798, 776, 736, 695; <sup>1</sup>H NMR (400 MHz, DMSO-*d*<sub>6</sub>) δ 9.92 (s, 1 H), 8.01 (dd, *J* = 6.8, 2.8 Hz, 1 H), 7.83 (s, 1 H), 7.76-7.72 (m, 1 H), 7.50 (app t, *J* = 9.2 Hz, 1 H), 7.19 (s, 1 H), 4.17 (t, *J* = 6.4 Hz, 1 H), 3.93 (s, 1 H), 3.58 (app t, *J* = 6.4 Hz, 1 H), 2.47-2.45 (m, 2 H), 2.38 (brd s, 4 H), 2.01-1.98 (m, 2 H); <sup>13</sup>C NMR (100 MHz, DMSO-*d*<sub>6</sub>) δ 158.2, 155.7, 154.4, 148.9, 148.6, 136.3, 124.8, 123.6, 123.5, 119.4, 117.3, 117.1, 107.6, 107.2, 103.3, 67.7, 66.6, 55.6, 55.4, 53.9, 26.3; <sup>19</sup>F NMR (376 MHz, DMSO-*d*<sub>6</sub>) δ -121.8; HRMS (LCMS ESI+) *m/z* calcd for C<sub>22</sub>H<sub>24</sub>Cl<sub>2</sub>FN<sub>4</sub>O<sub>3</sub> [M+H] 481.1204, found 481.1207.



**2-5** (Gefitinib)

***N*-(3-Chloro-4-fluorophenyl)-7-methoxy-6-(3-**

**morpholinopropoxy)quinazolin-4-amine (2-5, Gefitinib).**<sup>68</sup> To a suspension of zinc dust (2.96 g, 45.3 mmol, 10 equiv) and TMEDA (6.9 mL, 45 mmol, 10 equiv) in MeOH (110 mL) at 0 °C was added dropwise acetic acid (5.2 mL, 90.6 mmol, 20 equiv) followed by 2-chloro-*N*-(3-chloro-4-fluorophenyl)-7-methoxy-6-(3-morpholino-propoxy)-quinazolin-4-amine (2.18 g, 4.53 mmol). The temperature was monitored with an internal and external thermometer. The reaction mixture was heated at 40-45 °C for 24 h, cooled to rt, and diluted with MeOH (115 mL). To this solution was added 2-mercaptonicotinic acid (3.58 g, 22.6 mmol, 5 equiv). The suspension was vigorously stirred at rt for 30 min, diluted with MTBE (190 mL), and washed with 2 M NaOH (2 x 190 mL). The combined aqueous layers were back-extracted with MTBE (2 x 190 mL), and the combined organic layers were washed with sat. NaHCO<sub>3</sub> (190 mL), dried (Na<sub>2</sub>SO<sub>4</sub>, 65 g), filtered, and concentrated to give a white-yellow solid residue (7.25 g). The solid was dissolved in hot MeOH (55 mL) and allowed to crystallize for 3 h at rt. The colorless needles were collected by filtration, washed with MTBE (20 mL), and dried in vacuo (0.5 Torr, 20 °C) to provide a first batch of crystalline product (1.35 g). The mother liquor was concentrated (~30 mL) and allowed to crystallize overnight at rt. The resulting crystals were filtered and dried in vacuo (0.5 Torr, 20 °C) to provide a second batch of product (0.240 g) that was combined. The product was further dried in vacuo (0.5 Torr, 80 °C) for 24 h to provide (**2-5**, Gefitinib, Iressa®) as a colorless solid (1.51 g, 3.38 mmol, 75%): TLC 1:2:2, EtOH:EtOAc:Hex R<sub>f</sub>=0.2; Mp 195.2-197.3 °C; IR (ATR, neat) 3365, 3160, 1873, 2816, 1622, 1578, 1530, 1497, 1472, 1426, 1393, 1353, 1280, 1217, 1112, 1044, 993, 957, 850, 772 cm<sup>-1</sup>; <sup>1</sup>H NMR (400 MHz, DMSO-*d*<sub>6</sub>) δ 9.57 (s, 1 H), 8.50 (s, 1 H), 8.12 (dd, *J* = 6.8, 2.4 Hz, 1 H), 7.81-7.77 (m, 2 H), 7.45 (app t, *J* = 9.2 Hz, 1 H), 7.20 (s, 1 H), 4.18 (t, *J* = 6.4 Hz, 1 H), 3.94 (s, 3 H), 3.58 (app t, *J* = 4.4 Hz, 4 H), 2.48-2.46 (m, 2 H), 2.39 (brd s, 4 H), 2.03-1.96 (m, 2 H); <sup>13</sup>C NMR (100 MHz, DMSO-*d*<sub>6</sub>) δ 156.5, 155.0, 153.1, 148.8, 124.0, 122.9, 122.8, 117.1, 116.9, 109.2, 107.8, 103.0, 67.6, 66.6, 56.4, 55.4, 53.9, 26.3; <sup>19</sup>F NMR (376 MHz, DMSO-*d*<sub>6</sub>) δ -123.3; HRMS (LCMS ESI+) *m/z* calcd for C<sub>22</sub>H<sub>25</sub>ClFN<sub>4</sub>O<sub>3</sub> [M+H] 447.1594, found 447.1594.

### 3.0 Synthesis of JP4-039 Analogs Through a Vinylogous Mannich Reaction and Their In Vitro Activity as Ferroptosis Inhibitors

#### 3.1 Introduction

##### 3.1.1 Mitochondria Targeting Nitroxides and Their Therapeutic Indications

Our group has a great interest in mitochondria-targeting therapeutics. Our strategy is to use a mitochondrial-targeting moiety to deliver a potent payload across the membrane.<sup>77-79</sup> The mitochondrial-targeting fragment is designed based on gramicidin S (Figure 3-1), a cyclodecapeptide natural product combining natural and unnatural amino acids that has activity against Gram-positive and Gram-negative bacteria.<sup>80</sup>

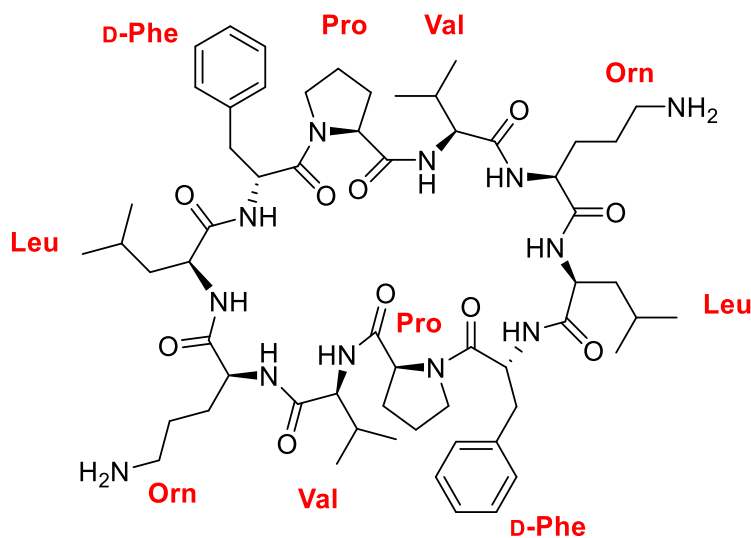
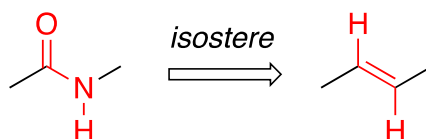


Figure 3-1 Structure of gramicidin S

Gramicidin S is amphipathic with an antiparallel  $\beta$ -sheet secondary structure that positions hydrophilic and hydrophobic amino acids on opposite sides of the molecule.<sup>80</sup> The biological

activity of gramicidin S derives from favorable interactions with cell membranes, however, as a single agent it has limited practical therapeutic value because of cytotoxic side effects such as hemolysis.<sup>81</sup> In our peptide mimics, we have replaced a polar, internal amide bond with an alkene dipeptide isostere (Figure 3-2).<sup>77-79, 82</sup> (*E*)-Alkene peptide isosters are innately rigid and, unlike amides, not susceptible to peptidase cleavage, thus increasing bioavailability.<sup>80</sup>



**Figure 3-2 (*E*)-alkene is an isostere of an amide**

We have utilized a nitroxide moiety, specifically 2,2,6,6-tetramethylpiperidin-*N*-oxyl (TEMPO) (Figure 3-3), as the payload in our design. Nitroxides are stable compounds that contain a nitroxyl moiety with an unpaired electron.<sup>83</sup> The most commonly utilized heterocyclic nitroxides have substitutions at each of the  $\alpha$ -carbons of the nitroxide to enhance stability.<sup>83</sup> 4-Hydroxy-TEMPO (TEMPOL) is one example of a simple nitroxide that has been shown to increase insulin responsiveness, provide protective effects in neurodegenerative models, and counteract oxidative stress (Figure 3-3).<sup>84</sup> Other nitroxide bearing compounds have shown efficacy in lung, breast, thyroid, and ovarian cancer.<sup>83</sup>

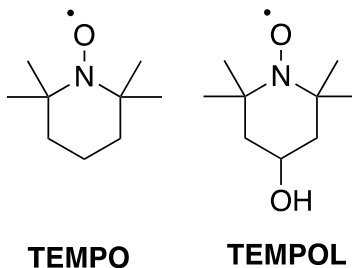


**Figure 3-3 Structures of TEMPO and TEMPOL**

Nitroxides act as radical-scavenging antioxidants.<sup>85</sup> An antioxidant is any compound that inhibits oxidation in the body.<sup>86</sup> Innate antioxidants to the body include ubiquinol (coenzyme Q),

glutathione (GSH) (Figure 3-4), and superoxide dismutase.<sup>87</sup> Vitamin C and vitamin E are examples of dietary antioxidants (Figure 3-4).<sup>87</sup>

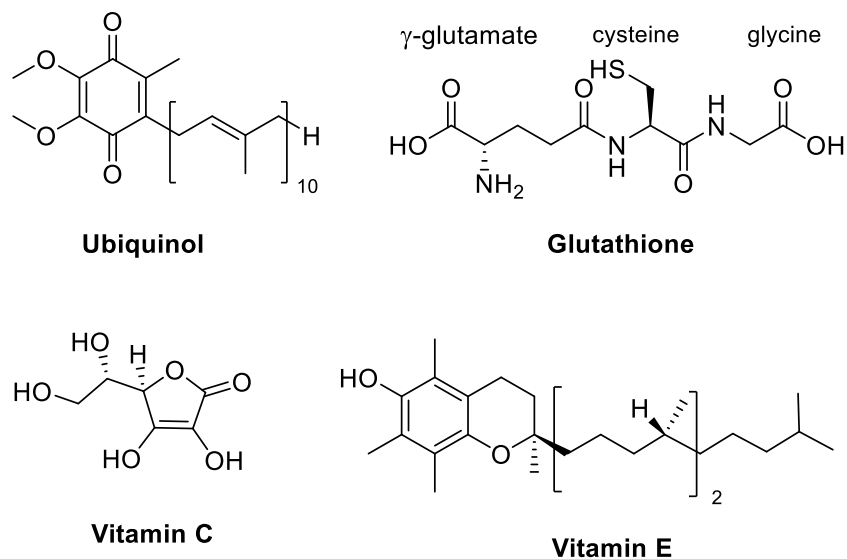


**Figure 3-4 Structure of natural and dietary antioxidants**

In the body, oxidation plays a critical role in cell signaling, the electron transport chain of the mitochondria, and a variety of other enzymatic and nonenzymatic reactions including the cytochrome P-450 system.<sup>88</sup> The majority of oxidation chemistry occurs in the mitochondria.<sup>89</sup> Reactive oxygen species (ROS) are a byproduct of these processes. The most common ROS are the superoxide anion ( $O_2^{\cdot-}$ ), hydrogen peroxide ( $H_2O_2$ ), hydroxyl radical ( $\cdot OH$ ), organic hydroperoxide ( $ROOH$ ), and alkoxy or peroxy radicals ( $RO\cdot$  or  $ROO\cdot$ ).<sup>87</sup> These species donate oxygen to other substances in the body. If the cell cannot properly break down these free radicals, oxidative stress occurs. Lipids, proteins, and DNA can be affected by oxidative stress driving age related diseases and cancers.<sup>90</sup> Nitroxides are able to quench ROS through a catalytic one- and two-electron redox cycle (Figure 3-5 A).<sup>84</sup> This process is reversible and occurs at physiological pH with rapid rate constants. Pratt and coworkers have proposed a redox cycle of nitroxides to quench peroxy radicals (Figure 3-5 B).<sup>91</sup> The catalytic redox cycle of nitroxides consists of electron transfer with peroxy radicals ( $ROO\cdot$ ) to form oxammonium ions. This species can undergo hydride transfer to form a hydroxylamine, and in turn regenerate the nitroxide.<sup>91</sup> Although they do not possess a nitroxide moiety, effective antioxidants such as vitamin E and liproxstatin-1

(Lip-1) are believed to proceed through a nitroxide moiety as part of their catalytic cycle supporting the general conception of nitroxide therapeutics.<sup>92</sup>

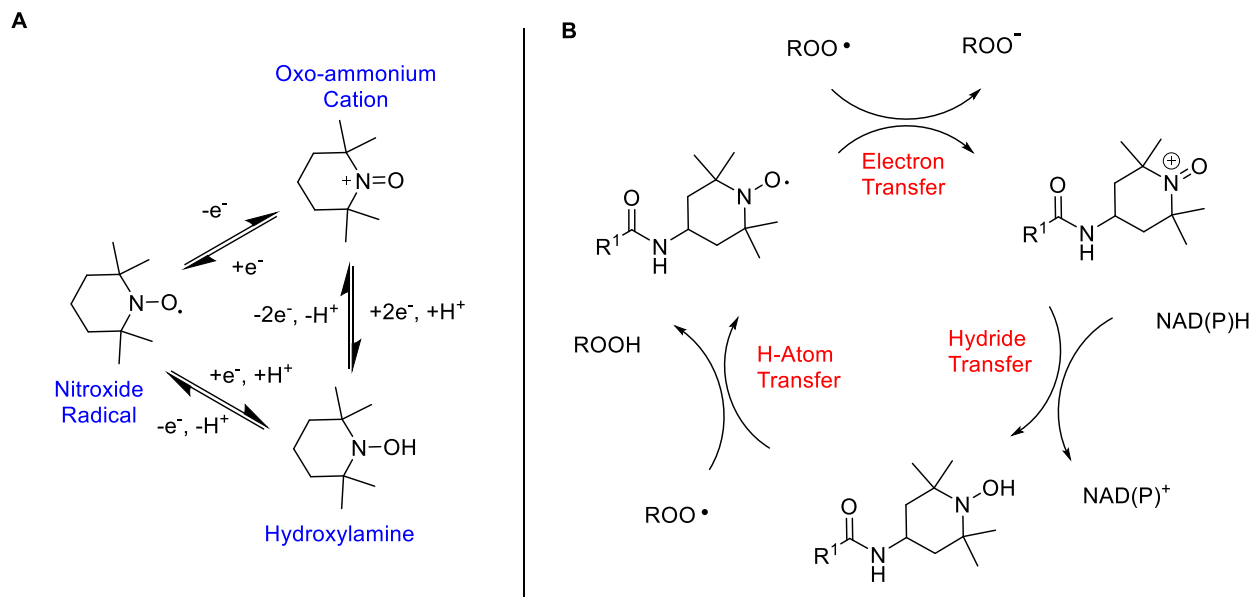
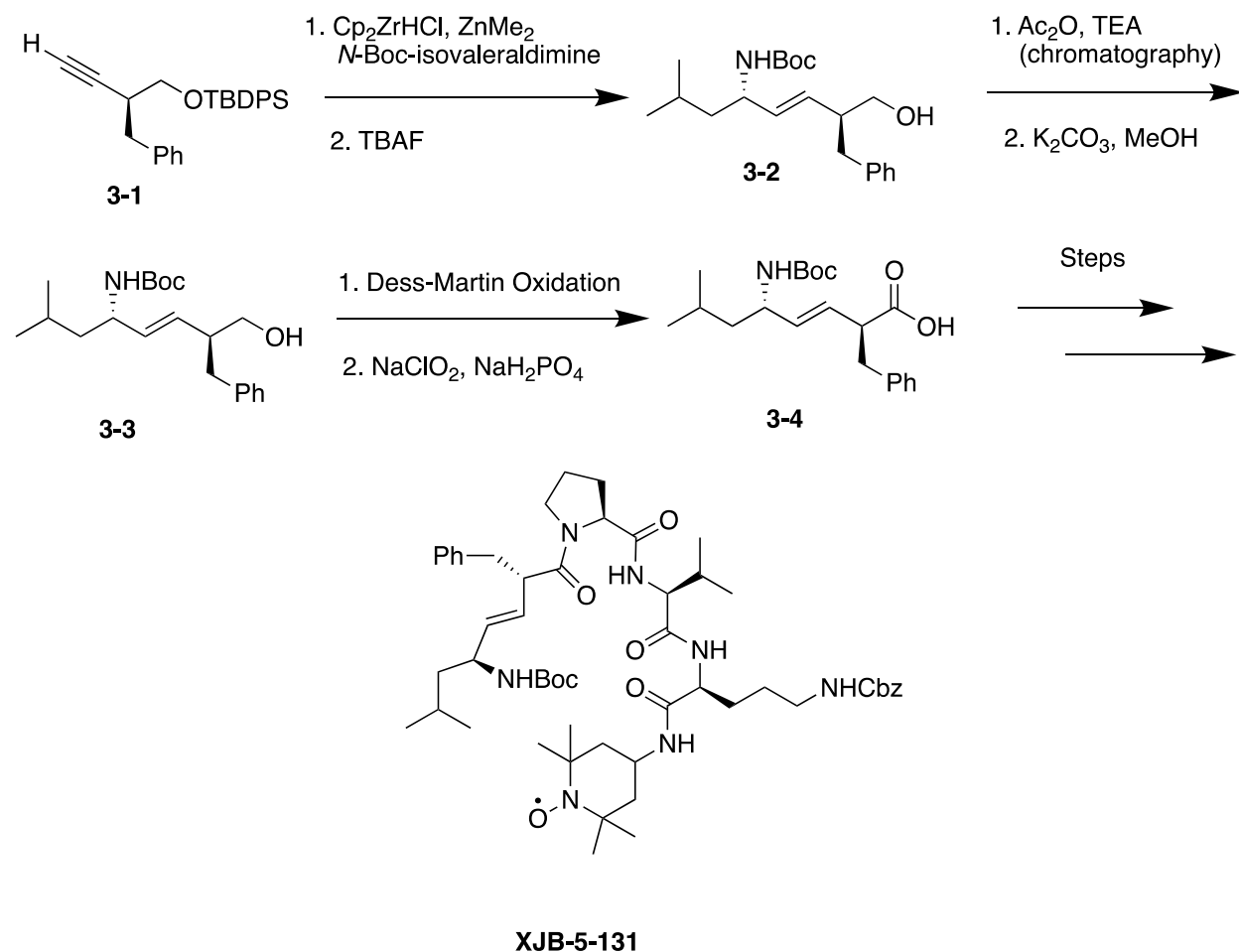


**Figure 3-5 A) TEMPO catalytic cycle B) Proposed nitroxide catalytic cycle to quench peroxy radicals<sup>91</sup>**

The first hemigramacidin-TEMPO conjugate therapeutics in our lab were developed through a 10-step synthesis sequence involving chromatographic resolution (Scheme 3-1).<sup>77</sup> (*S*)-((2-Benzylbut-3-yn-1-yl)oxy)(*tert*-butyl)diphenylsilane (**3-1**) was subjected to hydrozirconation and subsequent transmetallation to dimethylzinc followed by addition to *N*-Boc-isovaleraldimine to provide **3-2** as a mixture of diastereomers. The diastereomers were acylated, separated, and deprotected to provide **3-3** which then underwent a two-step oxidation procedure consisting of a Dess-Martin periodinane (DMP) oxidation to provide the aldehyde and a Pinnick oxidation to provide carboxylic acid **3-4**. This key intermediate was then coupled with tri-peptide *H*-Pro-Val-Orn(Cbz)-OMe and 4-amino-Tempo (4-AT) to provide the alkene isostere analog of gramicidin S, **XJB-5-131**. X-ray analysis confirmed the major diastereomer assignment.<sup>77</sup> This analog was characterized by quantitative mass spectrometry to preferentially locate to the mitochondria and protect cells against apoptosis.<sup>93</sup> The mitochondrial membrane has a unique negative potential, -180 mV, preferentially attracting cations; the resonance stabilized triphenylphosphonium ion is the most common mitochondrial targeting moiety for this reason.<sup>94</sup> XJB-5-131 can cross the

mitochondrial membrane in spite of the absence of a positive charge, through mechanisms that are not yet fully elucidated. Once inside the organelle, the nitroxide payload is able to scavenge for ROS and electrons escaping the oxidative phosphorylation process.<sup>78, 95</sup>



**Scheme 3-1** Synthesis of XJB-5-131<sup>77</sup>

In addition to efficiently locating to the mitochondria, these first analogs showed promise in bioassays of radiation, traumatic brain injury (TBI), hematopoietic syndrome, Huntington's disease, and in head and neck irradiation of Fanconi anemia models, among others.<sup>77, 96-98</sup> Promising biological activity lead to the desire to produce new analogs possessing superior potency and improved pharmacological properties. XJB-5-131 does not meet three out of four of Lipinski's rule of five to determine the drug-likeness of a chemical compound.<sup>99</sup> While XJB-5-131 has only 5 hydrogen bond donors, it has more than 10 hydrogen bond acceptors, a molecular

weight greater than 500, and an octanol-water partition coefficient (logP) greater than 5. Solubility and lipophilicity greatly limit the practicality of XJB-5-131 as a therapeutic. For analog development purposes, a new, more efficient route, was necessary to generate sufficient amounts of analogs with improved pharmacological properties for *in vitro* and possible *in vivo* testing. JP4-039, a smaller alkene dipeptide isostere composed of leucine and glycine residues, was synthesized in large quantity during this second campaign (Figure 3-6).<sup>79</sup>

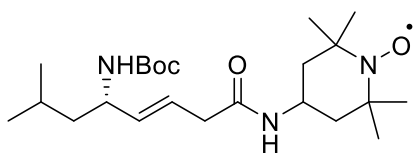
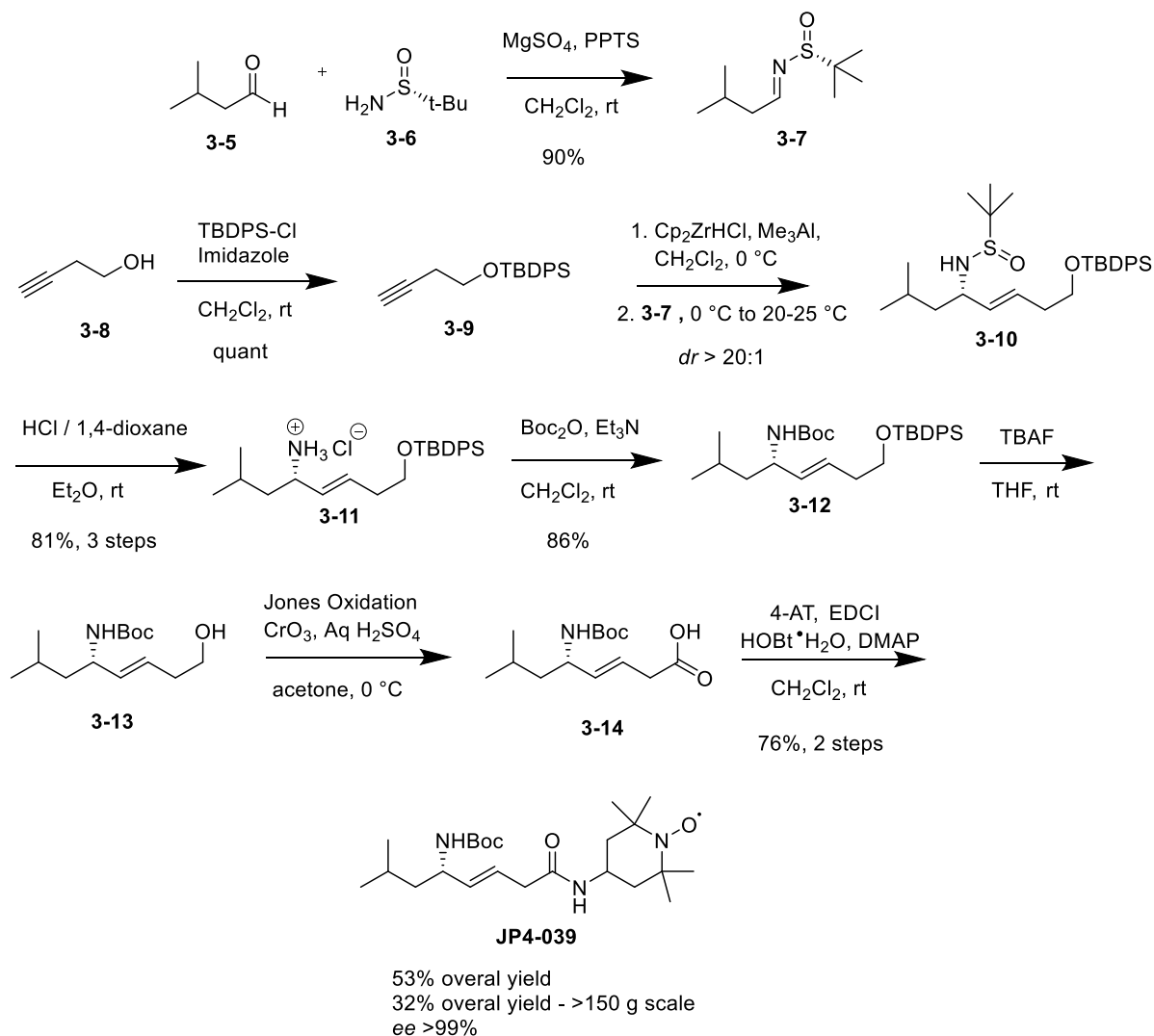


**Figure 3-6 Structure of JP4-039**

The synthesis of JP4-039 proceeded through a key coupling of an imine with a trimethylaluminum species (Scheme 3-2).<sup>79</sup> Isovaleraldehyde (**3-5**) was reacted with sulfinamide **3-6** at room temperature to provide stable imine **3-7**. This intermediate was then coupled with TBDPS protected alcohol **3-9** through a hydrozirconation and transmetallation via trimethylaluminum to provide the allylic amine **3-10** in >95:5 *dr*. The allylic amine was cleaved with HCl in diethyl ether to the hydrochloride **3-11**. Subsequent Boc-protection of the amine gave **3-12** and TBAF mediated deprotection of the silyl ether provided the desired alcohol **3-13**. This key alcohol was used to make a variety of derivatives including JP4-039. Jones oxidation with chromium trioxide provided carboxylic acid **3-14** that was then coupled with 4-AT to provide **JP4-039** in >98% purity as determined by supercritical fluid chromatography (SFC). The final purification of JP4-039 has been accomplished through recrystallization in heptane. Recently, this synthetic route by Wipf and Pierce was successfully employed to synthesize 275 g of JP4-039 at Albany Molecular Research Inc. (AMRI).





**Scheme 3-2 Synthesis of JP4-039 through a hydrozirconation/transmetalation reaction**<sup>79</sup>

There are several drawbacks to the synthetic route. The linear sequence is eight steps and the leucine side chain is introduced early in the sequence. To generate analogs with functional group substitutions for the leucine residue, there is not a common intermediate to build from. Even if these side-chain modifications must be introduced early in the synthesis, a shorter, four- to five-step sequence would be a great improvement for diverse analog development. An obvious way to reduce the synthesis length is to eliminate the need for the protecting group interchange from a sulfinylamine to a Boc-amine as well as a protection and deprotection of the primary alcohol. Another drawback to the synthetic route is the use of pyrophoric (trimethylaluminium,  $\text{Me}_3\text{Al}$ , and

toxic (Jones' reagent) chemicals.<sup>100-101</sup> Especially without a common intermediate, the repeated use of these reagents in analog development is not ideal from a safety perspective.

Similar to XJB-5-131, JP4-039 has shown efficacy in a selection of bioassays; the greatest therapeutic indication is as a potent radiation mitigator.<sup>102-106</sup> In total body irradiation models, JP4-039 is hypothesized to reduce oxidative stress events in the mitochondrial membrane which in turn limits signaling events that drive cell death.<sup>107</sup> Unlike XJB-5-131, JP4-039 conforms to all of Lipinski's rules, making it much more drug-like.<sup>99</sup> JP4-039 is more water soluble and thus easier to formulate for delivery.

Both mitochondrial targeting peptide-conjugates, XJB-5-131 and JP4-039, have been used as probes in oxidative cell death phenotypes.<sup>77, 98, 108-109</sup> Cell death is essential for life. In the first stages of life it is a necessary part of morphogenesis and development of the immune and nervous systems.<sup>110</sup> Throughout life, cell death maintains homeostasis, plays an active role in metabolism, and serves as an anti-cancer defense mechanism.<sup>110-111</sup> Unfortunately, uncontrolled cell death can drive tumor evolution by killing healthy cells and allowing the proliferation of cancer cells in their place (Figure 3-7).<sup>112</sup>

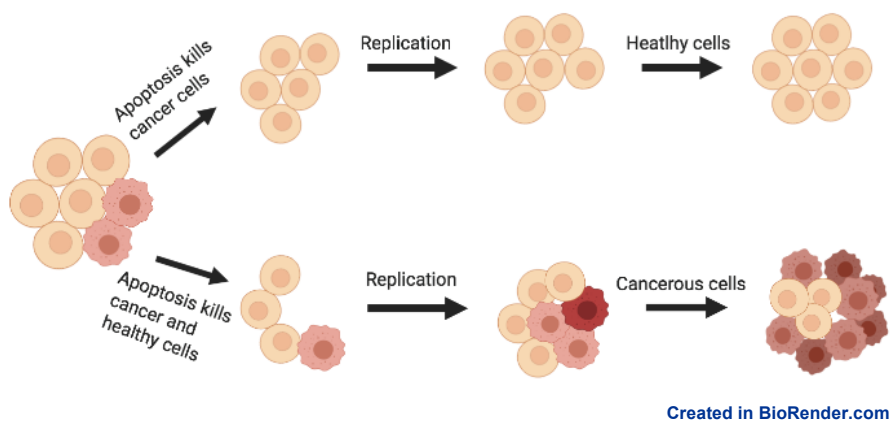


**Figure 3-7 Uncontrolled cell death can drive tumor evolution**

Several parallel cell death pathways can be activated independently. Death triggers a loss of cell membrane integrity, fragmentation of DNA, or activation of extracellular death receptors.<sup>113</sup> The Nomenclature Committee on Cell Death have defined over 34 different modes of regulated cell death.<sup>114</sup> A variety of internal or external perturbations such as  $\text{Ca}^{2+}$  overload, pathogen

invasions, inflammatory cues, and hypoxia provide unique cellular morphology features.<sup>114-115</sup> Cells also have compensatory survival pathways, such as the heat shock response, leading to a variety of different and distinct cell death phenotypes.

In 2012 Brent Stockwell and coworkers discovered a new, iron-dependent cell death phenotype, ferroptosis.<sup>116</sup> As our nitroxide conjugates have shown efficacy in other oxidative cell death phenotypes, we also wanted to probe their role in ferroptosis.

### **3.1.2 Ferroptosis, an Iron-Mediated Cell Death Pathway**

Ferroptosis is distinct from other regulated cell death pathways, particularly apoptosis and necroptosis (regulated necrosis).<sup>116</sup> Apoptosis is a caspase dependent process. Caspases (cysteine-aspartic proteases) are a group of twelve endoproteases that utilize a catalytic cysteine residue in the active site to hydrolyze peptide bonds after an aspartic acid residue to drive apoptosis or inflammation.<sup>117</sup> Apoptosis is characterized by nuclear fragmentation, an intact plasma membrane at an early stage, and a decrease in cellular size (Figure 3-8).<sup>118-119</sup> It can occur as a result of internal factors that lead to mitochondrial outer membrane permeabilization (MOMP) or external factors driven by the binding of ligands to death receptors or the decrease in binding to dependence receptors on the plasma membrane.<sup>119</sup> The deregulation of inhibitor of apoptosis proteins (IAP) is a frequent driver of cancer and often a target for therapy.<sup>120</sup> Inhibitors of apoptosis include navitoclax, ABT-199, and obatoclax mesylate among others.<sup>121</sup>

Necroptosis is a pro-inflammatory, passive process that generally affects large pockets of cells and is characterized by an increase in cellular volume, plasma membrane protrusions, and lack of nuclear fragmentation (Figure 3-8).<sup>114</sup> Necroptosis is dependent on receptor-interacting protein kinase 1 and 3 (RIPK1/RIPK3) and mixed lineage kinase domain like (MLKL); it is caspase independent.<sup>122-123</sup> Necroptosis cell death progression has been implicated in systemic inflammation, neurodegeneration, and ischemic reperfusion injury.<sup>124</sup> Necrostatin 1 (Nec-1), an inhibitor of RIPK1, and necrosulfonamide (NSA), an inhibitor of MLKL, are small molecules that target the necroptosis cell death pathway.<sup>125</sup>

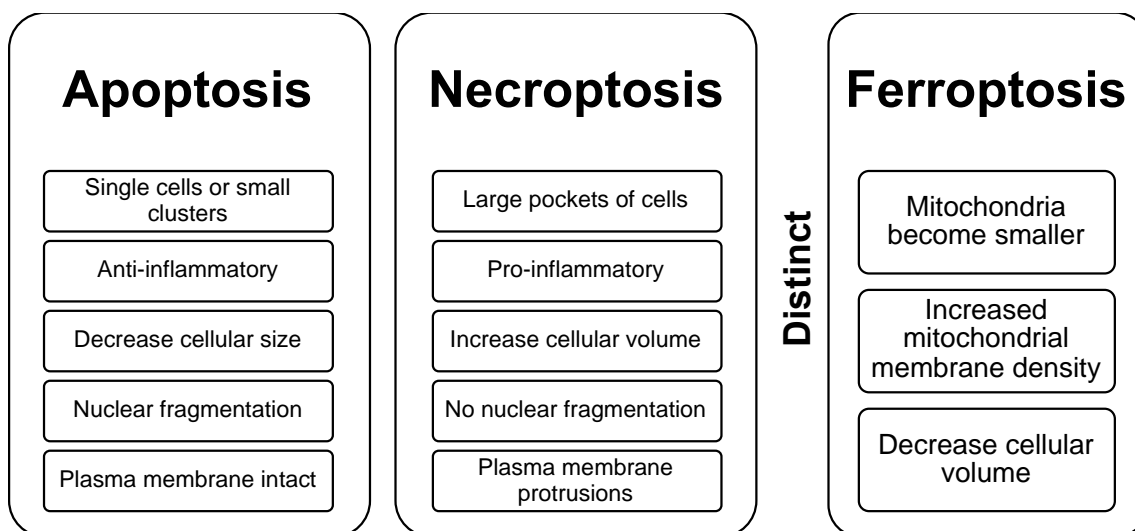


**Figure 3-8 Comparison of apoptosis, necroptosis, and ferroptosis<sup>114</sup>**

Ferroptosis was coined in 2012 to describe a distinct cell death pathway that occurred in RAS-mutated tumor cells.<sup>116</sup> RAS is a class of small GTPase proteins that have critical roles in cell signaling.<sup>126</sup> RAS mutations cause uncontrolled cell growth, which allow cells to avoid death signals and become immune to drug treatments; they are frequently used in biological models. When the Stockwell group exposed RAS-mutated cells to the small molecules erastin or RSL3, the cells did not undergo typical apoptotic (nuclear fragmentation) or necroptotic (plasma membrane protrusions) death phenotypes. Ferroptotic cell death was manifested through a decrease in cellular volume, mitochondrial shrinkage, and an increase in mitochondrial membrane density (Figure 3-8).<sup>116</sup>

The defining feature of ferroptosis is the accumulation of iron dependent lipid peroxides.<sup>114, 116, 127</sup> This distinguishing feature has been confirmed through LCMS oxidative lipidomics.<sup>127</sup> Ferroptosis has been implicated in ischemia reperfusion injury, traumatic brain injury, Huntington's disease, stroke, acute kidney injury, and several cancers, among others.<sup>128-130</sup>

As the defining feature of ferroptosis, it is important to understand what lipid peroxidation is, what drives it, and what counteracts it. Lipid peroxidation is the destruction of lipids in cell membranes by free radicals.<sup>131</sup> Polyunsaturated fatty acids (PUFAs) are highly prone to peroxidation because of the weak C-H bonds of the bisallylic carbons in the backbone structure.<sup>132</sup> LCMS oxidative lipidomics revealed three main PUFA classes prone to peroxidation:

phosphatidylethanolamine, phosphatidylserine, and phosphatidylinositol.<sup>127</sup> The specific length and location of double bonds in the lipid tails of these phospholipids are believed to be the reason why they are more prone to oxidation.<sup>127</sup> Although the mechanism for initiation of lipid peroxidation is not fully understood (it has been attributed to both enzymatic and non-enzymatic factors), it is generally hypothesized that the initiation event is a result of the removal of a bis-allylic hydrogen atom from PUFA phospholipids (Figure 3-9).<sup>131, 133</sup> This generates a carbon-centered phospholipid radical (PL•) that can react with molecular oxygen in the cell to form a phospholipid peroxy radical (PLOO•).<sup>134</sup> This peroxy radical can then remove another hydrogen atom from PUFA phospholipids to form a phospholipid hydroperoxide (PLOOH), the propagating species in the destructive cycle.<sup>131</sup> PLOOH react with labile iron in the cell through Fenton chemistry (Scheme 3-3) to generate further radical species (PLO• and PLOO•) that can participate in the cycle (Figure 3-9).<sup>135-136</sup>

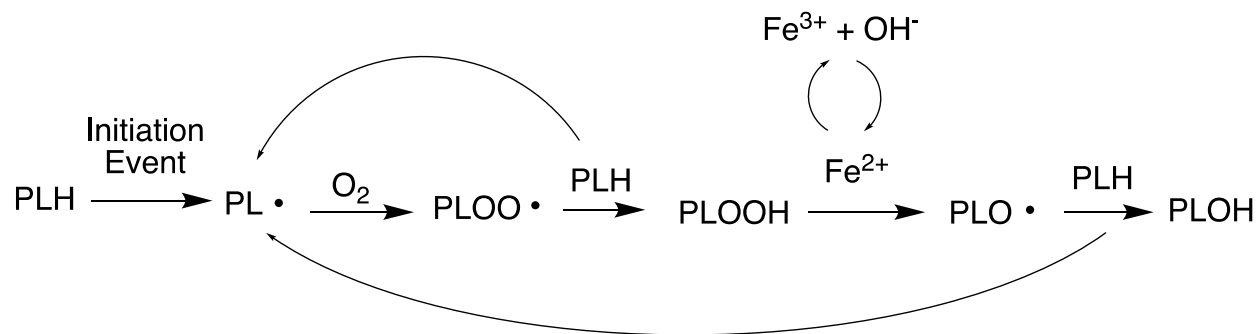


**Figure 3-9 Phospholipid peroxidation cycle**

Just as the mechanism of initiation is attributed to several possible cellular events, the termination event of lipid peroxidation is not fully elucidated. Ferroptotic cell death occurs when the amount of PLOOH reaches a level that causes a breakdown of organelle or cell membrane integrity. Depending on the level of PUFA phospholipids in their structure, the mitochondria, endoplasmic reticulum, and lysosome membranes have been shown to be affected by lipid peroxidation.<sup>131</sup> Recently, cathepsin B, a lysosomal cysteine protease, has been implicated as an executioner in ferroptosis by causing mitochondrial and cellular membrane disruptions (Figure 3-11).<sup>137</sup>

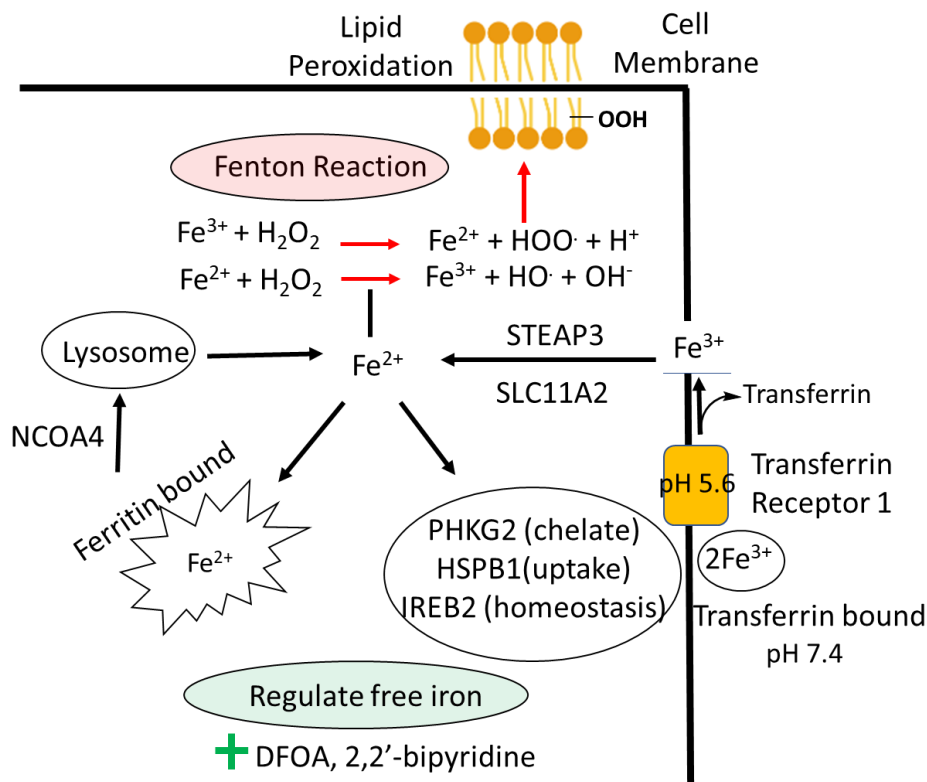
Other proposed initiators and drivers of lipid peroxidation include lipoxygenases (LOXs) and cytochrome P450 oxidoreductase (POR). LOX are iron-dependent dioxygenases that can directly oxygenate PUFAs and increase the amount of lipid hydroperoxides.<sup>138</sup> Knockout studies of GPX<sub>4</sub> demonstrate that LOX are not essential drivers of ferroptosis, but potentially contribute to initiation and propagation of lipid peroxidation<sup>139-140</sup> POR are ubiquitous in the cell and required for electron transfer from NADPH to cytochrome P450.<sup>141</sup> After accepting an electron, reduced cytochrome P450 is hypothesized to be able remove a hydrogen from PUFAs to contribute to lipid peroxidation or, alternatively, contribute to the conversion of Fe<sup>3+</sup> to Fe<sup>2+</sup> as part of the Fenton reaction (Scheme 3-3).<sup>141</sup>



**Scheme 3-3 The Fenton reaction<sup>136</sup>**

As evidenced by the Fenton reaction, iron is an essential driver of ferroptosis. The more cellular labile iron in the cell, the greater the propagation of lipid peroxidation. Extracellular iron is bound to transferrin, a glycoprotein that can bind two Fe<sup>3+</sup> tightly but reversibly with high turnover (Figure 3-10).<sup>142</sup> Transferrin is the most vital source of iron for the body.<sup>142</sup> Transferrin-bound iron enters the cell through endocytosis by Transferrin receptor 1. Transferrin receptor 1 has greater affinity for diferric bound transferrin as compared to monoferric bound transferrin and apo-transferrin.<sup>143</sup> At serum pH 7.4, Fe<sup>3+</sup> complexation to transferrin receptor 1 is favorable. However, inside the endosome, ATP-dependent H<sup>+</sup> pumps lower the pH to 5.6 facilitating the release of Fe<sup>3+</sup> from transferrin receptor 1.<sup>143</sup> Once uncomplexed, free Fe<sup>3+</sup> is reduced to Fe<sup>2+</sup> by transmembrane ferrireductase STEAP3 and it then enters the cytosol through solute carrier family 11 member 2 (SLC11A2).<sup>142</sup> In the cytosol, Fe<sup>2+</sup> is further stored in an inactive complex by the protein ferritin thus limiting oxidative damage.<sup>144</sup> To uncomplex Fe<sup>2+</sup>, the selective cargo receptor nuclear receptor coactivator 4 (NCOA4) binds ferritin and transports it to the lysosome for degradation (Figure 3-10).<sup>144-145</sup> When this process is overactivated or mis-regulated, an increased amount of ferritin is degraded through a process known as ferritinophagy, releasing large amounts of uncomplexed, reactive Fe<sup>2+</sup>.<sup>137</sup> In the cell, free iron is also regulated by phosphorylase kinase catalytic subunit gamma 2 (PHKG2), heat shock protein beta-1 (HSPB1), and iron responsive element binding protein 2 (IREB2) among others (Figure 3-10).<sup>132, 146</sup> Misregulation of any of

these storage elements increases the amount of intracellular reactive iron that participates in the Fenton reaction to drive lipid peroxidation.



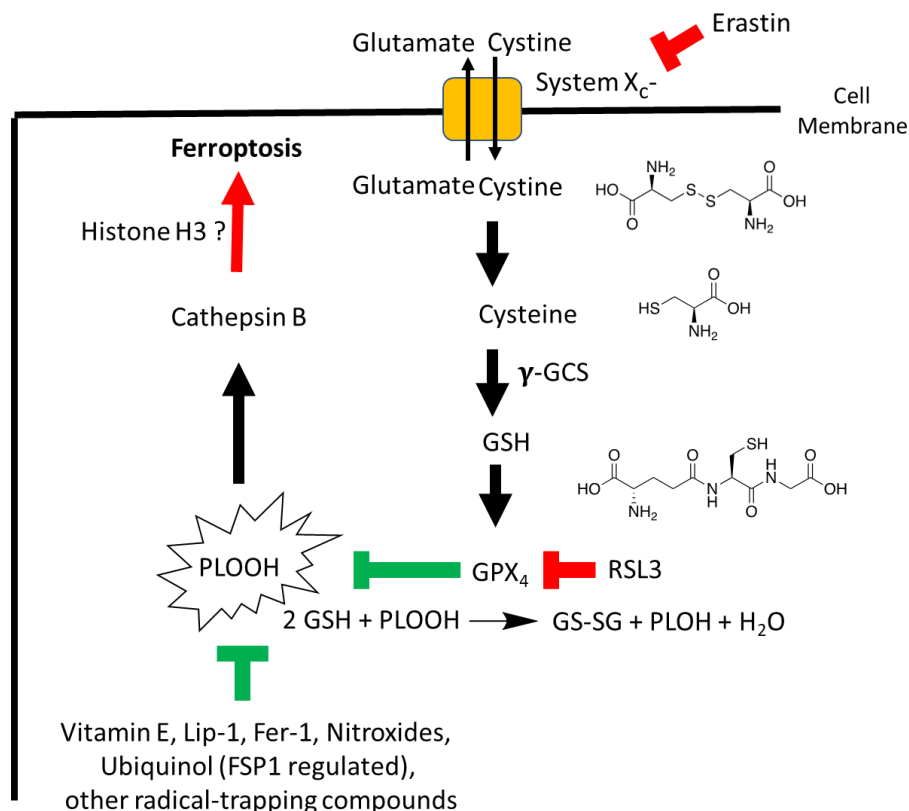
$\text{Fe}^{3+}$  is bound to transferrin at serum pH 7.4; transferrin receptor 1 has great affinity for diferric bound transferrin and at pH 5.6 uncomplexes  $\text{Fe}^{3+}$  from transferrin; STEAP3 reduces  $\text{Fe}^{3+}$  to  $\text{Fe}^{2+}$ ; solute carrier family 11 member 2 (SLC11A2) facilitates entry of  $\text{Fe}^{2+}$  to the cytosol; phosphorylase catalytic subunit gamma 2 (PHKG2) regulates free iron; heat shock protein family B (Small) Member 1 (HSPB1) reduces iron-mediated production of lipid ROS; iron responsive element binding protein 2 (IREB2) encodes a regulator of iron metabolism and homeostasis; nuclear receptor coactivator 4 (NCOA4) drives ferritin degradation; Fenton reaction converts labile  $\text{Fe}^{2+}$  and hydrogen peroxide to  $\text{Fe}^{3+}$  and highly reactive hydroxy radicals;  $\text{Fe}^{3+}$  then reacts with  $\text{H}_2\text{O}_2$  to form hydroperoxyl radicals that lead to lipid peroxidation; deferoxamine (DFOA) and 2,2'-bipyridine chelate iron.

**Figure 3-10 Mechanisms to regulate iron in the cell**

Under optimal biological conditions, the cell has well-defined mechanisms to counteract lipid peroxidation (Figure 3-11).<sup>116, 144</sup> Mechanisms discovered to date revolve around glutathione peroxidase 4 (GPX4) and more recently ferroptosis suppressor protein 1 (FSP1). GPX4 is a selenium-containing enzyme. It is the major enzyme responsible for the detoxification of PLOOHs in cells. While all members of the glutathione peroxidase family can degrade peroxides, only GPX4 can break down hydroperoxides in complex lipids. The absence of a twenty amino acid

sequence in the surface-exposed structural loop is hypothesized to contribute to this unique reactivity.<sup>147</sup> Before ferroptosis was officially recognized, GPX4 knockout studies revealed a non-apoptotic, lipid peroxidation driven cell death.<sup>148</sup> Activation of GPX4 is glutathione (GSH) and in turn cystine dependent. Cystine enters the cell through System Xc<sup>-</sup>, a membrane-bound Na<sup>+</sup> dependent exchange antiporter that shuttles cystine into the cell in exchange for glutamate.<sup>149</sup> Once in the cell, cystine is converted to cysteine which is then further converted to GSH by glutamate cysteine ligase ( $\gamma$ -GCS).<sup>144, 149</sup> GSH, a tripeptide consisting of glutamate, cysteine, and glycine, is a potent reductant critical for GPX4 mediation of lipid peroxidation.<sup>144</sup> At the selenocysteine catalytic center of GPX4, two molecules of GSH are used to convert lipid hydroperoxides to glutathione disulfide and the associated lipid alcohol and water (Figure 3-11). The selenol in the active site is oxidized by the lipid hydroperoxide to selenenic acid, reduced with GSH to form a selenodisulfide, and finally reactivated by a second GSH molecule releasing the glutathione disulfide.<sup>144</sup>





System X<sub>c</sub><sup>-</sup> brings cystine into and glutamate out of the cell; erastin is a system X<sub>c</sub><sup>-</sup> inhibitor; glutamate cystine ligase (γ-GCS) catalyzes the first and rate-limiting step to form gamma-glutamylcysteine (γ-GC) in the conversion of cystine to glutathione; glutathione (GSH) activates glutathione peroxidase 4 by donating two electrons; glutathione peroxidase 4 (GPX4) reduces lipid hydroperoxides to lipid alcohols effectively slowing the lipid peroxidation chain reaction; cathepsin B is proposed as a GPX4 independent executioner of ferroptosis through hypothesized histone H3 cleavage; histone H3 maintains the structure of chromatin in cells.

**Figure 3-11 Mechanisms to regulate lipid peroxidation and ferroptosis in the cell**

There are two main checkpoints for a small-molecule induction of ferroptosis. The first, most direct way is through inhibition of GPX4. The chloroketone RSL3 directly blocks GPX4 leading to uncontrolled lipid peroxidation and ferroptosis cell death (Figure 3-12).<sup>116</sup> The second, more indirect mechanism is through system X<sub>c</sub><sup>-</sup> inhibition. Inhibition of system X<sub>c</sub><sup>-</sup> deprives the cell of cystine. Without cystine, GSH cannot be synthesized and furthermore, GPX4 is not activated.<sup>150</sup> Erastin is a small molecule inhibitor of system X<sub>c</sub><sup>-</sup> (Figure 3-12).<sup>116</sup>

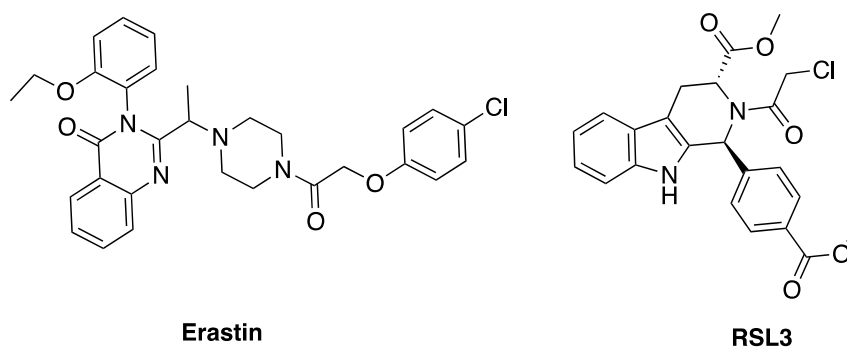


**Figure 3-12 Two ferroptosis inducers, erastin and RSL3**

A GPX4-independent pathway that was recently implicated in ferroptosis involves the flavoprotein apoptosis-inducing factor mitochondria-associated 2 (AIFM2), which was renamed ferroptosis-suppressor protein 1 (FSP1) (Figure 3-11). This gene was discovered through a genetic suppressor screen and shown to prevent ferroptosis driven by GPX4 deletion.<sup>151</sup> FSP1 is hypothesized to control lipid peroxidation as part of the oxidation-reduction cycle of the antioxidant ubiquinol (Figure 3-4). Ubiquinol quenches lipid peroxides to terminate autoxidation. FSP1 catalyzes the regeneration of ubiquinol from ubiquinone with NADP(H) so the cycle can continue.<sup>151</sup> Importantly, this pathway points to the critical role of radical-trapping antioxidants in preventing ferroptotic cell death induced by GPX4 inhibition. Other proteins and pathways critical to the overall antioxidant potential of the cell, including tumor protein 53 (Figure 3-11), continue to be investigated for their role in ferroptosis.<sup>152</sup>

Several classes of small, organic molecules have been developed to inhibit ferroptosis. Some of these compounds act as iron-chelators or as antioxidants based on the critical role iron and radical species have in driving ferroptosis. The first class, consisting of deferoxamine (DFOA) and 2,2'-bipyridine (Figure 3-10 and Figure 3-13), inhibits the accumulation of iron in the cell through chelation. Thus, iron-chelators limit lipid peroxidation resulting from the Fenton reaction and the iron-dependent LOX mediated oxidation of PUFAs.<sup>116</sup> The therapeutic benefit of iron chelators is limited because iron is essential to a variety of critical functions in the body. The second class of compounds are antioxidants, which can directly inhibit lipid peroxidation. Some examples are vitamin E, liproxstatin-1 (Lip-1), and ferrostatin-1 (Fer-1) which act as radical-trapping antioxidants (Figure 3-11 and 3-13).<sup>92</sup> Lip-1 and Fer-1 were discovered through high-throughput screens and have a half maximal effective concentration (EC<sub>50</sub>) in an erastin-induced

ferroptosis cell death model of 38 nM and 70 nM respectively.<sup>92</sup> Recently, a group from Sichuan University demonstrated a lead phenothiazine compound (Figure 3-13) with strong intrinsic antioxidant potential that has an EC<sub>50</sub> of 0.5 nM in an erastin-induced ferroptosis assay. This is one of the most potent ferroptosis inhibitors to date.<sup>153</sup>

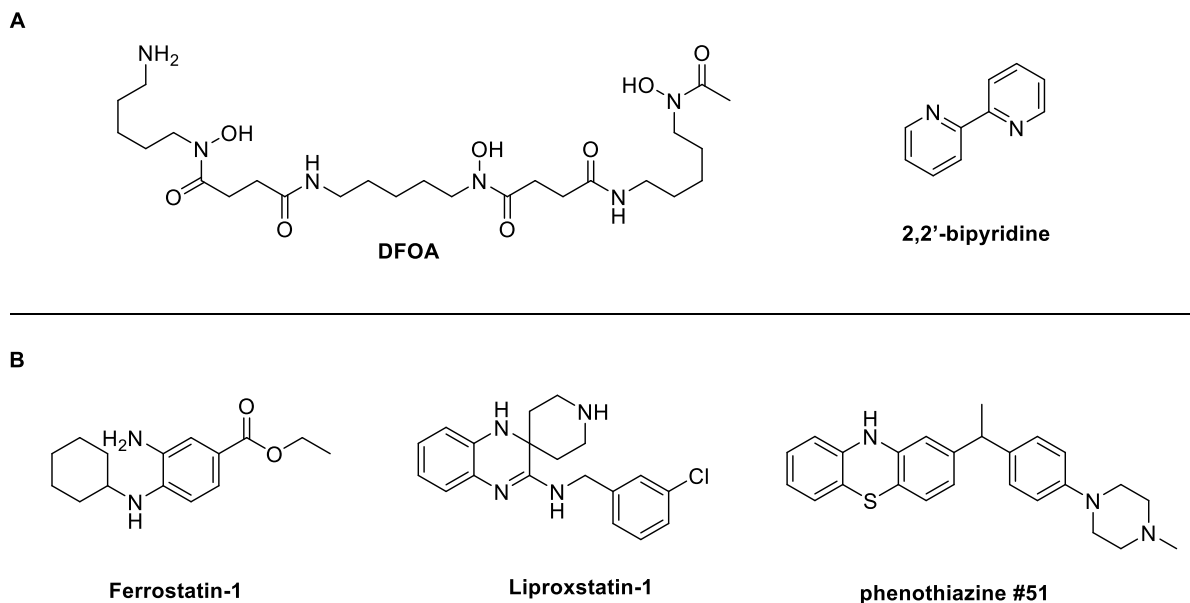


**Figure 3-13 A) Iron chelators DFOA and 2,2'-bipyridine B) Antioxidants Fer-1, Lip-1, and phenothiazine #51**

There remains a strong need for the further investigation of ferroptosis. Over the last eight years, mechanistic work has revealed interesting contrasting roles for ferroptosis in disease. For example, it has recently been proposed that certain classes of cancer cells are more likely to undergo ferroptotic cell death because they have a higher ROS load and iron requirement.<sup>131, 154</sup> In this scenario, ferroptosis inducers are attractive as they could be developed to selectively induce cell death in cancer cells which are prone to lipid peroxidation. Conversely, in ischemic diseases ferroptosis negatively contributes to the pathogenesis of the disease. In these indications, ferroptosis inhibitors are necessary to prevent stroke and heart injury.<sup>155</sup> Not only can ferroptosis inhibitors serve therapeutic purposes, they can also help elucidate the various biological pathways.

In 2016, in collaboration with the Stockwell laboratory, the radical-scavenging compounds XJB-5-131 and JP4-039 were tested in an erastin-induced ferroptosis assay in the fibrosarcoma cell line HT-1080.<sup>156</sup> Not only was the Wipf group interested in the therapeutic potential of these

compounds, they were also interested in using these compounds to probe the role of mitochondrial lipid peroxidation in ferroptosis. XJB-5-131 and JP4-039 both preferentially locate in the mitochondria over the cytosol; XJB-5-131 has a 600-fold enrichment factor while JP4-039 has only a 20-30 fold enrichment factor.<sup>93</sup> If XJB-5-131 and JP4-039 showed activity as ferroptosis inhibitors, this would indicate that protection of mitochondrial lipids was sufficient to prevent ferroptosis. The results supported this hypothesis. Owing to its efficiency in crossing the mitochondrial membrane and enriching in the mitochondria, XJB-5-131 exhibited superior protective effects with an EC<sub>50</sub> of 114 nM while JP4-039, which is less concentrated in the mitochondria, had an EC<sub>50</sub> of 3.6  $\mu$ M.<sup>156</sup> In this report, ten analogs of XJB-5-131 and JP4-039 were synthesized and examined for anti-ferroptotic activity. Most of these analogs were not more active than XJB-5-131 or JP4-039. Surprisingly, an exception was the bis-nitroxide analog of JP4-039 (Figure 3-14) with an EC<sub>50</sub> of 915 nM. The authors speculated to its enhanced ability to scavenge reactive oxygen species in the mitochondria. Importantly, there was no correlation between protective activity and lipophilicity.

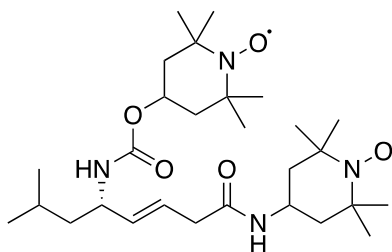


**Figure 3-14 JP4-039 bis-nitroxide analog**

### 3.1.3 SAR In Vitro Assay and JP4-039 Zones for Modification

Based on this early effort, there remained significant room for improvement in the activity of the JP4-039 scaffold. We chose to pursue the smaller JP4-039 scaffold because of its better drug like properties, including lower molecular weight and logP compared to XJB-5-131. The logP of JP4-039 is 2.76 while the logP of XJB-5-131 is 7.61. It has been difficult to pursue XJB-5-131 in other therapeutic indications because its lipophilicity and molecular weight make it hard to dose. Based on our previous work, it was hypothesized that XJB-5-131 is an effective ferroptosis

inhibitor because it locates to the mitochondria and specifically inhibits the peroxidation of mitochondrial lipids. JP4-039 is a less effective ferroptosis inhibitor because it is largely untargeted.<sup>156</sup> Based on this finding, to improve the anti-ferroptosis activity of the truncated series of nitroxides, we should improve the ability of these compounds to cross the mitochondrial membrane or their efficiency as global cellular antioxidants. We hypothesized that structural modifications that affect the secondary structure of the truncated analogs may improve their mitochondrial targeting ability. Structural modifications that affect lipophilicity and polar surface area may also improve global cellular antioxidant activity. Ultimately, our goal was to generate compounds with improved activity and determine whether the increase in activity was conformation- or lipophilicity-dependent.

To build a structure activity relationship (SAR), we utilized a CellTiter-Glo® ferroptosis assay in HT-1080 cells at the contract research organization (CRO) Pharmaron. CellTiter-Glo® is a method to measure the number of viable cells in a culture by measuring the amount of ATP, a metabolic marker, that is present. We chose to determine the 80% effective concentration (EC<sub>80</sub>) for each compound. EC<sub>80</sub>'s have been used previously to screen large libraries of compounds for ferroptosis activity.<sup>157</sup> For our compounds, EC<sub>80</sub> determinations were a more accurate representation of the data based on the concentration points screened and the resulting curves generated.

We analyzed the previously reported EC<sub>50</sub> data obtained in collaboration with the Stockwell laboratory to determine EC<sub>80</sub> values. The EC<sub>80</sub> for JP4-039 was between 4000-7000 nM in erastin (10  $\mu$ M) induced ferroptosis cell death in the fibrosarcoma cell line HT-1080.<sup>156</sup> The control Fer-1 had an EC<sub>80</sub> range of 80-100 nM. The assay utilized by the Stockwell group was fluorescence based; the greater the apparent fluorescence intensity, the greater the protective effect of the compound. Fluorescent assays measure the conversion of a substrate to a reaction product that fluoresces when excited by light of a certain wavelength.<sup>158</sup> In the assay at Pharmaron, JP4-039 had an EC<sub>80</sub> range of 4000-8500 nM while the control Fer-1 had an EC<sub>80</sub> of  $39 \pm 19$  nM. The assay conducted at Pharmaron was luminescence-based. Luminescence-based assays have a wide dynamic range and are one of the most sensitive detection methods used (significantly more sensitive than fluorescence) because of signal multiplication and amplification capabilities. In luminescent assays, a substrate is converted to a reaction product that emits photons of light as it returns from an electronically excited state to a ground state.<sup>158</sup> Across the two assay types, the

EC<sub>80</sub> values for JP4-039 were within error range. The EC<sub>80</sub> values for Fer-1 showed approximately a two-fold difference but we believe this difference falls into the assay error range, considering that the two assays are fundamentally different and were run in different labs. The advantage of the luminescence-based assay at Pharmaron is that we are more likely to discern subtle changes in activity and better observe the rank ordering of our compounds from most potent to less potent.

We targeted five zones for chemical modification on JP4-039 (Figure 3-15). We investigated replacements of the leucine side chain (Zone I - red), the chirality at the amine center (Zone II - blue) and substitutions at the  $\alpha$ -position of the amide (Zone III - green). We also considered the location of nitroxide, specifically relocating it from Zone IV (gold) to Zone V (purple). Finally, we looked at a replacement of the protecting group of the amine (Zone V - purple) as a way to introduce a second scavenging moiety to the molecule. These modifications were designed to improve the overall activity and analyze whether the improvement in activity was a result of structure conformation or lipophilicity. Thus, we were careful to consider the logP as part of our synthesis efforts. Generally, logP should not exceed 5.<sup>99</sup> There are several exceptions to this rule, especially when a portion of the molecule is a targeting moiety, as is the case with XJB-5-131.<sup>159</sup> We were concerned with logP to ensure that the activity was not correlated purely to how lipophilic the molecule was. Lipophilic antioxidants such as vitamin E are known to rescue cells from ferroptosis through a different mechanism than our compounds. Vitamin E is fat soluble and thus incorporated into cell membranes.<sup>160</sup>

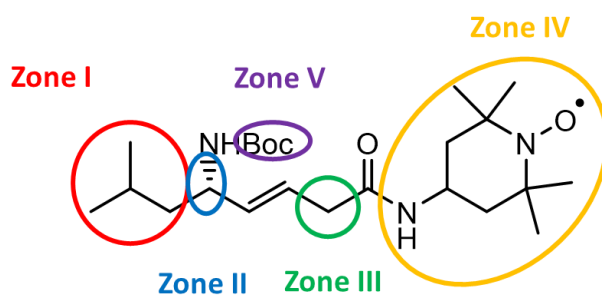
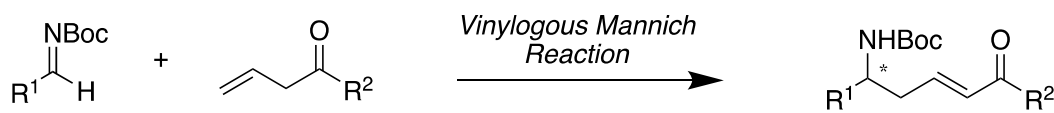


Figure 3-15 SAR zones of JP4-039

To make and test these structural modifications efficiently, a new synthetic route was required. The new route needed to be shorter so that we could more readily introduce substitutions for the leucine side chain (Zone I). It also needed to avoid the use of pyrophoric and toxic reagents

in order to facilitate scale-up when needed. A more robust and less water- and air-sensitive methodology for setting the chiral amine center would also be beneficial.

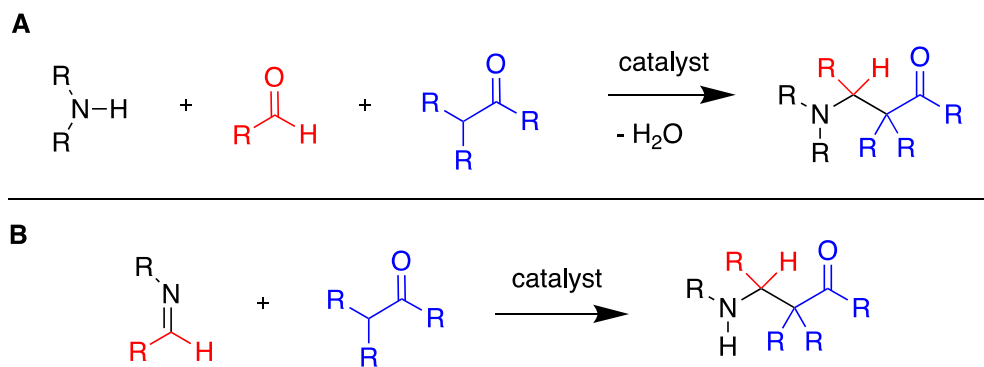
As the key step in our new synthesis, we proposed a vinylogous Mannich reaction, inspired by a 2017 report from the Yin group at the Chinese Academy of Sciences (Scheme 3-4).<sup>161</sup> With this carbon-carbon bond forming reaction we could avoid the use of a hydrozirconation step to set the stereocenter and eliminate the need for a change in the nitrogen protecting group. It would also avoid the use of toxic reagents. Most importantly, we believed we could rapidly synthesize a structurally diverse set of analogs to test for anti-ferroptotic activity.



**Scheme 3-4 Proposed vinylogous Mannich reaction towards JP4-039**

### 3.1.4 The Vinylogous Mannich Reaction

The Mannich reaction is one of the most useful carbon-carbon bond forming reactions in synthetic chemistry. The reaction is named after Carl Mannich who first described the mechanism in 1912.<sup>40</sup> The Mannich reaction is the reaction between a primary or secondary amine, a nonenolizable aldehyde, and an enolizable carbonyl compound (Scheme 3-5 A); the amine and aldehyde can also be pre-condensed to form the imine prior to reaction with an enolizable carbonyl compound (Scheme 3-5 B). The key to the reaction is the presence of a resonance-stabilized nucleophile and a highly reactive electrophile (imine).

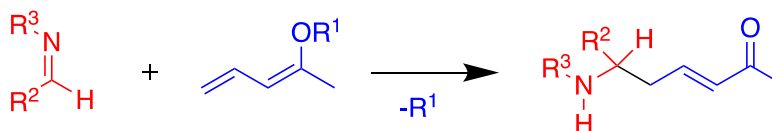


**Scheme 3-5 A) Three-component Mannich reaction and B) Two-component Mannich reaction**

The utility of the Mannich reaction is derived from not only the generality of the mechanism and reaction components but also from the vast number of specialized protocols applicable for numerous functional groups through specialty catalyst design and auxiliary incorporation. With optimized conditions, reactions are highly chemo- and stereospecific. Much of the innovation in Mannich reactions stems from the utility of the  $\beta$ -amino-carbonyl product as a precursor for natural products and pharmaceuticals.<sup>162-163</sup>  $\beta$ -Amino-carbonyl synthons are readily transformed to Michael acceptors, amino alcohols, and a variety of carbonyl derivatives.<sup>163</sup> In the early 2000's Shibasaki<sup>164</sup>, Jorgensen<sup>165</sup>, and Trost<sup>166</sup> introduced catalytic asymmetric Mannich reactions using chiral organometallic systems. Most of this work built on asymmetric aldol chemistry.

The vinylogous Mannich reaction is a logical two carbon extension of the Mannich reaction (Scheme 3-6). The term vinylogous describes functional groups where the standard moieties are separated by a double bond.<sup>167</sup> In the traditional Mannich reaction, addition occurs at the  $\alpha$ -position of the enolizable carbonyl compound. In the vinylogous equivalent, addition takes place at the  $\gamma$ -position of a dienol. The conjugated double bonds serve as an electron conducting channel in the molecule.<sup>168</sup> Both cyclic and acyclic as well as direct (dienolate not pre-formed) and indirect (Mukaiyama-Mannich reaction where the dienolate is pre-formed) variants have been extensively explored. Stephen F. Martin at the University of Texas is a pioneer in the field of vinylogous Mannich reactions, using the methodology to construct the core of numerous alkaloids.<sup>169</sup>

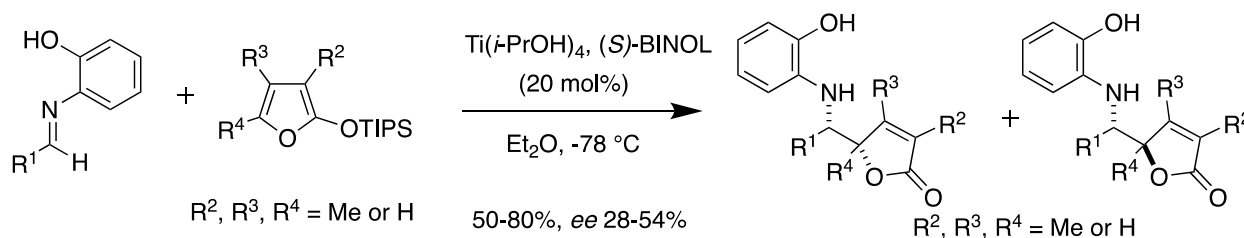




**Scheme 3-6 Acyclic, indirect vinylogous Mannich reaction**

Asymmetric vinylogous Mannich reactions were first introduced in 1999 and continue to be investigated today.<sup>170</sup> Asymmetric induction can occur in three ways: 1) chiral catalyst/ligand design; 2) introduction of a chiral auxiliary on the imine; and 3) introduction of a chiral auxiliary on the carbonyl component. To date, no vinylogous Mannich methodology has integrated two of these components in a cooperative system. Reaction development is significantly behind that of the closely related vinylogous aldol variant.<sup>168</sup>

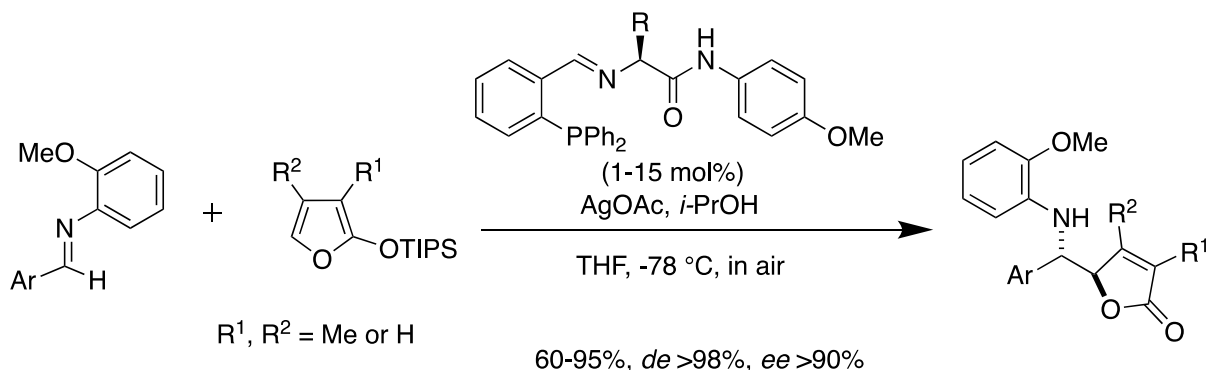
The first catalytic, asymmetric indirect vinylogous Mannich reaction was demonstrated by the Martin group in 1999 (Scheme 3-7).<sup>170</sup> The reaction involved an aryl aldimine and silyloxyfuran with 20 mol% of an optimized titanium-BINOL catalytic system. Yields were modest and the *ee* ranged from 28-54%. Martin noted that the hydroxy group on the aromatic ring of the imine was critical for the enantioselectivity of the reaction. The hydroxy group was hypothesized to coordinate to the titanium Lewis acid species in the proposed transition state. The catalyst system was prepared in a 2:1 ratio of (*S*)-BINOL to Ti(*i*-PrOH)<sub>4</sub> in a coordinating solvent. When the chiral ligand was omitted from the reaction, the yield remained high but the diastereomeric ratio was reduced from up to 91:9 to 2:1.



**Scheme 3-7 Martin et al. vinylogous Mannich reaction<sup>170</sup>**

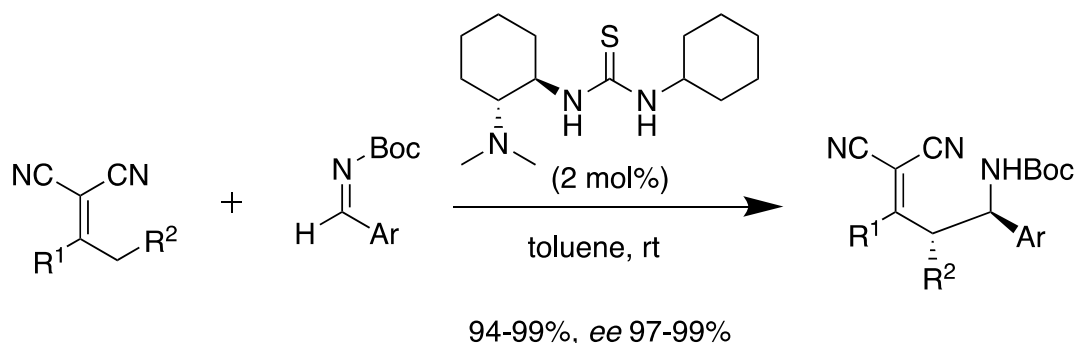
The next major advancement in catalytic and asymmetric vinylogous Mannich methodology was not until 2006 when Hoveyda at Boston College disclosed a silver-catalyzed

transformation of protected aldimines and silyloxyfurans that proceeded with >98% *de*, >90% *ee*, and 60-95% yield (Scheme 3-8).<sup>171</sup> A chiral phosphine ligand (1-15 mol%) and AgOAc with *i*-PrOH (1.1 equiv) as an additive in THF was an effective catalytic system for a variety of aryl substituted aldimines and methyl substituted silyloxyfurans. *i*-PrOH was a necessary proton source additive for reaction turnover. In the proposed mechanism, Ag(I) is coordinated to both the ligand (phosphorus and nitrogen atoms) and the aldimine (nitrogen and methoxy group) substrate. The substrate was bound *anti* to the bulky R substituent on the ligand. An *endo*-type addition was followed by an intramolecular desilylation by the Lewis basic amide end of the ligand through a process facilitated by the alcohol additive (*i*-PrOH). The amide moiety of the ligand was key for both yield and enantioselectivity. When a less Lewis basic substituent (OMe) or a less electron rich (N(H)-*p*-CF<sub>3</sub>C<sub>6</sub>H<sub>4</sub>) group was used, both the yield and *ee* decreased. Hoveyda hypothesized that the amide moiety prolonged the catalyst longevity through stabilization of the silver complexes.



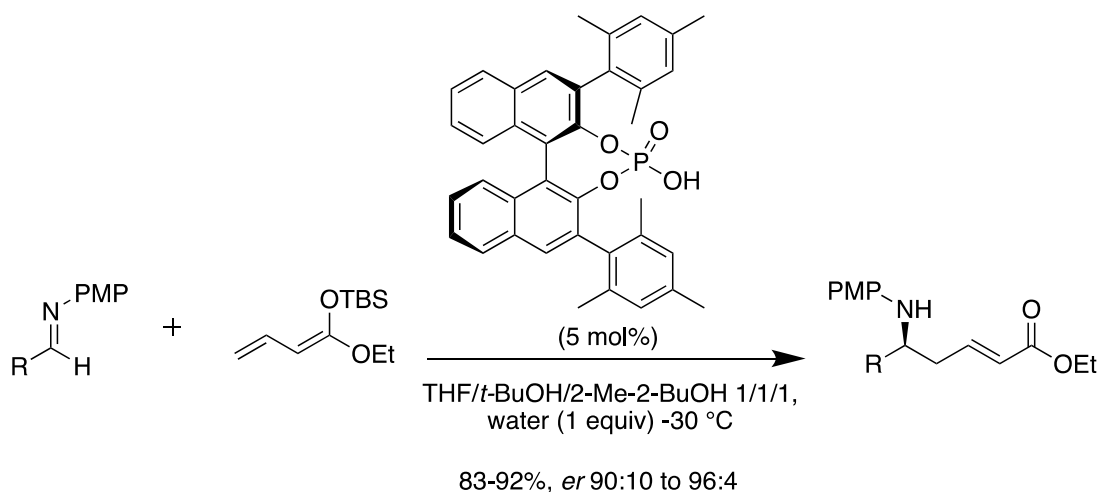
**Scheme 3-8 Hoveyda et al. Ag(I) catalyzed indirect vinylogous Mannich reaction<sup>171</sup>**

Also in 2006, the first direct, catalytic, asymmetric vinylogous Mannich reaction was disclosed by the Chen group (Scheme 3-9).<sup>172</sup> The reaction components were a *N*-Boc aldimine and an  $\alpha,\alpha$ -dicyanoolefin activated by a chiral bifunctional thiourea-tertiary amine organocatalyst. Berkessel's thiourea catalyst delivered product in nearly quantitative yield and >98% *ee* with only 2 mol% of catalyst. The group previously demonstrated the facile  $\gamma$ -deprotonation of  $\alpha,\alpha$ -dicyanoolefin under mildly basic conditions in the context of vinylogous Michael reactions. A variety of cyclic and acyclic dicyanoolefins and aryl aldimines were well tolerated.



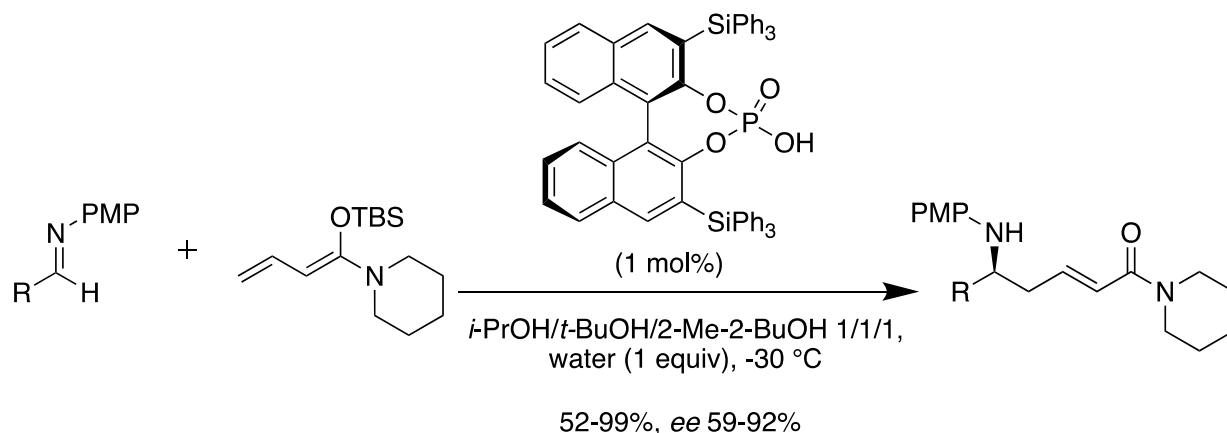
**Scheme 3-9** Chen et al. direct vinylogous Mannich reaction<sup>172</sup>

The first catalytic, enantioselective vinylogous indirect Mukaiyama-Mannich reaction of acyclic silyl dienolates and aldimines was accomplished by Schneider at the University of Leipzig in 2008 (Scheme 3-10).<sup>173</sup> Solvent selection was critical for the reaction, using a 1:1:1 mixture of THF:*t*-BuOH:2-Me-2-BuOH with 1 equivalent of water. THF was critical for enantioselectivity, the alcohol solvent for the reaction rate, 2-methyl-2-butanol for solubility, and water for turnover in the catalytic cycle. An *er* of 90:10 to 96:4 was achieved with aromatic imines; aliphatic imines were not tolerated. A key finding from the methodology was the formation of a contact ion pair through monocoordination of the phosphoric acid to the imine which could be detected and characterized by ESI(+)-MS/MS.



**Scheme 3-10** Schneider et al. acyclic vinylogous Mannich reaction<sup>173</sup>

Schneider also disclosed the first example of a vinylogous Mukaiyama-Mannich reaction to produce enantioenriched amides (Scheme 3-11).<sup>174</sup> A selection of silyl *N,O*-acetals were screened, including *N,N*-dimethyl-, *N,N*-diisopropylamide-, pyrrolidide-, piperidide-, and morpholide-, as nucleophiles in the reaction with aryl substituted PMP-protected aldimines. The alkyl substituted acetals were low yielding (19-34%) and had a poor *ee*. The piperidide substituent was optimal, providing amide products with yields from 52-99% and *ee* from 59-92%. While only 1 mol% of phosphine catalyst was required, a typical reaction took 9 days at -30 °C. Similar to the group's previous reports, alcohol or water in the solvent mixture was critical to trap the TBS species as the silanol (water) or silyl ether (alcohol) and to reprotonate the phosphate counterion to ensure catalyst turnover. The silyl *N,O*-acetal was used in three-fold excess in the reaction. Subsequent transformations of the amide product included conversion to the allylic alcohol with Schwartz reagent or reduction with lithium triethylborohydride and cyclization under Mitsunobu conditions.

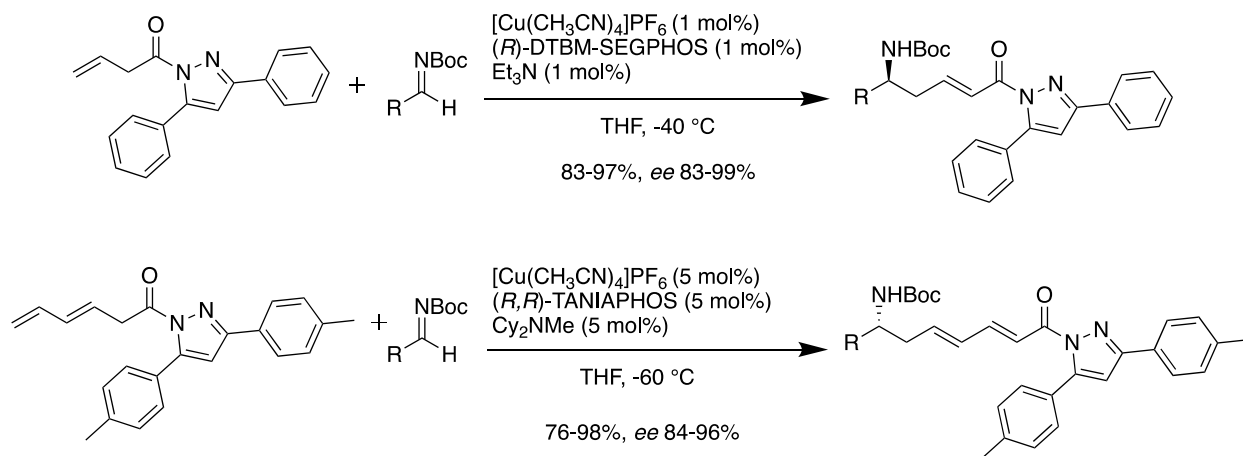


**Scheme 3-11 Schneider et al. vinylogous Mannich reaction of form amides**<sup>174</sup>

Several other groups published variants of the asymmetric vinylogous Mannich reaction of acyclic silyl dienolates and imines following these seminal works. Carretero at the University of Madrid disclosed the first copper catalyzed variant with *N*-2-thienylsulfonylimines and an in-situ catalyst (10 mol%) generated from CuBr<sub>2</sub> and a bulky Fesulphos ligand.<sup>175</sup> The Schneider group built on their previous work with PMP protected imines, silyl dienolates, and phosphoric acid catalysts to showcase improved yields, enantiomeric ratios (88-97%), and applicability to a three-component reaction. They were able to gain further mechanistic insights by obtaining a crystal

structure of their imine-bound phosphoric acid catalyst.<sup>176</sup> Schneider also used the methodology as a key step to generate the tobacco alkaloid (*S*)-anabasine<sup>177</sup> in the synthesis of four indolizidine based alkaloids (IBAs)<sup>178</sup>, and later in the synthesis of an additional 16 IBAs.<sup>179</sup> The Feng group at Sichuan University utilized a scandium(III)-*N,N'*-dioxide complex in a three-component vinylogous Mannich reaction with a benzaldehyde derivative, 2-aminophenyl, and silyl dienol ethylester.<sup>180</sup> Finally, in 2014 the List group used a dioxinone-derived silyl dienolate with a *N*-Boc aldimine and bulky disulfonimide catalyst derived from BINOL (1 mol%) to provide  $\gamma$ -selective products with high yields and modest *ee* (80:20 to 99:1) after 3 days of reaction time.<sup>181</sup>

In 2017, the Yin group at the Chinese Academy of the Sciences disclosed the first direct, catalytic vinylogous Mannich reaction of  $\beta,\gamma$ -unsaturated amides (Scheme 3-12).<sup>161</sup> Steric bulk provided by the amide substrate (3,5-diphenyl pyrazole), copper species ( $[\text{Cu}(\text{CH}_3\text{CN})_4]\text{PF}_6$ ), and ligand ((*R,R*)-DTBM-SEGPBOS) resulted in a  $\gamma$ -selective reaction with *ee* up to 99%. The reaction proceeded with only 1 mol% of the catalyst/base system. It should be noted that alkyl substituents on the imine resulted in much more modest *ee* values between 83-89%. The reaction was not successful with the analogous  $\alpha,\beta$ -unsaturated amides because of the high pKa values of the  $\gamma$ -proton necessary for deprotonation for the reaction to occur. The pKa of protons  $\alpha$  to amides (where deprotonation is necessary for  $\beta,\gamma$ -unsaturated amides) is approximately 30.<sup>182</sup> The authors extended the  $\beta,\gamma$ -unsaturated amide methodology to the  $\varepsilon$ -position for a bisvinylogous Mannich reaction. Re-optimization of the reaction was required, however, and the authors did not provide a rationale as to why the 3,5-di-*p*-tolyl pyrazole or TANIAPHOS ligand were optimal.



**Scheme 3-12** Yin et al. vinylogous and bisvinylogous Mannich reaction of  $\beta,\gamma$ -unsaturated amides<sup>161</sup>

Acyclic vinylogous Mannich reactions lead to a  $\delta$ -amino- $\alpha,\beta$ -unsaturated carbonyl compound.<sup>161</sup> Isomerization of the double bond to the  $\delta$ -amino- $\beta,\gamma$ -unsaturated carbonyl compound generates the backbone of JP4-039. The recent work from the Yin group matches up quite closely with JP4-039 because it utilizes a Boc-protecting group on the imine. While we could use the same pyrazole system to generate the backbone of JP4-039, we hypothesized that the introduction of a different auxiliary would further enhance the stereochemical outcome of the reaction and also be a useful directing group for our proposed  $\alpha$ -substitutions in Zone III (Figure 3-15). For this reason, we were interested in using the Evans oxazolidinone auxiliary in the vinylogous Mannich reaction with imines.

### 3.1.5 Oxazolidinone Auxiliaries in (Vinylogous) Mannich Reactions

To date, there has not been a report of a selective vinylogous Mannich reaction with a chiral auxiliary attached to the carbonyl nucleophile. The Liu and Chen groups at the Chinese Academy of Sciences incorporated chirality through a *N-tert*-butanesulfinylimino group on the imine while the Chen group at Nankai University used an *O*-pivaloylated *D*-galactosylamine as a chiral auxiliary on an imine to carry out a vinylogous Mannich reaction.<sup>183-184</sup> There are several examples for a nucleophilic chiral auxiliary in the more traditional Mannich reaction.<sup>185-187</sup> Evans' oxazolidinone is one of the most common auxiliaries.

Chiral auxiliaries gained attention in 1975 when E.J. Corey used 8-phenylmenthol in the synthesis of an enantiomerically enriched key prostaglandin intermediate.<sup>188</sup> For an aldol-type chiral auxiliary to be effective it must be: 1. easy to introduce; 2. predisposed to highly-selective enolizations; 3. provide a high degree of facial selectivity for addition post-enolization; and 4. easy to cleave without erosion of stereochemistry.<sup>189</sup> The *N*-acyloxazolidinone with a benzyl directing group at the 4-position was the first chiral oxazolidinone auxiliary developed by the Evans group at Harvard University in 1981 and has since become the gold standard in chiral auxiliaries.<sup>190</sup> Numerous variations with different directing groups and heteroatoms have since been developed by Fujiata, Crimmins, Davies, and Seebach (Figure 3-16).<sup>189</sup>

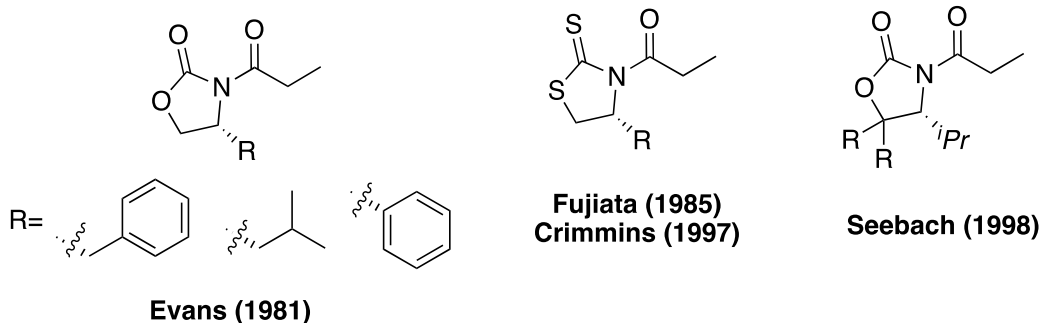


**Figure 3-16 Oxazolidinone derived chiral propanoates**

The oxazolidinone auxiliary is easy to introduce through coupling reactions with carboxylic acids or acyl chlorides (Figure 3-17). The oxazolidinone itself can be purchased or synthesized in two steps from an amino acid.<sup>191</sup> Generally, they direct highly selective (*Z*)-enolizations and permit high facial selectivity post-enolization through a substituent at the 4-position. Finally, they are easy to cleave through saponification or reduction conditions. The auxiliary has shown great utility in asymmetric alkylations, asymmetric *syn*- and *anti*-aldol reactions, and in Diels-Alder reactions.<sup>189, 192</sup> The discussion of oxazolidinones as chiral auxiliaries in asymmetric aldol reactions has been included in numerous review articles,<sup>193-196</sup> however, they have found very limited utility in Mannich reactions; they have not been used in vinylogous Mannich reactions.

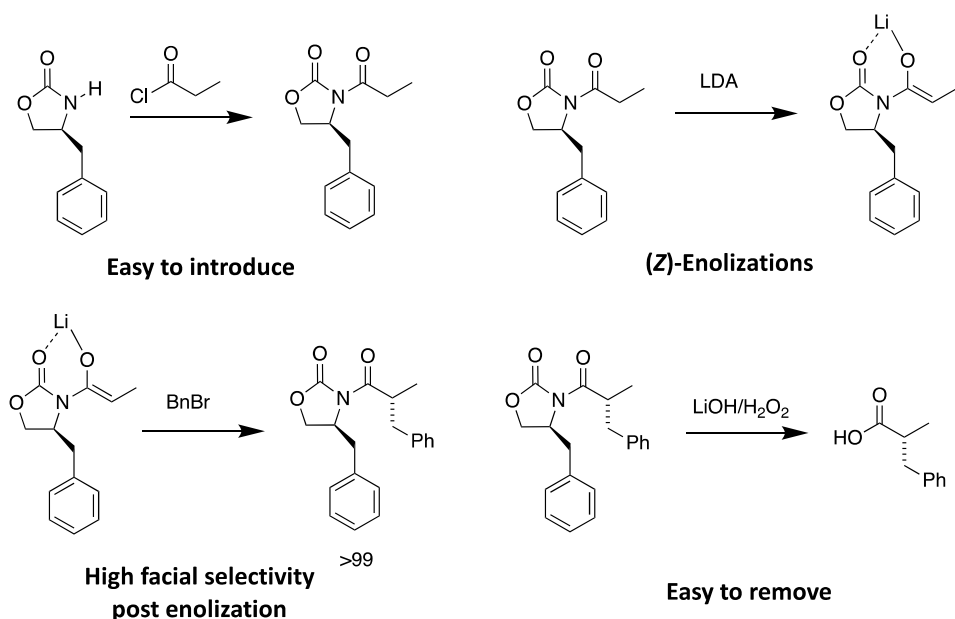
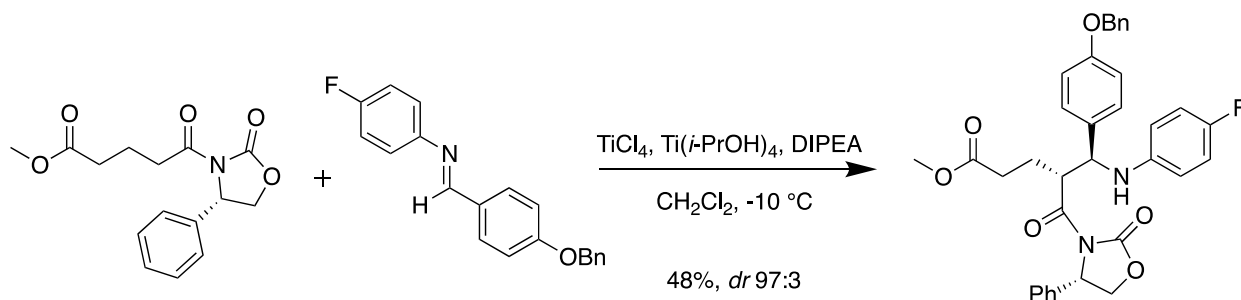


Figure 3-17 Oxazolidinone auxiliaries are the gold standard in chiral auxiliaries

Dr. Reddy's Laboratories, a pharmaceutical company in India, used chiral oxazolidinone chemistry to set the stereochemistry in a Mannich reaction towards the process scale synthesis of the anti-hypercholesterolemia drug, Ezetimibe (Scheme 3-13).<sup>185</sup> The reaction was performed on a 100-gram scale to provide product in 48% yield with *dr* 97:3.

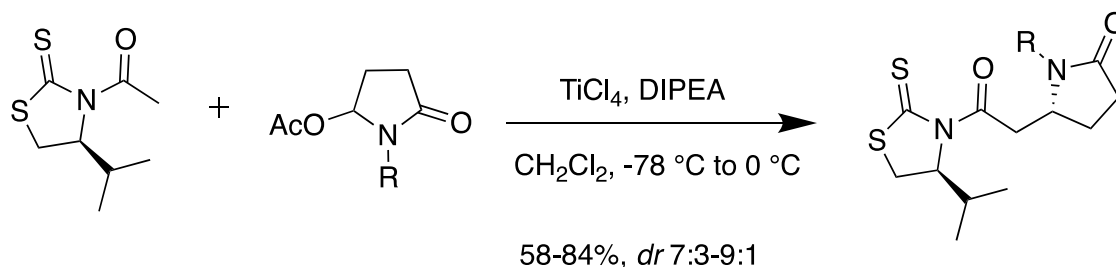


Scheme 3-13 Praveen et al. Mannich reaction with chiral phenyl-substituted oxazolidinone<sup>185</sup>

The Olivo group at the University of Iowa reported the Mannich type addition of a carbonyl compound bearing a thiazolidine auxiliary to *in situ* prepared *N*-substituted *N*-acyl iminium ions (Scheme 3-14).<sup>186</sup> A group of six imines provided the *anti*-product in modest yields and a *dr* from

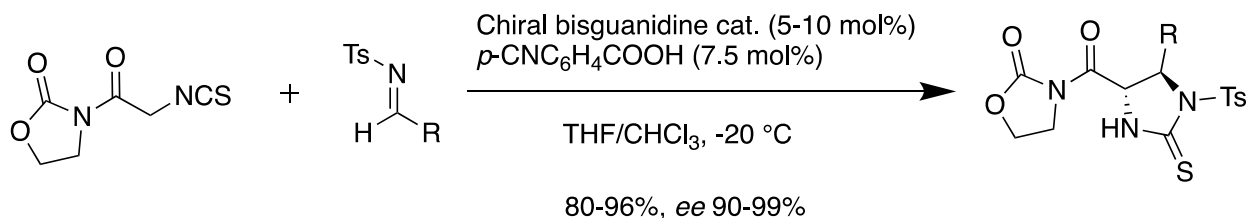


7:3 to 9:1. The investigators proposed a reaction mechanism that proceeded through an open antiperiplanar transition state.



**Scheme 3-14** Olivo et al. Mannich reaction with chiral thiazolidine auxiliary<sup>186</sup>

The Feng group at Sichuan University used an achiral oxazolidinone substituted isothiocyanate in a Mannich-type reaction with various sulfonyl imines (Scheme 3-15).<sup>197</sup> The phenyl imines all proceeded in >80% yield, and *ee* 90-99%. The reaction was catalyzed by a chiral bisguanidine derived from benzene-1,3-diamine. The Brønsted basicity of the guanidine was critical for initial activation of the isothiocyanate. The additive 4-cyanobenzoic acid provided an incremental improvement in enantioselectivity. This was hypothesized to occur by acid protonation of the guanidine catalyst to form a guanidinium salt which in turn activated the tosyl protected imine through H-bonding interactions.



**Scheme 3-15** Feng et al. Mannich reaction with achiral unsubstituted oxazolidinone<sup>197</sup>

The Praveen, Olivo, and Feng groups have demonstrated that with proper reaction conditions, oxazolidinone auxiliaries can direct highly stereoselective Mannich reactions. We hypothesized that this control would translate to vinylogous Mannich reactions. Specifically, we believed the incorporation of Evans' oxazolidinone auxiliary onto our nucleophile could improve

enantiomeric outcome in an asymmetric reaction or more ambitiously diastereomeric outcome in a double asymmetric reaction.

Double asymmetric reactions are controlled by two chiral sources.<sup>198</sup> The chiral sources can be two chiral substrates that combine in such a way to form a new stereogenic center or one chiral substrate and one prochiral substrate that utilize a chiral reagent to generate a new stereogenic center in the product (Figure 3-18).

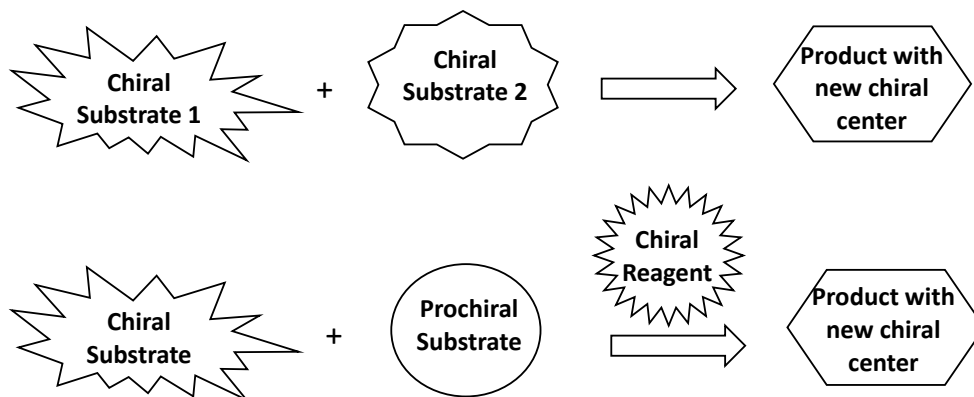
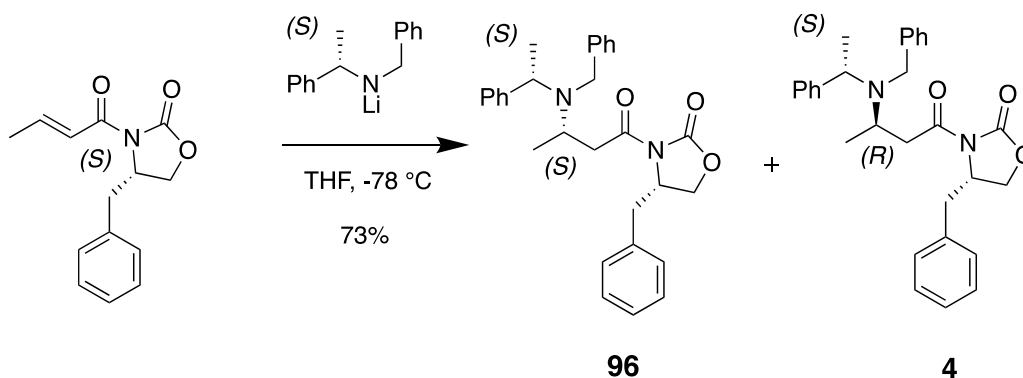


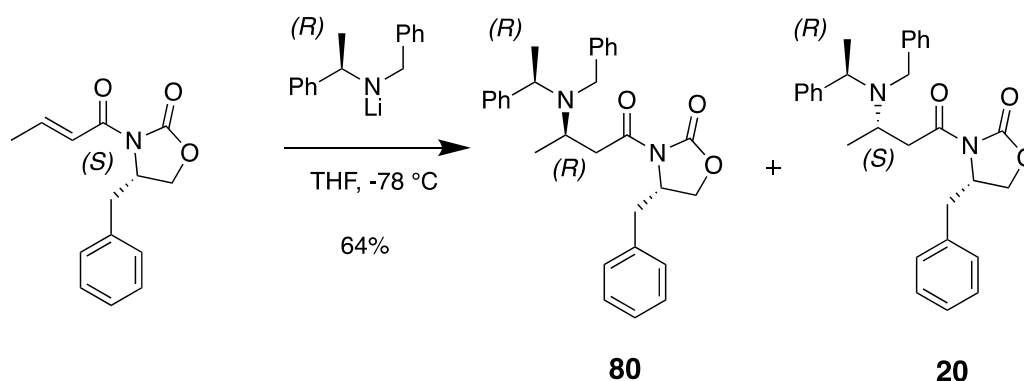
**Figure 3-18 Double asymmetric reaction to form product with new stereogenic center**

The Davies group at the University of Oxford has examined double asymmetric reactions between two chiral substrates. In 2010, they disclosed the double diastereoselective addition of enantiopure lithium amines to chiral oxazolidinones (Figure 3-19).<sup>199</sup> In a representative example, (*S,E*)-4-benzyl-3-(but-2-enoyl)oxazolidin-2-one formed a matched pair with lithium (*S*)-*N*-benzyl-*N*-( $\alpha$ -methylbenzyl)amine to provide the major (*S,S*)-enantiomer with a *dr* 96:4. With the mismatched (*R*)-lithium amine, the major product was the (*R,R*)-enantiomer with a *dr* of 80:20. The (*S*)-oxazolidinone, (*R*)-amine system was determined to be the mismatched pair because of the reduction in overall *dr*. When the (*S*)-oxazolidinone was reacted with an achiral Li-amine, the major product was the (*S*)-enantiomer with an *er* 76:24, indicating that the double asymmetric catalytic system provided a distinct advantage. The group did not report selectivity when only a chiral Li-amine was used.

### Matched



### Mismatched



### Oxazolidinone Substrate Controlled

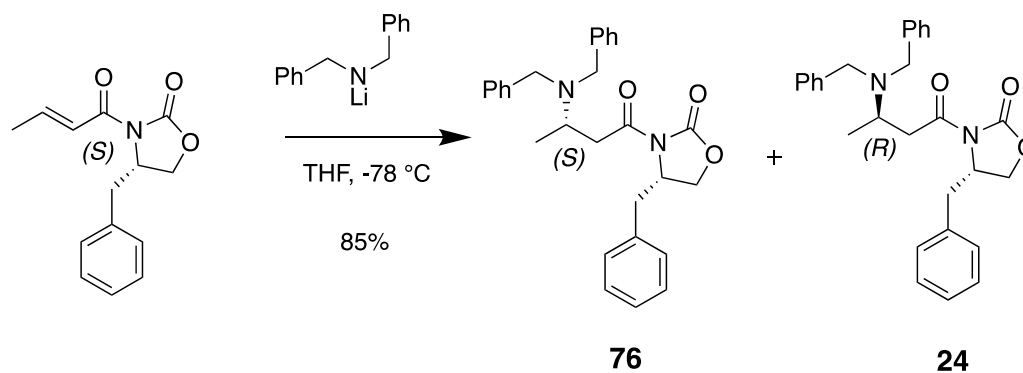


Figure 3-19 Analysis of matched/mismatched product outcome in a conjugate addition reaction<sup>199</sup>

While some matched-mismatched pairs result in equally high yielding reactions, albeit with lower *dr*, this is not always the case. Work by Fernandez-Mayoralas and Houk investigating aldol reactions of an  $\alpha$ -chiral azide-substituted aldehyde, ketone, and chiral proline catalyst resulted in a 5-membered ring azasugar in 60% yield (*dr* >20:1) in the matched scenario and only a 10% yield (*dr* 5:1) in the mismatched scenario.<sup>200</sup>

An advantage of double asymmetric reactions is that the diastereomeric ratio can often be improved by chromatography. In many cases, the desired diastereomer can be purified from the undesired diastereomer through silica gel chromatography to enhance the overall *dr*.<sup>201</sup> This type of separation is not possible with enantiomers.

Although Evans' oxazolidinone auxiliaries have not been used in vinylogous Mannich reactions, we were encouraged by the reactivity and stereocontrol in Mannich reactions. Chiral appendages of various sizes and flexibilities at the 4-position or 5-position of the oxazolidinone can be screened in order to optimize the selectivity. We also hypothesized that the carbonyl group of the oxazolidinone may coordinate more strongly than the pyrazole to copper(I), stabilizing the enolate and allowing for greater control of the enantio- or diastereochemical outcome. With the right substituent we believed the auxiliary would be sufficiently bulky to block  $\alpha$ -attack.

## 3.2 Results and Discussion

### 3.2.1 Synthesis of JP4-039 Through a Vinylogous Mannich Reaction with a Pyrazole

#### Auxiliary

We designed a new synthesis of JP4-039 with a vinylogous Mannich reaction as the key transformation. In a retrosynthetic analysis from JP4-039, we envisioned three requisite transformations: a direct (or indirect) amide coupling, isomerization of the backbone double bond from a  $\beta,\gamma$ -unsaturated carbonyl compound to  $\alpha,\beta$ -unsaturated carbonyl compound, and a carbon-carbon bond forming vinylogous Mannich reaction (Figure 3-20). Before exploring oxazolidinone auxiliaries, we first set out with a proof of concept synthesis of JP4-039 using the same pyrazole auxiliary with which the Yin group had success.<sup>161</sup>

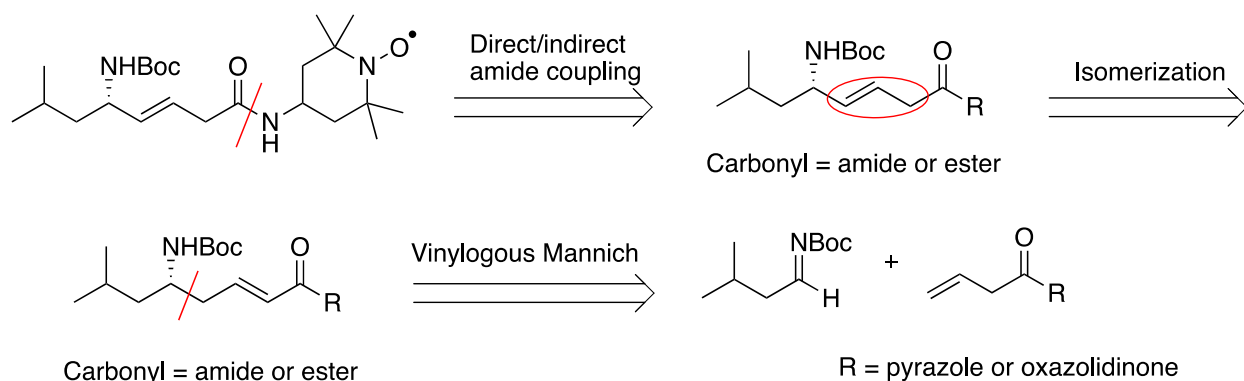
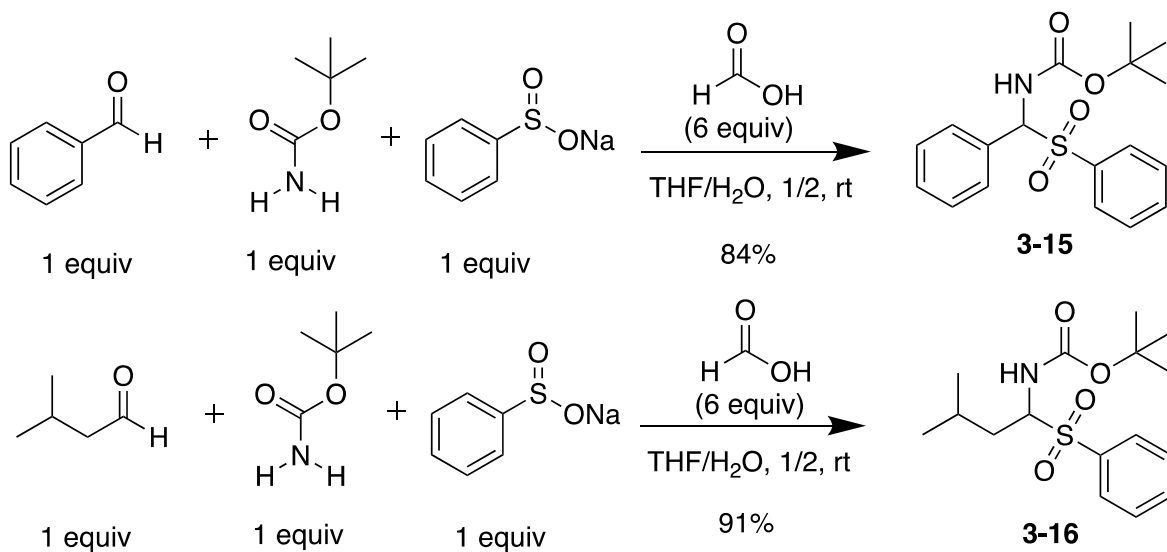


**Figure 3-20 Retrosynthetic analysis of JP4-039**

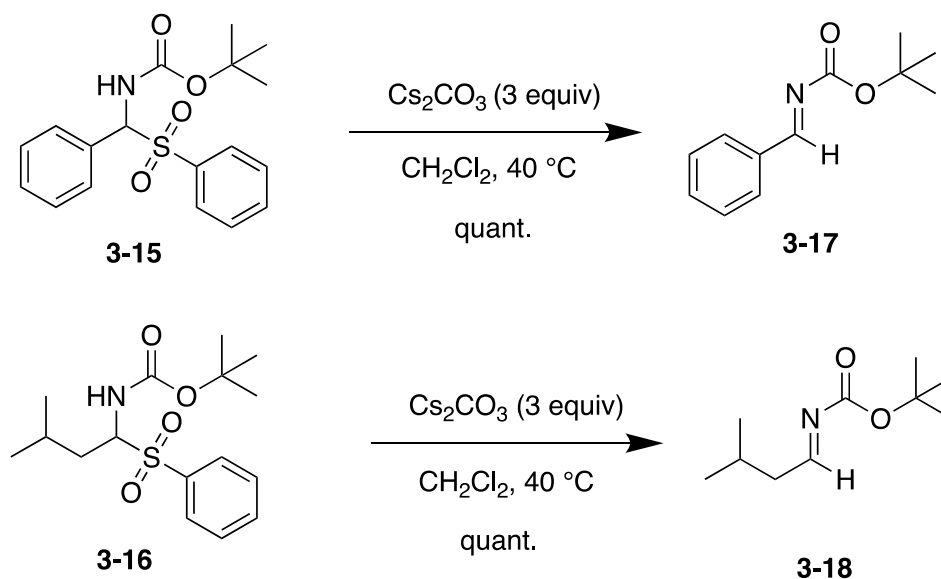
The formation of protected imines is not a trivial step. *N*-Boc protected alkyl substituted imines, especially, are highly prone to decomposition even upon exposure to room temperature for a few minutes.<sup>202</sup> We began with the synthesis of sulfone **3-15** from benzaldehyde, *t*-butyl carbamate, and sodium benzenesulfinate under acidic conditions in good yields (Scheme 3-16).<sup>203</sup> This procedure was also amenable for the synthesis of sulfone **3-16** from 3-methylbutanal, *t*-butyl carbamate, and sodium benzenesulfinate.



**Scheme 3-16 Synthesis of sulfones 3-15 and 3-16**

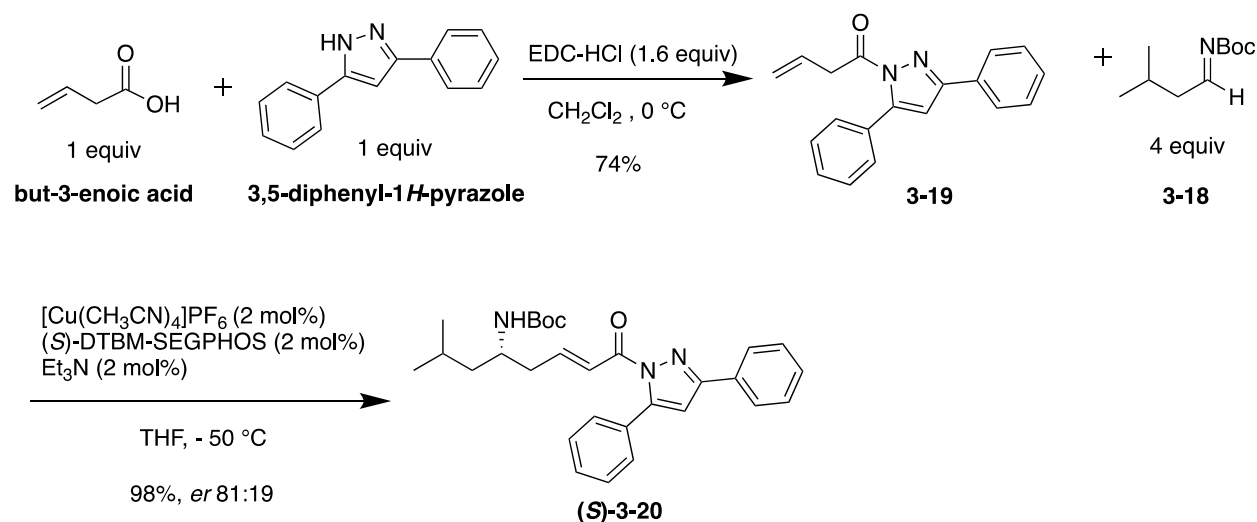
Following protocols similar to Greene and Shibasaki,<sup>204-205</sup> exposure of sulfone **3-15** to cesium carbonate at reflux or at room temperature in CH<sub>2</sub>Cl<sub>2</sub> for extended periods of time (4-5 h)

led to inconsistent product formation, most often contaminated with large amounts of benzaldehyde. There have been multiple reports that even trace impurities from the imine formation step can suppress reactivity in subsequent reactions.<sup>206</sup> We tried including magnesium sulfate (MgSO<sub>4</sub>) as a drying reagent in the reaction, but that did not improve reproducibility or the reaction profile. A report from Pihko in 2014 noted the use of Hyflo® Super Cel® as the filter aid in the reaction.<sup>202</sup> Hyflo® Super Cel® has a pH of 10.0 as a 10% solution in water and a pore size of 7.0 microns.<sup>207</sup> Our previous trials involved simple filtration through a medium coarse filter frit. The authors noted that, in their hands, this type of filtration resulted in isomerization of the imine and dimerization. Based on this report, sulfone **3-15** and cesium carbonate were dried under high vacuum for 1 h, stirred for 45 min at 40 °C in CH<sub>2</sub>Cl<sub>2</sub>, and filtered through a plug of Hyflo® Super Cel® two times (Scheme 3-17). <sup>1</sup>H NMR indicated that the formation of imine **3-17** was clean without any dimerization or decomposition. This pre-drying/filtration protocol was also compatible with alkyl substituted sulfone **3-16** to provide imine **3-18** without decomposition or isomerization to the enamine (Scheme 3-17). This two-step sequence (synthesis of sulfone and conversion to imine) was later used to synthesize a selection of imines.



**Scheme 3-17** Synthesis of aryl- or alkyl-substituted Boc-protect imines

With a reliable synthesis of protected imines, we first set out to see if we could use the methodology developed by the Yin group in 2017 with a  $\beta,\gamma$ -unsaturated pyrazole amide to synthesize the backbone of JP4-039 (Scheme 3-18).<sup>161</sup>  $\beta,\gamma$ -Unsaturated carbonyl compound **3-19** was formed through an EDC coupling of but-3-enoic acid with 3,5-diphenyl-1*H*-pyrazole in 74% yield. A freshly prepared *N*-Boc protected *i*-butyl substituted imine **3-18** was reacted with **3-19** in the presence of base ( $\text{Et}_3\text{N}$ ) and the pre-formed catalyst solution of (*S*)-DTBM-SEGPHOS and  $[\text{Cu}(\text{CH}_3\text{CN})_4]\text{PF}_6$  at  $-50\text{ }^\circ\text{C}$  to form the vinylogous Mannich product (*S*)-**3-20** in 98% yield with an *er* of 81:19 determined by chiral HPLC analysis (Scheme 3-18). The pyrazole auxiliary was highly activating and sufficiently bulky to allow for selective  $\gamma$ -attack. The bulky copper catalyst system also contributed to selective  $\gamma$ -attack; however, the *er* was lower than the authors' report of 92:8 with the leucine substituted imine.



**Scheme 3-18 Vinylogous Mannich reaction with pyrazole auxiliary to form JP4-039 backbone**

We attempted to optimize the formation of vinylogous Mannich product **3-20** (Table 3-1). After 4.5 h at  $-40\text{ }^\circ\text{C}$  with 2% catalyst loading we obtained 90% of the desired product with an *er* of 80:20 (entry 1). Longer reaction times at a slightly lower temperature of  $-50\text{ }^\circ\text{C}$  increased the yield slightly to 98% but did not improve the selectivity (entry 2). We increased the catalyst loading in an attempt to improve the *er*, but an increase from 2% to 5% did not enhance the selectivity (entry 3). Despite maintaining nearly quantitative conversion and excellent

regioselectivity, the reaction was very temperature sensitive, perhaps contributing to why we were not able to achieve an *er* of >9:1.

**Table 3-1 Vinylogous Mannich reaction optimizations with (S)-DTBM-SEGPBOS<sup>a</sup>**

Entry	Catalyst loading (%)	Temperature (°C)	Time (h)	Yield (%) <sup>b</sup>	<i>er</i> <sup>c</sup>
1	2	-40	4.5	90	80:20
2	2	-50	17.5	98	81:19
3	5	-50	18	98	78:22

<sup>a</sup>Conditions: **3-19** (1 equiv), **3-18** (4 equiv), THF, (S)-DTBM-SEGPBOS, [Cu(CH<sub>3</sub>CN)<sub>4</sub>]PF<sub>6</sub>, Et<sub>3</sub>N (ligand, Cu, and Et<sub>3</sub>N all 2 mol% or all 5 mol%)

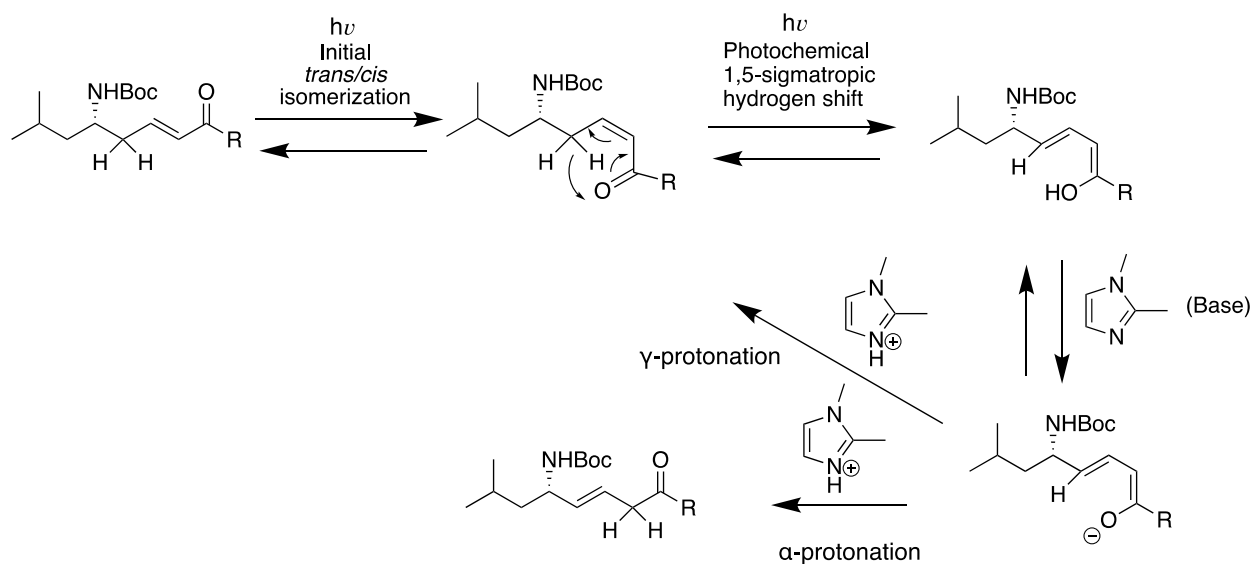
<sup>b</sup>Isolated yield

<sup>c</sup>Determined by chiral HPLC

Although the *er* was not as high as anticipated, we proceeded with our synthesis of JP4-039 as a proof of principle of the methodology originating from the vinylogous Mannich reaction of amides. From the vinylogous Mannich product there were two key steps remaining to obtain the final compound: an isomerization from the conjugated to the skipped alkene and coupling to 4-AT (directly or indirectly through saponification). Our initial approach was to isomerize and then couple to 4-AT. We first attempted a base mediated isomerization with LiOH saponification conditions; we had success synthesizing analogs of JP4-039 with this methodology previously. However, under these conditions we saw a trace to no conversion and partial loss of the pyrazole functionality that complicated the reaction profile. We next used a protocol from a 1985 paper that disclosed the photochemical deconjugation of  $\alpha,\beta$ -unsaturated esters to their  $\beta,\gamma$ -unsaturated isomers.<sup>208</sup> In the presence of the weak base, 1,2-dimethylimidazole, a wide range of substrates underwent isomerization under mercury lamp irradiation. The protocol from Duhaime et al. was shown to be applicable on multi-gram scale reactions. For our substrate, we envisioned an initial *trans/cis* isomerization of the vinylogous Mannich product (Scheme 3-19). The isomerization sets up a photochemical 1,5-sigmatropic hydrogen shift to the enol. The base serves as a proton shuffle, deprotonating the hydroxy group and reprotonating the  $\alpha$ -position. If reprotonation occurs at the  $\gamma$ -position, then the cycle continues.  $\alpha,\beta$ -Unsaturated esters typically possess strong absorption



bands in the 220-250 nm region while the  $\beta,\gamma$ -unsaturated isomers do not absorb strongly above 220 nm, so with the proper lamp, the reaction is non-reversible.<sup>208</sup>

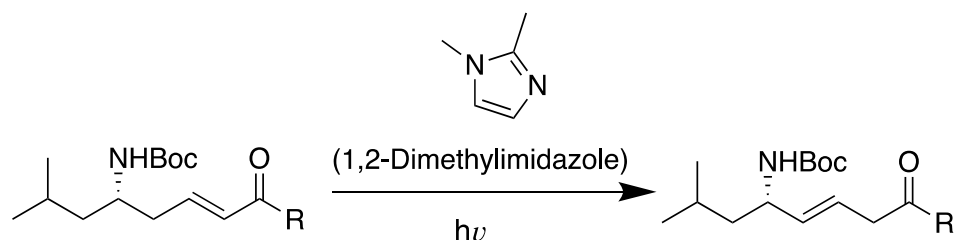


**Scheme 3-19 Proposed photochemical isomerization mechanism**

We believed these conditions would be feasible on our system, but we needed to determine what species would be most amenable to the transformation (Table 3-2). First, we tried to directly isomerize **3-20**. We thought the pyrazole substrate may be sufficiently basic to catalyze the reaction without the addition of 1,2-dimethylimidazole. However, it did not catalyze the reaction; rather we saw loss of the pyrazole moiety in both methanol and *t*-butylmethylether (TBME) solvents (entries 1, 2). Inclusion of the weak base 1,2-dimethylimidazole also did not improve the reaction profile (entry 3). Since the pyrazole functionality has a strong UV absorbance, we hypothesized that it may be a liability for the photochemical process. Accordingly, **3-20** was converted to corresponding methyl ester **3-21** in 82% yield by stirring in methanol at 60 °C for 18 h.<sup>161</sup> Encouragingly, with the methyl ester derivative we were able to obtain the desired  $\beta,\gamma$ -unsaturated isomer in 36% yield after purification of the 5:1 - *trans*:*cis* isomer mixture (entry 4). The ratio of *trans*:*cis* isomers was determined by <sup>1</sup>H coupling constants and integration of the alkene peaks. We analyzed these three species by UV-Vis spectroscopy and, as proposed by Duhaime, only the  $\alpha,\beta$ -unsaturated ester **3-21** showed absorbance in the 220-250 nm range; *trans*- and *cis*-isomers **3-23** did not have absorbance in this region. If desired, we could re-subject the

*cis*-isomer to the photochemical isomerization conditions, but, on a small scale, this yield was satisfactory. To obtain JP4-039, we had to convert the methyl ester to the carboxylic acid before coupling to 4-AT. With a goal of reducing the total number of steps, we speculated we could convert **3-20** to a species amenable for direct coupling with 4-AT following isomerization. Several groups have demonstrated the direct conversion of activated esters to amides.<sup>209</sup> Therefore, **3-20** was stirred in 2,2,2-trifluoroethanol for 7 h at 75 °C to provide activated ester substrate **3-22** in 84% yield. Under mercury lamp irradiation for 24 h, we obtained isomerized activated ester product **3-24** in 34% yield after purification of the 5:1 – *trans*: *cis* isomer mixture (entry 5). Overall, however, photochemical isomerization conditions proved time intensive and did not provide a high yield of  $\beta,\gamma$ -unsaturated product (without requiring re-subjection of the *cis*-isomer).

**Table 3-2 Photochemical isomerization substrates and conditions<sup>a</sup>**



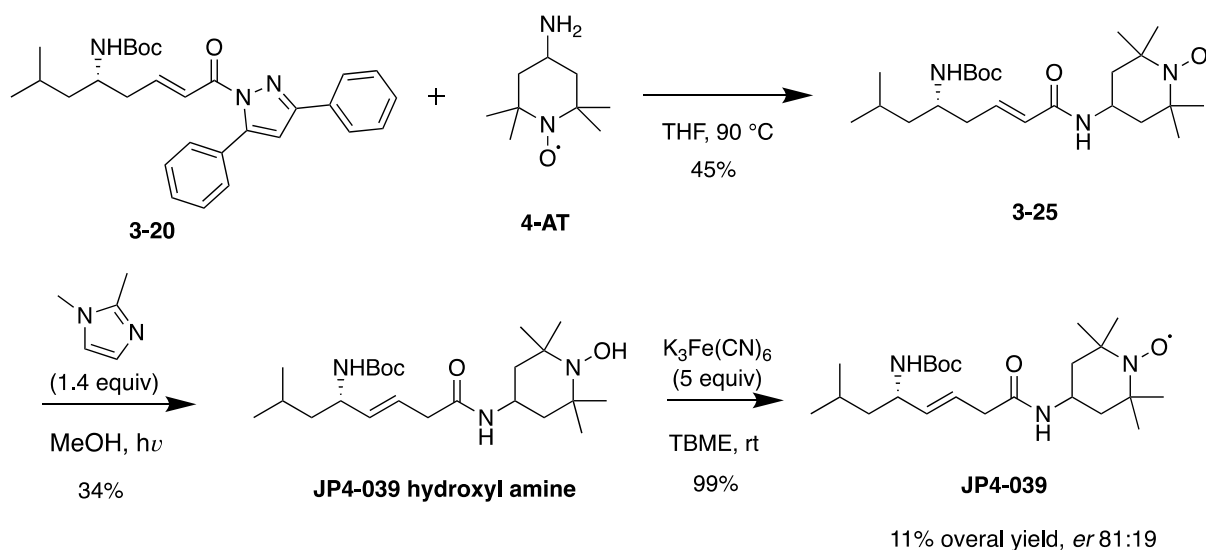
Entry	Starting Material	R	1,2-Dimethylimidazole (equiv)	Solvent	Result <sup>b</sup>
1	<b>3-20</b>	3,5-Diphenyl-1 <i>H</i> -pyrazole	0	MeOH	No isomerization, loss of pyrazole, decomposition
2	<b>3-20</b>	3,5-Diphenyl-1 <i>H</i> -pyrazole	0	TBME	No isomerization, loss of pyrazole, decomposition
3	<b>3-20</b>	3,5-Diphenyl-1 <i>H</i> -pyrazole	1.4	MeOH	Trace isomerization, loss of pyrazole
4	<b>3-21</b>	OMe	1.4	MeOH	36% Desired <i>trans</i> isomer, <b>3-23</b> 5:1 - <i>trans</i> : <i>cis</i> ratio
5	<b>3-22</b>	OCH <sub>2</sub> CF <sub>3</sub>	1.4	MeOH	34% Desired <i>trans</i> isomer, <b>3-24</b> 5:1 – <i>trans</i> : <i>cis</i> ratio

<sup>a</sup>Conditions: quartz reaction flask, 15-low pressure Hanovia mercury lamps, 0.1 M, 23 h

<sup>b</sup>Isolated yield

Simultaneously, we explored isomerization conditions of the vinylogous Mannich product **3-20**, and evaluated direct coupling reactions of **3-20** to 4-AT (Scheme 3-20). Conventional heating at 90 °C with 2 equiv of 4-AT provided a 1:2 ratio of product:SM, but the reaction seemed to stall as reaction times >24 h did not promote additional conversion. The addition of DMAP also did not improve the conversion. However, we were able to obtain 45% of the desired coupled product **3-25** through microwave heating conditions with 4 equiv of 4-AT at 90 °C in THF for 1 h. Since the starting material was entirely consumed, we believe the lower yield was a result of a retro-Mannich process. We investigated catalytic conditions for the coupling that would be milder and possibly promote a clean reaction. Unfortunately, boric acid<sup>210</sup>, scandium triflate<sup>211</sup>, and iron(III) nitrate<sup>212</sup> did not provide sufficient conversion to **3-25** at temperatures below 60 °C.

We used the most promising isomerization conditions developed to synthesize JP4-039 (Scheme 3-20). With 1,2-dimethylimidazole (1.4 equiv) in methanol under mercury lamp irradiation for 24 h, we were able to isolate JP4-039 as the hydroxylamine species in 34% yield. Irradiation in the presence of weak base at least partially converted the 4-AT radical to the hydroxylamine. Fortunately, we were able to oxidize the hydroxyl amine to **JP4-039** with 5 equiv of potassium ferricyanide at rt for 2.5 h in quantitative yield (Scheme 3-20).<sup>213</sup>



**Scheme 3-20** Coupling of vinylogous Mannich product to 4-AT and isomerization/oxidation to JP4-039

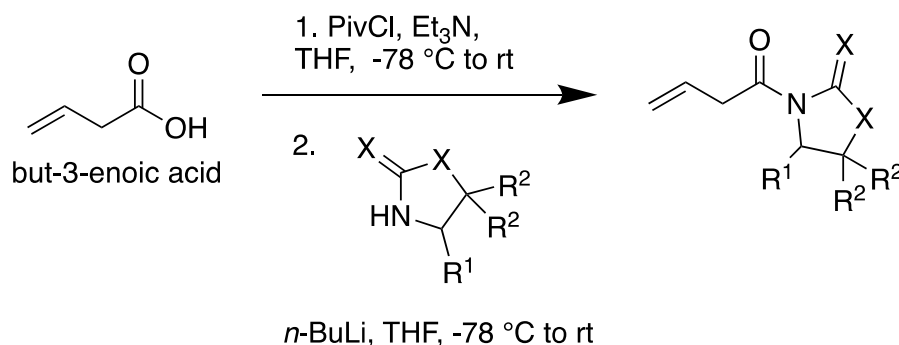
We attempted to convert **3-25** to the hydroxylamine prior to isomerization. We hypothesized that this would improve the overall yield. We suspended the crude reaction product **3-25** in various reducing agents, including sodium dithionite ( $\text{Na}_2\text{S}_2\text{O}_4$ )<sup>214</sup>, a solution of zinc and ammonium chloride ( $\text{Zn}/\text{NH}_4\text{Cl}$ )<sup>215</sup>, and ascorbic acid.<sup>79</sup> However, we were not able to see full conversion to the hydroxylamine.

With a pyrazole amide starting material we achieved proof of concept that a vinylogous Mannich reaction could be used to synthesize JP4-039 in 5 linear steps with 11% overall yield and *er* 81:19. The yield and selectivity were both reduced compared to the previous synthesis which was completed in 53% overall yield with *er* >99:1. The advantage of the vinylogous Mannich route is that it did not require moisture or air sensitive reagents. The use of pyrophoric or toxic chemicals was also not necessary. We hypothesized that the double bond isomerization protocol and the selectivity of the vinylogous Mannich reaction could improve through incorporation of an oxazolidinone nucleophile chiral auxiliary. The chiral auxiliary would provide a second source of stereochemical control for the vinylogous Mannich reaction and would allow us to investigate subsequent isomerization/alkylations controlled by the auxiliary. Arguably, this optimization should further facilitate the goal of a rapid synthesis of structurally diverse JP4-039 analogs for the study of ferroptosis.

### 3.2.2 Vinylogous Mannich Reaction with an Oxazolidinone Auxiliary

To investigate the second approach to JP4-039, we synthesized a selection of substituted analogs through a pivaloyl chloride, *n*-butyl lithium coupling reaction (Table 3-3). The auxiliaries included the more traditional Evans auxiliaries: *i*-propyl (entry 1-2), (1*H*-indol-2-yl)methyl (entry 3), and benzyl (entry 4-5). We also explored a much more bulky auxiliary with phenyl groups in the R<sup>2</sup> positions (entry 6) as well as a thiazolidinethione auxiliary introduced by Fujita and Nagao (entry 7), and finally the unsubstituted oxazolidinone (entry 8).

**Table 3-3 Synthesis of oxazolidinone derivatives<sup>a</sup>**



Entry	X	R <sup>1</sup>	R <sup>2</sup>	Product	Yield (%) <sup>b</sup>
1	O	<i>i</i> -Propyl	H	( <i>R</i> )- <b>3-26</b>	47
2	O	<i>i</i> -Propyl	H	( <i>S</i> )- <b>3-26</b>	60
3	O	(1 <i>H</i> -Indol-2-yl)methyl	H	( <i>R</i> )- <b>3-27</b>	74
4	O	Benzyl	H	( <i>R</i> )- <b>3-28</b>	45
5	O	Benzyl	H	( <i>S</i> )- <b>3-28</b>	40
6	O	Benzyl	Phenyl	( <i>R</i> )- <b>3-29</b>	28
7 <sup>c</sup>	S	Benzyl	H	( <i>R</i> )- <b>3-30</b>	66
8	O	H	H	<b>3-31</b>	43

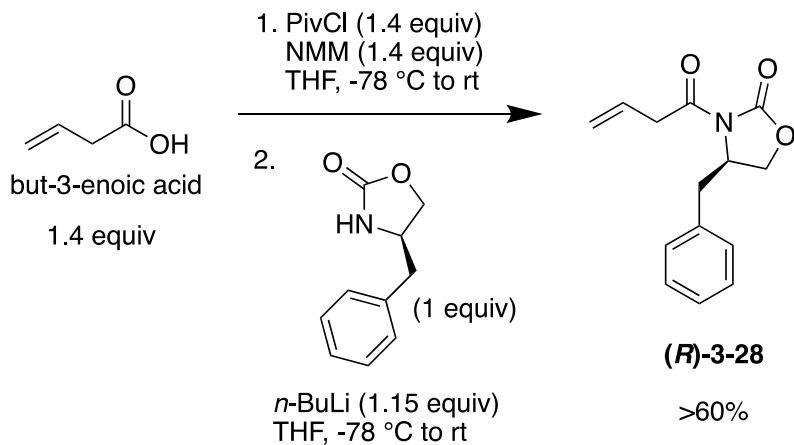
<sup>a</sup>Conditions: oxazolidinone (1 equiv), but-3-enoic acid (1.4 equiv), PivCl (1.4 equiv), Et<sub>3</sub>N (1.4 equiv), *n*-BuLi (1.15 equiv), THF (0.2 M)

<sup>b</sup>Isolated yield

<sup>c</sup>Conditions: oxazolidinone (1 equiv), but-3-enoic acid (1.4 equiv), DCC (1.4 equiv), DMAP (0.1 equiv), CH<sub>2</sub>Cl<sub>2</sub> (0.2 M)

We obtained inconsistent and often lower than expected yields when acylating the auxiliaries because of the formation of an isomerized, conjugated side-product. The conjugated side-product was impossible to separate from the desired product. Similar limitations have been reported for  $\beta,\gamma$ -unsaturated acids in the literature.<sup>216</sup> In these examples, using *N*-methylmorpholine (NMM) as the base, opposed to the more classical base triethylamine, provided exclusively the deconjugated product. NMM is a nucleophilic but weaker base that is often used in peptide coupling reactions because it leads to reduced racemization and isomerization in the activation of acids.<sup>217</sup> The pK<sub>a</sub>'s of protonated triethylamine and protonated NMM are 10.75 and 7.61 respectively.<sup>217</sup> As a weaker base, NMM is less prone to deprotonate the  $\alpha$ -position of the activated carbonyl compound which results in isomerized, conjugated side product. We were able

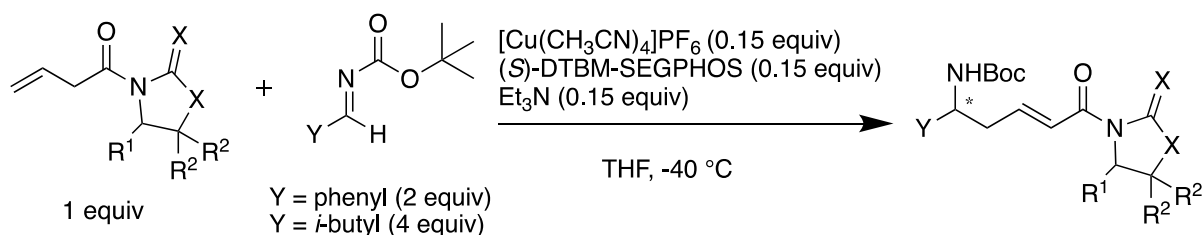
to reproduce the conditions with NMM to obtain  $\beta,\gamma$ -unsaturated amides in consistently higher yields with no isomerized side-product (Scheme 3-21).



**Scheme 3-21** *N*-Methylmorpholine mediated synthesis of  $\beta,\gamma$ -unsaturated oxazolidinone

We evaluated each  $\beta,\gamma$ -unsaturated acyl oxazolidinone using the same reaction conditions as for the pyrazole-substituted derivatives (Table 3-4). With *i*-propyl-substituted oxazolidinone **3-26** and *i*-butyl imine **3-18**, vinylogous Mannich product **3-32** was obtained in 60% yield but with a *dr* of only 60:40 determined by chiral HPLC analysis (entry 1). With the same *i*-butyl imine **3-18**, we observed trace product with (1*H*-indol-2-yl)methyl-substituted compound **3-27** (entry 2) and no product formation with the much more bulky 5,5-diphenyl-4-benzyl-substituted oxazolidinone **3-29** (entry 3). We explored the vinylogous Mannich reaction between the phenyl-substituted imine and thiazolidine substrate **3-30** but only isolated trace amounts of product (entry 4); possibly the sulfur atoms of **3-30** were not favorable for copper coordination. When we switched to the benzyl-substituted auxiliary **3-28** with *i*-butyl imine **3-18**, we obtained 50% of desired vinylogous Mannich product **3-33** with a *dr* 70:30 (entry 5). With phenyl-substituted imine **3-17**, the yield of product **3-34** dropped to 31%, but the *dr* improved to 86:14 as determined by SFC analysis (entry 6). With this encouraging diastereomeric ratio, we pursued further optimization of the benzyl-substituted Evans auxiliary **3-28** in our vinylogous Mannich reaction.

**Table 3-4 Oxazolidinone auxiliary screen in the vinylogous Mannich reaction<sup>a</sup>**



Entry	X	R <sup>1</sup>	R <sup>2</sup>	Y	Yield (%) <sup>b</sup> (product)	<i>dr</i> <sup>c</sup>
1 <sup>d</sup>	O	<i>i</i> -Propyl	H	<i>i</i> -Butyl	60, ( <b>3-32</b> )	60:40
2	O	Indolylmethyl	H	<i>i</i> -Butyl	Trace	NA
3	O	Benzyl	Phenyl	<i>i</i> -Butyl	0	NA
4	S	Benzyl	H	Phenyl	Trace	NA
5	O	Benzyl	H	<i>i</i> -Butyl	50, ( <b>3-33</b> )	70:30
6	O	Benzyl	H	Phenyl	31, ( <b>3-34</b> )	86:14

<sup>a</sup>Conditions: Oxazolidinone (1 equiv), imine (2 or 4 equiv), THF (0.1 M), catalyst solution ((*S*)-DTBM-SEGPHOS, [Cu(CH<sub>3</sub>CN)<sub>4</sub>]PF<sub>6</sub>, Et<sub>3</sub>N) (0.15 equiv)

<sup>b</sup>Isolated yield

<sup>c</sup>Determined by chiral HPLC or SFC

<sup>d</sup>((*S*)-DTBM-SEGPHOS, [Cu(CH<sub>3</sub>CN)<sub>4</sub>]PF<sub>6</sub>) (0.1 equiv), Et<sub>3</sub>N (1.0 equiv)

With (*R*)-benzyl oxazolidinone **3-28**, we screened various ligands, copper sources, additives, the inclusion of water, solvents, and reaction temperatures without significant improvement in yield or diastereomeric outcome. For example, increasing catalyst loading from 0.15 equiv to 0.25 equiv was slightly beneficial for the yield.

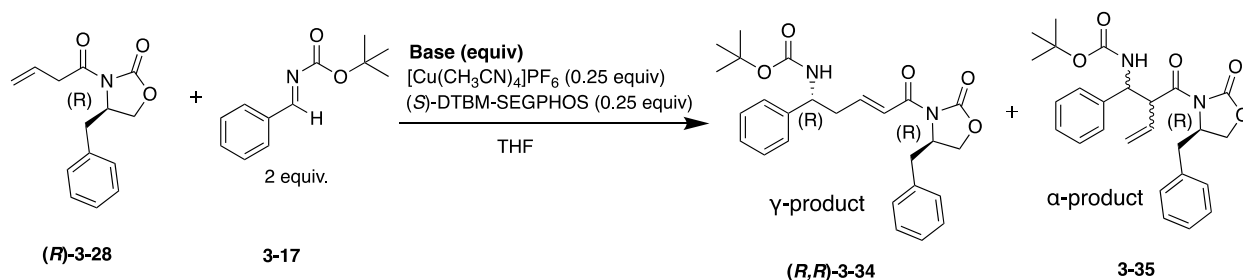
One key finding was that only the very bulky DTBM-SEGPHOS ligand efficiently catalyzed the reaction. We hypothesized that the reactivity was dependent on more than just ligand dihedral- and bite-angle. The Liu group at the University of Pittsburgh and the Buchwald group at MIT recently reported the success of the DTBM-SEGPHOS ligand in the hydroamination of unactivated olefins.<sup>218-219</sup> Through experimental calculations they confirmed that stabilizing, “through space” ligand-substrate interactions ( $\Delta E_{\text{int-space}}$ ) were responsible for the difference in reactivity of substrates with DTBM-SEGPHOS versus the less bulky SEGPHOS ligand. Dispersion interactions between the *t*-butyl groups of the ligand and the alkyl substituents on the olefin substrates were weakly stabilizing and the additive effects of these ~1 kcal/mol stabilizations

significantly increased the reaction rate. All of the “through bond” ( $\Delta E_{\text{int-bond}}$ ) interactions for DTBM-SEGPPOS and SEGPPOS were nearly identical and thus did not contribute to the reactivity difference.<sup>218</sup> We hypothesized that our system could benefit from these “through space” interactions. Unique London dispersion interactions between the bulky DTBM-SEGPPOS ligand and oxazolidinone nucleophile lower the activation barrier leading to increased product formation as compared to less sterically demanding ligands.

While most reaction parameter optimizations were unsuccessful, a small screen of bases was beneficial (Table 3-5). Standard conditions with Et<sub>3</sub>N (0.15 equiv) provided vinylogous Mannich product (***R,R***)-**3-34** in 31% yield (entry 1). When Et<sub>3</sub>N was increased to 0.45 equiv, we did not see a corresponding increase in conversion (entry 2). With the success of NMM as a base in the auxiliary coupling reaction, we used it in the vinylogous Mannich reaction at -20 °C but only obtained 16% of desired product (***R,R***)-**3-34** (entry 3). Neither did the strong base DBU (pKaH 12) nor less basic pyridine (pKaH 5.2) catalyze the reaction (entries 4-5). Next, we switched to 1,4-diazabicyclo[2.2.2]octane (DABCO) which was shown to be selective in a vinylogous Aza-Morita-Baylis-Hillman with Boc protected imines.<sup>220</sup> DABCO is a cyclic, tertiary amine that is highly nucleophilic. Protonated DABCO has a pKaH of 8.8 making DABCO a weak base, however, the two nitrogen atoms of DABCO lead to unique properties including that of an uncharged supernucleophile.<sup>221</sup> With DABCO (0.15 equiv) at -40 °C, we obtained product (***R,R***)-**3-34** in 34% yield and a much cleaner overall reaction profile; the pKaH of 8.8 was sufficient for the required  $\alpha$ -deprotonation (entry 6). We increased the equivalents of DABCO to 0.5 and 1.0 equivalents at -20 °C (entries 7-8) and observed improved results with DABCO (0.5 equiv) as the yield was improved to 58%. Interestingly, when we switched to the very strong, non-nucleophilic phosphazene bases P4-*t*-Bu (entry 9) and P2-*t*-Bu (entry 10), we obtained the  $\alpha$ -addition product **3-35** in greater than 50% yield.<sup>222</sup>



**Table 3-5 Base screen for the vinylogous Mannich reaction between 3-28 and 3-17<sup>a</sup>**



Entry	Base	Base equiv	Temp (°C)	(R,R)-3-34 yield (%)	3-35 yield (%)
1	Et <sub>3</sub> N	0.15	-40	31	-
2	Et <sub>3</sub> N	0.45	-40	30	-
3	NMM	0.15	-20	16	-
4	DBU	0.15	-40	-	-
5	Pyridine	0.15	-40	-	-
6	DABCO	0.15	-40	34	-
7	DABCO	0.50	-20	58	-
8	DABCO	1.0	-20	39	-
9	P4- <i>t</i> -Bu	0.50	-20	-	50
10	P2- <i>t</i> -Bu	0.50	-20	-	53

<sup>a</sup>Conditions: **(R)-3-28** (1 equiv), **3-17** (2 equiv), **(S)-DTBM-SEGPHOS** (0.25 equiv), **[Cu(CH<sub>3</sub>CN)<sub>4</sub>]PF<sub>6</sub>** (0.25 equiv), base (equiv), THF (0.1 M)

<sup>b</sup>Isolated yield

The optimal conditions for the reaction were two equivalents of imine **3-17**, a catalyst system of **DTBM-SEGPHOS** (0.25 equiv) and **[Cu(CH<sub>3</sub>CN)<sub>4</sub>]PF<sub>6</sub>** (0.25 equiv), **DABCO** (0.5 equiv), and **THF** (0.1 M) at -20 °C for 5 h. Previously, reaction times were >15 h, but with these optimized conditions we found that the reaction was complete in less than five hours.

After determining the optimized conditions, we performed a systematic analysis of the reaction outcome to determine if the double asymmetric reaction was more selective than the single asymmetric reaction.

A double asymmetric synthesis reaction can be analyzed mathematically. Masamune proposed that the degree of asymmetric induction obtained in double asymmetric reaction is approximated as  $(a \times b)$  in a matched pair and  $(a / b)$  in a mismatched pair where  $a$  and  $b$  are the individual diastereoselectivities for each of the chiral reactants.<sup>198</sup> This equation was later fully derived by Nakayama.<sup>223</sup> Noteworthy, this equation is valid in a qualitative sense for reaction design. There are eight total reactions that can be considered in the analysis (Figure 3-21). In consideration is the following scenario: 1) a substrate that exists in (*S*)-X and (*R*)-X enantiomeric forms along with a closely related achiral form X; 2) a prochiral substrate, Y; and 3) a reagent that exists in (*S*)-Z and (*R*)-Z enantiomeric forms along with a closely related achiral form Z. For the single asymmetric reactions, product formation can be controlled by the reagent (Figure 3-21 A) or by the substrate (Figure 3-21 B). Control by the reagent leads to two major enantiomeric products. Control by the substrate leads to two major diastereomeric products; the other two possible diastereomeric products will be minor. For the double asymmetric reactions, both the chirality of the reagent and chirality of the substrate control the stereochemical outcome (Figure 3-21 C). From four reaction combinations, four possible diastereomeric products can form as the major product. The diastereomeric outcome from the single asymmetric substrate-controlled reactions will most often be different from the diastereomeric outcome of the double asymmetric reactions.

Major products					
<b>A</b>	Single asymmetric reagent controlled reactions	X + Y	(S)-Z	(S)-XY	2 Enantiomeric products
			(R)-Z	(R)-XY	
<b>B</b>	Single asymmetric substrate controlled reactions	(S)-X + Y	Z	(R,S)-XY	2 Diastereomeric products
		(R)-X + Y		(S,R)-XY	
<b>C</b>	Double asymmetric reagent and substrate controlled reactions	(S)-X + Y	(S)-Z	(S,S)-XY	4 Diastereomeric products
		(R)-X + Y		(R,S)-XY	
		(S)-X + Y	(R)-Z	(S,R)-XY	
		(R)-X + Y		(R,R)-XY	

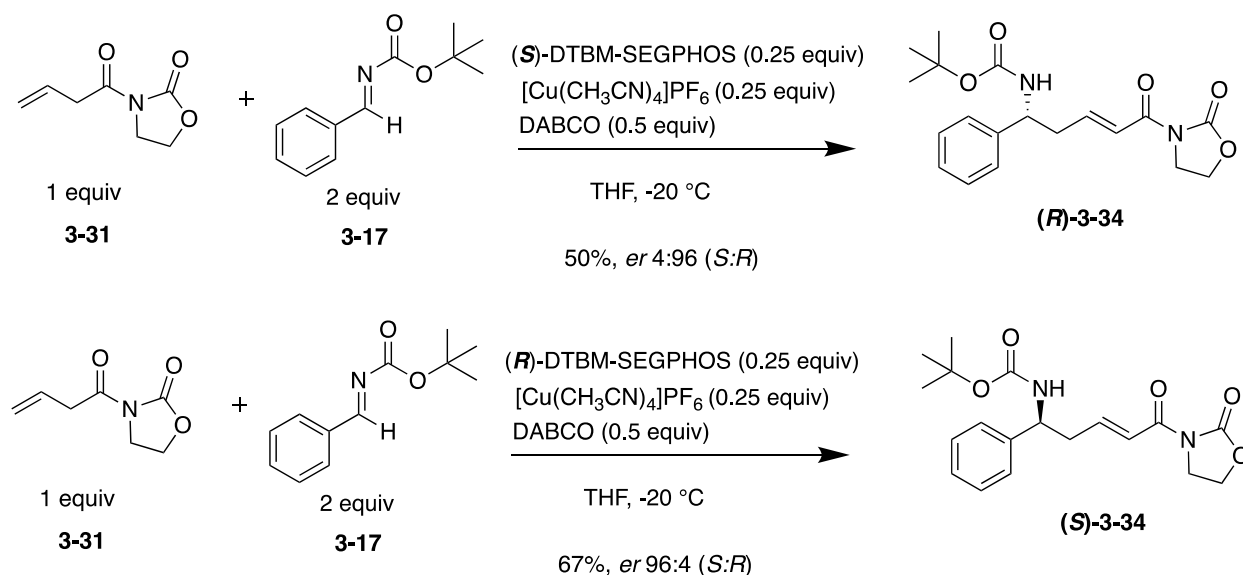
**Figure 3-21 Experimental designs for determining the outcome of a double asymmetric synthesis**

#### methodology

Similar to the scenario in Figure 3-21, our vinylogous Mannich reaction can proceed under single asymmetric control or double asymmetric control. The vinylogous Mannich reaction results in the formation of one new stereogenic center. When an achiral oxazolidinone substrate reacts with a prochiral imine under chiral DTBM-SEGPHOS ligand conditions, two major enantiomeric products can form (reagent control). When a chiral oxazolidinone substrate reacts with a prochiral imine under achiral (or racemic) reagent conditions, two major diastereomeric products can form (substrate control). When a chiral oxazolidinone substrate reacts with a prochiral imine under chiral DTBM-SEGPHOS ligand conditions, four possible diastereomeric products can form as the major product (reagent and substrate control). Based on the classical sense of double asymmetric induction as defined in Figure 3-21, two of these reaction pairs will represent a “matched” case and two will represent a “mismatched” case. A matched case leads to an increase in diastereomeric outcome while a mismatched case results in a decrease in diastereomeric outcome. The mismatched outcome can also manifest itself as a decrease in reaction rate/product formation. It is important to evaluate the single asymmetric induction scenarios for baseline selectivity values to

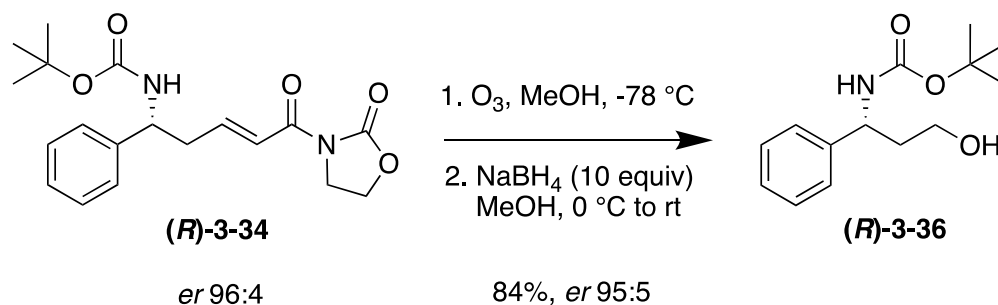
determine if a double asymmetric induction is warranted. Additionally, the selectivity ratios may be used to rationalize the selectivity seen in the double asymmetric induction products.

We analyzed these reactions with Evans' benzyl oxazolidinone and phenyl substituted imine **3-17** (Table 3-6). First, we considered the single asymmetric reactions. With unsubstituted oxazolidinone **3-31**, the (*S*)-ligand provided the (*R*)-product with an *er* of 4:96 (*S*:*R*) while the (*R*)-ligand provided the (*S*)-product with an *er* of 96:4 (*S*:*R*) as determined by SFC analysis (Entry 1-2) (Scheme 3-22). Both reactions resulted in conversion of starting material to product in >50% yield. The remaining mass balance was recovered starting material. There was no evidence of  $\alpha$ -addition by  $^1\text{H}$  NMR analysis.



**Scheme 3-22** Single asymmetric synthesis reactions controlled by chiral ligand

The absolute configuration was determined by conversion of (*R*)-product (entry 1) to primary alcohol (*R*)-**3-36** by a two-step ozonolysis, reduction sequence and comparison of the specific rotation to the known literature value (Scheme 3-23).<sup>161, 224</sup>



**Scheme 3-23** Determination of absolute configuration of (*R*)-3-34

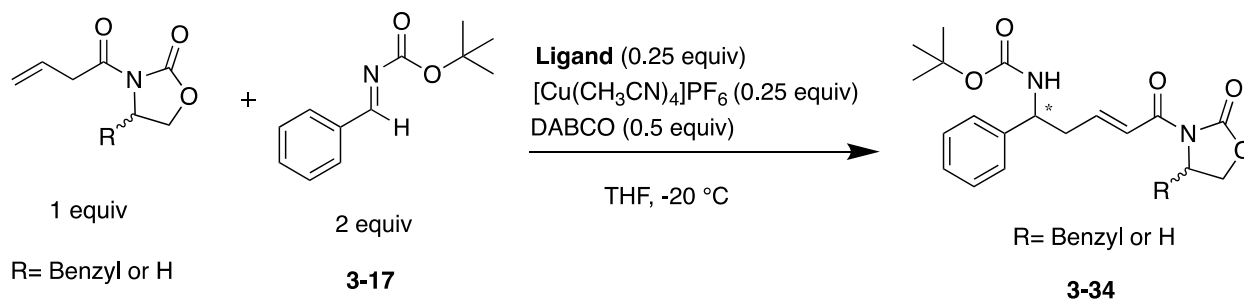
When the ligand rac-BINAP was used and the stereocontrol was provided by the substrate, (*R*)-3-28 or (*S*)-3-28, we obtained products with only 2:1 selectivity (entry 3-4). As a ligand, rac-BINAP should not be compared directly to DTBM-SEGPHOS because of its different size and electronic properties; however, this result indicates that the ligand has a stronger stereochemical control over the reaction compared to the chiral substrate. From the single stereochemical control reactions, we determined that the (*S*)-ligand directs to the (*R*)-product while the (*R*)-ligand directs to the (*S*)-product. These results are consistent to the Yin group's results with the pyrazole auxiliary.<sup>161</sup> We also determined that the (*R*)-oxazolidinone directs preferentially to the (*S*)-product while the (*S*)-oxazolidinone directs preferentially to the (*R*)-product. Taken together, the (*S*)-ligand forms a matched pair with the (*S*)-oxazolidinone and the (*R*)-ligand with the (*R*)-oxazolidinone.

Next, we looked at the double asymmetric synthesis conditions. (*R*)-Oxazolidinone, (*R*)-3-28, and the (*S*)-ligand provided the (*R*)-product with a *dr* of 14:86 (*S*:*R*) (entry 5). The absolute configuration was confirmed by conversion to the primary alcohol as previously described.<sup>161, 224</sup> The (*R*)-oxazolidinone substrate with the (*R*)-ligand provided the (*S*)-product with a slightly lower yield (33%) but with an improved *dr* of 92:8 (*S*:*R*) (entry 6). The same result was achieved with (*S*)-oxazolidinone (*S*)-3-28: an enhanced diastereomeric outcome with the (*S*)-ligand that formed a matched-pair compared to the (*R*)-ligand that formed a mismatched-pair (entry 7-8).

In our system, the ligand provides significantly more control than the substrate. Interestingly, even in the matched-pair double asymmetric reactions, the stereocontrol was reduced compared to the reaction controlled only by the ligand. These results do not conform to Masamune's mathematical analysis because there was not an enhancement in stereocontrol in the double asymmetric reaction. We hypothesized that the flexible chiral appendage on the substrate interferes with the orderly transition state controlled by the ligand. The results where selectivity

was controlled only by the substrate (entry 3-4) confirms that there is interplay between the ligand and chiral auxiliary; the benzyl appendage has some effect on the stereochemical outcome because the product outcome was not racemic. The mismatched-pair occurs when the chiral auxiliary and ligand direct towards different amine stereocenters resulting in a lower selectivity of 86:14 compared to the matched-pair selectivity of 92:8 where both the chiral auxiliary and the ligand direct towards the same amine stereocenter. Unless we intend to use the chiral substrate appendage for further selective additions, a double asymmetric reaction was not advantageous.

**Table 3-6 Analysis of stereochemical outcome with phenyl imine<sup>a</sup>**



Entry	R	Substrate	Ligand	Yield (%)	Product	<i>er</i> <sup>b</sup> <i>S</i> : <i>R</i> <sup>c</sup>	<i>dr</i> <sup>b</sup> <i>S</i> : <i>R</i> <sup>c</sup>
1	H	<b>3-31</b>	( <i>S</i> )-DTBM-SEGPPOS	67	( <i>R</i> )- <b>3-34</b>	4:96 <sup>d</sup>	
2	H	<b>3-31</b>	( <i>R</i> )-DTBM-SEGPPOS	50	( <i>S</i> )- <b>3-34</b>	96:4	
3	( <i>R</i> )-Benzyl	( <i>R</i> )- <b>3-28</b>	rac-BINAP	10	( <i>S,R</i> )- <b>3-34</b>		67:33
4	( <i>S</i> )-Benzyl	( <i>S</i> )- <b>3-28</b>	rac-BINAP	10	( <i>R,S</i> )- <b>3-34</b>		35:65
5	( <i>R</i> )-Benzyl	( <i>R</i> )- <b>3-28</b>	( <i>S</i> )-DTBM-SEGPPOS	58	( <i>R,R</i> )- <b>3-34</b>		14:86 <sup>e</sup>
6	( <i>R</i> )-Benzyl	( <i>R</i> )- <b>3-28</b>	( <i>R</i> )-DTBM-SEGPPOS	33	( <i>S,R</i> )- <b>3-34</b>		92:8
7	( <i>S</i> )-Benzyl	( <i>S</i> )- <b>3-28</b>	( <i>R</i> )-DTBM-SEGPPOS	50	( <i>S,S</i> )- <b>3-34</b>		86:14
8	( <i>S</i> )-Benzyl	( <i>S</i> )- <b>3-28</b>	( <i>S</i> )-DTBM-SEGPPOS	26	( <i>R,S</i> )- <b>3-34</b>		9:91

<sup>a</sup>Conditions: Oxazolidinone (1 equiv), **3-17** (2 equiv), ligand (0.25 equiv), [Cu(CH<sub>3</sub>CN)<sub>4</sub>]PF<sub>6</sub> (0.25 equiv), DABCO (0.5 equiv), THF (0.1 M)

<sup>b</sup>Determined by SFC analysis

<sup>c</sup>Assignment of stereocenter at amine

<sup>d</sup>Converted to primary alcohol (*R*)-**3-36** by ozonolysis and reduction – *er* 5:95

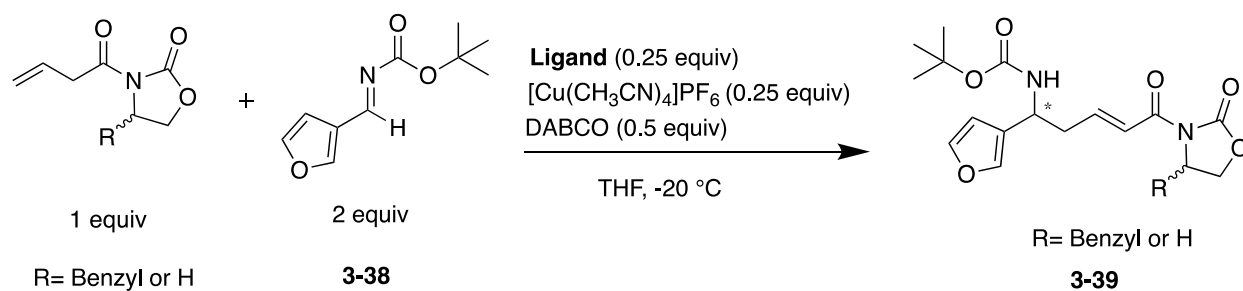
<sup>e</sup>Converted to primary alcohol (*R*)-**3-36** by ozonolysis and reduction – *er* 15:85

We considered two other imine substrates to confirm this unique reactivity. First, we synthesized furan imine **3-38** from sulfone **3-37** and then subjected it to our optimized vinylogous Mannich conditions with oxazolidinone substrate (*R*)-**3-28**, (*S*)-**3-28**, or **3-31** (Table 3-7). The furan imine with unsubstituted oxazolidinone **3-31** provided product with less stereoselectivity, ~4:1 for both chiral ligands, compared to the phenyl substituent (entry 1-2). Unfortunately, the control reaction with rac-BINAP did not provide any product to aid in the analysis (entry 3). For the double asymmetric reactions, utilizing the (*R*)-oxazolidinone with the (*S*)-ligand provided product that was essentially racemic at the amine stereogenic center (entry 4). The (*R*)-ligand was significantly better, as product was obtained in slightly lower yield (40%) but an improved *dr* of 84:16 (entry 5). A similar improved result was achieved with the (*S*)-oxazolidinone and (*S*)-ligand (entry 6). These matched-pair double asymmetric outcomes (entry 5-6) were actually a slight improvement compared to the stereochemical outcome obtained with the single asymmetric reaction controlled by the chiral ligand (entry 1-2).

The results with the furan imine demonstrate the importance of the imine substituent on the stereochemical outcome. The furan is slightly electron donating while the phenyl substituent is slightly electron withdrawing; this electronic difference may contribute to the stereochemical outcome when controlled only by the ligand. In the Yin group's system with a pyrazole auxiliary, alkyl substituted imines and furan substituted imines resulted in decreased enantiomeric outcome compared to phenyl substituted imines.<sup>161</sup> The matched, mismatched systems lead to a significant difference in diastereomeric outcome. This cannot be solely attributed to the interplay between the substrate auxiliary and ligand; if it was, the outcome would match the phenyl imine. We hypothesize that the furan imine size and electronic properties contribute to the difference. The furan imine was more reactive than the phenyl imine which may also contribute to the decreased stereochemical outcome by lowering  $\Delta\Delta G^\ddagger$ .



**Table 3-7 Analysis of stereochemical outcome with furan imine<sup>a</sup>**



Entry	R	Substrate	Ligand	Yield (%)	Product	<i>er</i> <sup>b</sup> <i>S</i> : <i>R</i> <sup>c</sup>	<i>dr</i> <sup>b</sup> <i>S</i> : <i>R</i> <sup>c</sup>
1	H	<b>3-31</b>	( <i>S</i> )-DTBM-SEGPPOS	74	( <i>R</i> )- <b>3-39</b>	18:82	
2	H	<b>3-31</b>	( <i>R</i> )-DTBM-SEGPPOS	62	( <i>S</i> )- <b>3-39</b>	79:21	
3	( <i>R</i> )-Benzyl	( <i>R</i> )- <b>3-28</b>	rac-BINAP	NR	-	-	
4	( <i>R</i> )-Benzyl	( <i>R</i> )- <b>3-28</b>	( <i>S</i> )-DTBM-SEGPPOS	62	( <i>R,R</i> )- <b>3-39</b>		47:53
5	( <i>R</i> )-Benzyl	( <i>R</i> )- <b>3-28</b>	( <i>R</i> )-DTBM-SEGPPOS	40	( <i>S,R</i> )- <b>3-39</b>		84:16
6	( <i>S</i> )-Benzyl	( <i>S</i> )- <b>3-28</b>	( <i>S</i> )-DTBM-SEGPPOS	34	( <i>R,S</i> )- <b>3-39</b>		17:83

<sup>a</sup>Conditions: Oxazolidinone (1 equiv), **3-38** (2 equiv), ligand (0.25 equiv),  $[\text{Cu}(\text{CH}_3\text{CN})_4]\text{PF}_6$  (0.25 equiv), DABCO (0.5 equiv), THF (0.1 M)

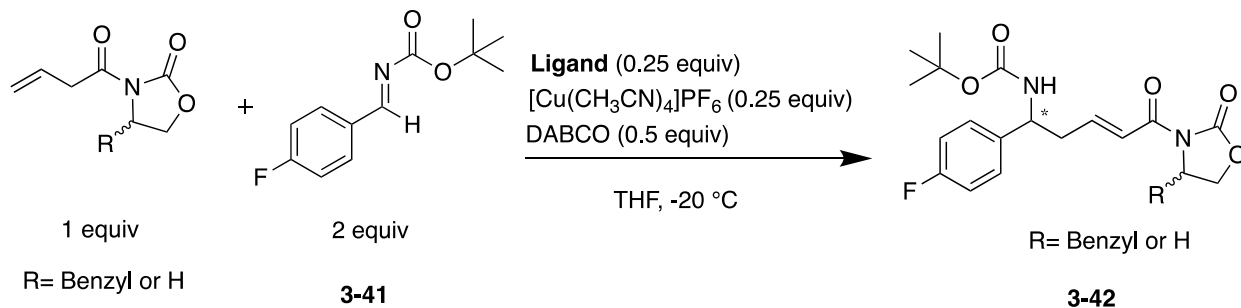
<sup>b</sup>Determined by SFC analysis

<sup>c</sup>Assignment of stereocenter at amine

Next, we synthesized 4-fluorophenyl imine **3-41** from sulfone **3-40** and subjected it to our optimized vinylogous Mannich conditions with the oxazolidinone substrate. We obtained a similar stereochemical outcome to that of the phenyl derivative (Table 3-8). The reaction of unsubstituted oxazolidinone **3-31** with (*R*)-DTBM-SEGPPOS provided the best stereochemical outcome with a *dr* of 94:6 (entry 1). The (*R*)-substrate with the (*S*)-ligand formed a mismatched pair resulting in

product with a *dr* of 85:15 while the reaction with the (*R*)-ligand in the matched pair improved the *dr* to 91:9 (entry 2-3).

**Table 3-8 Analysis of stereochemical outcome with fluorenyl imine<sup>a</sup>**



Entry	R	Substrate	Ligand	Yield (%)	Product	<i>er</i> <sup>b</sup> <i>S</i> : <i>R</i> <sup>c</sup>	<i>dr</i> <sup>b</sup> <i>S</i> : <i>R</i> <sup>c</sup>
1	H	<b>3-31</b>	( <i>R</i> )-DTBM-SEGPPOS	39	( <i>S</i> )- <b>3-42</b>	94:6	
2	( <i>R</i> )-Benzyl	( <i>R</i> )- <b>3-28</b>	( <i>S</i> )-DTBM-SEGPPOS	34	( <i>R,R</i> )- <b>3-42</b>		15:85
3	( <i>R</i> )-Benzyl	( <i>R</i> )- <b>3-28</b>	( <i>R</i> )-DTBM-SEGPPOS	17	( <i>S,R</i> )- <b>3-42</b>		91:9

<sup>a</sup>Conditions: Oxazolidinone (1 equiv), **3-41** (2 equiv), ligand (0.25 equiv), [Cu(CH<sub>3</sub>CN)<sub>4</sub>]PF<sub>6</sub> (0.25 equiv), DABCO (0.5 equiv), THF (0.1 M)

<sup>b</sup>Determined by SFC analysis

<sup>c</sup>Assignment of stereocenter at amine

Based on these experimental data, we considered the mechanism and transition state of the reaction. Copper(I) prefers to adopt a tetrahedral orientation coordinating to the two phosphorus atoms of the ligand.<sup>225</sup> We considered a cyclic transition state with the copper species bonded at the  $\alpha$ -position of the carbonyl nucleophile (Figure 3-22 A) and an open transition with the copper placed on the oxygen of the enolate and coordinated to the oxazolidinone carbonyl for additional stability (Figure 3-22 B).<sup>187, 226</sup> The cyclic transition state model leads to the formation of a favorable 6-membered ring with the oxazolidinone carbonyl group oriented *anti* to the acyl carbonyl and the copper species coordinated to the imine nitrogen (Figure 3-22 A). We briefly

considered the cyclic transition state with copper coordinated to the carbonyl of the oxazolidinone and the imine nitrogen, however, this led to the formation of an unfavorable 8-membered ring and distorted bond angles of 101 and 132° for sp<sup>2</sup>-carbons in the ring.

In the open transition state, the oxazolidinone carbonyls must be *syn* to one other thus adopting a *syn-s-cis* confirmation that leads to the (*Z*)-enolate (Figure 3-22 B). Chelation to both carbonyls impedes free rotation around the carbon-nitrogen sigma bond thus locking the oxazolidinone in place. *Anti*-periplanar attack occurs on the prochiral center of the imine. With this orientation, bond angles of approximately 120° are maintained for the sp<sup>2</sup>-carbons of the nucleophile.

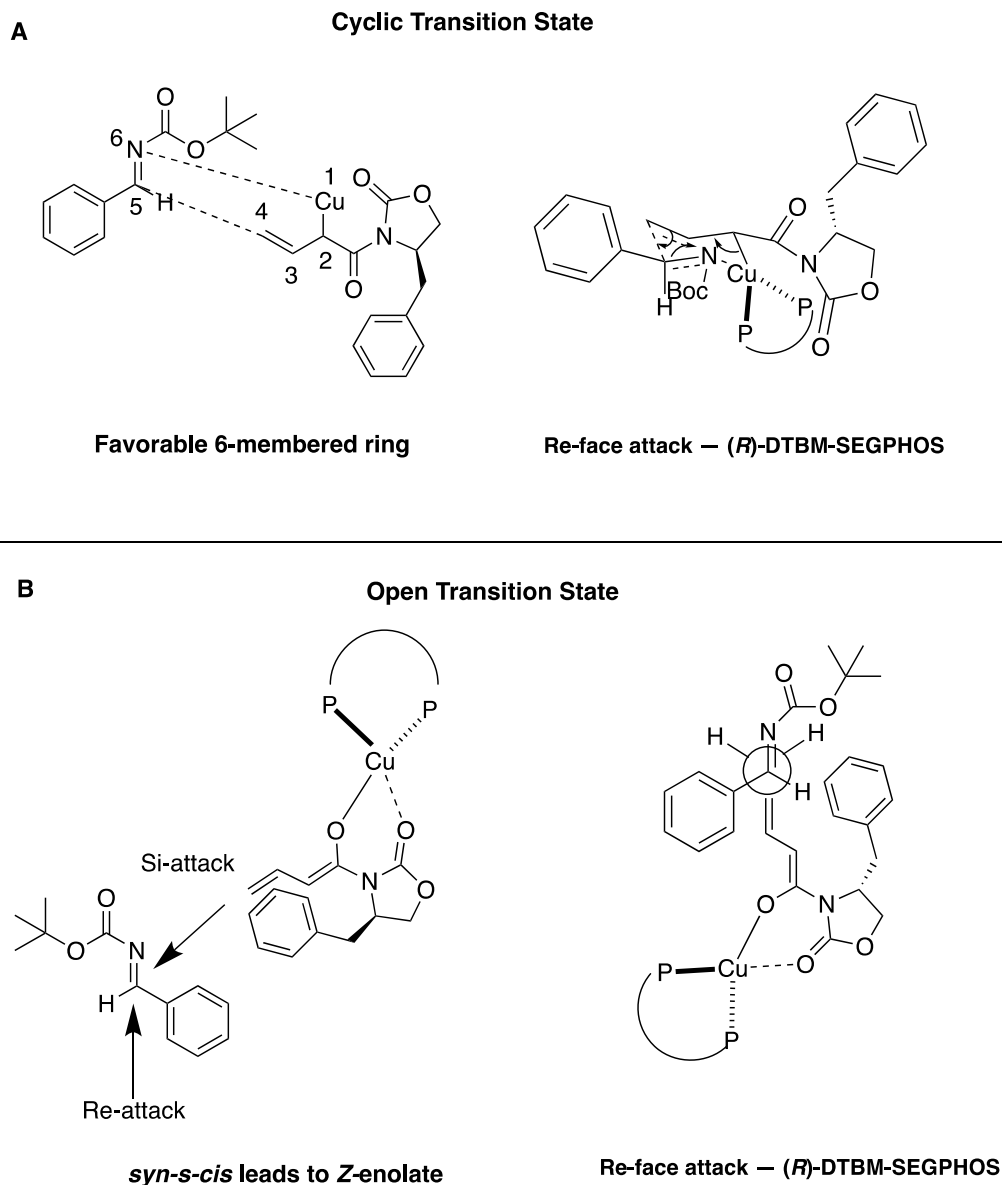


**Figure 3-22 A) Proposed cyclic transition state and B) Proposed open transition state**

We modeled the cyclic and open transition states with (*R*)-benzyl oxazolidinone substituted (***R***)-**3-28** and (*S*)-DTBM-SEGPHOS leading to the major (*R,R*)-product and the minor (*S,R*)-product in Scigress with MM3 force field parameters (Figure 3-23 and 3-24).<sup>161, 226-228</sup> In the cyclic transition state, the chiral ligand is oriented such that it may block one face of the imine, however, control from the oxazolidinone auxiliary appears limited. The benzyl oxazolidinone auxiliary is positioned over 8.5 Å from the prochiral center so it is unlikely to have much of an effect on the newly formed stereocenter (Figure 3-23). Non-covalent interactions between the substrate and

ligand may be altered by the chiral appendage but not in a significant effect for the prochiral center. From our experiments, the oxazolidinone chiral appendage provides a 2:1 selectivity when a racemic ligand is used so it must be orientated in such a way to impact the prochiral center. Additionally, in the cyclic transition state there is steric clash between the Boc-protecting group of the imine and the large phenyl substituent of the imine. In the open transition state it is easier to visualize how the benzyl oxazolidinone auxiliary could have some effect on the new stereogenic center. The benzyl appendage is less than 5 Å from the imine center and the  $sp^2$ -carbons of the phenyl group of the imine are 3.7 Å from then benzyl  $sp^2$ -carbons (Figure 3-24). In the major (*R,R*)-product the (small) hydrogen from the imine prochiral center is on the same face as the benzyl directing group. In the minor (*S,R*)-product the (large) phenyl group of the prochiral imine is on the same face as the benzyl directing group leading to an unfavorable interaction. From modeling the antiperiplanar transition state, it is easier to rationalize how there can be matched and mismatched pairs leading to different stereochemical outcomes as well as how the unsubstituted oxazolidinone generates a simpler transition state when controlled only by the ligand. We hypothesize that the matched pair occurs when the ligand blocks the face that the oxazolidinone appendage is on while the mismatched pair occurs when the ligand blocks the face that the oxazolidinone appendage directs to. At this time, we cannot definitively conclude which transition state is responsible for the reactivity, but the open transition state seems more probable.

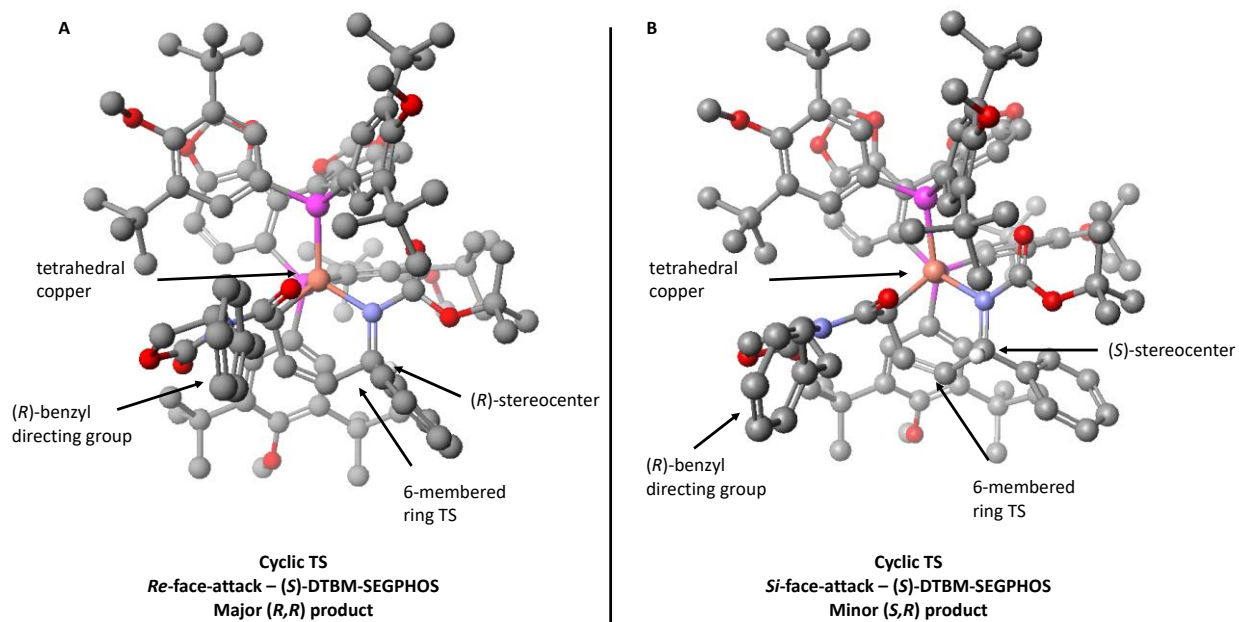


**Figure 3-23** Scigress modeled cyclic transition state with (R)-auxiliary and (S)-ligand leading to A) (R,R)-major product and B) (S,R)-minor product

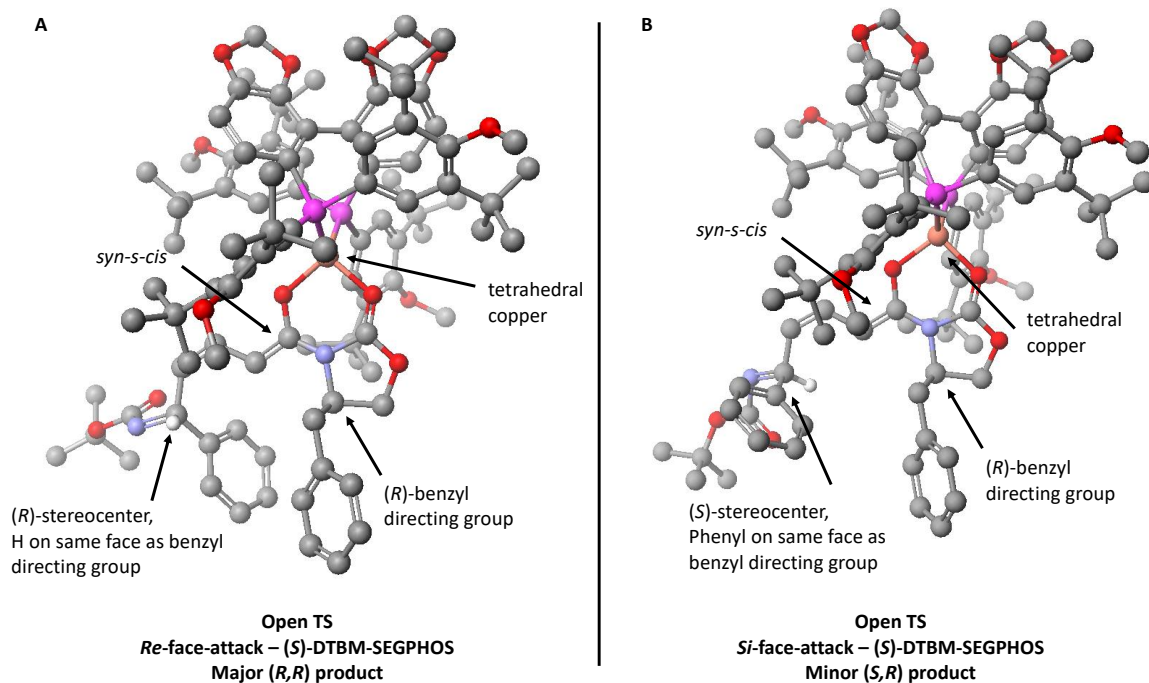
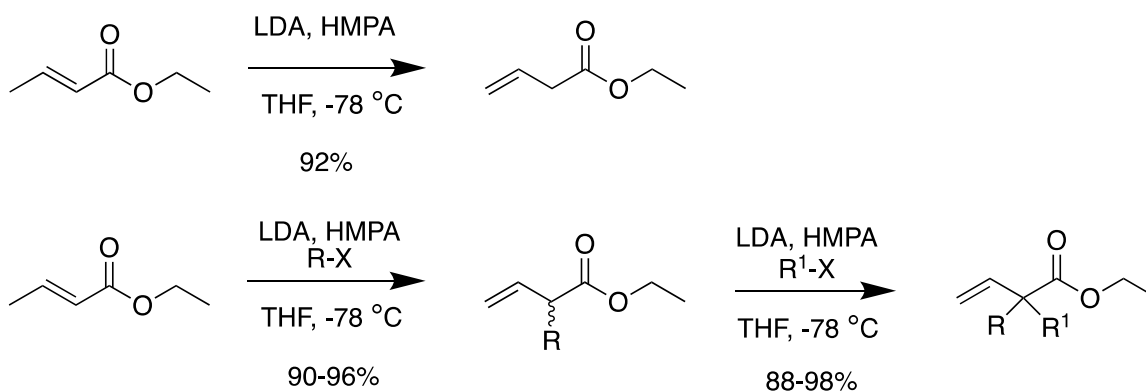


**Figure 3-24** Scigress modeled open transition state with (R)-auxiliary and (S)-ligand leading to A) (R,R)-major product and B) (S,R)-minor product

Ultimately the vinylogous Mannich reaction allowed the rapid formation of the backbone of JP4-039. The previous synthesis took six-steps to get to the Boc-protected amine, whereas this new route only required two synthetic steps. Additionally, various imines could be used to diversify the molecule in Zone I (Figure 3-15). With these vinylogous Mannich products, we set out to accomplish our primary objective: to probe the structure-activity relationship of JP4-039 analogs in the ferroptosis cell death pathway and determine whether activity was sequence-dependent or lipophilicity-dependent.

### 3.2.3 Synthesis of JP4-039 Analogs

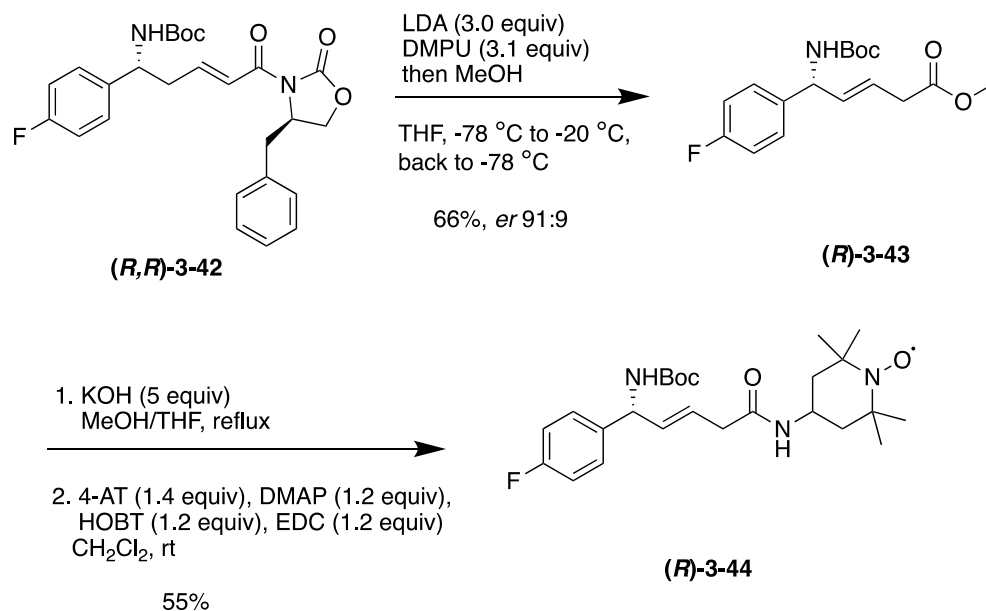
We began the analog efforts with (*R,R*)-vinylogous Mannich product **3-42** with a 4-fluorophenyl side chain. We attempted our optimized photochemical isomerization conditions on the substrate but were unable to observe any  $\beta,\gamma$ -unsaturated product. Instead, the oxazolidinone auxiliary was highly prone to eliminate which led to decomposition products. Similar to the pyrazole auxiliary, the benzyl side chain on the oxazolidinone likely affected the photochemistry of the molecule. Alternatively, we explored strong base-mediated isomerizations. In 1973, Herrmann demonstrated the use of an LDA-mediated deconjugation reaction of ethyl crotonate (Scheme 3-24).<sup>229</sup> Herrmann and coworkers performed simple molecular orbital calculations on the lithium enolate of ethyl crotonate and determined that the maximum negative partial charge existed on the  $\alpha$ -carbon, indicating that this would be the site of a charge-controlled electrophilic addition.



**Scheme 3-24** LDA mediated deconjugation reaction<sup>229</sup>

For our isomerization conditions, we replaced HMPA with the cyclic urea DMPU as it is less carcinogenic (Scheme 3-25).<sup>230</sup> Our first aim was to use a hydrogen source to isomerize the double bond out of conjugation. The LDA reagent (3.0 equiv) was formed at -78 °C followed by the addition of DMPU (3.1 equiv). Vinylogous Mannich product **(R)-3-42** was added and the solution was allowed to warm slowly from -78 °C to -40 °C and then -20 °C. Upon recooling to -78 °C, methanol was added. Our expected product was the skipped diene with the oxazolidinone still in place. However, we were pleasantly surprised that under these conditions not only did we achieve isomerization of the double bond but also elimination of the oxazolidinone to the methyl ester. We believe that the LDA-DMPU complex deprotonated an allylic hydrogen which generated an extended enolate system and upon quenching with methanol, a hydrogen was preferentially added at the  $\alpha$ -carbon. Under the strongly basic LDA conditions, methanolysis led to the formation of methyl ester product, **(R)-3-43**, in 66% yield. To the best of our knowledge, these conditions have not been reported to cleave an oxazolidinone auxiliary. From here only two steps were necessary to prepare a direct JP4-039 analog with a 4-fluorophenyl side chain. Saponification followed by amidation with 4-AT under standard conditions used in our group provided nitroxide **(R)-3-44** in 55% yield (Scheme 3-25). The synthetic route to **(R)-3-44** required only five linear steps and only four purifications, however the yield was 8% because of the low yield in the vinylogous Mannich step. Despite the yield, this is a dramatic improvement over the previously developed synthesis in terms of our ability to quickly synthesize and test a diverse set of analogs for their anti-ferroptosis activity. It also avoids the use of experimentally challenging transmetalation chemistry and a toxic chromium oxidation.

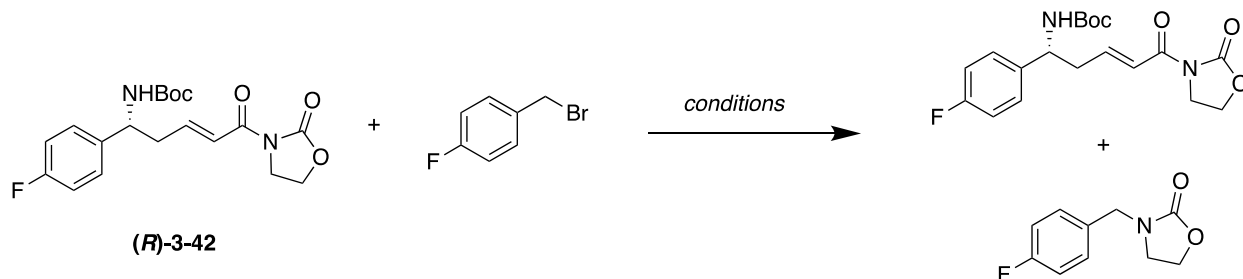




**Scheme 3-25 Synthesis of analog (*R*)-3-44**

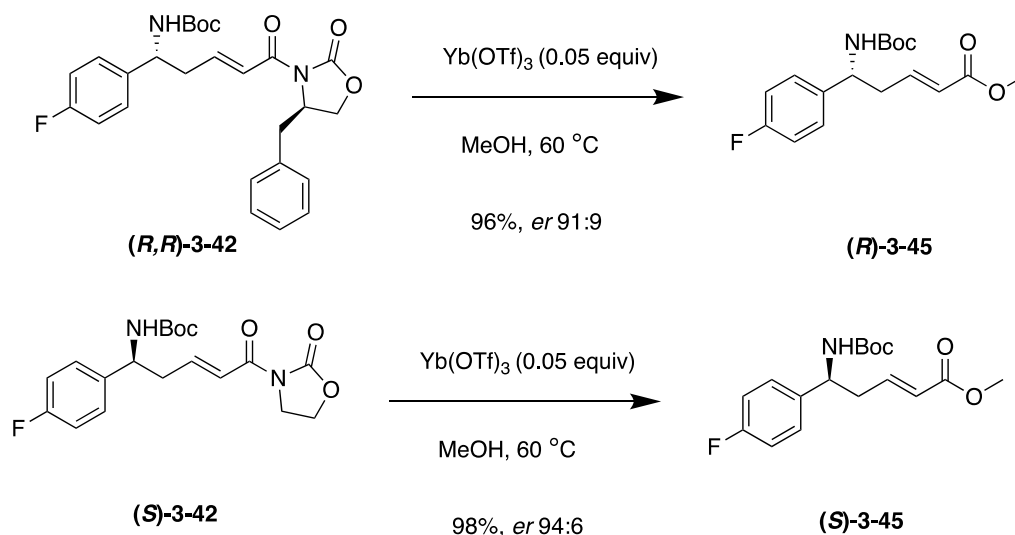
While we were interested in modifications of Zone I, we were also interested in substitutions at the  $\alpha$ -position of the carbonyl in Zone III. We previously only explored a small number of modifications at this position and we know that these substitutions can affect how the molecule folds and crosses the mitochondrial membrane.<sup>79,93</sup> Despite multiple attempts to isomerize and alkylate both the 4-benzyl oxazolidinone and unsubstituted oxazolidinone **3-42**, we were unsuccessful. Conditions we attempted included: 1) replacing HMPA with DMPU; 2. exploring both NaHMDS and LDA; 3. modifying temperature; 4. modifying equivalents of LDA and DMPU; and 5. using alkylating agents of various sizes and in various equivalents. In brief, reactions with HMPA were not as high yielding as DMPU. Since NaHMDS is not as strong of a base as LDA (pKa 26 vs 36), we were not surprised to observe no reactivity under these conditions as most likely NaHMDS did not lead to deprotonation and formation of the enolate.<sup>231</sup> We noted that when the reaction was not warmed up, alkylation did not occur. However, when the reaction temperature reached rt too quickly, decomposition was evident. As our substrate possessed a NH, we required at least two equivalents of base. In some cases, excess base drove the formation of decomposition products. The smaller electrophile methyl iodide or the more reactive electrophile methyl triflate did not lead to deconjugated alkylated product. From all these unsuccessful

reactions, we generally isolated starting material or alkylated oxazolidinone auxiliary along with decomposition products (Scheme 3-26).

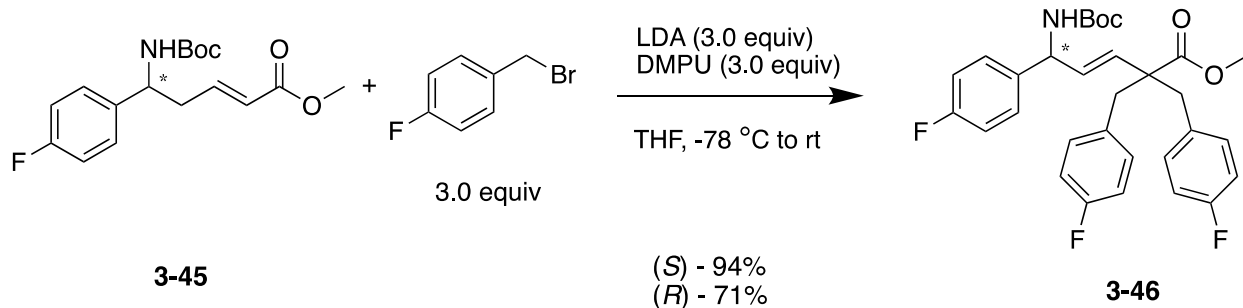


**Scheme 3-26 Attempted deconjugative alkylation reaction with oxazolidinone auxiliary**


As the deconjugative alkylation did not work with the oxazolidinone auxiliary, we hypothesized that the corresponding methyl ester may be more amenable to the transformation. In the literature, the most common way to cleave Evans oxazolidinone auxiliary is with LiOH/H<sub>2</sub>O.<sup>231</sup> However, this method generates the carboxylic acid and we wanted to streamline the synthesis directly to the methyl ester. In 2018, a group at Bristol-Myers Squibb disclosed one-pot Yb(OTf)<sub>3</sub> conditions to convert *N*-acyl oxazolidinones directly to esters or amides.<sup>232</sup> The authors did not comment specifically on the mechanism but through a high-throughput screen determined that the smaller the ionic-radius of the Lewis acid (104.2 Å for Yb(OTf)<sub>3</sub>), the shorter the reaction time. According to the literature, Yb(OTf)<sub>3</sub> does have unique reactivity with oxazolidinones; it has been utilized in annulations and free-radical-mediated intramolecular conjugate addition reactions.<sup>233-234</sup> To our delight, the ytterbium conditions worked well for both 4-benzyl oxazolidinone substituted (**(R,R)**-3-42) and unsubstituted oxazolidinone substrate (**(S)**-3-42 (Scheme 3-27). Both methyl ester products were obtained in over 95% yield with no degradation in *er*.



With the (*S*)- and (*R*)-methyl ester products in hand, we attempted the deconjugative alkylation chemistry again. Upon reaction with LDA (3.0 equiv), DMPU (3.1 equiv), and 4-fluorobenzyl bromide (3.0 equiv) at -78 °C, followed by slow warming to rt, we isolated the (*S*)- and (*R*)-bis alkylated product **3-46** in 94% and 71% yield respectively (Scheme 3-28). With less than 2 equivalents of alkylating agent, we always isolated the bis-alkylated product. Mono- versus di-alkylation was hard to control; the second alkylation was very energetically favorable on our substrate.



From this intermediate we synthesized three analogs for direct activity comparison in a ferroptosis assay. Both (*S*)- and (*R*)-**3-46** were saponified and coupled to 4-AT to provide (*S*)- and



**3-46**

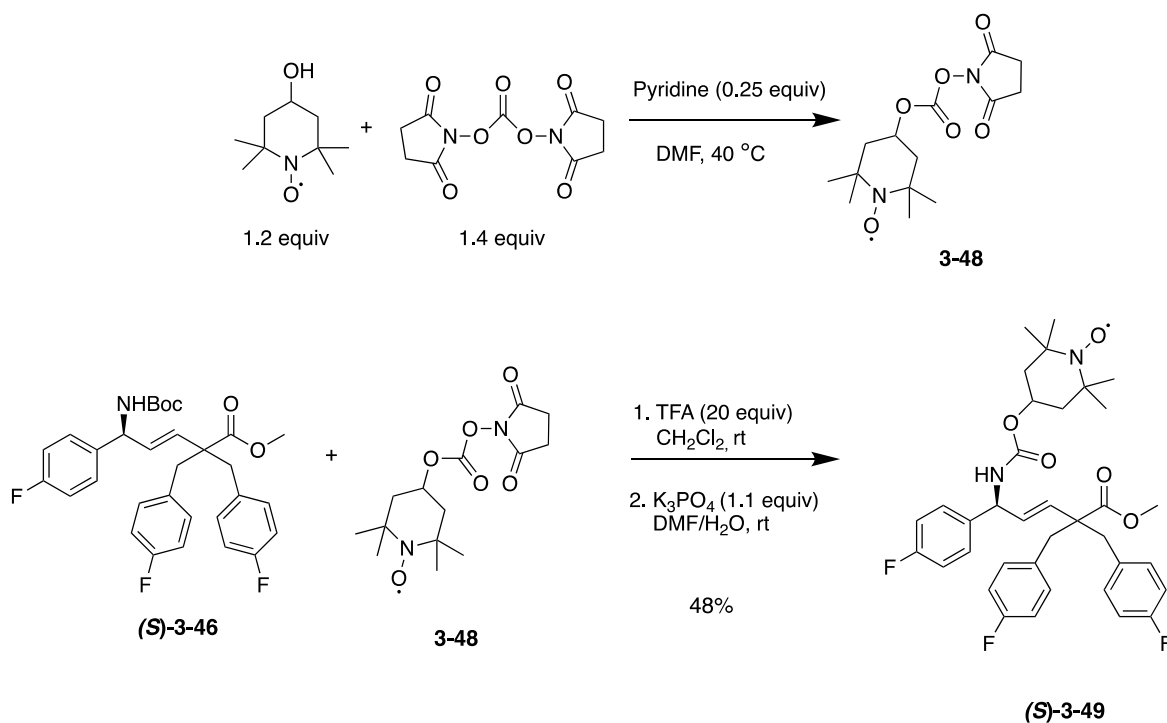
1. KOH (5 equiv)  
 MeOH/THF, reflux

2. 4-AT (1.4 equiv), DMAP (1.2 equiv)  
 HOBT (1.2 equiv), EDC (1.2 equiv)  
 CH<sub>2</sub>Cl<sub>2</sub>, rt

**3-47**

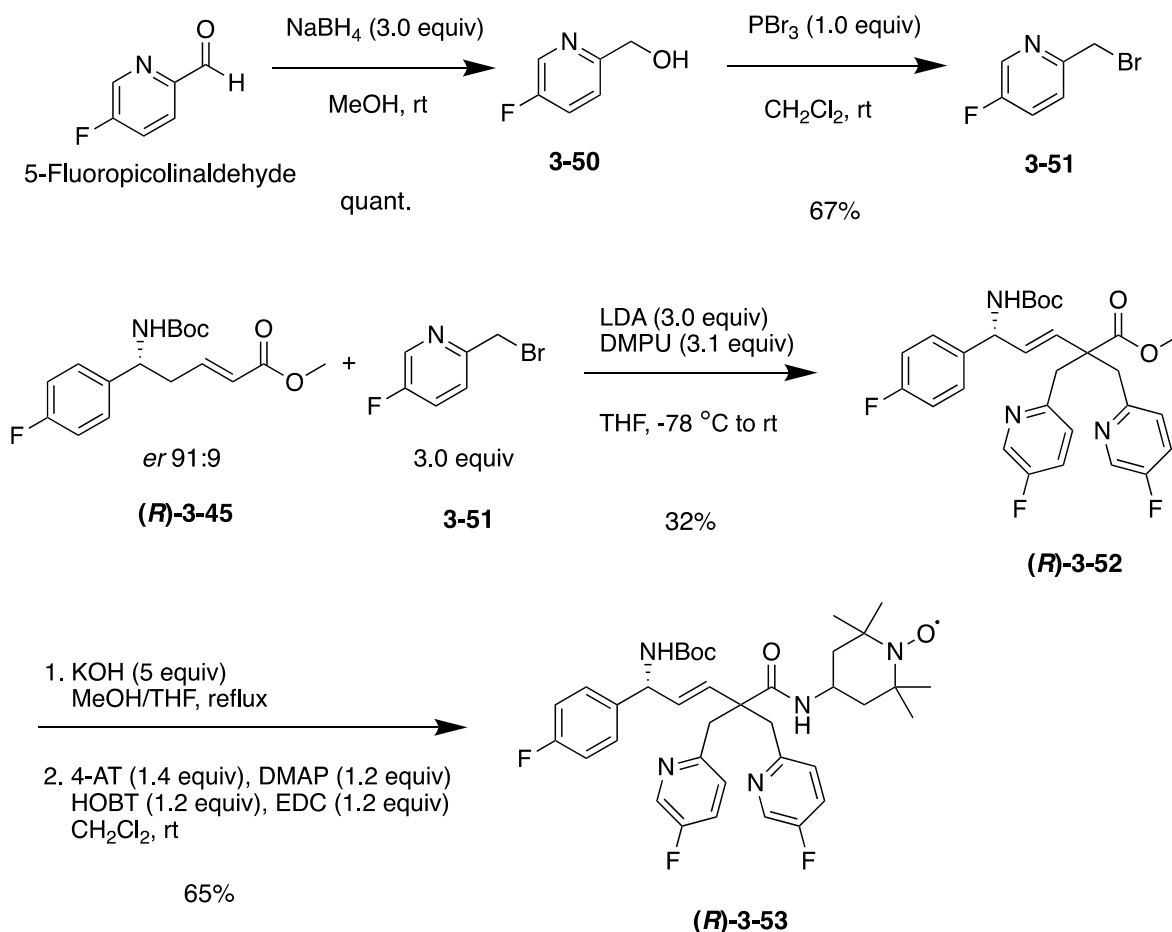
(S) - 62%  
 (R) - 37%

109



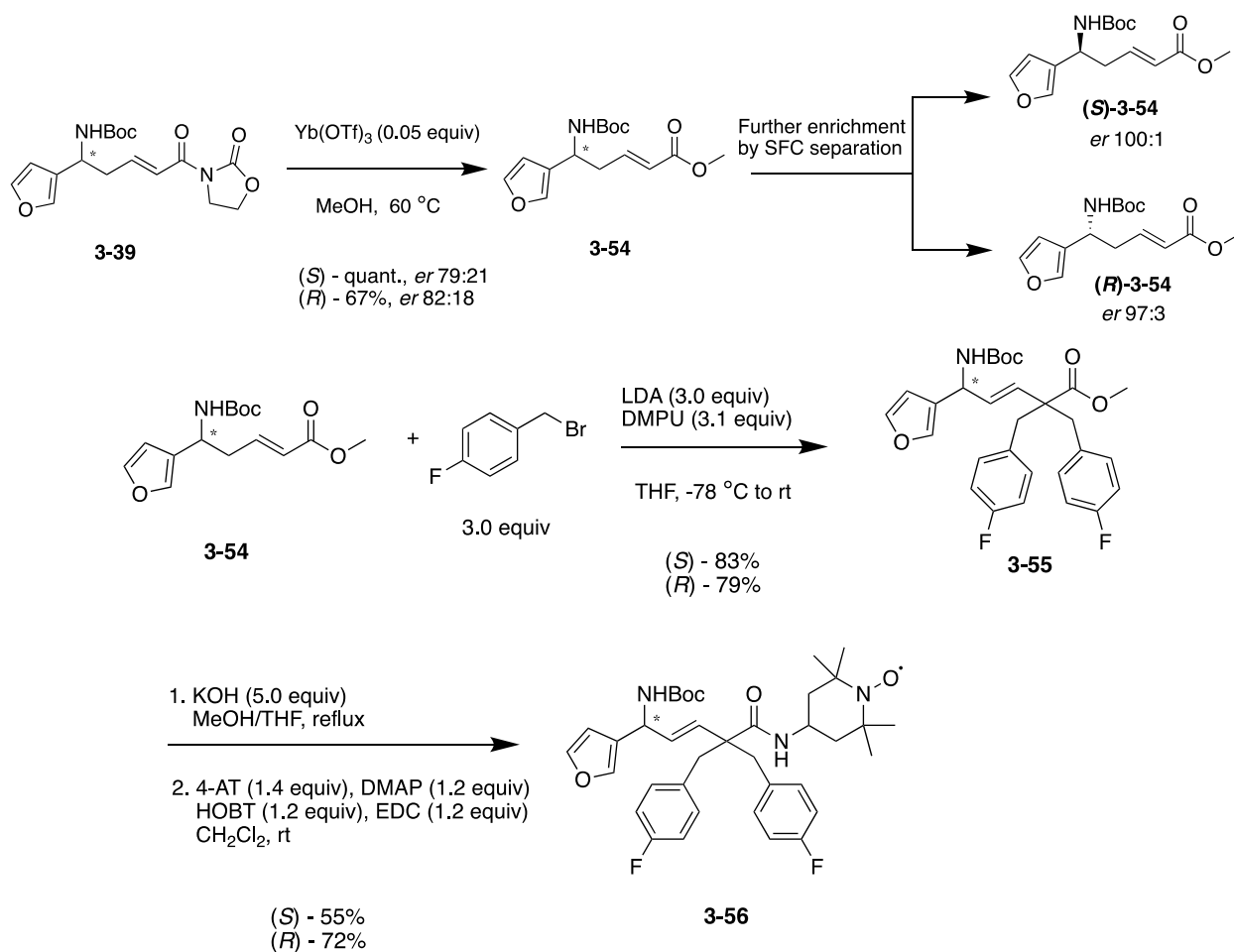
Scheme 3-30 Synthesis of anlaog (S)-3-49

To reduce the logP in this series of compounds, we incorporated a hetero-atom in the  $\alpha$ -alkylation reagent. 5-Fluoropicolinaldehyde was reduced with sodium borohydride to benzylic alcohol **3-50** and converted to allylic bromide **3-51** by an  $\text{S}_{\text{N}}2$ -substitution with the activated primary alcohol generated upon reaction with phosphorus tribromide (Scheme 3-31). (*R*)-Methyl ester **3-45** did not react as smoothly with alkylating agent **3-51** but did provide product (*R*)-**3-52** in 32% yield. Saponification followed by amide coupling with 4-AT provided nitroxide (*R*)-**3-53** in 65% yield over two steps with a logP of 5.78 (Scheme 3-31).



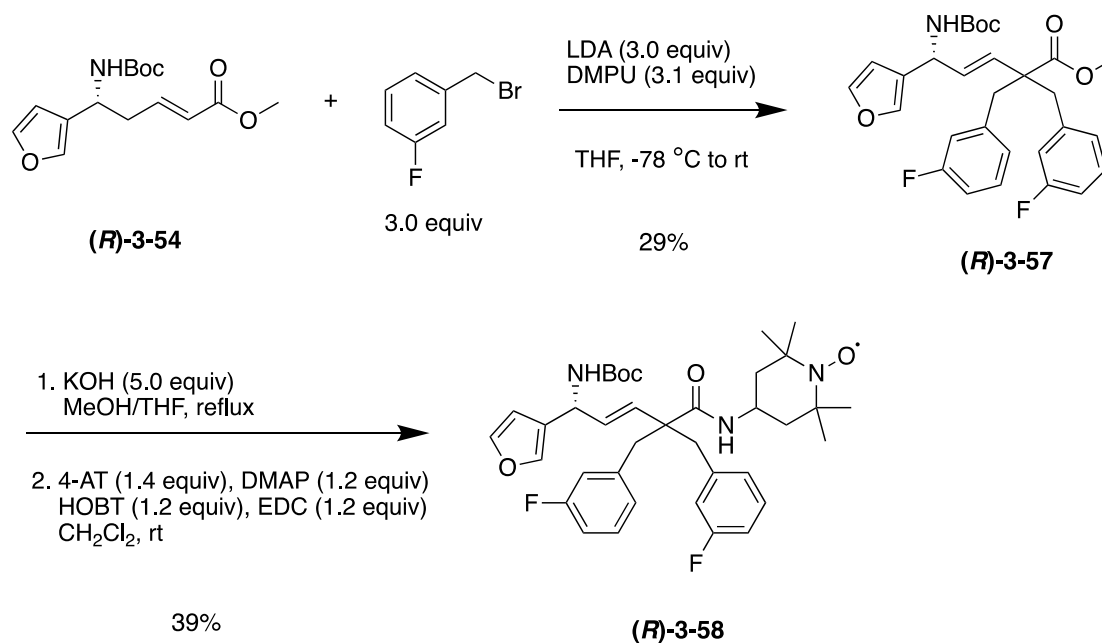
Scheme 3-31 Synthesis of analog **(R)-3-53**

We next turned our attention to the incorporation of a furan in Zone I that would reduce the overall logP. We converted (*S*)- and (*R*)-**3-39** to methyl ester, **3-54**, with the Yb(OTf)<sub>3</sub> conditions (Scheme 3-32). The enantiomeric ratios of these products (established in the vinylogous Mannich reaction) were much lower than that of the 4-fluorophenyl derivative. Accordingly, we carried out semi-preparative purification by SFC to provide the (*S*)-product with *er* of >99:1 and the (*R*)-product with *er* 97:3 (Scheme 3-28). Subsequent deconjugative alkylation with 4-fluorobenzyl bromide provided (*S*)-**3-55** in 83% yield and (*R*)-**3-55** in 79% yield (Scheme 3-32). Saponification followed by amide coupling with 4-AT provided nitroxides (*S*)-**3-56** and (*R*)-**3-56** in 55% and 72% yield respectively with a logP of 6.03.



**Scheme 3-32 Synthesis of analogs (*S*)- and (*R*)-3-56**

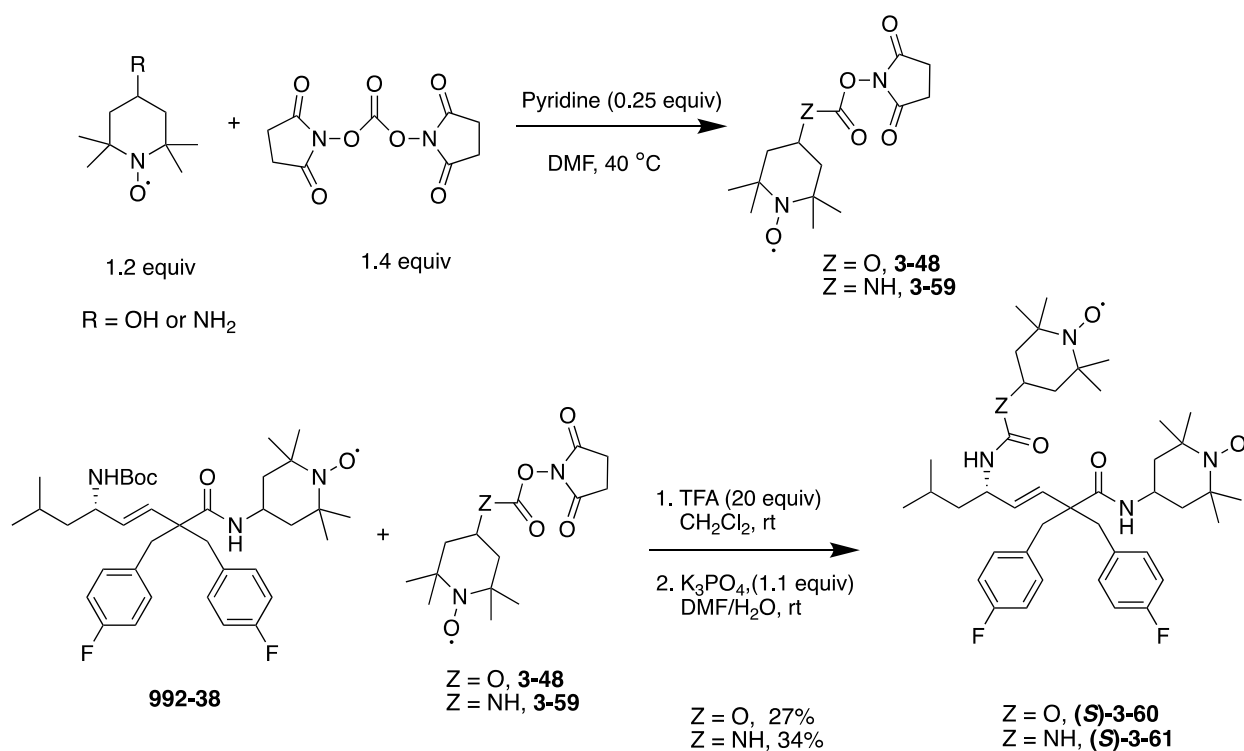
As a single point change that would allow us to look at the SAR in Zone III, we used 3-fluorobenzyl bromide as the alkylating reagent (Scheme 3-33). (*R*)-**3-54** underwent deconjugative alkylation with 3-fluorobenzyl bromide to provide bis-substituted compound (*R*)-**3-57** in 29% yield. Subsequent saponification and amide coupling to 4-AT provided nitroxide (*R*)-**3-58** in 39% yield.



Scheme 3-33 Synthesis of analog  $(R)$ -3-58

In collaboration with group members who also carried out research on the SAR of JP4-039, nitroxide  $(S)$ -992-38 became a lead compound. When our group first tested the ferroptosis activity of JP4-039 in 2016, the bis-nitroxide derivative of JP4-039 was 3.5x more active. It was proposed that the improvement in activity was due to its increased ability to scavenge reactive oxygen species.<sup>156</sup> Accordingly, as a modification in Zone V, we synthesized both the carbamate and urea linked bis-nitroxide of nitroxide  $(S)$ -992-38 to test the ROS scavenging of a dual nitroxide analog (Scheme 3-34). Similar to the chemistry used to synthesize nitroxide  $(S)$ -3-49, 4-hydroxy-tempo or 4-AT was reacted with  $N,N'$ -disuccinimidyl carbonate to form the respective carbonate or carbamate, 3-48 or 3-59. The Boc-protecting group of nitroxide  $(S)$ -992-38 was cleaved with TFA and the resulting free amine was coupled to the carbonate/carbamate with  $\text{K}_3\text{PO}_4$  to provide bis-nitroxide  $(S)$ -3-60 possessing a carbamate linker or bis-nitroxide  $(S)$ -3-61 with a urea linker.





**Scheme 3-34** Synthesis of analogs (*S*)-**3-60** and (*S*)-**3-61**

### 3.2.4 Activity of JP4-039 Analogs in an Erastin-Induced Ferroptosis Assay

We considered the SAR (Table 3-9) based on the five designated zones for modifications (Figure 3-15). We first considered Zone I and II modifications. JP4-039 has a leucine residue in Zone I and (*S*)-stereochemistry in Zone II. (*R*)-**3-44** has 4-fluorophenyl in Zone I and (*R*)-stereochemistry in Zone II. (*R*)-**3-44** was >10x more active than JP4-039 (Figure 3-25). (*R*)-**3-44** is more than twice as lipophilic as JP4-039; further modifications of (*R*)-**3-44** could help indicate whether this activity increase was sequence-dependent or lipophilicity-dependent. We cannot make any conclusions about preferred stereochemistry from this result. Ultimately, residues other than leucine can, and should, be incorporated in Zone I.

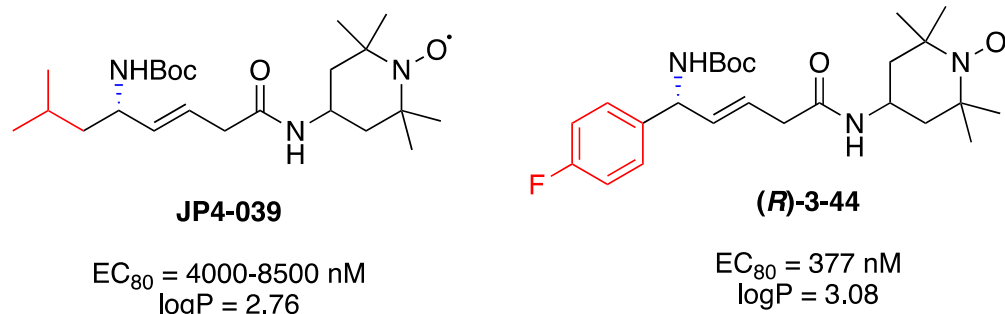


**Figure 3-25 Activity and logP comparison of JP4-039 and (R)-3-44**

Next, we looked at specific modifications to Zone III in **(R)-3-44** as well as the impact of stereochemistry in Zone II (Figure 3-26). When 4-fluorophenyl is in Zone I, substitution  $\alpha$  to the amide was not significantly beneficial for activity. **(R)-3-47**, the direct comparison to **(R)-3-44**, had an  $EC_{80}$  of 355 nM and a greatly increased logP of 7.88. The enantiomer of this compound, **(S)-3-47**, also had a similar  $EC_{80}$  of 371 nM. If activity was lipophilicity-dependent, we would expect that these  $\alpha$ -substituted analogs would have improved activity. Our previous work points to the role  $\alpha$ -amide substitutions have in determining the secondary structure of the compound and how it interacts with the mitochondrial membrane.<sup>79, 93</sup> We do not know the exact mechanism of action of these analogs but the  $EC_{80}$  activities indicate that both substituted analogs **(R)-3-47** and **(S)-3-47** and unsubstituted **(R)-3-44** may have similar mitochondrial locating efficiency.

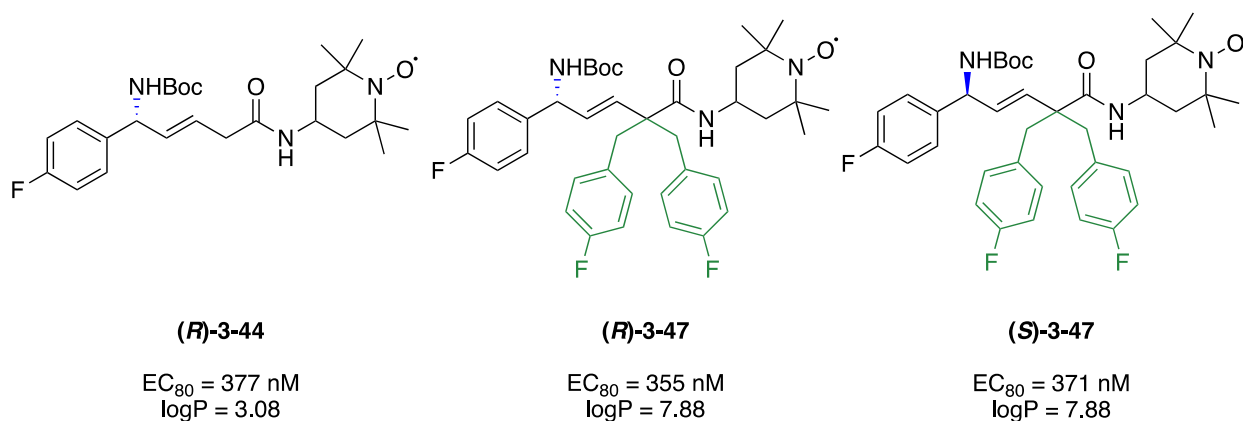


**Figure 3-26 Activity and logP comparison of (R)-3-44, (R)-3-47 and (S)-3-47**

To further test the effect of lipophilicity, we looked at an additional modification in Zone III in this series of 4-fluorophenyl analogs. Incorporation of a heteroatom in the  $\alpha$ -substituents of **(R)-3-53** reduced the logP from 7.88 to 5.78 but lead to a complete loss of activity (Figure 3-27). If the activity trend in this series of analogs was correlated to logP, we would expect **(R)-3-53** to have intermediate activity between **(R)-3-44**, which has a lower logP, and **(R)-3-47**, which has a higher logP. The pyridine heterocycles may affect secondary structure or interactions with the mitochondrial membrane.

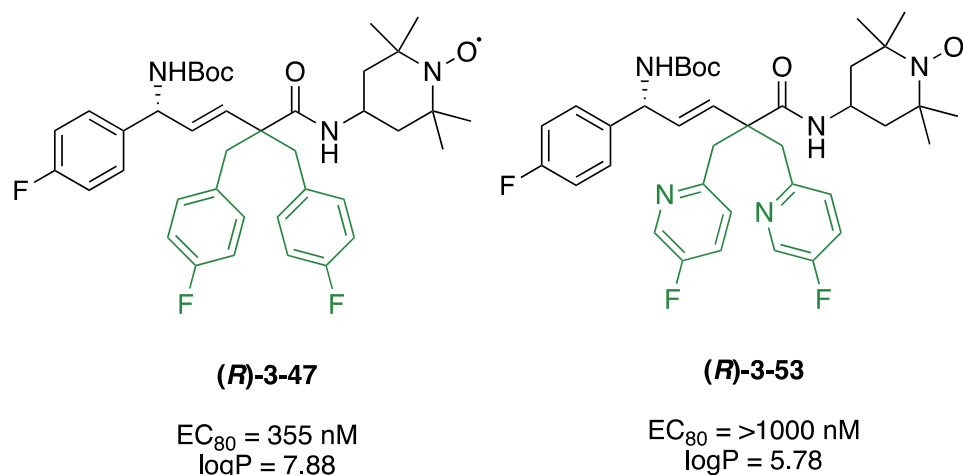


**Figure 3-27 Activity and logP comparison of (R)-3-47 and (R)-3-53**

Finally, for this series of Zone I, 4-fluorophenyl analogs we looked at the location of the nitroxide by moving it from Zone IV to Zone V (Figure 3-28). **(S)-3-49** with a methyl ester in Zone IV and TEMPO radical scavenging moiety in Zone V had an  $EC_{80}$  of 225 nM and similar logP of 7.68. This analog was 1.6x more active than its direct comparison **(S)-3-47**. This is the first time we have moved the lone-nitroxide around the molecule and the SAR indicates that it is better positioned on the allylic amine. Further modifications of nitroxide species and linkers should be investigated at this position.

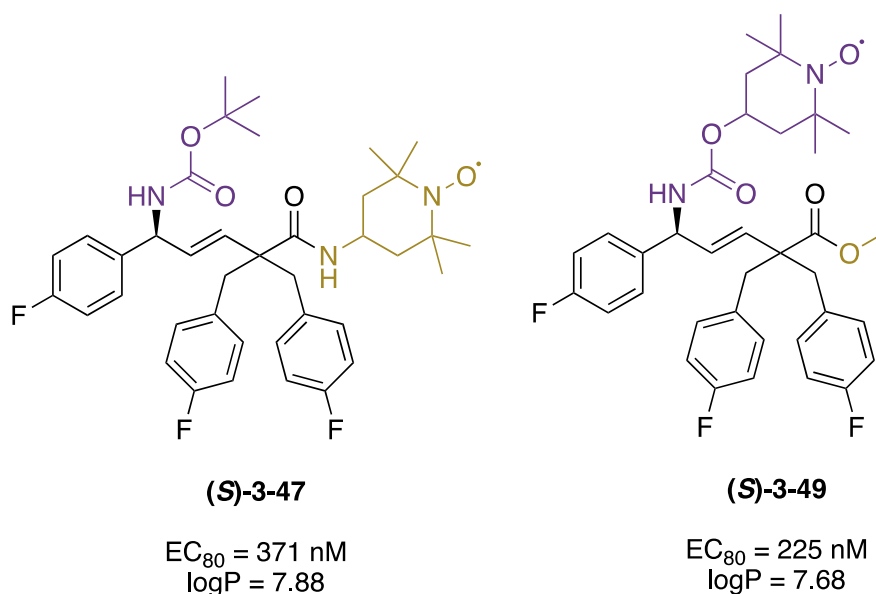


**Figure 3-28 Activity and logP comparison of (S)-3-47 and (S)-3-49**

With the success of the 4-fluorophenyl side chain in Zone I, we looked at the incorporation of a furan in Zone I because it would lower the overall logP thus improving the drug-like properties (Figure 3-29). Incorporation of a furan in Zone I of (*R*)- and (*S*)-**3-56** reduced the logP from 7.88 to 6.03 but did not improve the activity; almost equivalent activity was maintained. This supported our hypothesis that the activity is not correlated to lipophilicity only. Analog (*S*)-**3-56** was 1.7x more active than (*R*)-**3-56**. With the 4-fluorophenyl residue in Zone I, we did not see a significant difference in activity. Substitutions in Zone I affect the activity of enantiomers differently.

In the furan series, we also compared analog (*R*)-**3-58** with a 3-fluorobenzyl side chain to (*R*)-**3-56** with a 4-fluorobenzyl side chain. There was not a statistically significant difference in activity indicating that some variations in the benzyl side chain in Zone III are tolerated.

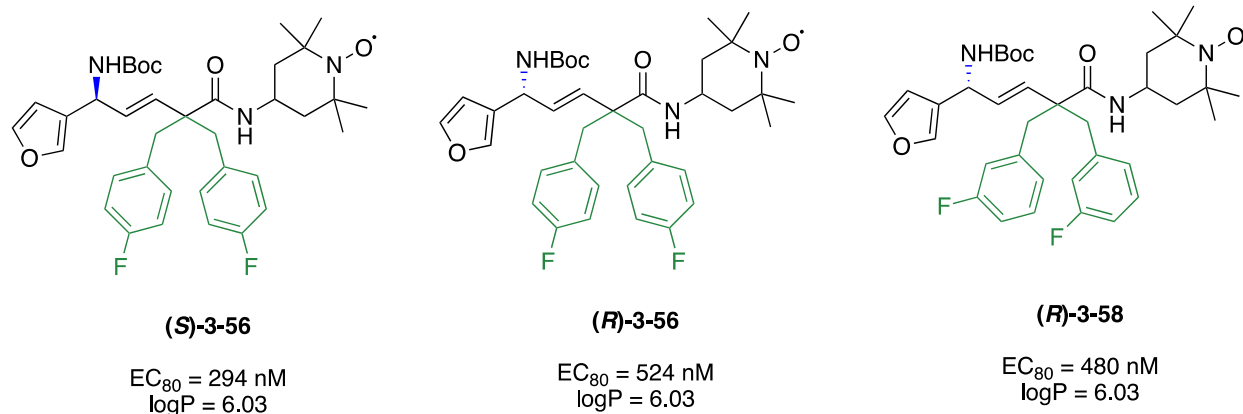


**Figure 3-29 Activity and logP comparison of (R)-3-56 and (R)-3-58**

Finally, we looked at modifications in Zone V through introduction of a second nitroxide moiety (Figure 3-30). Our previous results indicated that the introduction of a second nitroxide increased activity by enhancing the innate radical-scavenging ability of the compound. This result was confirmed as introduction of a carbamate linked nitroxide in **(S)-3-60** resulted in a 2.2x increase in activity (Figure 3-30). Bis-nitroxide **(S)-3-60** was one of the most potent compounds to date. Introduction of a urea linked nitroxide in **(S)-3-61** also increased activity but to a lesser extent (1.2x).

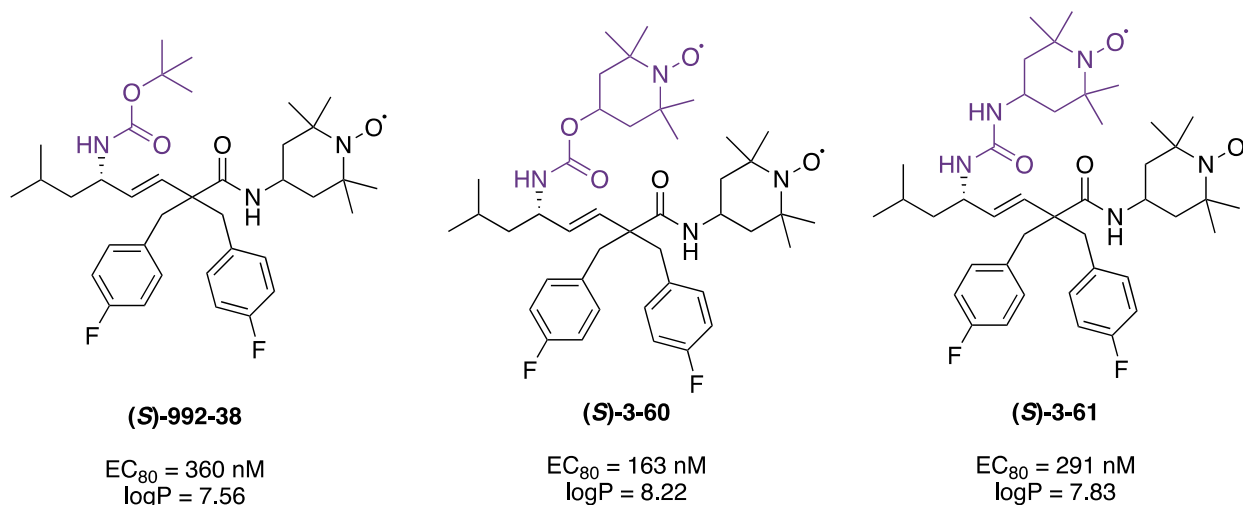


**Figure 3-30 Activity and logP comparison of (S)-992-38 and (S)-3-60 and (S)-3-61**

**Table 3-9 Activity of analogs in erastin induced CellTiter-Glo® ferroptosis assay**

Entry	Structure	ID	EC <sub>80</sub> ± STDev (nM) <sup>a</sup>	logP <sup>b</sup>	er <sup>c</sup>
1		JP4-039	4000-8500 <sup>d</sup>	2.76	>99:1
2		(R)-3-44	377 ± 85	3.08	91:9
3 <sup>e</sup>		(R)-3-47	355 ± 78	7.88	91:9
4		(S)-3-47	371 ± 20	7.88	94:6
5		(S)-3-49	225 ± 19	7.68	94:6
6		(R)-3-53	>1000	5.78	91:9
7		(R)-3-56	524 ± 32	6.03	97:3
8		(S)-3-56	294 ± 17	6.03	>99:1

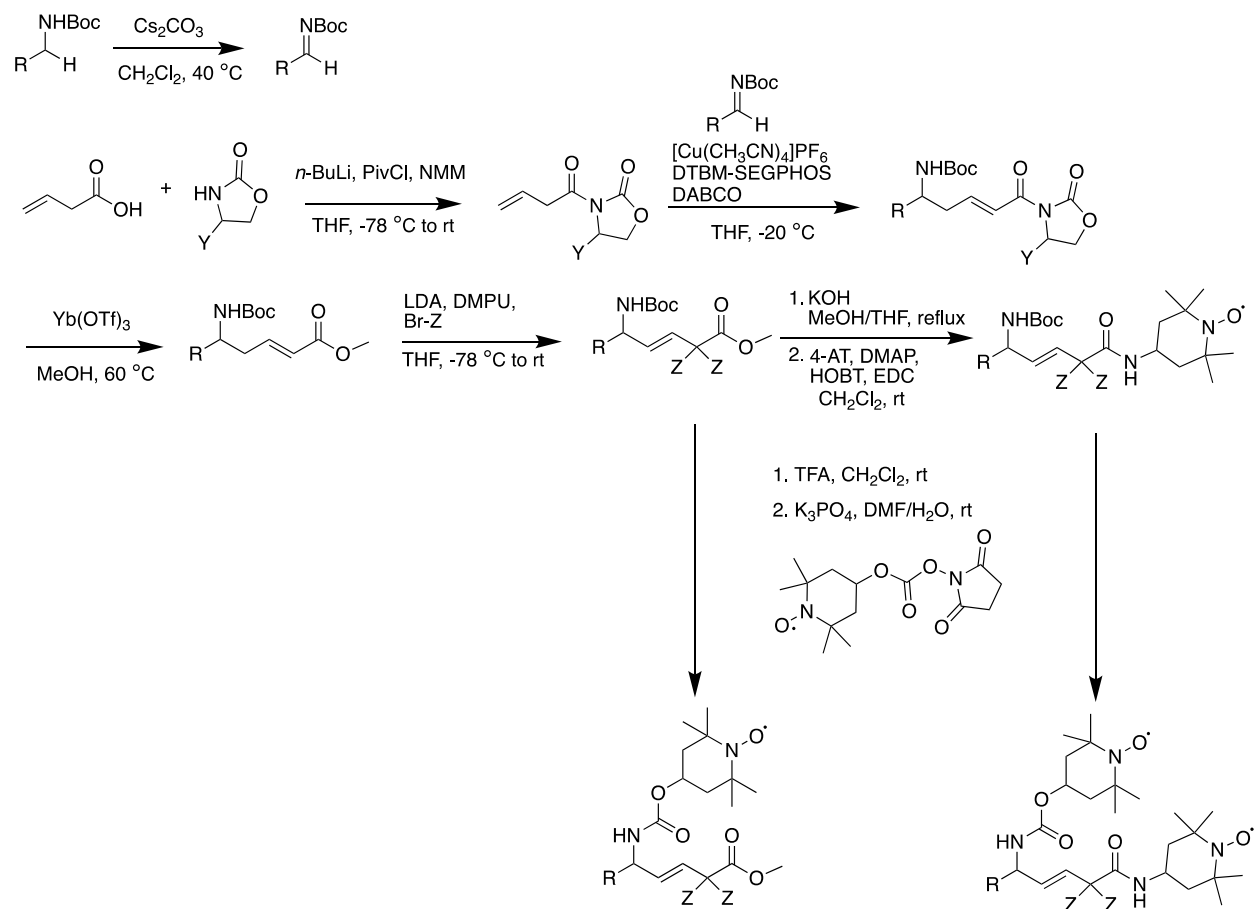


time that activity can be improved by installing the nitroxide on the allylic amine in Zone V. The presence of a nitroxide in Zone IV and Zone V, however, is optimal from purely an activity standpoint.

### 3.3 Conclusions

We have developed a new synthetic route to analogs of the nitroxide JP4-039 (Scheme 3-35). The key step of the sequence, a vinylogous Mannich reaction, allows the formation of the JP4-039 backbone and chiral amine in a single step; protecting group interchange is not necessary. Isomerization and amide coupling lead to JP4-039 analogs in five steps and only four purifications while deconjugative alkylation and amide coupling from the corresponding methyl ester allowed the synthesis of analogs with substitutions at the  $\alpha$ -position of the carbonyl group. Several analogs that are more protective in preventing erastin-induced ferroptosis cell death were synthesized. Various functionalities could be incorporated in Zone I and substitutions  $\alpha$  to the amide in Zone III were effective. Activity was sequence-dependent but did show some lipophilicity-dependence as, generally, the most active compounds had a higher logP. The two most potent compounds, (*S*)-**3-49** ( $EC_{80} = 225$  nM) and (*S*)-**3-60** ( $EC_{80} = 163$  nM) incorporated a Tempo-nitroxide in Zone V on the allylic amine.





**Scheme 3-35** Synthetic scheme proceeding through a vinylogous Mannich reaction and deconjugative alkylation towards JP4-039 analogs

### 3.4 Experimental Procedures

**General.** All glassware was flame-dried or oven-dried and cooled under dry  $\text{N}_2$  or Ar prior to use. All moisture sensitive reactions were performed under dry  $\text{N}_2$  or Ar. Reactions carried out below  $0^\circ\text{C}$  employed an acetone/dry ice bath or a cryocool and an isopropanol or acetone bath. Reagents obtained from commercial sources were used as received unless otherwise specified. THF,  $\text{Et}_2\text{O}$ , and 1,4-dioxane were distilled from sodium/benzophenone ketyl; DIPEA and TEA were distilled from  $\text{CaH}_2$  and stored over  $\text{KOH}$ ; and  $\text{CH}_2\text{Cl}_2$  and toluene were purified by passage through an activated alumina filtration system. Concentrating under reduced pressure refers to the use of a

rotary evaporator connected to a membrane vacuum pump to remove solvent.

Melting points were determined using a Laboratory Devices Mel-Temp II in open capillary tubes and are uncorrected. Infrared spectra were determined as neat solids or oils (unless otherwise specified) on a Perkin Elmer Spectrum 100. Low-resolution mass spectra were obtained on a Agilent Technologies 1260 Infinity II LCMS. High-resolution mass spectra were obtained on a Thermo Scientific Exactive Orbitrap LCMS or Agilent QTOF LCMS 6545A. Purity of compounds tested in biological assays was assessed using an Agilent Technologies 1260 Infinity II LC at 220 nm UV absorption (Waters XBridge BEH C<sub>18</sub> 2.1 x 50 mm, 2.5  $\mu$ m). Microwave reactions were performed using a Biotage Initiator in glass microwave vials (cap sealed) with continuous magnetic stirring and an external surface temperature sensor.

<sup>1</sup>H and <sup>13</sup>C NMR spectra were recorded on a Bruker Avance III 300MHz, 400 MHz, 500 MHz, and a cryoprobe equipped 600 MHz instruments. CDCl<sub>3</sub> was filtered through basic Al<sub>2</sub>O<sub>3</sub> immediately prior to sample preparation. Chemical shifts ( $\delta$ ) were reported in parts per million with the residual solvent peak used as an internal standard  $\delta$  <sup>1</sup>H / <sup>13</sup>C (Solvent); 7.26 / 77.16 (CDCl<sub>3</sub>); 2.50 / 39.52 (DMSO-d<sub>6</sub>); 3.31 / 49.00 (MeOD) and are tabulated as follows: chemical shift, multiplicity (s = singlet, brd = broad, d = doublet, t = triplet, q = quartet, m = multiplet), number of protons, and coupling constant(s). <sup>13</sup>C NMR spectra were obtained at 75 MHz, 100 MHz, 125, and 150 MHz using a proton-decoupled pulse sequence and are tabulated by observed peak. All 1D NMR spectra were processed using Bruker Topspin NMR. Thin-layer chromatography was performed using pre-coated silica gel 60 F<sub>254</sub> plates (EMD, 250  $\mu$ m thickness) and visualization was accomplished with a 254 nm UV light and by staining with a phosphomolybdic acid solution (5 g of phosphomolybdic acid in 100 mL of 95% EtOH), a *p*-anisaldehyde solution (2.5 mL of *p*-anisaldehyde, 2 mL of AcOH, and 3.5 mL of conc. H<sub>2</sub>SO<sub>4</sub> in 100 mL of 95% EtOH), a KMnO<sub>4</sub> solution (1.5 g of KMnO<sub>4</sub> and 1.5 g of K<sub>2</sub>CO<sub>3</sub> in 100 mL of a 0.1% NaOH solution), or Vaughn's reagent (4.8 g of (NH<sub>4</sub>)<sub>6</sub>Mo<sub>7</sub>O<sub>24</sub>•4 H<sub>2</sub>O and 0.2 g of Ce(SO<sub>4</sub>)<sub>2</sub> in 100 mL of a 3.5 N H<sub>2</sub>SO<sub>4</sub> solution). Flash chromatography on SiO<sub>2</sub> (Silicycle, Silia-P Flash Silica Gel or SiliaFlash® P60, 40-63  $\mu$ m) was used to purify crude reaction mixtures.

Enantiomeric and diastereomeric ratios were determined either by analytical HPLC on Rainin Dynamax HPLC (Dual Pump, Model SD-200) with Dynamax UV-1 absorbance detector using Chiralpak AD-H column, or analytical SFC performed on Mettler Toledo instrument using Chiralpak-IC semiprep or Cellulose-2 column.

**HT-1080 ferroptosis assay at CRO pharmaron.** A 50,000 cell/mL solution (200  $\mu$ L) of HT-1080 cells was added to a 96-well plate and incubated at 37  $^{\circ}$ C, 5% CO<sub>2</sub>, 95% humidity for 24 h. The compounds were dissolved in DMSO and a serial dilution was performed to achieve the desired testing concentration. This compound dilution (1  $\mu$ L) was added to culture medium (1 mL) containing erastin (10  $\mu$ M) to make the working solution. This working solution replaced the culture medium in each cell and the plate was incubated at 37  $^{\circ}$ C, 5% CO<sub>2</sub>, 95% humidity for 24 h. After 24 h, medium (100  $\mu$ L) was removed from each well and CellTiter-Glo® (50  $\mu$ L) reagent was added to each well. The plate was incubated for 30 min at rt to stabilize the luminescence signal. The plate was sealed, centrifuged for 1 min at 1,000 rpm to remove bubbles, and shaken for 1 min on an orbital shaker. Replicates of N=4 was used for all sample wells and ferrostatin-1 was used as a control in all assays. The luminescence was read in Enspire. The % remaining activity was determined by Equation 3-1:

$$\%Remaining\ Activity = \frac{S - M}{V - M} \times 100\% \quad \text{Equation 3-1}$$

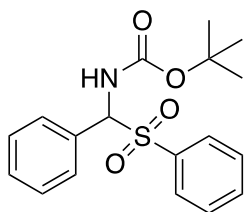
where S = readout of the test sample, V = readout of the vehicle sample, and M = readout of well with only Erastin treatment. Accordingly, the greater the luminescence signal the more protective the compound was. EC<sub>80</sub>'s were determined by plotting the data in GraphPad Prism and fitting the curves to a nonlinear regression model, either : [Agonist] vs. response -- variable slope (4-parameters) or [Agonist] vs. normalized response -- variable slope depending on the data type. The generated EC<sub>50</sub> and Hill slope were plugged into Equation 3-2 to generate the EC<sub>80</sub>:

$$EC_{80} = \frac{80}{100 - 80}^{\sqrt{H}} \times EC_{50} \quad \text{Equation 3-2}$$

where H is the Prism determined Hill slope.

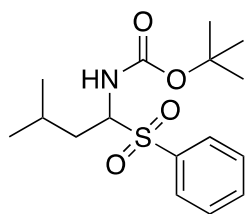
**General procedure A.** For the preparation of Boc-sulfones. The reaction was carried out according to a literature procedure and the product was prepared as described.<sup>235</sup> A mixture of aldehyde (16.3 mmol, 1.0 equiv), *t*-butyl carbamate (16.3 mmol, 1.0 equiv), and sodium benzene

sulfinate (16.3 mmol, 1.0 equiv) was treated sequentially, and under vigorous stirring, with THF (6.5 mL), H<sub>2</sub>O (14.9 mL), and formic acid (3.9 mL, 98.1 mmol, 6.0 equiv). The reaction mixture was stirred at room temperature for 72 h under a N<sub>2</sub> atmosphere. The white precipitate was filtered, washed with H<sub>2</sub>O (50 mL), suspended in a mixture of hexanes (25 mL) and CH<sub>2</sub>Cl<sub>2</sub> (2.5 mL), and stirred for 2 h at room temperature. The residue was filtered and washed with hexanes. The colorless sulfone was dried under high vacuum and used without further purification.



**3-15** *tert*-Butyl (phenyl(phenylsulfonyl)methyl)carbamate (**3-15**).<sup>236</sup> According

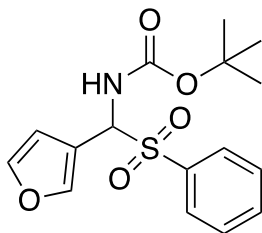
to General Procedure A, benzaldehyde (2.00 mL, 19.5 mmol, 1 equiv), *t*-butyl carbamate (2.28 g, 19.5 mmol, 1 equiv), sodium benzene sulfinate (3.27 g, 19.5 mmol, 1 equiv), and formic acid (4.65 mL, 117 mmol, 6 equiv) afforded **3-15** (5.70 g, 16.4 mmol, 84%) as a white solid: <sup>1</sup>H NMR (400 MHz, CDCl<sub>3</sub>) δ 7.91 (d, *J* = 7.6 Hz, 2H), 7.66-7.62 (m, 1H), 7.56-7.43 (m, 2H), 7.42 (brd s, 5H), 5.92 (d, *J* = 10.8 Hz, 1H), 5.75 (d, *J* = 10.8 Hz, 1H), 1.26 (s, 9H); <sup>13</sup>C NMR (100 MHz, CDCl<sub>3</sub>) δ 192.5, 136.4, 134.5, 132.0, 130.1, 129.9, 129.84, 129.78, 129.5, 129.1, 129.0, 128.9, 128.8, 128.7, 126.4, 124.9, 28.2.



**3-16** *tert*-Butyl (3-methyl-1-(phenylsulfonyl)butyl)carbamate (**3-16**).<sup>235</sup>

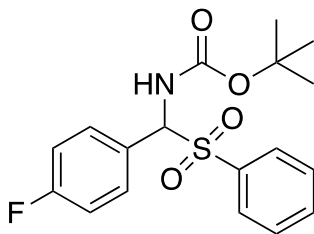
According to General Procedure A, isovaleraldehyde (2.03 mL, 18.4 mmol, 1 equiv), *t*-butyl carbamate (2.15 g, 18.4 mmol, 1 equiv), sodium benzene sulfinate (3.07 g, 18.4 mmol, 1 equiv), and formic acid (5.12 mL, 110 mmol, 6 equiv) afforded **3-16** (5.45 g, 16.6 mmol, 91%) as a white solid: Mp 119.8-121.9 °C; IR (ATR, neat) 3301, 2967, 1692, 1523, 1447, 1306, 1245, 1104, 1085, 1047, 1025, 873, 845, 750, 688 cm<sup>-1</sup>; <sup>1</sup>H NMR (400 MHz, CDCl<sub>3</sub>) δ 7.91 (app d, *J* = 7.6 Hz, 2H), 7.64-7.61 (m, 1H), 7.55-7.52 (m, 2H), 4.92 (d, *J* = 5.2 Hz, 1H), 2.05-2.00 (m, 1H), 1.80-1.70 (m,

2H), 1.20 (s, 9H), 1.00 (d,  $J = 6.4$  Hz, 3H), 0.92 (d,  $J = 6.4$  Hz, 3H);  $^{13}\text{C}$  NMR (100 MHz,  $\text{CDCl}_3$ )  $\delta$  153.6, 137.0, 133.8, 129.3, 129.2, 129.0, 80.8, 69.6, 34.5, 28.0, 24.8, 23.2, 21.1; HRMS (HESI)  $m/z$  calcd for  $\text{C}_{16}\text{H}_{26}\text{NO}_4\text{SNa}$   $[\text{M}+\text{H}]^+$  350.1393, found 350.1393.



**3-37** *tert*-Butyl (furan-3-yl(phenylsulfonyl)methyl)carbamate (**3-37**).<sup>237</sup>

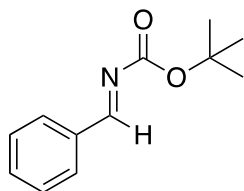
According to General Procedure A, 3-furaldehyde (2.88 mL, 33.0 mmol, 1 equiv), *t*-butyl carbamate (3.86 g, 33.0 mmol, 1 equiv), sodium benzene sulfinate (5.58 g, 33.0 mmol, 1 equiv), and formic acid (7.86 mL, 198 mmol, 6 equiv) afforded **3-37** (6.32 g, 18.7 mmol, 57%) as a white solid: Mp 164.0-167.5 °C; IR (ATR, neat) 3248, 1686, 1529, 1448, 1369, 1317, 1250, 1132, 1083, 1016, 872, 859, 680  $\text{cm}^{-1}$ ;  $^1\text{H}$  NMR (300 MHz,  $\text{CDCl}_3$ )  $\delta$  7.93 (d,  $J = 7.5$  Hz, 2H), 7.68-7.48 (m, 4H), 7.47 (s, 1H), 5.93 (d,  $J = 10.5$  Hz, 1H), 5.57 (d,  $J = 10.5$  Hz, 1H), 1.25 (s, 9H);  $^{13}\text{C}$  NMR (75 MHz,  $\text{CDCl}_3$ )  $\delta$  184.5, 153.4, 151.4, 145.0, 143.8, 142.6, 134.0, 131.8, 129.5, 129.1, 129.0, 124.9, 115.4, 109.7, 107.0, 28.2.



**3-40** *tert*-Butyl ((4-fluorophenyl)(phenylsulfonyl)methyl)carbamate (**3-40**).<sup>236</sup>

According to General Procedure A, 4-fluorobenzaldehyde (3.60 mL, 32.7 mmol, 1 equiv), *t*-butyl carbamate (3.83 g, 32.7 mmol, 1 equiv), sodium benzene sulfinate (5.53 g, 32.7 mmol, 1 equiv), and formic acid (7.79 mL, 196 mmol, 6 equiv) afforded **3-40** (4.87 g, 13.3 mmol, 82% yield) as a white solid:  $^1\text{H}$  NMR (300 MHz,  $\text{CDCl}_3$ )  $\delta$  7.93-7.90 (app d,  $J = 7.2$  Hz, 2H), 7.68-7.64 (m, 1H), 7.58-7.53 (m, 2H), 7.46-7.41 (m, 2H), 7.12 (t,  $J = 8.4$  Hz, 2H), 5.90 (br d,  $J = 10.5$  Hz, 1H), 5.68 (br d,  $J = 10.5$  Hz, 1H), 1.25 (s, 9H).  $^{19}\text{F}$  NMR (470 MHz,  $\text{CDCl}_3$ )  $\delta$  -110.8.

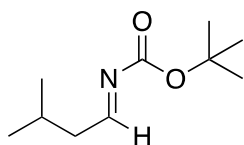
**General procedure B.** For the preparation of Boc-imines. The reaction was carried out according to a literature procedure and the product was prepared as described.<sup>202</sup> A mixture of sulfone (0.903 mmol, 1.0 equiv) and cesium carbonate (2.71 mmol, 3.0 equiv) was dried under high vacuum for 1 h in a 50 mL round bottom flask. Anhydrous CH<sub>2</sub>Cl<sub>2</sub> (0.2 M, 5.0 mL) was added and the suspension was stirred for 45 min at 40 °C under an N<sub>2</sub> atmosphere. The reaction mixture was diluted with cold hexanes (3.0 mL, 0 °C) and filtered through a plug of Hyflo® Super-Cel®. The plug was washed with hexanes (10.0 mL), and the filtrate was concentrated under reduced pressure (bath temperature maintained at 20 °C) and dried under high vacuum to afford the desired Boc-imine that was used in the following step without further purification.



**3-17**

***tert*-Butyl benzylcarbamate (3-17).**<sup>236</sup> According to General Procedure B, **3-**

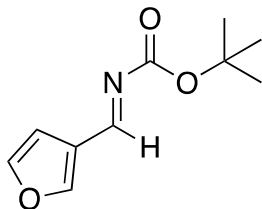
**15** (0.825 g, 2.26 mmol, 1 equiv) and Cs<sub>2</sub>CO<sub>3</sub> (2.23 g, 6.77 mmol, 3 equiv) afforded **3-17** (quant.) as a colorless oil: <sup>1</sup>H NMR showed quantitative conversion and minor impurities. Diagnostic NMR peaks: <sup>1</sup>H NMR (300 MHz, CDCl<sub>3</sub>) δ 8.87 (s, 1H), 7.91 (d, *J* = 6.9 Hz, 2H), 7.59-7.53 (m, 1H), 7.49-7.44 (m, 2H), 1.59 (s, 9H).



**3-18**

***tert*-Butyl (3-methylbutylidene)carbamate (3-18).**<sup>235</sup> According to General

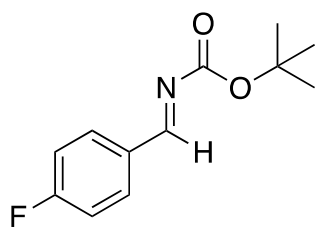
Procedure B, **3-16** (0.535 g, 1.63 mmol, 1 equiv) and Cs<sub>2</sub>CO<sub>3</sub> (1.61 g, 4.90 mmol, 3 equiv) afforded **3-18** (quant) as a colorless oil: <sup>1</sup>H NMR showed quantitative conversion and minor impurities. Diagnostic NMR peak: <sup>1</sup>H NMR (CDCl<sub>3</sub>, 400 MHz) δ 8.24 (s, 1 H).



**3-38**

***tert*-Butyl (furan-3-ylmethylidene)carbamate (3-38).**<sup>237</sup> According to General

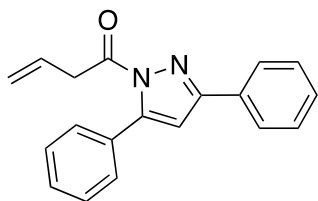
Procedure B, **3-37** (0.750 g, 2.22 mmol, 1 equiv) and Cs<sub>2</sub>CO<sub>3</sub> (2.17 g, 6.67 mmol, 3 equiv) afforded **3-38** (0.360 g, 1.84 mmol, 83%) as a white solid: <sup>1</sup>H NMR (300 MHz, DMSO-*d*<sub>6</sub>) δ 8.82 (s, 1H), 8.48 (s, 1H), 7.56 (d, *J* = 2.1 Hz, 1H), 6.85 (d, *J* = 2.1 Hz, 1H), 1.48 (s, 9H).



**3-41**

***tert*-Butyl (*E*)-(4-fluorobenzylidene)carbamate (3-41).**<sup>236</sup> According to

General Procedure B, **3-40** (1.00 g, 2.74 mmol, 1 equiv) and Cs<sub>2</sub>CO<sub>3</sub> (2.67 g, 8.21 mmol, 3 equiv) afforded **3-41** (0.590 g, 2.64 mmol, 97%) as a white solid: <sup>1</sup>H NMR (300 MHz, CDCl<sub>3</sub>) δ 8.85 (s, 1H), 7.96-7.91 (m, 2H), 7.16 (t, *J* = 8.4 Hz, 2H), 1.58 (s, 9H).

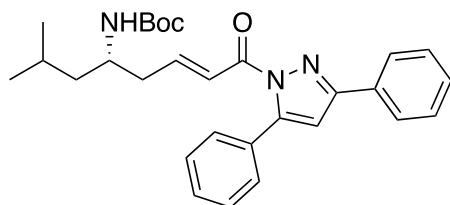


**3-19**

**1-(3,5-Diphenyl-1H-pyrazol-1-yl)but-3-en-1-one (3-19).**<sup>161</sup> To a

mixture of but-3-enoic acid (1.00 mL, 11.4 mmol, 1 equiv) and 3,5-diphenylpyrazole (2.56 g, 11.4 mmol, 1 equiv) in dry CH<sub>2</sub>Cl<sub>2</sub> (23 mL, 0.5 M) was added EDC·HCl (3.49 g, 18.2 mmol, 1.6 equiv) at 0 °C. After stirring for 60 min, the reaction was quenched with saturated brine (10 mL). The organic layer was separated and the aqueous phase was extracted with CH<sub>2</sub>Cl<sub>2</sub> (50 mL x 2). The combined organic layers were dried (MgSO<sub>4</sub>) and the solvent was removed under reduced pressure. The crude product was purified by chromatography on SiO<sub>2</sub> (9:1, hexanes:EtOAc) to afford **3-19** (4.38 g, 15.2 mmol, 67%) as a white solid: Mp 70.5-72.4 °C; IR (ATR) 3059, 1736, 1557, 1487, 1459, 1439, 1399, 1340, 1247, 1195, 1026, 986, 945, 921, 907, 800, 760, 698 cm<sup>-1</sup>;

$^1\text{H}$  NMR ( $\text{CDCl}_3$ , 500 MHz)  $\delta$  7.90 (dd,  $J$  = 14.0, 3.0 Hz, 2H), 7.46-7.40 (m, 8H), 6.72 (s, 1H), 6.15-6.01 (m, 1H), 5.32-5.22 (m, 2H), 4.05 (d,  $J$  = 11.5 Hz, 2H);  $^{13}\text{C}$  NMR ( $\text{CDCl}_3$ , 125 MHz)  $\delta$  171.1, 153.5, 147.5, 131.8, 131.0, 130.2, 129.2, 129.0, 128.8, 127.9, 126.3, 119.3, 109.8, 40.5; HRMS (LCMS ESI+)  $m/z$  calcd for  $\text{C}_{19}\text{H}_{17}\text{N}_2\text{O}$   $[\text{M}+\text{H}]^+$  289.1335, found 289.1332.



**(S)-3-20**

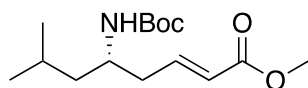
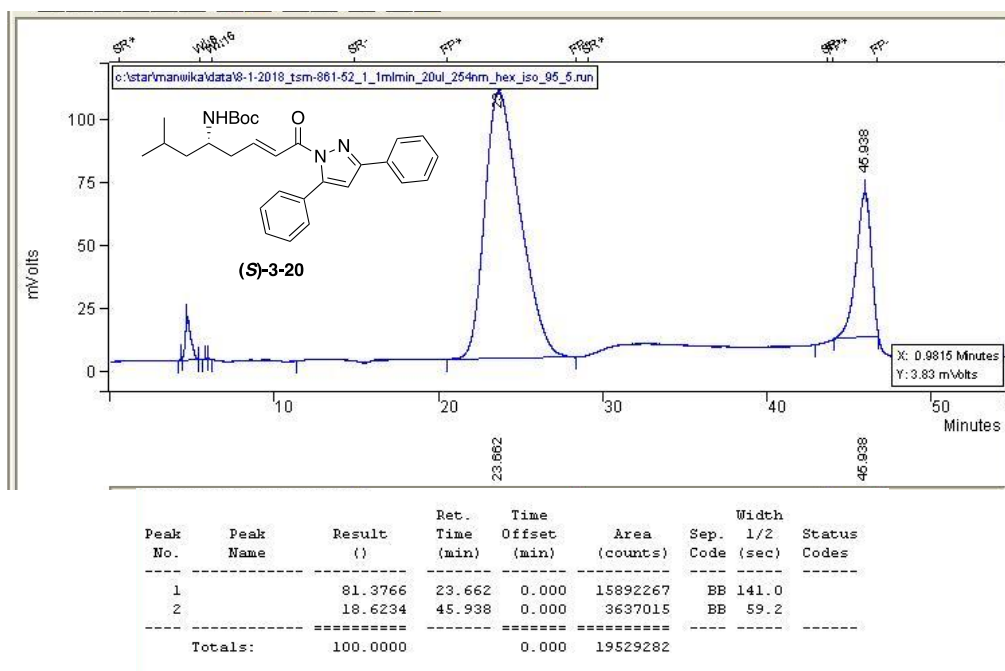
*tert*-Butyl (S,E)-(8-(3,5-diphenyl-1H-pyrazol-1-yl)-2-

**methoxy-8-oxooct-6-en-4-yl)carbamate ((S)-3-20).**<sup>161</sup> A dried 25 mL round bottom flask equipped with a magnetic stir bar was charged with  $[\text{Cu}(\text{CH}_3\text{CN})_4]\text{PF}_6$  (0.010 g, 0.028 mmol, 0.02 equiv) and (S)-DTBM-SEGPHOS (0.033 g, 0.028 mmol, 0.02 equiv) under an Ar atmosphere. Distilled anhydrous THF (12.5 mL) was added via syringe. The mixture was stirred for 15 min to give a colorless catalyst solution that was kept sealed under Ar at room temperature until the imine was prepared (3 h). To a freshly prepared **3-18** (1.11 g by mass - residual hexanes and  $\text{CH}_2\text{Cl}_2$ , 4 equiv) was added the catalyst solution containing the copper(I) complex via syringe (12.5 mL), and, immediately, the combined solution was added to **3-19** (0.400 g, 1.39 mmol, 1 equiv) in a dried 25-mL round bottom flask equipped with a magnetic stir bar under Ar atmosphere at room temperature. Upon addition of imine and catalyst, the reaction turned a faint yellow color. The reaction mixture was cooled to  $-50\text{ }^\circ\text{C}$  and  $\text{Et}_3\text{N}$  (0.02 M in THF, 0.70 mL, 0.028 mmol, 0.02 equiv) was added. Immediately upon addition of  $\text{Et}_3\text{N}$ , the reaction turned a golden yellow color. The resulting reaction mixture was stirred at  $-50\text{ }^\circ\text{C}$  for 17.5 h, filtered through a plug of basic alumina, and concentrated under reduce pressure. The crude product was purified by chromatography on  $\text{SiO}_2$  (8:1, hexanes:EtOAc) to afford (S)-**3-20** (0.644 g, 1.36 mmol, 98%) as a colorless crystalline solid: Mp  $134.3\text{--}137.2\text{ }^\circ\text{C}$ ; IR (ATR, neat) 3348, 2955, 1701, 1640, 1524, 1438, 1350, 1275, 1242, 1166, 971, 945, 886, 760, 668  $\text{cm}^{-1}$ ;  $[\alpha]_D^{25}$  -16.0 ( $c$  0.50,  $\text{CH}_2\text{Cl}_2$ );  $^1\text{H}$  NMR ( $\text{CD}_3\text{OD}$ , 400 MHz)  $\delta$  7.98 (d,  $J$  = 6.8 Hz, 2H), 7.50-7.40 (m, 9H), 7.19-7.12 (m, 1H), 6.94 (s, 1H), 6.63 (d,  $J$  = 9.2 Hz, 1H), 3.83-3.73 (m, 1H), 2.58-2.52 (m, 1H), 2.45-2.38 (m, 1H), 1.74-1.67 (m, 1H), 1.49-1.44 (m, 1H), 1.34 (s, 9H), 1.30-1.22 (m, 1H), 0.95-0.89 (m, 6 H);  $^{13}\text{C}$  NMR (100 MHz,  $\text{CD}_3\text{OD}$ )  $\delta$  164.0, 148.4, 147.6, 131.8, 131.3, 128.9, 128.6, 128.4, 128.3, 127.5, 126.0,



123.0, 109.6, 78.5, 43.8, 39.2, 27.3, 24.7, 22.2, 20.9; HRMS (LCMS ESI+)  $m/z$  calcd for  $C_{29}H_{36}N_3O_3$   $[M+H]^+$  474.2751, found 474.2751. The enantiomeric ratio was determined as 81:19 by chiral HPLC (Chiralcel ADH; 98:2 hexane:EtOH, 254 nm; 1.0 mL/min; Rt 23.7 min).

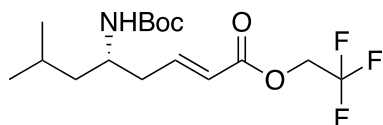
HPLC (Chiralcel-AD-H) 98:2, hexane:EtOH, 254 nm, 1.0 mL/min



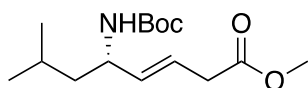
**(S)-3-21**

**Methyl (S,E)-5-((tert-butoxycarbonyl)amino)-7-methyloct-2-enoate**

**((S)-3-21).** To a flame-dried round bottom flask containing MeOH (1 mL, 0.2 M) was added (S)-**3-20** (0.107 g, 0.226 mmol, 1 equiv). The mixture was stirred at 60 °C for 18 h, the solvent was removed under reduced pressure, and the residue was purified by chromatography on  $SiO_2$  (9:1, hexanes:EtOAc) to afford (S)-**3-21** (0.053 g, 0.18 mmol, 88%) as a white solid:  $^1H$  NMR ( $CD_3OD$ , 300 MHz)  $\delta$  6.99-6.88 (m, 1H), 6.51 (d,  $J$  = 9.0 Hz, 1H), 5.87 (d,  $J$  = 15.6 Hz, 1H), 3.70 (s, 3H), 2.43-2.34 (m, 1H), 2.28-2.18 (m, 1H), 1.69-1.60 (m, 1H), 1.45 (s, 9H), 1.26-1.22 (m, 2H), 0.93-0.89 (m, 6H);  $^{13}C$  NMR (100 MHz,  $CD_3OD$ )  $\delta$  167.0, 156.7, 146.2, 122.4, 78.4, 50.5, 43.7, 38.6, 27.3, 24.6, 22.2, 20.8; HRMS (LCMS ESI+)  $m/z$  calcd for  $C_{15}H_{28}NO_4$   $[M+H]^+$  286.2013, found 286.2009.

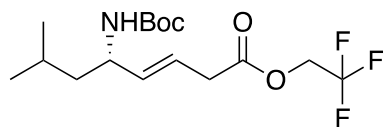


**(S)-3-22**      **2,2,2-Trifluoroethyl**      **(S,E)-5-((tert-butoxycarbonyl)amino)-7-methyloct-2-enoate ((S)-3-22)**. To a flame-dried round bottom flask containing 2,2,2-trifluoroethanol (10 mL, 0.1 M) was added (S)-3-20 (0.546 g, 1.15 mmol). The mixture was stirred at 75 °C for 7 h, the solvent was removed under reduced pressure, and the residue was purified by chromatography on SiO<sub>2</sub> (9:1, hexanes:EtOAc) to afford (S)-3-22 (0.344 g, 0.973 mmol, 84%) as a colorless solid: Mp 69.5-71.3 °C; IR (ATR, neat) 3342, 296, 2931, 1736, 1678, 1654, 1526, 1440, 1365, 1338, 1280, 1207, 1170, 1059, 981, 844, 751 cm<sup>-1</sup>; <sup>1</sup>H NMR (CDCl<sub>3</sub>, 400 MHz) δ 7.09-6.99 (m, 1H), 5.92 (d, *J* = 15.6 Hz, 1H) 4.50 (q, *J* = 8.8 Hz, 2H), 4.28 (d, *J* = 8.4 Hz, 1H), 3.81 (t, *J* = 6.0 Hz, 1H), 2.45 (q, *J* = 6.0 Hz, 1H), 2.31 (q, *J* = 6.4 Hz, 1H), 1.70-1.65 (m, 1H), 1.45 (s, 9H), 1.34-1.24 (m, 2H), 0.91 (d, *J* = 6.8 Hz, 6H); <sup>13</sup>C NMR (CDCl<sub>3</sub>, 400 MHz) δ 162.4, 159.1, 155.2, 148.2, 139.0, 134.2, 122.0, 60.3, 50.2, 28.3, 27.0, 24.9, 23.0; HRMS (LCMS ESI+) *m/z* calcd for C<sub>11</sub>H<sub>19</sub>F<sub>3</sub>NO<sub>2</sub> (MW – C<sub>5</sub>H<sub>8</sub>O<sub>2</sub> (Boc group)) [M+H]<sup>+</sup> 254.1362, found 254.1361.



**(S)-3-23**      **Methyl (S,E)-5-((tert-butoxycarbonyl)amino)-7-methyloct-3-enoate ((S)-3-23)**.<sup>79</sup> A solution of (S)-3-21 (50 mg, 0.17 mmol, 1 equiv) and 1,2-dimethylimidazole (24 mg, 0.24 mmol, 1.4 equiv) in methanol (1.5 mL, 0.1 M) was irradiated in a quartz cuvette in a Rayonet reactor with 15 low-pressure mercury lamps. The reaction was monitored by NMR to determine the ratio of conjugated to unconjugated product. After 23 h under irradiation, TLC analysis (5:1, hexanes:EtOAc, developed 2x) indicated that starting material was entirely consumed. The crude reaction mixture (5:1, *trans:cis*) was purified by chromatography on SiO<sub>2</sub> (9:1, hexanes:EtOAc) to afford (S)-3-23 (0.018 g, 0.063 mmol, 36%) as a white solid: Mp 55.0-56.4 °C; IR (ATR, neat) 3322, 2954, 1735, 1685, 1534, 1436, 1390, 1364, 1250, 1176, 1051, 972, 873, 752, 686 cm<sup>-1</sup>; <sup>1</sup>H NMR (CD<sub>3</sub>OD, 400 MHz) δ 6.63 (d, *J* = 6.8 Hz, 1H), 5.65 (ddt, *J* = 15.6, 7.2, 0.9 Hz, 1H) 5.48 (dd, *J* = 15.6, 6.4 Hz, 1H), 4.06 (brd s, 1H), 3.66 (s, 3H), 3.07 (d, *J* = 6.8 Hz, 2H), 1.68-1.61 (m, 1H), 1.44 (s, 9H), 1.37-1.29 (m, 2H), 0.91 (d, *J* = 6.8 Hz, 6H); <sup>13</sup>C NMR

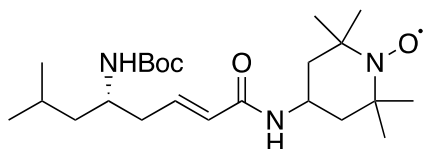
(CD<sub>3</sub>OD, 400 MHz)  $\delta$  172.5, 156.5, 135.3, 121.5, 50.9, 50.1, 43.9, 36.8, 27.4, 24.5, 21.7, 21.1; HRMS (LCMS ESI+)  $m/z$  calcd for C<sub>15</sub>H<sub>28</sub>NO<sub>4</sub> [M+H]<sup>+</sup> 286.2013, found 286.2009.



**(S)-3-24**

**2,2,2-Trifluoroethyl (S,E)-5-((tert-butoxycarbonyl)amino)-7-**

**methyloct-3-enoate ((S)-3-24).** A solution containing (S)-3-22, (0.160 g, 0.453 mmol, 1 equiv) and 1,2-dimethylimidazole (0.062 g, 0.63 mmol, 1.4 equiv) in methanol (1.5 mL, 0.3 M) was irradiated in a quartz cuvette in a Rayonet reactor with 15 low-pressure mercury lamps. The reaction was monitored by NMR to determine the ratio of conjugated to unconjugated product. After 24 h under irradiation, TLC (5:1, hexanes:EtOAc, developed 2x) indicated that starting material was entirely consumed. The crude reaction mixture (5:1, *trans:cis*) was purified by chromatography on SiO<sub>2</sub> (9:1, hexanes:EtOAc) to afford (S)-3-24 (0.054 g, 0.15 mmol, 34%) as a colorless solid: <sup>1</sup>H NMR (MeOD, 400 MHz)  $\delta$  6.64 (d,  $J$  = 7.6 Hz, 1H), 5.70-5.63 (m, 1H), 5.53 (dd,  $J$  = 15.2, 6.0 Hz, 1H), 4.59 (q,  $J$  = 8.4 Hz, 2H), 4.06 (brd s, 1H), 3.18 (d,  $J$  = 6.4 Hz, 2H), 1.69-1.58 (m, 1H), 1.43 (s, 9H), 1.33-1.24 (m, 2H), 0.91 (d,  $J$  = 6.8 Hz, 6H).

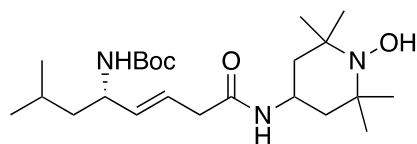


**(S)-3-25**

**(S,E)-N-(2,2,6,6-Tetramethyl-1-oxo-piperidin-4-yl)-5-(tert-**

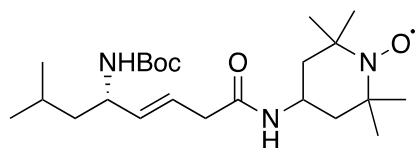
**butoxycarbonylamino)-7-methyloct-2-enamide (4-25).** To a dried microwave vial equipped with a magnetic stir bar was added (S)-3-20, (0.200 g, 0.422 mmol, 1 equiv) and 4-AT (0.304 g, 1.69 mmol, 4 equiv.). Anhydrous THF (6 mL, 0.07 M) was added and the mixture was heated in the microwave at 90 °C for 1 h. The reaction was concentrated under reduced pressure and purified by chromatography on SiO<sub>2</sub> with gradient elution (2:1 to 1:1, hexanes:EtOAc) to afford (S)-3-25 (0.070 g, 0.16 mmol, 39%) as an orange solid: Mp 175.5-178.3 °C; IR (ATR, neat) 3088, 1671, 1606, 1509, 1457, 1224, 1107, 1039, 900, 822, 765, 705 cm<sup>-1</sup>; HRMS (LCMS ESI+)  $m/z$  calcd for C<sub>23</sub>H<sub>43</sub>N<sub>3</sub>O<sub>4</sub> [M+H]<sup>+</sup> 425.3248, found 425.3247.

For  $^1\text{H}$  NMR characterization, 16 mg of the nitroxide was reduced to the corresponding hydroxylamine: A solution of (*S*)-**3-25** (16 mg, 0.038 mmol, 1 equiv) in MeOH (1.5 mL, 0.1 M) was treated with ascorbic acid (33 mg, 0.19 mmol, 5 equiv) and stirred for 1 h until it turned from orange to colorless. The solution was diluted with ether, washed with sat.  $\text{NaHCO}_3$  and water, and the organic layer was dried ( $\text{MgSO}_4$ ), concentrated, and dissolved in  $\text{CD}_3\text{OD}$  for analysis:  $^1\text{H}$  NMR ( $\text{CD}_3\text{OD}$ , 500 MHz)  $\delta$  6.65-6.59 (m, 1H), 6.38 (d,  $J$  = 9.0 Hz, 1H), 5.80 (d,  $J$  = 15.5 Hz, 1H), 4.45 (s, 1H), 4.08-4.03 (m, 1H), 3.58 (brd s, 1H), 2.26-2.22 (m, 1H), 2.15-2.12 (m, 1H), 1.67-1.63 (m, 2H), 1.61-1.57 (m, 1H), 1.44 (s, 9H) 1.34-1.32 (m, 4H), 1.19 (s, 6H), 1.09 (s, 6H), 0.82-0.80 (d,  $J$  = 6.5 Hz, 6H).



***tert*-Butyl (*S,E*)-(8-((1-hydroxy-2,2,6,6-tetramethylpiperidin-**

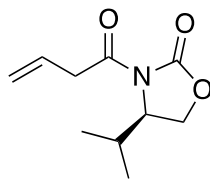
**4-yl)amino)-2-methyl-8-oxooct-5-en-4-yl)carbamate (JP4-039 hydroxyl amine).**<sup>79</sup> A solution of (*S*)-**3-25**, (58 mg, 0.14 mmol, 1 equiv) and 1,2-dimethylimidazole (19 mg, 0.19 mmol, 1.4 equiv) in methanol (1.0 mL, 0.1 M) in a quartz cuvette was irradiated with 15 low-pressure mercury lamps for 24 h. After 24 h under irradiation, TLC analysis (1:2, hexanes:EtOAc, developed 2x) indicated that starting material was consumed. The mixture was concentrated under reduced pressure and purified by chromatography on  $\text{SiO}_2$  with gradient elution (3:1 to 1:1, hexanes:EtOAc) to afford **JP4-039 hydroxyl amine** (19.4 mg, 0.046 mmol, 34%) as a white solid: Mp 69.3-72.0 °C; IR (ATR, neat) 3311, 2931, 1644, 1523, 1365, 1244, 1176, 972  $\text{cm}^{-1}$ ;  $^1\text{H}$  NMR ( $\text{CD}_3\text{OD}$ , 400 MHz)  $\delta$  6.65 (brd s, 1H), 5.65 (ddt,  $J$  = 14.8, 7.2, 0.9 Hz, 1H) 5.50 (dd,  $J$  = 14.8, 6.8 Hz, 1H), 4.13-4.04 (m, 2H), 2.88 (d,  $J$  = 6.8 Hz, 2H), 1.74-1.70 (m, 2 H), 1.66-1.61 (m, 1H), 1.44 (s, 9H), 1.36-1.29 (m, 4H), 1.17 (s, 6H), 1.15 (s, 6H), 0.91 (d,  $J$  = 6.0 Hz, 6H); HRMS (LCMS ESI+)  $m/z$  calcd for  $\text{C}_{23}\text{H}_{44}\text{N}_3\text{O}_4$   $[\text{M}+\text{H}]^+$  426.3326, found 426.3325.



(*S,E*)-*N*-(2,2,6,6-Tetramethyl-1-oxo-piperidin-4-yl)-5-(*tert*-

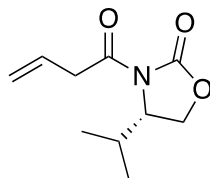
**butoxycarbonylamino)-7-methyloct-3-enamide (JP4-039).**<sup>79</sup> To a solution of **JP4-039 hydroxyl amine** (18 mg, 0.042 mmol, 1 equiv) in *t*-butyl methyl ether (1.0 mL, 0.04 M) was added a 10% aqueous solution of potassium ferricyanide (0.37 mL, 0.21 mmol, 5 equiv). The solution was stirred vigorously at rt. The conversion was monitored by TLC analysis (1:1, hexanes:EtOAc). After 2.5 h, the mixture was extracted with EtOAc (3 mL) and the combined organic layers were filtered through a plug of sand and SiO<sub>2</sub> to afford **JP4-039** (17.9 mg, 0.042 mmol, quant) as an orange solid: R<sub>f</sub>=0.6 (1:1, hexanes:EtOAc), HRMS (LCMS ESI+) *m/z* calcd for C<sub>23</sub>H<sub>43</sub>N<sub>3</sub>O<sub>4</sub> [M+H]<sup>+</sup> 425.3248, found 425.3245.

**General procedure C.** For the preparation of acyl oxazolidinones. To a solution of but-3-enoic acid (7.90 mmol, 1.4 equiv) in dry THF (30 mL, 0.3 M) at 0 °C under N<sub>2</sub> atmosphere was added *N*-methylmorpholine (7.90 mmol, 1.4 equiv) and pivaloyl chloride (7.90 mmol, 1.4 equiv). The colorless mixture was stirred at -78 °C for 1 h. In a separate flask, *n*-BuLi (2.5 M solution in hexane, 2.60 mL, 6.49 mmol, 1.15 equiv) was added to a solution of oxazolidinone (5.64 mmol, 1 equiv) in dry THF (30 mL, 0.2 M) under an N<sub>2</sub> atmosphere at -78 °C. After 30 min at -78 °C, the clear solution of the lithium anion of the oxazolidinone was transferred dropwise to the flask containing the mixed anhydride and stirred at -78 °C for 1 h and then warmed to rt and stirred for 16 h. The reaction mixture was diluted with saturated aqueous NH<sub>4</sub>Cl (20 mL) and the aqueous layer was extracted with EtOAc (3 x 20 mL). The combined organic layers were dried (MgSO<sub>4</sub>) and the solvent was evaporated. The residue was purified by chromatography on SiO<sub>2</sub> with gradient elution (6:1 to 3:1, hexanes:EtOAc) to afford the desired acyl oxazolidinone.



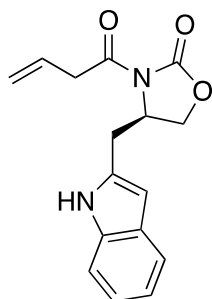
**(R)-3-26**

**(R)-3-(But-3-enoyl)-4-isopropylloxazolidin-2-one ((R)-3-26).** According to General Procedure C but using Et<sub>3</sub>N instead of NMM, but-3-enoic acid (0.494 mL, 5.58 mmol, 1 equiv), (R)-4-isopropyl-2-oxazolidinone (0.798 g, 6.13 mmol, 1.1 equiv), Et<sub>3</sub>N (0.871 mL, 6.13 mmol, 1.1 equiv), *n*-BuLi (2.5 M in hexanes, 2.45 mL, 6.13 mmol, 1.1 equiv), and pivaloyl chloride (0.735 mL, 5.85 mmol, 1.05 equiv) afforded **(R)-3-26** (0.520 g, 2.64 mmol, 47%) as a light yellow liquid: IR (ATR, neat) 2965, 2878, 1771, 1698, 1387, 1366, 1300, 1197, 1144, 1095, 1057, 1021, 974, 923, 773, 716 cm<sup>-1</sup>; [ $\alpha$ ]<sub>D</sub><sup>25</sup> -99.2 (*c* 0.9, CHCl<sub>3</sub>); <sup>1</sup>H NMR (500 MHz, CDCl<sub>3</sub>)  $\delta$  6.03-5.95 (m, 1H), 5.24-5.20 (m, 2H), 4.45-4.42 (m, 1H), 4.30-4.21 (m, 2H), 3.72 (dq, *J* = 7.0, 1.5 Hz, 2H), 2.42-2.35 (m, 1H), 0.91 (d, *J* = 7.0 Hz, 3H), 0.87 (d, *J* = 7.0 Hz, 3H); <sup>13</sup>C NMR (75 MHz, CDCl<sub>3</sub>)  $\delta$  171.2, 154.0, 129.9, 119.1, 63.4, 58.4, 40.2, 28.3, 18.0, 14.7; HRMS (LCMS ESI+) *m/z* calcd for C<sub>10</sub>H<sub>16</sub>NO<sub>3</sub> [M+H] 198.1125, found 198.1124.



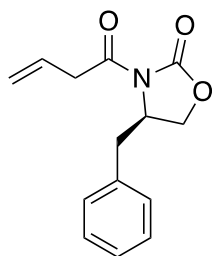
**(S)-3-26**

**(S)-3-(But-3-enoyl)-4-isopropylloxazolidin-2-one ((S)-3-26).** According to General Procedure C but using Et<sub>3</sub>N instead of NMM, but-3-enoic acid (0.988 mL, 11.2 mmol, 1 equiv), (S)-4-isopropyl-2-oxazolidinone (1.62 g, 12.3 mmol, 1.1 equiv), Et<sub>3</sub>N (1.74 mL, 12.3 mmol, 1.1 equiv), *n*-BuLi (2.5 M in hexanes, 4.91 mL, 12.3 mmol, 1.1 equiv), and pivaloyl chloride (1.47 mL, 11.7 mmol, 1.05 equiv) afforded **(S)-3-26** (1.31 g, 6.64 mmol, 60%) as a light yellow liquid: [ $\alpha$ ]<sub>D</sub><sup>25</sup> +94.1 (*c* 1.4, CHCl<sub>3</sub>).



**(R)-3-27** **(R)-4-((1H-Indol-2-yl)methyl)-3-(but-3-enoyl)oxazolidin-2-one ((R)-3-27).**

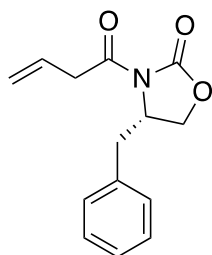
According to General Procedure C but using Et<sub>3</sub>N instead of NMM, but-3-enoic acid (0.247 mL, 2.79 mmol, 1 equiv), (R)-(-)-4-(1H-indol-3-ylmethyl)-2-oxazolidinone (0.677 g, 3.07 mmol, 1.1 equiv), Et<sub>3</sub>N (0.435 mL, 3.07 mmol, 1.1 equiv), *n*-BuLi (2.5 M in hexanes, 1.23 mL, 3.07 mmol, 1.1 equiv), and pivaloyl chloride (0.367 mL, 2.93 mmol, 1.05 equiv) afforded **(R)-3-27** (0.587 g, 2.06 mmol, 74%) as a colorless semi-solid: IR (ATR, neat) 3394, 2981, 2917, 1768, 1692, 1424, 1386, 1363, 1339, 1199, 1095, 1044, 991, 925, 726, 710 cm<sup>-1</sup>; [ $\alpha$ ]<sub>D</sub><sup>25</sup> -80.0 (*c* 0.1, CHCl<sub>3</sub>); <sup>1</sup>H NMR (500 MHz, CDCl<sub>3</sub>)  $\delta$  8.11 (s, 1H), 7.76 (d, *J* = 8.0 Hz, 1H), 7.38 (d, *J* = 8.5 Hz, 1H), 7.25-7.18 (m, 1H), 7.16-7.15 (m, 1H), 7.07 (s, 1H), 6.09-6.03 (m, 1H), 5.29-5.25 (m, 2H), 4.80-4.77 (m, 1H), 4.24-4.19 (m, 2H), 3.76 (dq, *J* = 7.0, 1.5 Hz, 2H), 3.49-3.46 (m, 1H), 2.95-2.90 (m, 1H); <sup>13</sup>C NMR (125 MHz, CDCl<sub>3</sub>)  $\delta$  171.4, 153.6, 136.3, 130.5, 129.21, 129.19, 127.4, 123.3, 122.0, 120.7, 120.6, 119.5, 118.3, 118.1, 112.0, 110.7, 109.7, 68.2, 67.0, 65.8, 55.0, 53.8, 41.3, 40.3, 39.2, 29.1, 28.1, 27.0; HRMS (LCMS ESI+) *m/z* calcd for C<sub>16</sub>H<sub>17</sub>N<sub>2</sub>O<sub>3</sub> [M+H] 285.1234, found 285.1230.



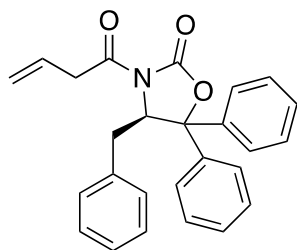
**(R)-3-28** **(R)-4-Benzyl-3-(but-3-enoyl)oxazolidin-2-one ((R)-3-28).**<sup>216</sup> According to

General Procedure C, but-3-enoic acid (0.700 mL, 7.90 mmol, 1.4 equiv), (R)-4-benzyl-2-oxazolidinone (1.00 g, 5.64 mmol, 1 equiv), NMM (0.877 mL, 7.90 mmol, 1.4 equiv), *n*-BuLi (2.5 M in hexanes, 2.60 mL, 6.49 mmol, 1.15 equiv), and pivaloyl chloride (0.992 mL, 7.90 mmol, 1.4 equiv) afforded **(R)-3-28** (0.938 g, 3.82 mmol, 68%) as a colorless oil: IR (ATR, neat) 3084, 3029, 2981, 2919, 1771, 1697, 1354, 1208, 1197, 1099, 994, 922, 750, 700 cm<sup>-1</sup>; [ $\alpha$ ]<sub>D</sub><sup>25</sup> -61.0 (*c* 0.2,

CHCl<sub>3</sub>); <sup>1</sup>H NMR (300 MHz, CDCl<sub>3</sub>) δ 7.36-7.29 (m, 3H), 7.22-7.19 (m, 2H), 6.07-5.98 (m, 1H), 5.28-5.22 (m, 2H), 4.70-4.65 (m, 1H), 4.22-4.17 (m, 2H), 3.74 (dq, *J* = 7.0, 1.5 Hz, 2H), 3.34-3.28 (m, 1H), 2.81-2.74 (m, 1H); <sup>13</sup>C NMR (75 MHz, CDCl<sub>3</sub>) δ 171.3, 153.5, 135.3, 129.8, 129.5, 129.1, 127.5, 119.4, 66.4, 55.3, 40.3, 38.0; HRMS (LCMS ESI+) *m/z* calcd for C<sub>14</sub>H<sub>16</sub>NO<sub>3</sub> [M+H]<sup>+</sup> 246.1125, found 246.1124.



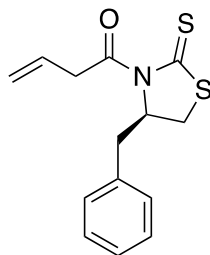
**(S)-3-28** **(S)-4-Benzyl-3-(but-3-enoyl)oxazolidin-2-one ((S)-3-28).**<sup>216</sup> According to General Procedure C, but-3-enoic acid (0.693 mL, 7.82 mmol, 1.4 equiv), (S)-4-benzyl-2-oxazolidinone (1.00 g, 5.59 mmol, 1 equiv), NMM (0.869 mL, 7.82 mmol, 1.4 equiv), *n*-BuLi (2.5 M in hexanes, 2.57 mL, 6.42 mmol, 1.15 equiv), and pivaloyl chloride (0.982 mL, 7.82 mmol, 1.4 equiv) afforded **(S)-3-28** (0.827 g, 3.37 mmol, 61%) as a colorless oil: [ $\alpha$ ]<sub>D</sub><sup>25</sup> +63.2 (*c* 0.2, CHCl<sub>3</sub>).



**(R)-3-29** **(R)-4-Benzyl-3-(but-3-enoyl)-5,5-diphenyloxazolidin-2-one ((R)-3-29).** According to General Procedure C but using Et<sub>3</sub>N instead of NMM, but-3-enoic acid (0.148 mL, 1.67 mmol, 1 equiv), (R)-(+)-5,5-diphenyl-4-benzyl-2-oxazolidinone (0.612 g, 1.84 mmol, 1.1 equiv), Et<sub>3</sub>N (0.261 mL, 1.84 mmol, 1.1 equiv), *n*-BuLi (2.5 M in hexanes, 0.736 mL, 1.84 mmol, 1.1 equiv), and pivaloyl chloride (0.220 mL, 1.76 mmol, 1.05 equiv) afforded **(R)-3-29** (0.183 g, 0.460 mmol, 28%) as a colorless liquid: IR (ATR, neat) 2955, 2873, 1783, 1702, 1450, 1356, 1216, 1167, 996, 918, 758, 702 cm<sup>-1</sup>; [ $\alpha$ ]<sub>D</sub><sup>25</sup> +206.7 (*c* 0.1, CHCl<sub>3</sub>); <sup>1</sup>H NMR (500 MHz, CDCl<sub>3</sub>) δ 7.44-7.42 (m, 3H), 7.36-7.30 (m, 4H), 7.23-7.19 (m, 4H), 7.09-7.08 (m, 4H), 5.85-5.60 (m, 1H), 5.62-

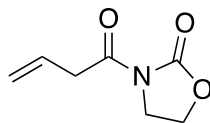


5.59 (m, 1H), 5.13-5.07 (m, 2H), 3.57 (dq,  $J = 7.0, 1.5$  Hz, 2H), 2.88-2.95 (m, 1H), 2.77-2.73 (m, 1H);  $^{13}\text{C}$  NMR (75 MHz,  $\text{CDCl}_3$ )  $\delta$  170.4, 152.0, 141.3, 137.4, 136.1, 129.5, 129.0, 128.83, 128.77, 128.2, 128.1, 126.44, 126.40, 125.9, 119.0, 88.6, 62.0, 39.9, 36.5; HRMS (LCMS ESI+)  $m/z$  calcd for  $\text{C}_{26}\text{H}_{24}\text{NO}_3$   $[\text{M}+\text{H}]$  398.1751, found 398.1747.



**(R)-3-30**

**(R)-1-(4-benzyl-2-thioxothiazolidin-3-yl)but-3-en-1-one ((R)-3-30).** To a suspension of (R)-4-benzyl-1,3-thiazolidine-2-thione (0.100 g, 0.468 mmol), DMAP (0.006 g, 0.05 mmol, 0.1 equiv), and but-3-enoic acid (0.058 mL, 0.65 mmol, 1.4 equiv) in  $\text{CH}_2\text{Cl}_2$  (2 mL, 0.2 M) at 0 °C was added DCC (0.147 g, 0.655 mmol, 1.4 equiv) in one portion and the mixture was stirred at rt for 20 h. The dicyclohexylurea formed was filtered and the precipitate washed with  $\text{CH}_2\text{Cl}_2$ . The filtrate was washed with sat.  $\text{NaHCO}_3$ , dried ( $\text{MgSO}_4$ ), concentrated under reduced pressure, and the residue was purified by chromatography on  $\text{SiO}_2$  (6:1, hexanes:EtOAc) to afford **(R)-3-30** (0.086 g, 0.31 mmol, 66%) as a yellow viscous oil: IR (ATR, neat) 3079, 32026, 2923, 1691, 1495, 1338, 1291, 1258, 1156, 1140, 1039, 991, 920, 888, 740, 700  $\text{cm}^{-1}$ ;  $[\alpha]_D^{25}$  -211.4 ( $c$  0.1,  $\text{CHCl}_3$ );  $^1\text{H}$  NMR (500 MHz,  $\text{CDCl}_3$ )  $\delta$  7.36-7.33 (m, 2H), 7.30-7.27 (m, 3H), 6.03-5.97 (m, 1H), 5.39-5.36 (m, 1H), 5.25-5.18 (m, 2H), 4.16 (dq,  $J = 6.5, 1.5$  Hz, 1H), 3.98 (dq,  $J = 4.0, 1.5$  Hz, 1H), 3.41-3.37 (m, 1H), 3.22 (dd,  $J = 13.5, 4.0$  Hz, 1H), 3.04 (dd,  $J = 13.0, 10.5$  Hz, 1H), 2.89 (app d,  $J = 11.5$  Hz, 1H); HRMS (LCMS ESI+)  $m/z$  calcd for  $\text{C}_{14}\text{H}_{16}\text{NOS}_2$   $[\text{M}+\text{H}]$  278.0668, found 278.0676.

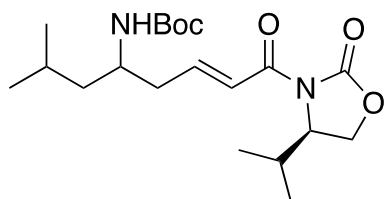


**3-31**

**3-(But-3-enoyl)oxazolidin-2-one (3-31).**<sup>238</sup> According to General Procedure C, but-3-enoic acid (2.09 mL, 23.6 mmol, 1.4 equiv), 2-oxazolidinone (1.50 g, 16.9 mmol, 1 equiv), NMM (2.62 mL, 23.6 mmol, 1.4 equiv),  $n\text{-BuLi}$  (2.5 M in hexanes, 7.60 mL, 19.4 mmol, 1.15

equiv), and pivaloyl chloride (2.97 mL, 23.6 mmol, 1.4 equiv) afforded **3-31** (1.16 g, 7.48 mmol, 44%) as a colorless oil: IR (ATR, neat) 2989, 2920, 1768, 1694, 1637, 1479, 1386, 1362, 1219, 1196, 1102, 1038, 1020, 970, 921, 758, 709  $\text{cm}^{-1}$ ;  $^1\text{H}$  NMR ( $\text{CDCl}_3$ , 300 MHz)  $\delta$  6.06-5.86 (m, 1H), 5.25 (dd,  $J = 3.3, 1.8$  Hz, 1H), 5.20 (d,  $J = 1.2$  Hz, 1H), 4.43 (t,  $J = 7.8$  Hz, 2H), 4.03 (t,  $J = 7.8$  Hz, 2H), 3.72 (d,  $J = 6.9$  Hz, 2H);  $^{13}\text{C}$  NMR ( $\text{CDCl}_3$ , 75 MHz)  $\delta$  171.4, 153.6, 129.8, 119.3, 62.2, 42.6, 39.9; HRMS (LCMS ESI+)  $m/z$  calcd for  $\text{C}_7\text{H}_{10}\text{NO}_3$   $[\text{M}+\text{H}]^+$  156.0655, found 156.0656.

**General procedure D.** For the vinylogous Mannich reaction. A dried 50-mL round bottom flask equipped with a magnetic stirring bar was charged with  $[\text{Cu}(\text{CH}_3\text{CN})_4]\text{PF}_6$  (0.306 mmol, 0.25 equiv) and (*S*)- or (*R*)-DTBM-SEGPPOS (0.306 mmol, 0.25 equiv) under an  $\text{N}_2$  atmosphere. Anhydrous THF (13 mL, 0.1 M) was added and the colorless catalyst solution was stirred for ca. 15 min at rt, then at  $-20^\circ\text{C}$  for 15 min until the imine was prepared. The oxazolidinone (1.22 mmol, 1.0 equiv) was added to the catalyst solution followed by the freshly prepared *N*-Boc imine (2.45 mmol, 2.0 equiv). After 5 min, DABCO (1.0 M in THF, 0.611 mmol, 0.5 equiv) was added. The resulting reaction mixture was stirred at  $-20^\circ\text{C}$  for 5-18 h, filtered through a plug of basic alumina ( $\text{EtOAc}$ ), washed with 1M  $\text{NH}_4\text{OH}$  (3 x 15 mL),  $\text{NaHCO}_3$  (1 x 15 mL), brine (2 x 15 mL), dried ( $\text{MgSO}_4$ ), filtered, and concentrated under reduced pressure. The residue was purified by chromatography on  $\text{SiO}_2$  with gradient elution (9:1 to 2:1, hexanes: $\text{EtOAc}$ ) to afford the desired  $\beta,\alpha$ -unsaturated vinylogous Mannich product.



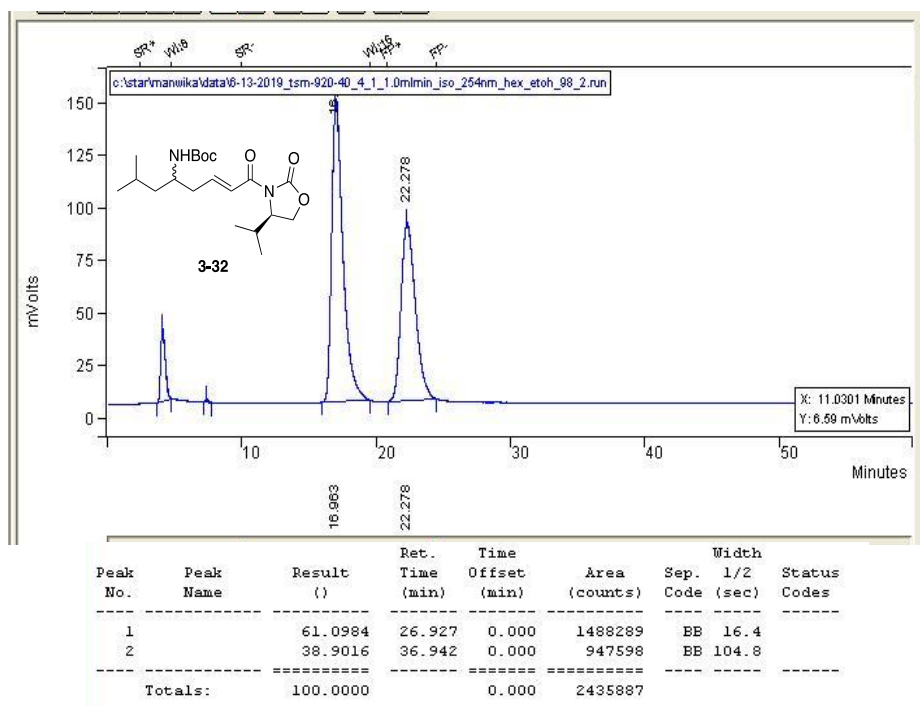
**3-32**

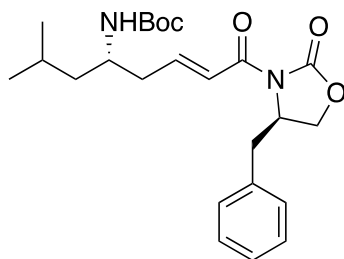
*tert*-Butyl ((*S,E*)-8-((*R*)-4-isopropyl-2-oxooxazolidin-3-yl)-2-

methy-8-oxooct-6-en-4-yl)carbamate (**3-32**). According to General Procedure D but using  $\text{Et}_3\text{N}$  instead of DABCO, (*R*)-**3-26** (0.150 g, 0.760 mmol, 1 equiv), **3-18** (0.563 g, 3.04 mmol, 4 equiv),  $[\text{Cu}(\text{CH}_3\text{CN})_4]\text{PF}_6$  (0.029 g, 0.076 mmol, 0.1 equiv), (*S*)-DTBM-SEGPPOS (0.091 g, 0.076 mmol, 0.1 equiv), and  $\text{Et}_3\text{N}$  (0.76 mL, 0.078 mmol, 1 equiv) afforded **3-32** (0.186 g, 0.486 mmol, 60%) as a colorless viscous oil: IR (ATR, neat) 3354, 2960, 1776, 1686, 1634, 1520, 1364, 1239,

1204, 1184, 1014, 772, 753, 715  $\text{cm}^{-1}$ ;  $^1\text{H}$  NMR (600 MHz,  $\text{CDCl}_3$ )  $\delta$  7.28 (d,  $J$  = 15.6 Hz, 1H), 7.11-7.06 (m, 1H), 4.48-4.47 (m, 1H), 4.30 (brd s, 1H), 4.28-4.25 (m, 1H), 4.20 (dd,  $J$  = 8.4, 2.4 Hz, 1H), 3.81 (brd s, 1H), 2.50-2.47 (m, 1H), 2.44-2.39 (m, 2H), 1.72-1.65 (m, 1H), 1.44 (s, 9H), 1.32-1.27 (m, 2H), 1.25-0.90 (m, 12H);  $^{13}\text{C}$  NMR (150 MHz,  $\text{CDCl}_3$ )  $\delta$  164.6, 155.3, 153.9, 146.7, 123.0, 79.6, 63.4, 58.6, 28.6, 28.3, 28.2, 24.9, 22.9, 22.1, 17.9, 14.8; HRMS (LCMS ESI+)  $m/z$  calcd for  $\text{C}_{20}\text{H}_{35}\text{N}_2\text{O}_5$   $[\text{M}+\text{H}]$  383.2540, found 383.2540. The diastereomeric ratio was determined to be 60:40 by chiral HPLC (Chiralcel-AD-H; 95:5, hexanes:EtOH; 254 nm; 1.0 mL/min; Rt 16.96 min).

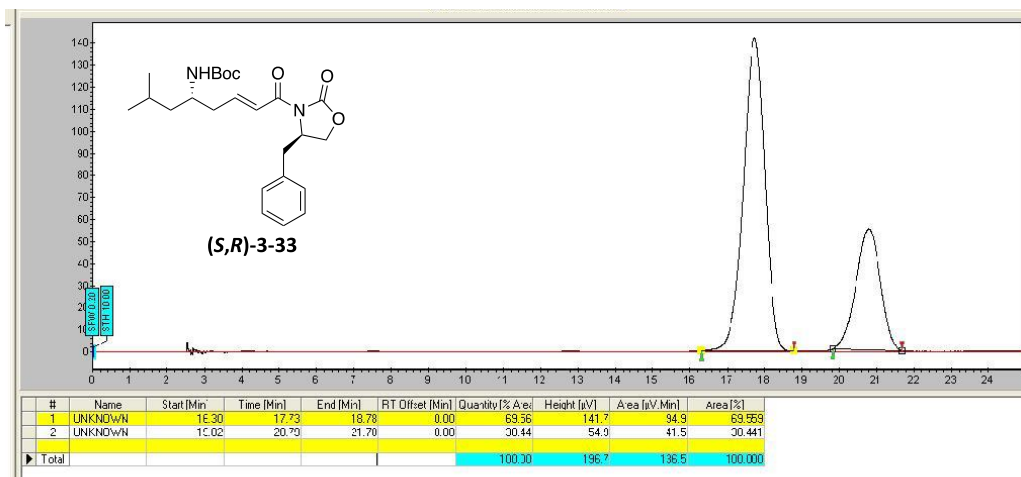
HPLC (Chiralcel-AD-H; 95:5, hexane:EtOH; 254 nm; 1.0 mL/min)

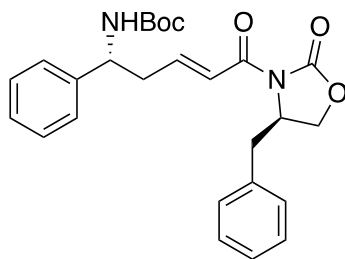




**(*S,R*)-3-33** *tert*-Butyl ((*S,E*)-8-((*R*)-4-benzyl-2-oxooxazolidin-3-yl)-2-methyl-8-oxooct-6-en-4-yl)carbamate ((*S,R*)-3-33). According to General Procedure D but using Et<sub>3</sub>N instead of DABCO, (*R*)-3-28 (0.100 g, 0.408 mmol, 1 equiv), 3-18 (0.302 g, 1.63 mmol, 4 equiv), [Cu(CH<sub>3</sub>CN)<sub>4</sub>]PF<sub>6</sub> (0.023 g, 0.061 mmol, 0.15 equiv), (*S*)-DTBM-SEPHOS (0.073 g, 0.061 mmol, 0.15 equiv), and Et<sub>3</sub>N (0.61 mL, 0.061 mmol, 0.15 equiv) afforded (*S,R*)-3-33 (0.175 g, 0.203 mmol, 50%) as a colorless solid: Mp 77.5-79.2 °C; IR (ATR, neat) 3358, 2961, 1775, 1685, 1634, 1499, 1353, 1258, 1284, 1103, 1006, 761, 700 cm<sup>-1</sup>; <sup>1</sup>H NMR (500 MHz, CDCl<sub>3</sub>) δ 7.35-7.27 (m, 4H), 7.23-7.21 (m, 2H), 7.16 (dt, *J* = 15.0, 7.5 Hz, 1H), 4.75-4.70 (m, 1H), 4.35 (d, *J* = 8.0 Hz, 1H), 4.23-4.16 (m, 2H), 3.86 (d, *J* = 5.0 Hz, 1H), 3.34 (dd, *J* = 13.5, 3.5 Hz, 1H), 2.82-2.76 (m, 1H), 2.55-2.51 (m, 1H), 2.43-2.40 (m, 1H), 1.69-1.65 (m, 1H), 1.43 (s, 9H), 1.35-1.24 (m, 2H), 0.92 (d, *J* = 6.5 Hz, 6H); <sup>13</sup>C NMR (150 MHz, CDCl<sub>3</sub>) δ 164.6, 155.3, 153.4, 147.9, 146.7, 135.4, 130.1, 129.64, 129.58, 128.8, 128.4, 128.3, 128.0, 126.7, 123.4, 66.2, 64.9, 56.0, 54.8, 38.9, 37.9, 28.92, 28.89, 27.9; HRMS (LCMS ESI+) *m/z* calcd for C<sub>24</sub>H<sub>35</sub>N<sub>2</sub>O<sub>5</sub> [M+H] 431.2540, found 431.2537. The diastereomeric ratio was determined to be 70:30 by chiral SFC (Chiralpak-IC (250 x 10 mm); 10% MeOH; 254 nm; 5.0 mL/min; Rt 17.73 min).

SFC (Chiralpak-IC (250 x 10 mm); 10% MeOH; 254 nm; 5.0 mL/min)

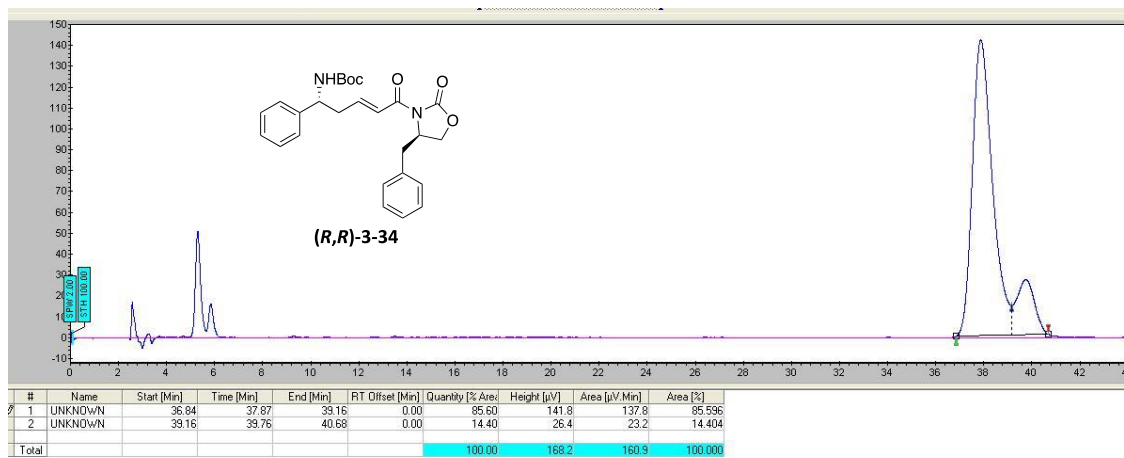


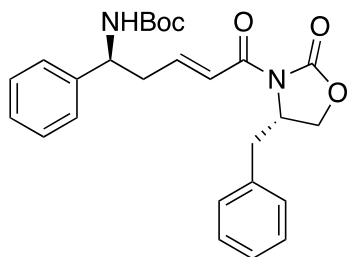


**(*R,R*)-3-34**

***tert*-Butyl ((*R,E*)-5-((*R*)-4-benzyl-2-oxooxazolidin-3-yl)-5-oxo-1-phenylpent-3-en-1-yl)carbamate ((*R,R*)-3-34).** According to General Procedure D, (*R*)-3-28 (0.050 g, 0.204 mmol, 1 equiv), **3-17** (0.084 g, 0.408 mmol, 2 equiv), [Cu(CH<sub>3</sub>CN)<sub>4</sub>]PF<sub>6</sub> (0.019 g, 0.051 mmol, 0.25 equiv), (*S*)-DTBM-SEGPPOS (0.061 g, 0.051 mmol, 0.25 equiv), and DABCO (2 M solution in THF, 0.051 mL, 0.101 mmol, 0.5 equiv) afforded (*R,R*)-3-34 (0.053 g, 0.118 mmol, 58%) as a colorless solid: Mp 59.6-62.7 °C; IR (ATR, neat) 3358, 2974, 2927, 1774, 1685, 1635, 1496, 1355, 1243, 1209, 1164, 1000, 752, 681 cm<sup>-1</sup>; [ $\alpha$ ]<sub>D</sub><sup>25</sup> -33.5 (*c* 1.3, CHCl<sub>3</sub>); <sup>1</sup>H NMR (500 MHz, CDCl<sub>3</sub>)  $\delta$  7.37-7.27 (m, 9H), 7.21-7.19 (m, 2H), 7.07 (dt, *J* = 15.2, 7.6 Hz, 1H), 4.89 (brd s, 2H), 4.72-4.67 (m, 1H), 4.22-4.15 (m, 2H), 3.30 (dd, *J* = 13.6, 3.2 Hz, 1H), 2.79-2.75 (m, 3H), 1.42 (s, 9H); <sup>13</sup>C NMR (75 MHz, CDCl<sub>3</sub>)  $\delta$  164.4, 155.0, 153.4, 146.3, 135.3, 129.4, 129.0, 128.8, 127.6, 127.4, 126.3, 123.1, 79.8, 77.2, 66.2, 55.3, 39.9, 37.9, 31.7, 28.3; HRMS (LCMS ESI+) *m/z* calcd for C<sub>26</sub>H<sub>31</sub>N<sub>2</sub>O<sub>5</sub> [M+H] 451.2227, found 451.2224. The diastereomeric ratio was determined to be 86:14 by chiral SFC (Cellulose-2, (250 x 4.6 mm); 11% MeOH; 220 nm; 1.25 mL/min; Rt 37.9 min).

SFC (Cellulose-2, (250 x 4.6 mm); 11% MeOH; 220 nm; 1.25 mL/min)

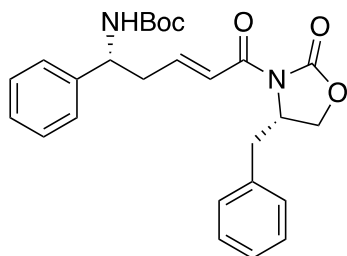
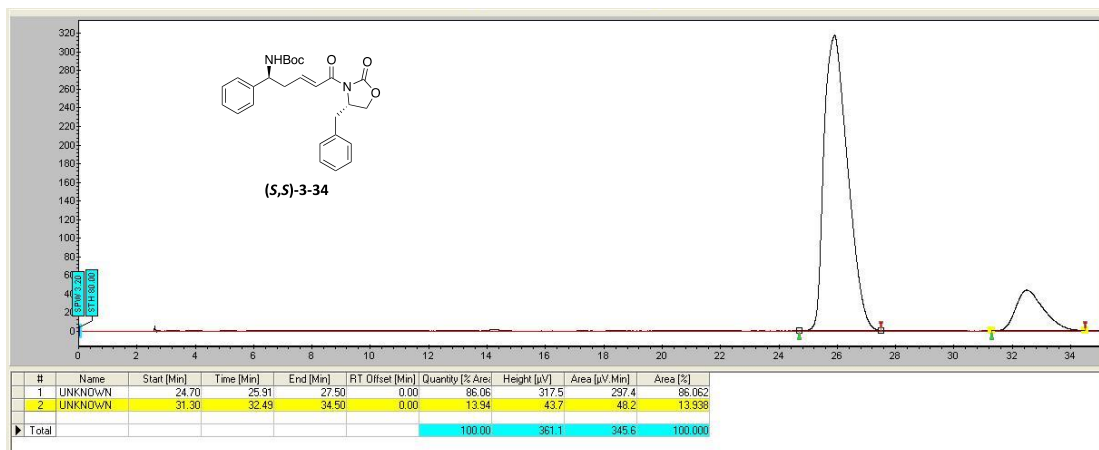




**(*S,S*)-3-34**

**tert-Butyl ((*S,E*)-5-((*S*)-4-benzyl-2-oxooxazolidin-3-yl)-5-oxo-1-phenylpent-3-en-1-yl)carbamate ((*S,S*)-3-34).** According to General Procedure D, (*S*)-3-28 (0.050 g, 0.204 mmol, 1 equiv), **3-17** (0.084 g, 0.408 mmol, 2 equiv), [Cu(CH<sub>3</sub>CN)<sub>4</sub>]PF<sub>6</sub> (0.019 g, 0.051 mmol, 0.25 equiv), (*R*)-DTBM-SEGPPOS (0.061 g, 0.051 mmol, 0.25 equiv), and DABCO (2 M solution in THF, 0.051 mL, 0.101 mmol, 0.5 equiv) afforded (*S,S*)-3-34 (0.046 g, 0.103 mmol, 50%) as a colorless solid:  $[\alpha]_D^{25} +30.7$  (*c* 0.5, CHCl<sub>3</sub>). The diastereomeric ratio was determined to be 86:14 by chiral SFC (Chiralpak-IC (250 x 10 mm); 13% MeOH; 254 nm; 5.0 mL/min; Rt 25.9 min).

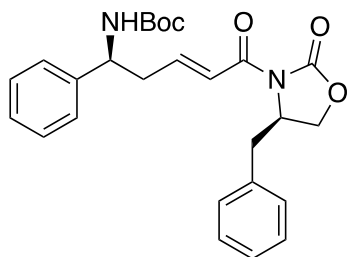
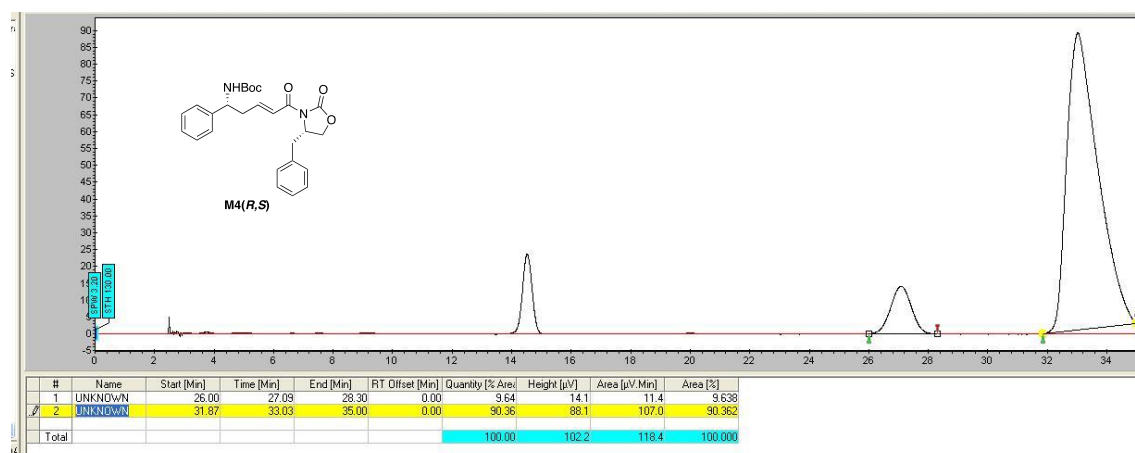
SFC, Chiralpak-IC (250 x 10 mm); 13% MeOH; 254 nm; 5.0 mL/min)



**(*R,S*)-3-34**

**tert-Butyl ((*R,E*)-5-((*S*)-4-benzyl-2-oxooxazolidin-3-yl)-5-oxo-1-phenylpent-3-en-1-yl)carbamate ((*R,S*)-3-34).** According to General Procedure D, (*S*)-3-28 (0.050 g, 0.204 mmol, 1 equiv), **3-17** (0.084 g, 0.408 mmol, 2 equiv), [Cu(CH<sub>3</sub>CN)<sub>4</sub>]PF<sub>6</sub> (0.019 g,

0.051 mmol, 0.25 equiv), (*S*)-DTBM-SEGPHOS (0.061 g, 0.051 mmol, 0.25 equiv), and DABCO (2 M solution in THF, 0.051 mL, 0.101 mmol, 0.5 equiv) afforded (*R,S*)-**3-34** (0.024 g, 0.053 mmol, 26%) as a colorless solid: Mp 60.2-64.1 °C; IR (ATR, neat) 3374, 2981, 2924, 1785, 1719, 1676, 1516, 1348, 1243, 1216, 1169, 1023, 1011, 816, 755, 702 cm<sup>-1</sup>; [ $\alpha$ ]<sub>D</sub><sup>25</sup> +32.4 (c 0.4, CHCl<sub>3</sub>); <sup>1</sup>H NMR (300 MHz, CDCl<sub>3</sub>)  $\delta$  7.41-7.27 (m, 9H), 7.20-7.17 (m, 2H), 7.06 (dt, *J* = 15.3, 7.8 Hz, 1H), 4.88 (brd s, 2H), 4.72-4.67 (m, 1H), 4.19-4.16 (m, 2H), 3.30 (dd, *J* = 13.5, 3.3 Hz, 1H), 2.81-2.74 (m, 3H), 1.41 (s, 9H); <sup>13</sup>C NMR (75 MHz, CDCl<sub>3</sub>)  $\delta$  164.4, 155.0, 153.3, 146.2, 138.4, 129.4, 128.9, 128.6, 127.6, 127.3, 126.2, 123.1, 79.2, 77.2, 66.2, 55.3, 39.9, 37.9, 31.7, 28.3; HRMS (LCMS ESI+) *m/z* calcd for C<sub>26</sub>H<sub>31</sub>N<sub>2</sub>O<sub>5</sub> [M+H] 451.2219, found 451.2224. The diastereomeric ratio was determined to be 91:9 by chiral SFC (Chiralpak-IC (250 x 10 mm); 13% MeOH; 254 nm; 5.0 mL/min; Rt 33.0 min).



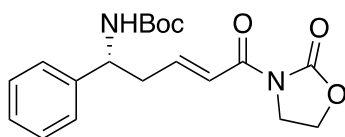
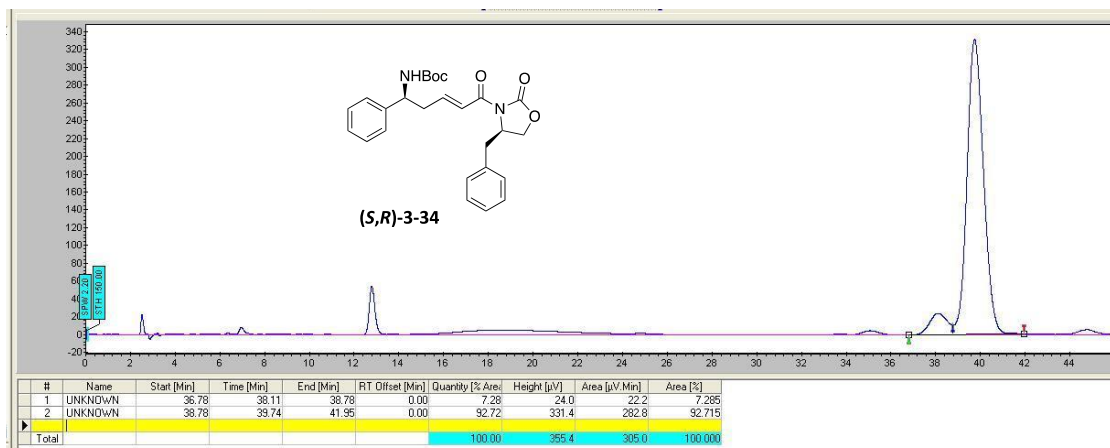
**(*S,R*)-3-34**

*tert*-Butyl ((*S,E*)-5-((*R*)-4-benzyl-2-oxooxazolidin-3-yl)-5-oxo-1-

phenylpent-3-en-1-yl)carbamate ((*S,R*)-**3-34**). According to General Procedure D, (*R*)-**3-28** (0.050 g, 0.204 mmol, 1 equiv), **3-17** (0.084 g, 0.408 mmol, 2 equiv), [Cu(CH<sub>3</sub>CN)<sub>4</sub>]PF<sub>6</sub> (0.019 g, 0.051 mmol, 0.25 equiv), (*S*)-DTBM-SEGPHOS (0.061 g, 0.051 mmol, 0.25 equiv), and DABCO (2 M solution in THF, 0.051 mL, 0.101 mmol, 0.5 equiv) afforded (*S,R*)-**3-34** (0.030 g, 0.067

mmol, 33%) as a colorless solid:  $[\alpha]_D^{25}$  -35.5 (*c* 0.8, CHCl<sub>3</sub>). The diastereomeric ratio was determined to be 92:8 by chiral SFC (Cellulose-2 (250 x 4.6 mm); 11% MeOH; 220 nm; 1.25 mL/min; Rt 39.7 min).

SFC (Cellulose-2 (250 x 4.6 mm); 11% MeOH; 220 nm; 1.25 mL/min)



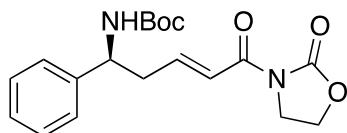
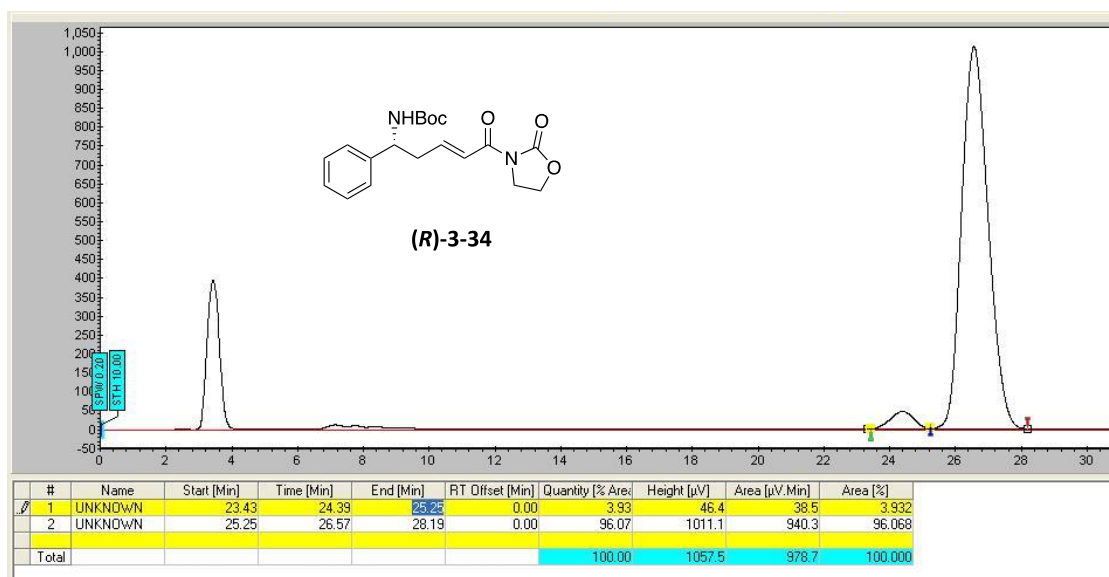
**(R)-3-34**

*tert*-Butyl (*R,E*)-(5-oxo-5-(2-oxooxazolidin-3-yl)-1-phenylpent-3-

en-1-yl)carbamate ((*R*)-3-34). According to General Procedure D, **3-31** (0.031 g, 0.200 mmol, 1 equiv), **3-17** (0.082 g, 0.400 mmol, 2 equiv), [Cu(CH<sub>3</sub>CN)<sub>4</sub>]PF<sub>6</sub> (0.019 g, 0.050 mmol, 0.25 equiv), (*S*)-DTBM-SEGPHOS (0.060 g, 0.050 mmol, 0.25 equiv), and DABCO (2 M solution in THF, 0.050 mL, 0.100 mmol, 0.5 equiv) afforded (*R*)-3-34 (0.048 g, 0.134 mmol, 67%) as a colorless solid: Mp 142.3-145.4 °C; IR (ATR, neat) 3371, 2978, 2921, 1789, 1774, 1680, 1636, 1517, 1327, 1334, 1246, 1223, 1203, 1171, 1121, 1046, 1015, 971, 747, 683 cm<sup>-1</sup>;  $[\alpha]_D^{25}$  +14.7 (*c* 0.3, CHCl<sub>3</sub>); <sup>1</sup>H NMR (300 MHz, CDCl<sub>3</sub>) δ 7.36-7.32 (m, 6H), 7.02 (dt, *J* = 15.0, 7.8 Hz, 1H), 4.85 (brd s, 2H), 4.41 (t, *J* = 7.8 Hz, 2H), 4.04 (t, *J* = 7.8 Hz, 2H), 2.77 (brd s, 2H), 1.41 (s, 9H); <sup>13</sup>C NMR (75 MHz, CDCl<sub>3</sub>) δ 164.7, 155.1, 153.5, 146.3, 128.9, 127.7, 126.4, 122.8, 62.2, 42.8, 28.5; HRMS (LCMS ESI+) *m/z* calcd for C<sub>19</sub>H<sub>25</sub>N<sub>2</sub>O<sub>5</sub> [M+H] 360.1685, found 360.1687. The enantiomeric ratio was determined to be 96:4 by chiral SFC (Chiralpak-IC (250 x 10 mm); 13% MeOH; 254 nm; 5.0 mL/min; Rt 26.6 min).

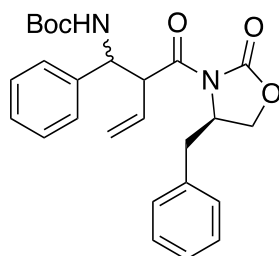
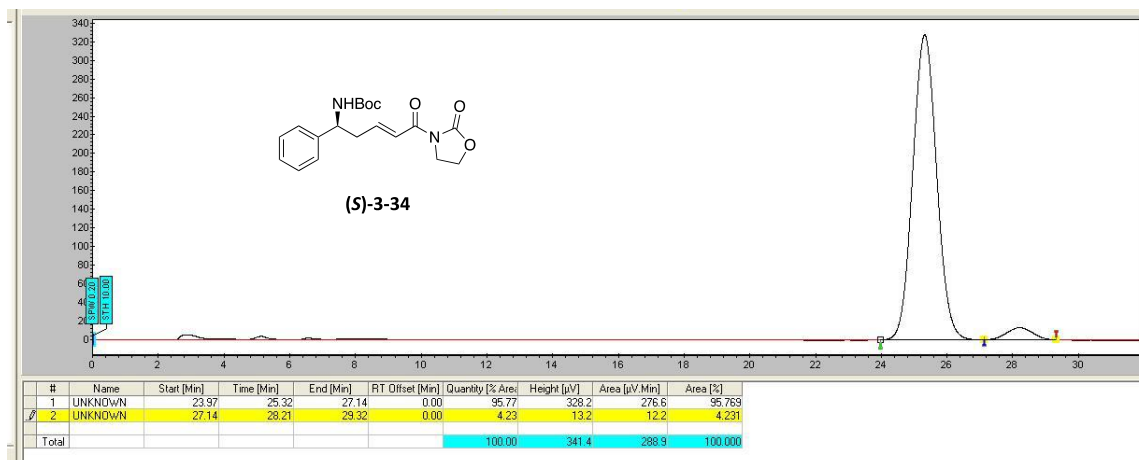


SFC (Chiralpak-IC (250 x 10 mm); 13% MeOH; 254 nm; 5.0 mL/min)



**(S)-3-34** *tert*-Butyl (*S,E*)-(5-oxo-5-(2-oxooxazolidin-3-yl)-1-phenylpent-3-en-1-yl)carbamate ((*S*)-3-34). According to General Procedure D, **3-31** (0.031 g, 0.200 mmol, 1 equiv), **3-17** (0.082 g, 0.400 mmol, 2 equiv), [Cu(CH<sub>3</sub>CN)<sub>4</sub>]PF<sub>6</sub> (0.019 g, 0.050 mmol, 0.25 equiv), (*R*)-DTBM-SEPHOS (0.060 g, 0.050 mmol, 0.25 equiv), and DABCO (2 M solution in THF, 0.050 mL, 0.100 mmol, 0.5 equiv) afforded (*S*)-3-34 (0.036 g, 0.100 mmol, 50%) as a colorless solid:  $[\alpha]_D^{25}$  -20.4 (*c* 0.7, CHCl<sub>3</sub>). The enantiomeric ratio was determined to be 96:4 by chiral SFC (Chiralpak-IC (250 x 10 mm); 13% MeOH; 220 nm; 5.0 mL/min; Rt 25.3 min).

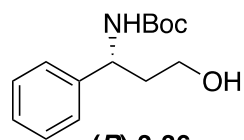
SFC (Chiralpak-IC (250 x 10 mm); 13% MeOH; 220 nm; 5.0 mL/min)



**3-35**

***tert*-Butyl (2-((*R*)-4-benzyl-2-oxooxazolidine-3-carbonyl)-1-phenylbut-**

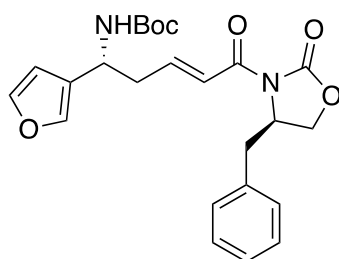
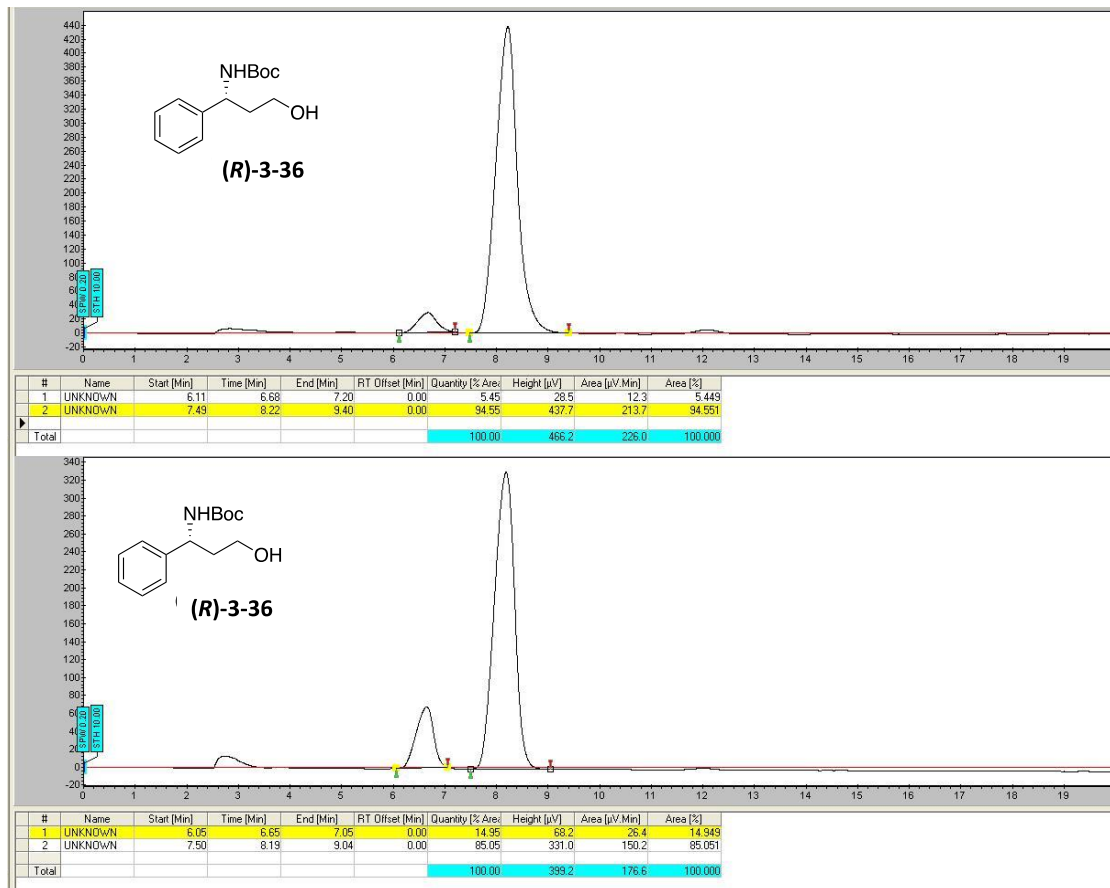
**3-en-1-yl)carbamate (3-35).** According to General Procedure D using P2-*t*-Bu instead of DABCO, (***R***)-**3-28** (0.050 g, 0.204 mmol, 1 equiv), **3-17** (0.084 g, 0.408 mmol, 2 equiv), [Cu(CH<sub>3</sub>CN)<sub>4</sub>]PF<sub>6</sub> (0.019 g, 0.051 mmol, 0.25 equiv), (*S*)-DTBM-SEPHOS (0.061 g, 0.051 mmol, 0.25 equiv), and DABCO (2 M solution in THF, 0.051 mL, 0.101 mmol, 0.5 equiv) afforded **3-35** (0.0918 g, 0.108 mmol, 53%) as a colorless solid: Mp 55.7-58.2 °C; IR (ATR, neat) 3369, 2977, 1773, 1691, 1495, 1364, 1288, 1165, 1102, 1048, 1020, 995, 926, 757, 702 cm<sup>-1</sup>; [α]<sub>D</sub><sup>25</sup> -64.0 (*c* 0.1, CHCl<sub>3</sub>); <sup>1</sup>H NMR (300 MHz, CDCl<sub>3</sub>) δ 7.31-7.22 (m, 8H), 7.16-7.13 (m, 2H), 6.11-5.98 (m, 1H), 5.32-5.22 (m, 3H), 4.95 (t, *J* = 8.4 Hz, 2H), 4.32 (t, *J* = 8.4 Hz, 1H), 4.00 (dd, *J* = 9.0, 1.8 Hz, 1H), 3.87 (brd s, 1H), 3.17 (dd, *J* = 13.5, 3.0 Hz, 1H), 2.72-2.65 (m, 1H), 1.39 (s, 9H); <sup>13</sup>C NMR (100 MHz, CDCl<sub>3</sub>) δ 171.6, 155.3, 135.3, 129.6, 129.0, 128.6, 127.7, 127.4, 127.0, 121.5, 66.2, 55.6, 54.1, 37.8, 28.4; HRMS (LCMS ESI+) *m/z* calcd for C<sub>26</sub>H<sub>31</sub>N<sub>2</sub>O<sub>5</sub> [M+H] 451.2228, found 451.2229.



**(*R*)-3-36** *tert*-Butyl (*R*)-(3-hydroxy-1-phenylpropyl)carbamate ((*R*)-3-36).<sup>161, 224</sup>

Ozone was bubbled through a solution of (*R*)-3-34 (0.028 g, 0.078 mmol, 1 equiv) or (*R,R*)-3-34 (100 mg, 0.222 mmol, 1 equiv) in MeOH (0.06 M) at -78 °C until the appearance of a light persistent blue color (20 min). The reaction solution was then allowed to warm to 0 °C and the mixture was subsequently treated with NaBH<sub>4</sub> (10 equiv) at 0 °C. The reaction mixture was allowed to warm to rt and stirred for an additional 2 h, quenched with H<sub>2</sub>O (5 mL) and extracted with CH<sub>2</sub>Cl<sub>2</sub> (3 x 10 mL). The combined organic layers were dried (Na<sub>2</sub>SO<sub>4</sub>), filtered, and the solvent was removed under reduced pressure. The crude product was purified by chromatography on SiO<sub>2</sub> (3:1, hexanes:EtOAc) to afford (*R*)-3-36 (0.020 g, 0.047 mmol, 61%) or (46.8 mg, 0.186 mmol, 84%) as a colorless oil:  $[\alpha]_D^{25} +48.3$  (*c* 0.3, CHCl<sub>3</sub>); <sup>1</sup>H NMR (600 MHz, MeOD) δ 7.36-7.28 (m, 5H), 4.99 (s, 1H), 4.90 (s, 1H), 3.70 (dd, *J* = 7.8, 3.0 Hz, 2H), 2.40 (brd s, 1H), 2.08-2.07 (m, 1H), 1.84-1.80 (m, 1H), 1.44 (s, 9H). The enantiomeric ratio was determined to be 95:5 (from (*R*)-3-33 and 85:15 from (*R,R*)-3-33 by chiral SFC (Chiralpak-IC (250 x 10 mm); 5% MeOH; 210 nm; 5.0 mL/min; Rt 8.2 min).

SFC (ChiralPak-IC (250 x 10 mm); 5% MeOH; 210 nm; 5.0 mL/min)



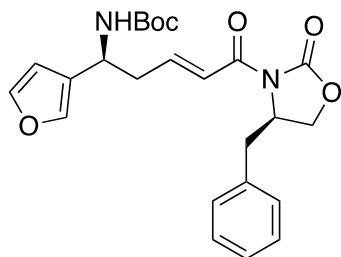
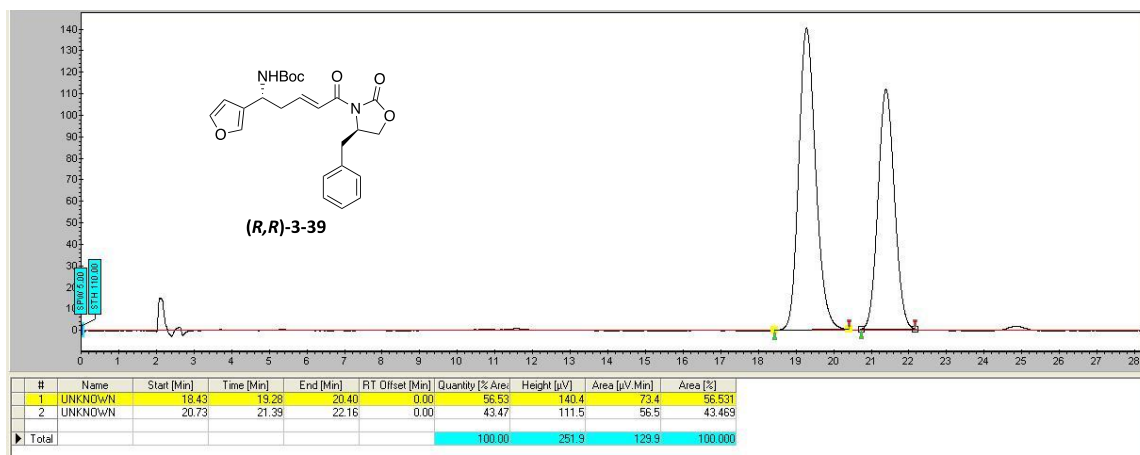
**(*R,R*)-3-39**

*tert*-Butyl ((*R,E*)-5-((*R*)-4-benzyl-2-oxooxazolidin-3-yl)-1-(furan-3-

yl)-5-oxopent-3-en-1-yl)carbamate ((*R,R*)-3-39). According to General Procedure D, (*R*)-3-28 (0.250 g, 1.02 mmol, 1 equiv), 3-38 (0.398 g, 2.04 mmol, 2 equiv), [Cu(CH<sub>3</sub>CN)<sub>4</sub>]PF<sub>6</sub> (0.098 g, 0.254 mmol, 0.25 equiv), (*S*)-DTBM-SEGPHOS (0.307 g, 0.255 mmol, 0.25 equiv), and DABCO (1 M solution in THF, 0.501 mL, 0.501 mmol, 0.5 equiv) afforded (*R,R*)-3-39 (0.276 g, 0.627 mmol, 62%) as a white solid: Mp 41.5-44.3 °C; IR (ATR, neat) 3358, 2978, 2929, 1773, 1683, 1635, 1499, 1389, 1361, 1212, 1172, 1020, 1000, 874, 761, 701 cm<sup>-1</sup>; [α]<sub>D</sub><sup>25</sup> -21.7 (*c* 0.2, CHCl<sub>3</sub>);

$^1\text{H}$  NMR (600 MHz,  $\text{CDCl}_3$ )  $\delta$  7.39 (d,  $J$  = 1.2 Hz, 1H), 7.38-7.28 (m, 5H), 7.20 (d,  $J$  = 7.2 Hz, 2H), 7.10 (dt,  $J$  = 15.0, 7.2 Hz, 1H), 6.35 (d,  $J$  = 1.2 Hz, 1H), 4.88 (brd s, 1H), 4.73-4.69 (m, 2H), 4.23-4.16 (m, 2H), 3.32 (dd,  $J$  = 13.2, 3.0 Hz, 1H), 2.81-2.75 (m, 3H), 1.45 (s, 9H);  $^{13}\text{C}$  NMR (150 MHz,  $\text{CDCl}_3$ )  $\delta$  164.4, 155.0, 153.4, 146.2, 143.6, 139.2, 135.3, 129.4, 129.0, 127.3, 126.0, 123.2, 108.9, 79.8, 66.2, 55.3, 46.1, 38.7, 37.8, 28.3; HRMS (LCMS ESI+)  $m/z$  calcd for  $\text{C}_{24}\text{H}_{28}\text{N}_2\text{O}_6$   $[\text{M}+\text{Na}]$  463.1840, found 463.1831. The enantiomeric ratio was determined to be 57:43 by chiral SFC (Cellulose-2 (OZ-H) (250 x 4.6 mm); 12% MeOH; 220 nm; 1.5 mL/min; Rt 19.3 min).

SFC (Cellulose-2 (OZ-H) (250 x 4.6 mm); 12% MeOH; 220 nm; 1.5 mL/min)



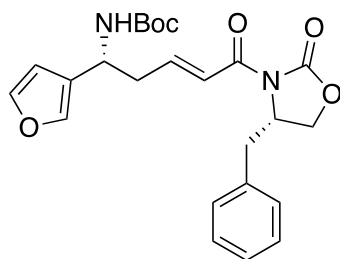
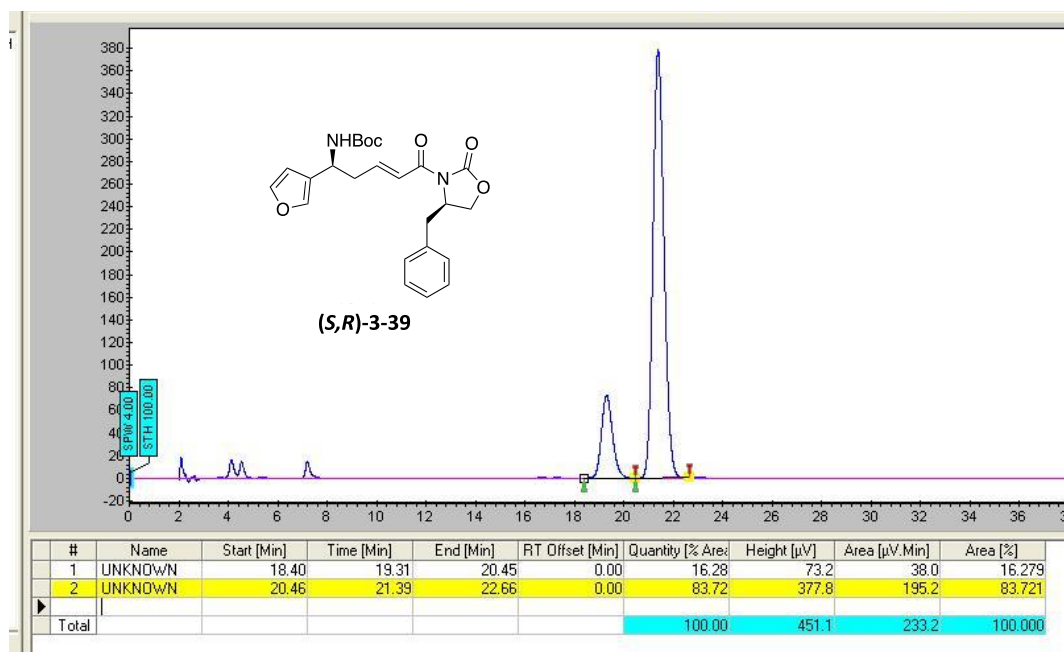
**(S,R)-3-39**

**tert-Butyl ((S,E)-5-((R)-4-benzyl-2-oxooxazolidin-3-yl)-1-(furan-3-**

**yl)-5-oxopent-3-en-1-yl)carbamate ((S,R)-3-39).** According to General Procedure D, **(R)-3-28** (0.088 g, 0.359 mmol, 1 equiv), **3-38** (0.147 g, 0.718 mmol, 2 equiv),  $[\text{Cu}(\text{CH}_3\text{CN})_4]\text{PF}_6$  (0.034 g, 0.090 mmol, 0.25 equiv), *(R)*-DTBM-SEGPHOS (0.107 g, 0.090 mmol, 0.25 equiv), and DABCO (1 M solution in THF, 0.179 mL, 0.179 mmol, 0.5 equiv) afforded **(S,R)-3-39** (0.063 g, 0.143 mmol, 40%) as a white solid: Mp 50.7-53.3 °C; IR (ATR, neat) 3978, 2977, 2929, 1784, 1682, 1638, 1513, 1352, 1247, 1214, 1190, 1022, 874, 797, 748, 700  $\text{cm}^{-1}$ ;  $[\alpha]_D^{25}$  -39.7 ( $c$  0.3,  $\text{CHCl}_3$ );  $^1\text{H}$  NMR (300 MHz,  $\text{CDCl}_3$ )  $\delta$  7.40 (d,  $J$  = 1.2 Hz, 1H), 7.37-7.27 (m, 5H), 7.21 (d,  $J$  = 6.6 Hz, 2H), 7.10 (dt,  $J$  = 15.2, 7.2 Hz, 1H), 6.37 (d,  $J$  = 1.2 Hz, 1H), 4.87 (brd s, 1H), 4.75-4.70 (m, 2H),

4.25-4.14 (m, 2H), 3.33 (dd,  $J = 13.5, 3.3$  Hz, 1H), 2.84-2.76 (m, 3H), 1.46 (s, 9H);  $^{13}\text{C}$  NMR (75 MHz,  $\text{CDCl}_3$ )  $\delta$  164.4, 155.0, 153.3, 146.1, 143.6, 139.2, 135.3, 129.4, 128.9, 127.3, 126.0, 123.2, 108.9, 77.8, 66.2, 55.3, 46.1, 38.5, 37.8, 28.3; HRMS (LCMS ESI+)  $m/z$  calcd for  $\text{C}_{24}\text{H}_{28}\text{N}_2\text{O}_6$   $[\text{M}+\text{Na}]$  463.1840, found 463.1836. The diastereomeric ratio was determined to be 16:84 by chiral SFC (Cellulose-2 (OZ-H) (250 x 4.6 mm); 12% MeOH; 220 nm; 1.5 mL/min;  $R_t$  21.4 min).

SFC (Cellulose-2 (OZ-H) (250 x 4.6 mm); 12% MeOH; 220 nm; 1.5 mL/min)

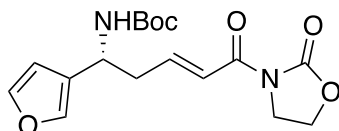
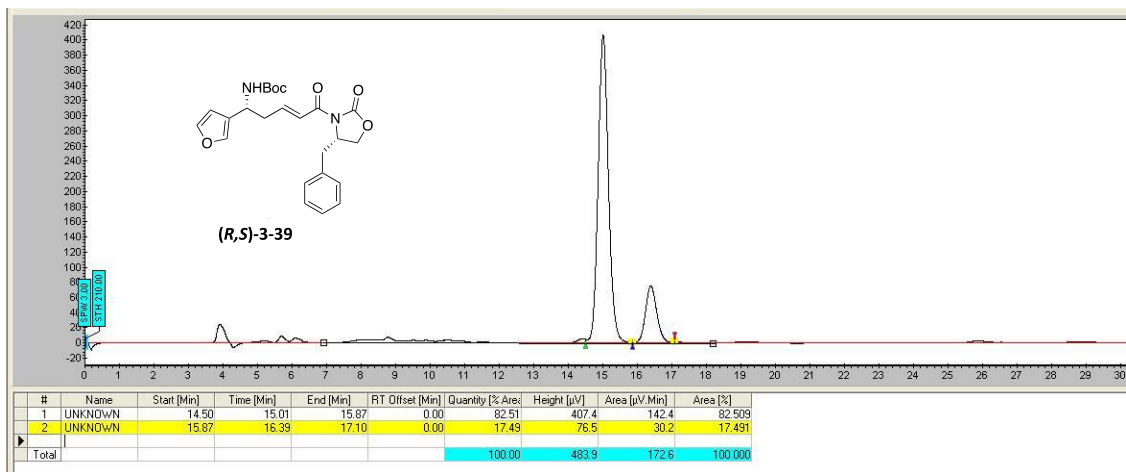


**(R,S)-3-39**

***tert*-Butyl ((R,E)-5-(S)-4-benzyl-2-oxooxazolidin-3-yl)-1-(furan-3-yl)-5-oxopent-3-en-1-yl)carbamate ((R,S)-3-39).** According to General Procedure D, (*S*)-**3-28** (0.300 g, 1.22 mmol, 1 equiv), **3-38** (0.48 g, 2.45 mmol, 2 equiv),  $[\text{Cu}(\text{CH}_3\text{CN})_4]\text{PF}_6$  (0.118 g, 0.306 mmol, 0.25 equiv), (*S*)-DTBM-SEGPHOS (0.368 g, 0.306 mmol, 0.25 equiv), and DABCO (1 M solution in THF, 0.612 mL, 0.612 mmol, 0.5 equiv) afforded (*R,S*)-**3-39** (0.181 g, 0.411 mmol, 34%) as a white solid:  $[\alpha]_D^{25} +46.5$  ( $c$  0.2,  $\text{CHCl}_3$ ). The diastereomeric ratio was determined

to be 83:17 by chiral SFC (Cellulose-2 (OZ-H) (250 x 4.6 mm); 12% MeOH; 220 nm; 1.5 mL/min; Rt 15.0 min).

SFC (Cellulose-2 (OZ-H) (250 x 4.6 mm); 12% MeOH; 220 nm; 1.5 mL/min)



**(R)-3-39**

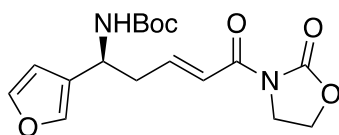
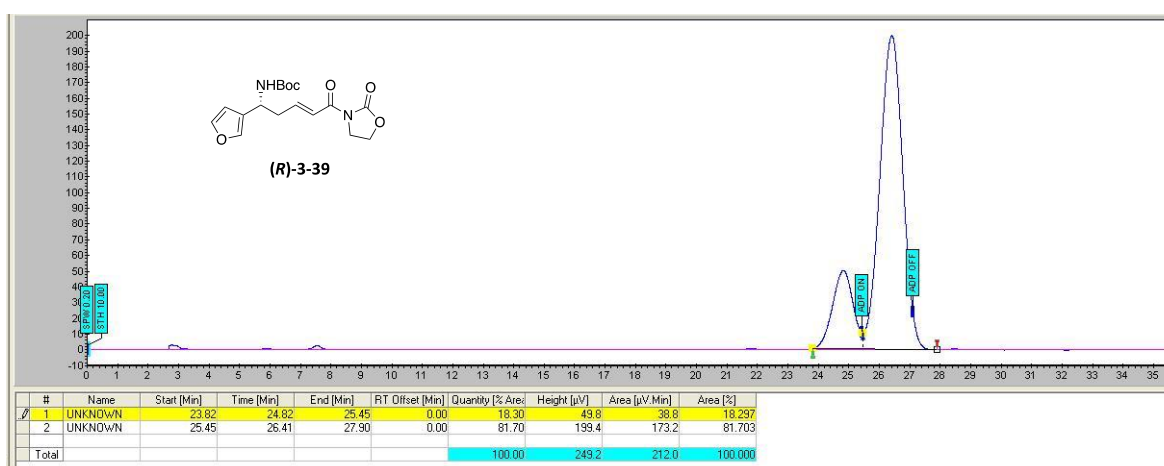
*tert*-Butyl

**(R,E)-(1-(furan-3-yl)-5-oxo-5-(2-oxooxazolidin-3-**

**yl)pent-3-en-1-yl)carbamate ((R)-3-39).** According to General Procedure D, **3-31** (0.214 g, 1.38 mmol, 1 equiv), **3-38** (0.538 g, 2.76 mmol, 2 equiv), [Cu(CH<sub>3</sub>CN)<sub>4</sub>]PF<sub>6</sub> (0.132 g, 0.345 mmol, 0.25 equiv), (*S*)-DTBM-SEPHOS (0.415 g, 0.345 mmol, 0.25 equiv), and DABCO (1 M solution in THF, 0.690 mL, 0.690 mmol, 0.5 equiv) afforded **(R)-3-39** (0.358 g, 1.02 mmol, 74%) as a white solid: Mp 145.8-147.1 °C; IR (ATR, neat) 3370, 2983, 2782, 1792 1774, 1664, 1640, 1520, 187, 1363, 1327 1249, 1223, 1207, 1172, 1120, 1046, 1018, 972, 873, 753, 708 cm<sup>-1</sup>; [α]<sub>D</sub><sup>25</sup> -22.3 (c 0.2, CHCl<sub>3</sub>); <sup>1</sup>H NMR (300 MHz, CDCl<sub>3</sub>) δ 7.38 (d, *J* = 1.5 Hz, 1H), 7.34-7.28 (m, 2H), 7.06 (dt, *J* = 15.0, 7.5 Hz, 1H), 6.34 (d, *J* = 1.2 Hz, 1H), 4.84 (brd s, 1H), 4.71 (s, 1H), 4.42 (t, *J* = 7.8 Hz, 2H), 4.05 (t, *J* = 7.8 Hz, 1H), 2.75 (t, *J* = 6.9 Hz, 2H), 1.44 (s, 9H); <sup>13</sup>C NMR (75 MHz, CDCl<sub>3</sub>) δ 164.6, 153.4, 145.9, 143.6, 139.8, 139.2, 126.0, 122.8, 108.9, 79.9, 62.0, 45.9, 42.6, 38.6, 28.3; HRMS (LCMS ESI+) *m/z* calcd for C<sub>17</sub>H<sub>22</sub>N<sub>2</sub>O<sub>6</sub> [M+Na] 373.1370, found 373.1375. The enantiomeric ratio was determined to be 18:82 by chiral SFC (ChiralPak-IC (250 x 10 mm); 10% MeOH; 220 nm; 5.0 mL/min; Rt 26.4 min).

Alternative purification 1.5 mmol scale: According to General Procedure D, **3-31** (0.220 g, 1.42 mmol, 1 equiv), **3-38** (0.554 g, 2.84 mmol, 2 equiv), [Cu(CH<sub>3</sub>CN)<sub>4</sub>]PF<sub>6</sub> (0.136 g, 0.355 mmol, 0.25 equiv), (*S*)-DTBM-SEGP<sub>HOS</sub> (0.427 g, 0.355 mmol, 0.25 equiv), and DABCO (1 M solution in THF, 0.709 mL, 0.709 mmol, 0.5 equiv) were stirred at -20 °C, filtered through a plug of basic alumina (EtOAc) and washed with NH<sub>4</sub>OH (3 x 15 mL), NaHCO<sub>3</sub> (1 x 10 mL), and brine (2 x 15 mL). The combined organic layers were dried (MgSO<sub>4</sub>), filtered, and concentrated under reduced pressure. The resulting solid was washed with additional hexanes (2 x 5 mL) and dried, to afford (*R*)-**3-39** (0.495 g, 1.41 mmol, quant) as a white solid.

SFC (ChiralPak-IC (250 x 10 mm); 10% MeOH; 220 nm; 5.0 mL/min)



**(S)-3-39**

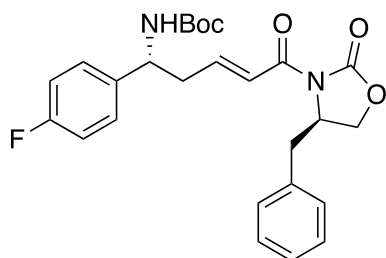
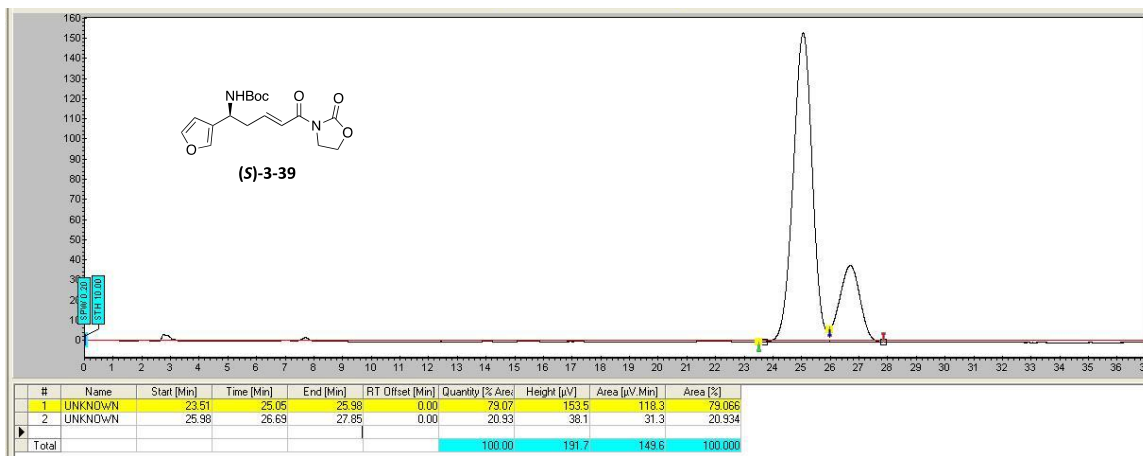
*tert*-Butyl

(*S,E*)-(1-(furan-3-yl)-5-oxo-5-(2-oxooxazolidin-3-

yl)pent-3-en-1-yl)carbamate ((*S*)-**3-39**). According to General Procedure D, **3-31** (0.091 g, 0.586 mmol, 1 equiv), **3-38** (0.229 g, 1.17 mmol, 2 equiv), [Cu(CH<sub>3</sub>CN)<sub>4</sub>]PF<sub>6</sub> (0.056 g, 0.147 mmol, 0.25 equiv), (*R*)-DTBM-SEGP<sub>HOS</sub> (0.176 g, 0.147 mmol, 0.25 equiv), and DABCO (1 M solution in THF, 0.293 mL, 0.293 mmol, 0.5 equiv) afforded (*S*)-**3-39** (0.128 g, 0.365 mmol, 62%) as a white solid:  $[\alpha]_D^{25} +11.3$  (*c* 0.2, CHCl<sub>3</sub>). The enantiomeric ratio was determined to be 79:21 by chiral SFC (ChiralPak-IC (250 x 10 mm); 10% MeOH; 220 nm; 5.0 mL/min; Rt 25.0 min).



SFC (ChiralPak-IC (250 x 10 mm); 10% MeOH; 220 nm; 5.0 mL/min)

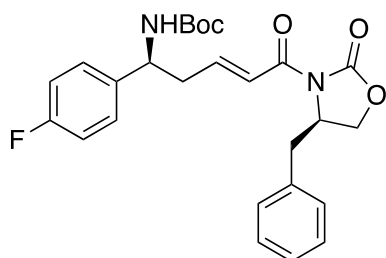
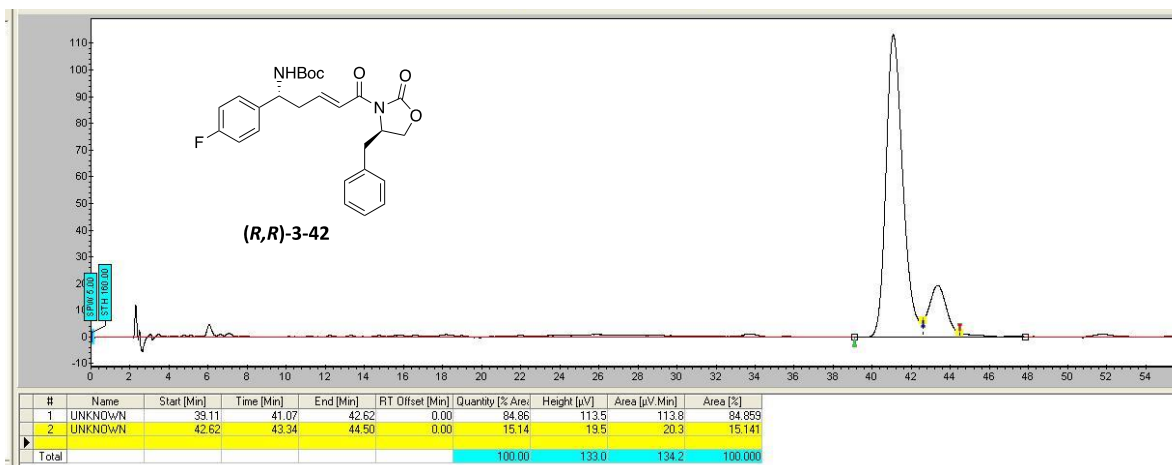


**(*R,R*)-3-42**

***tert*-Butyl ((*R,E*)-5-((*R*)-4-benzyl-2-oxooxazolidin-3-yl)-1-(4-**

**fluorophenyl)-5-oxopent-3-en-1-yl)carbamate ((*R,R*)-3-42).** According to General Procedure D, (*R*)-3-28 (0.300 g, 1.22 mmol, 1 equiv), 3-41 (0.502 g, 2.45 mmol, 2 equiv), [Cu(CH<sub>3</sub>CN)<sub>4</sub>]PF<sub>6</sub> (0.116 g, 0.306 mmol, 0.25 equiv), (*S*)-DTBM-SEGPBOS (0.364 g, 0.306 mmol, 0.25 equiv), and DABCO (1 M solution in THF, 0.612 mL, 0.612 mmol, 0.5 equiv) afforded (*R,R*)-3-42 (0.199 g, 0.425 mmol, 34%) as a white solid: Mp 53.5-55.8 °C; IR (neat) 3356, 2978, 2929, 1774, 1683, 1509, 1356, 1220, 1190, 836, 701 cm<sup>-1</sup>; [ $\alpha$ ]<sub>D</sub><sup>25</sup> -32.3 (*c* 0.5, CHCl<sub>3</sub>); <sup>1</sup>H NMR (500 MHz, CDCl<sub>3</sub>)  $\delta$  7.34-7.25 (m, 6H), 7.20-7.16 (m, 2H), 7.04-7.01 (m, 3H), 4.85 (brd s, 2H), 4.71-4.67 (m, 1H), 4.22-4.15 (m, 2H), 3.30 (dd, *J* = 13.5, 3.0 Hz, 1H), 2.79-2.73 (m, 3H), 1.41 (s, 9H); <sup>13</sup>C NMR (150 MHz, CDCl<sub>3</sub>)  $\delta$  164.3, 162.9, 161.3, 154.9, 153.4, 145.8, 135.2, 129.43, 129.40, 129.0, 127.91, 127.86, 127.4, 123.3, 115.7, 115.6, 79.9, 66.2, 55.3, 53.2, 39.7, 37.8, 28.3; <sup>19</sup>F NMR (470 MHz, CDCl<sub>3</sub>)  $\delta$  -114.9; HRMS (LCMS ESI+) *m/z* calcd for C<sub>26</sub>H<sub>30</sub>FN<sub>2</sub>O<sub>5</sub> [M+H] 469.2133, found 469.2135. The diastereomeric ratio was determined to be 85:15 by chiral SFC (Cellulose-2 (OZ-H) (250 x 4.6 mm); 8% MeOH; 220 nM; 1.5 mL/min; Rt 41.1 min).

SFC (Cellulose-2 (OZ-H) (250 x 4.6 mm); 8% MeOH; 220 nM; 1.5 mL/min)

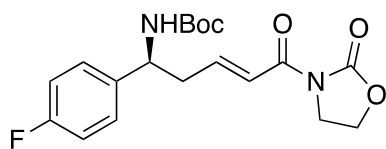
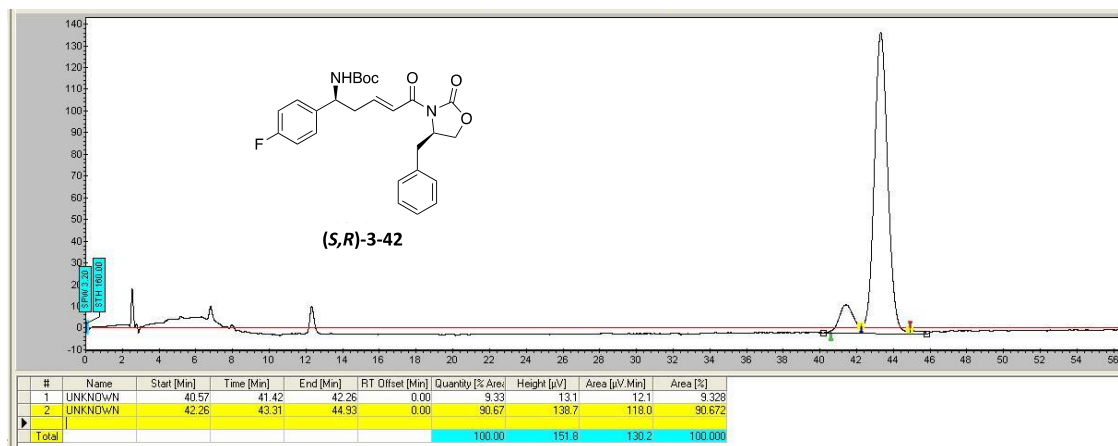


**(S,R)-3-42**

*tert*-Butyl ((S,E)-5-((R)-4-benzyl-2-oxooxazolidin-3-yl)-1-(4-

fluorophenyl)-5-oxopent-3-en-1-yl)carbamate ((S,R)-3-42). According to General Procedure D, (R)-3-28 (0.130 g, 0.530 mmol, 1 equiv), 3-41 (0.237 g, 1.06 mmol, 2 equiv), [Cu(CH<sub>3</sub>CN)<sub>4</sub>]PF<sub>6</sub> (0.051 g, 0.132 mmol, 0.25 equiv), (R)-DTBM-SEPHOS (0.158 g, 0.132 mmol, 0.25 equiv), and DABCO (1 M solution in THF, 0.265 mL, 0.265 mmol, 0.5 equiv) afforded (S,R)-3-42 (0.041 g, 0.088 mmol, 17%) as a white solid: Mp 61.1-64.2 °C; IR (neat) 3380, 2981, 1800, 1772, 1674, 1636, 1604, 1507, 1356, 1239, 1211, 1172, 1134, 1013, 972, 832, 760, 712, 699 cm<sup>-1</sup>; [α]<sub>D</sub><sup>25</sup> -26.3 (c 0.2, CHCl<sub>3</sub>); <sup>1</sup>H NMR (300 MHz, CDCl<sub>3</sub>) δ 7.33-7.18 (m, 6H), 7.21-7.18 (m, 2H), 7.07-6.97 (m, 3H), 4.84 (brd s, 2H), 4.73-4.68 (m, 1H), 4.21-4.17 (m, 2H), 3.30 (dd, *J* = 13.5, 3.0 Hz, 1H), 2.82-2.74 (m, 3H), 1.41 (s, 9H); <sup>13</sup>C NMR (75 MHz, CDCl<sub>3</sub>) δ 164.3, 163.7, 160.5, 154.9, 153.3, 145.7, 135.2, 129.4, 129.0, 127.93, 127.86, 127.82, 127.4, 123.3, 115.8, 115.5, 77.2, 66.2, 55.3, 52.3, 39.7, 37.8, 28.3; δ <sup>19</sup>F NMR (282 MHz, CDCl<sub>3</sub>) δ -114.9; HRMS (LCMS ESI+) *m/z* calcd for C<sub>26</sub>H<sub>30</sub>FN<sub>2</sub>O<sub>5</sub> [M+H] 469.2133, found 469.2139. The diastereomeric ratio was determined to be 91:9 by chiral SFC (Cellulose-2 (OZ-H) (250 x 4.6 mm); 8% MeOH; 220 nM; 1.5 mL/min; Rt 43.3 min).

SFC (Cellulose-2 (OZ-H) (250 x 4.6 mm); 8% MeOH; 220 nM; 1.5 mL/min)

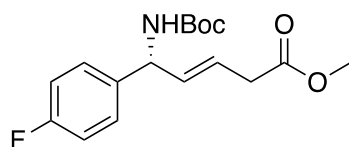
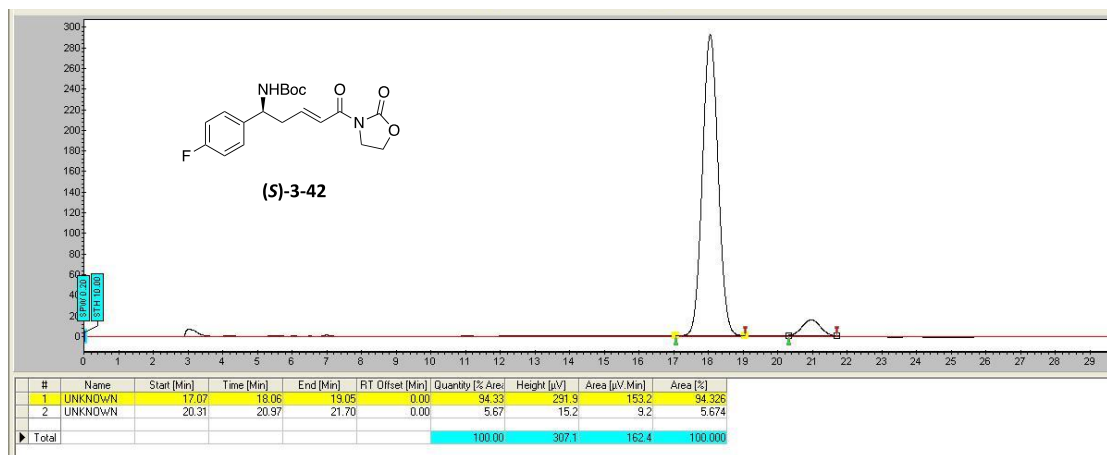


**(S)-3-42**

***tert*-Butyl (S,E)-(1-(4-fluorophenyl)-5-oxo-5-(2-oxooxazolidin-**

**3-yl)pent-3-en-1-yl)carbamate ((S)-3-42).** According to General Procedure D, **3-31** (0.206 g, 1.33 mmol, 1 equiv), **3-41** (0.593 g, 2.66 mmol, 2 equiv), [Cu(CH<sub>3</sub>CN)<sub>4</sub>]PF<sub>6</sub> (0.127 g, 0.332 mmol, 0.25 equiv), (*R*)-DTBM-SEGPPOS (0.395 g, 0.332 mmol, 0.25 equiv), and DABCO (1 M solution in THF, 0.664 mL, 0.664 mmol, 0.5 equiv) afforded **(S)-3-42** (0.197 g, 0.521 mmol, 39%) as a white solid: Mp 144.5-147.6 °C; IR (neat) 3371, 2981, 2921, 1791, 1774, 1680, 1637, 1607, 1501, 1475, 1363, 1327, 1223, 1203, 1172, 1220, 1046, 1015, 970, 824, 753, 708 cm<sup>-1</sup>; [α]<sub>D</sub><sup>25</sup> -19.2 (*c* 0.2, CHCl<sub>3</sub>); <sup>1</sup>H NMR (500 MHz, CDCl<sub>3</sub>) δ 7.29-7.23 (m, 3H), 7.05-6.96 (m, 3H), 4.83 (brd s, 2H), 4.42 (t, *J* = 7.5 Hz, 2H), 4.05 (t, *J* = 7.5 Hz, 2H), 2.74 (brd s, 2H), 1.41 (s, 9H); <sup>13</sup>C NMR (150 MHz, CDCl<sub>3</sub>) δ 164.5, 163.1, 161.1, 154.9, 153.4, 145.6, 127.9, 127.8, 122.9, 115.7, 115.5, 79.9, 62.0, 53.2, 42.6, 39.6, 28.3; <sup>19</sup>F NMR (470 MHz, CDCl<sub>3</sub>) δ -115.0; HRMS (LCMS ESI+) *m/z* calcd for C<sub>19</sub>H<sub>24</sub>FN<sub>2</sub>O<sub>5</sub> [M+H] 379.1669, found 379.1671. The enantiomeric ratio was determined to be 94:6 by chiral SFC (ChiralPak-IC (250 x 10 mm); 13% MeOH; 220 nM; 5 mL/min; Rt 18.1 min).

SFC (ChiralPak-IC (250 x 10 mm); 13% MeOH; 220 nM; 5 mL/min)



**(R)-3-43**

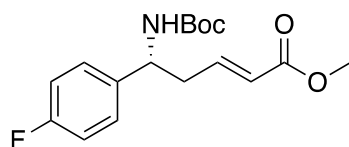
**Methyl**

**(R,E)-5-((tert-butoxycarbonyl)amino)-5-(4-**

**fluorophenyl)pent-3-enoate ((R)-3-43).** A solution of *n*-BuLi (0.29 mL, 0.728 mmol, 3.1 equiv) was added dropwise to a solution of DIPEA (0.10 mL, 0.704 mmol, 3.0 equiv) in anhydrous THF (3.0 mL) at  $-78^{\circ}\text{C}$ . The reaction mixture was kept at  $-78^{\circ}\text{C}$  for 15 min, then cooled to  $0^{\circ}\text{C}$  for 15 min, and re-cooled to  $-78^{\circ}\text{C}$ . DMPU (0.09 mL, 0.704 mmol, 3.0 equiv) was added and the reaction was stirred for 15 min. A solution of oxazolidinone **(R,R)-3-42** (0.110 g, 0.235 mmol, 1.0 equiv) in anhydrous THF (0.7 mL) was added over a period of 2 min. After the addition was complete, the mixture was stirred for 15 min at  $-78^{\circ}\text{C}$ , 15 min at  $-40^{\circ}\text{C}$ , and 60 min at  $-20^{\circ}\text{C}$ . The solution was re-cooled to  $-78^{\circ}\text{C}$ , treated with and MeOH (0.5 mL), stirred for 45 min at  $-78^{\circ}\text{C}$ . The reaction was quenched with saturated aqueous  $\text{NH}_4\text{Cl}$  (5 mL) and  $\text{H}_2\text{O}$  (5 mL). The aqueous layer was extracted with  $\text{CH}_2\text{Cl}_2$  ( $3 \times 5$  mL). The combined organic layer was dried ( $\text{MgSO}_4$ ), filtered, and concentrated. Purification by chromatography on  $\text{SiO}_2$  (20:1, hexanes:EtOAc) afforded **(R)-3-43** (0.0498 g, 0.154 mmol, 66% yield) as a pale yellow oil: IR (ATR, neat) 3354, 2978, 1694, 1508, 1222, 1188, 1014, 838  $\text{cm}^{-1}$ ;  $[\alpha]_D^{25} +16.3$  (*c* 0.2,  $\text{CHCl}_3$ );  $^1\text{H}$  NMR (400 MHz,  $\text{CDCl}_3$ )  $\delta$  7.26-7.23 (m, 2H), 7.02 (t, *J* = 8.4 Hz, 2H), 5.74-5.71 (m, 2H), 5.26 (brd s, 1H), 4.88-4.83 (m, 1H), 3.69 (s, 3H), 3.11 (d, *J* = 5.2 Hz, 2H), 1.43 (s, 9H);  $^{13}\text{C}$  NMR (125 MHz,  $\text{CDCl}_3$ )  $\delta$  171.8, 162.9, 161.3, 154.8, 137.0, 133.7, 128.6, 123.6, 115.5, 115.4, 51.9, 37.3,

28.3;  $^{19}\text{F}$  NMR (376 MHz,  $\text{CDCl}_3$ )  $\delta$  -115.1; HRMS (LCMS ESI+)  $m/z$  calcd for  $\text{C}_{17}\text{H}_{23}\text{FNO}_4$  [ $\text{M} + \text{H}$ ] 324.1606, found 324.1618.

**General procedure E.** For the preparation of  $\beta,\alpha$ -unsaturated methyl esters. A solution of  $\text{Yb}(\text{OTf})_3$  (0.0437 mmol, 0.05 equiv) in MeOH (10 mL, 0.08 M) was stirred at rt for 30 min. The  $\beta,\alpha$ -unsaturated vinylogous Mannich product (0.875 mmol, 1 equiv) was added and the mixture was stirred at 60 °C for 2 h. The solvent was removed under reduced pressure and the crude product was purified by chromatography on  $\text{SiO}_2$  (3:1, hexanes:EtOAc) to afford the desired  $\beta,\alpha$ -unsaturated methyl ester.



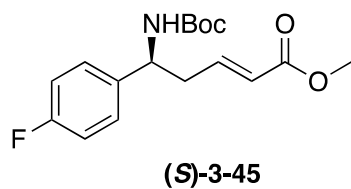
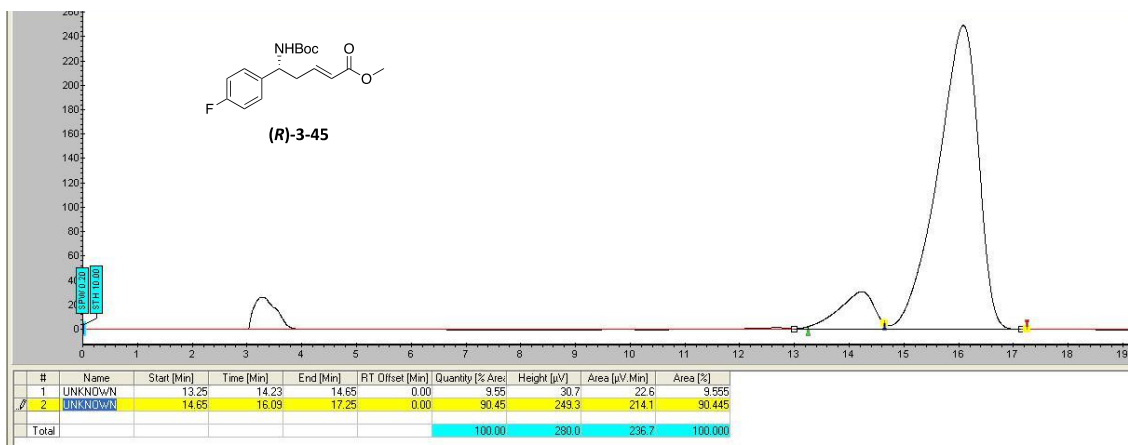
**(*R*)-3-45**

**Methyl**

**(*R,E*)-5-((*tert*-butoxycarbonyl)amino)-5-(4-**

**fluorophenyl)pent-2-enoate ((*R*)-3-45).** According to General Procedure E,  $\text{Yb}(\text{OTf})_3$  (27.9 mg, 0.044 mmol, 0.05 equiv) and **(*R,R*)-3-42** (0.410 g, 0.875 mmol, 1 equiv) afforded **(*R*)-3-45** (0.273 g, 0.844 mmol, 96%) as a white solid: Mp 59.9-61.2 °C; IR (ATR, neat) 3380, 2983, 2957, 1717, 1680, 1509, 1435, 1366, 1266, 1223, 1164, 1042, 1018, 980, 838, 780, 760  $\text{cm}^{-1}$ ;  $[\alpha]_D^{25} +16.8$  ( $c$  0.2,  $\text{CHCl}_3$ );  $^1\text{H}$  NMR (600 MHz,  $\text{CDCl}_3$ )  $\delta$  7.25-7.22 (m, 2H), 7.03 (t,  $J$  = 8.4 Hz, 2H), 6.81 (dt,  $J$  = 15.6, 7.8 Hz, 1H), 5.86 (d,  $J$  = 15.6 Hz, 1H), 4.80 (brd s, 2H), 3.71 (s, 3H), 2.67 (brd s, 2H), 1.41 (s, 9H);  $^{13}\text{C}$  NMR (150 MHz,  $\text{CDCl}_3$ )  $\delta$  166.4, 162.9, 161.3, 154.9, 143.8, 127.9, 124.0, 115.7, 115.5, 51.6, 28.3;  $^{19}\text{F}$  NMR (564 MHz,  $\text{CDCl}_3$ )  $\delta$  -114.88; HRMS (LCMS ESI+)  $m/z$  calcd for  $\text{C}_{17}\text{H}_{22}\text{FNO}_4\text{Na}$  [ $\text{M} + \text{Na}$ ] 346.1431, found 346.1419. The enantiomeric ratio was determined to be 9:91 by chiral SFC (ChiralPak-IC (250 x 10 mm); 5% MeOH; 220 nm; 5.0 mL/min; Rt 16.1 min).

SFC (ChiralPak-IC (250 x 10 mm); 5% MeOH; 220 nm; 5.0 mL/min)

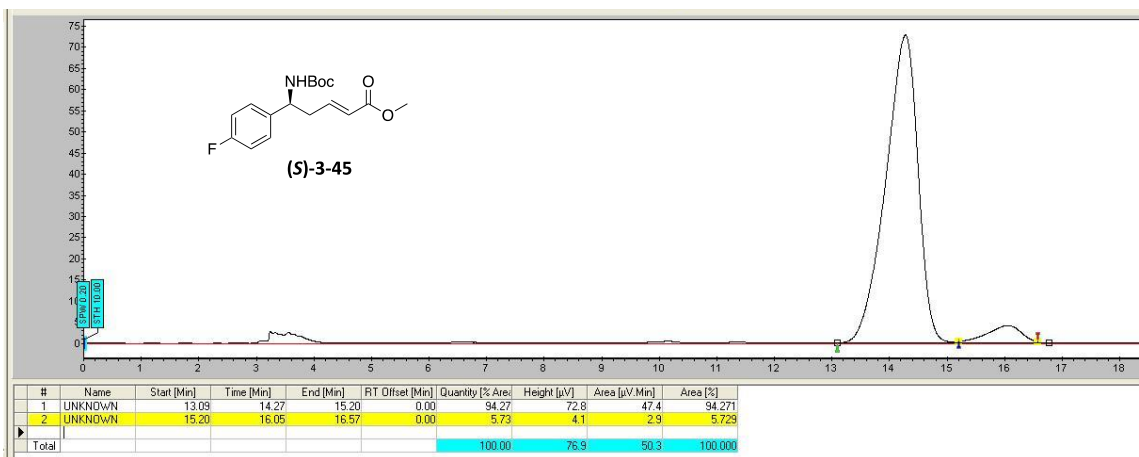


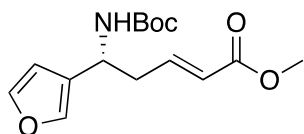
Methyl

**(S,E)-5-((tert-butoxycarbonyl)amino)-5-(4-**

**fluorophenyl)pent-2-enoate ((S)-3-45).** According to General Procedure E, Yb(OTf)<sub>3</sub> (20.3 mg, 0.031 mmol, 0.05 equiv) and (*S*)-**3-42** (0.238 g, 0.629 mmol, 1 equiv) afforded (*S*)-**3-45** (0.199 g, 0.615 mmol, 98%) as a white solid:  $[\alpha]_D^{25}$  -19.3 (*c* 0.1, CHCl<sub>3</sub>). The enantiomeric ratio was determined to be 94:6 by chiral SFC (ChiralPak-IC (250 x 10 mm); 5% MeOH; 220 nm; 5.0 mL/min; Rt 14.3 min).

SFC (ChiralPak-IC (250 x 10 mm); 5% MeOH; 220 nm; 5.0 mL/min)

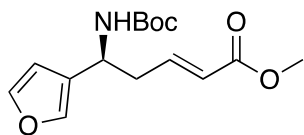
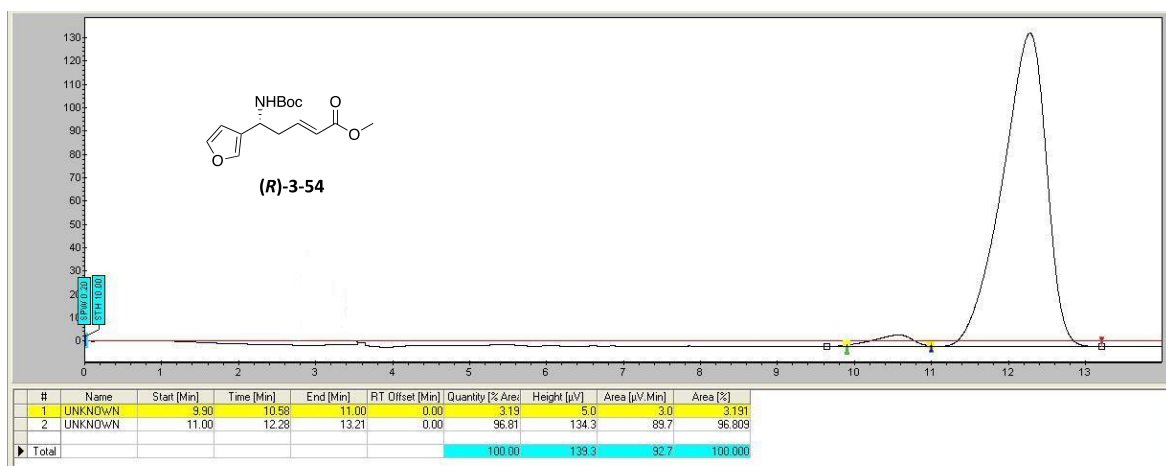




**(R)-3-54**

**Methyl (R,E)-5-((tert-butoxycarbonyl)amino)-5-(furan-3-yl)pent-2-enoate ((R)-3-54).** According to General Procedure E, Yb(OTf)<sub>3</sub> (35.8 mg, 0.056 mmol, 0.05 equiv) and (R,R)-3-39 (0.490 g, 1.11 mmol, 1 equiv) afforded (R)-3-54 (0.307 g, 1.04 mmol, 93%) as a colorless viscous oil: IR (ATR, neat) 3350, 2978, 1702, 1502, 1436, 1366, 1271, 149, 1184, 1022, 874, 783 cm<sup>-1</sup>; [α]<sub>D</sub><sup>25</sup> +14.1 (c 0.1, CHCl<sub>3</sub>); <sup>1</sup>H NMR (600 MHz, CDCl<sub>3</sub>) δ 7.38 (d, *J* = 1.2 Hz, 1H), 7.34 (s, 1H), 6.88 (dt, *J* = 15.6, 7.2 Hz, 1H), 6.33 (d, *J* = 1.2 Hz, 1H), 5.89 (d, *J* = 15.6, 1H), 4.82 (brd s, 1H), 4.67 (brd s, 1H), 3.71 (s, 3H), 2.70-2.66 (m, 2H), 1.44 (s, 9H); <sup>13</sup>C NMR (150 MHz, CDCl<sub>3</sub>) δ 166.5, 155.0, 144.1, 143.6, 139.2, 126.0, 123.9, 108.9, 79.9, 51.5, 46.0, 38.2, 28.3; HRMS (LCMS ESI+) *m/z* calcd for C<sub>15</sub>H<sub>21</sub>NO<sub>5</sub>Na [M+Na] 318.1212, found 318.1317. The enantiomers were separated by SFC and the resulting enantiomeric ratio was determined to be 3:97 by chiral SFC (ChiralPak-IC (250 x 10 mm); 6% MeOH; 220 nm; 5.0 mL/min; Rt 12.3 min).

SFC (ChiralPak-IC (250 x 10 mm); 6% MeOH; 220 nm; 5.0 mL/min)

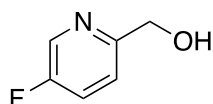
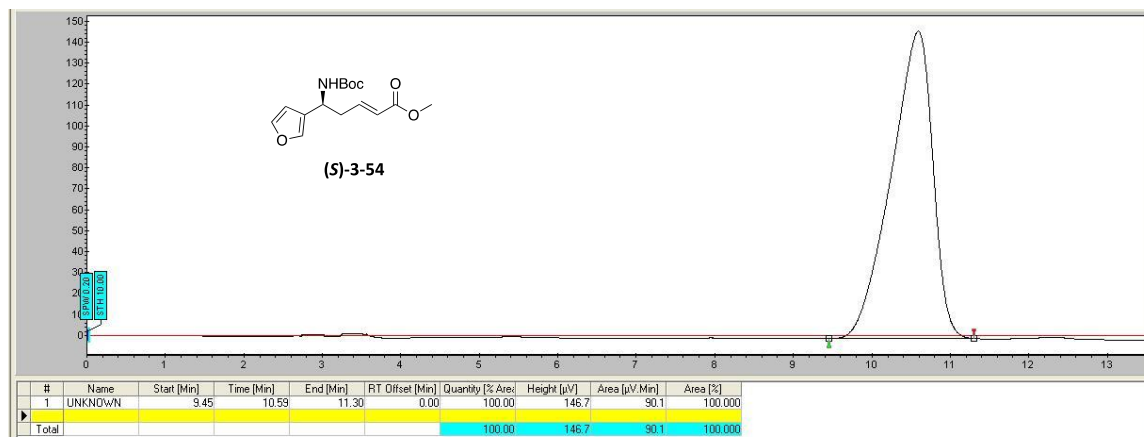


**(S)-3-54**

**Methyl (S,E)-5-((tert-butoxycarbonyl)amino)-5-(furan-3-yl)pent-2-enoate ((S)-3-54).** According to General Procedure E, Yb(OTf)<sub>3</sub> (10.5 mg, 0.016 mmol, 0.05 equiv) and (S,S)-3-39 (0.114 g, 0.323 mmol, 1 equiv) afforded (S)-3-54 (0.095 g, 0.322 mmol, 99%)

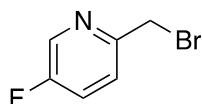
as a colorless viscous oil:  $[\alpha]_D^{25}$  -8.8 (*c* 0.1, CHCl<sub>3</sub>). The enantiomers were separated by SFC and the resulting enantiomeric ratio was determined to be >99:1 by chiral SFC (ChiralPak-IC (250 x 10 mm); 6% MeOH; 220 nm; 5.0 mL/min; Rt 10.6 min).

SFC (ChiralPak-IC (250 x 10 mm); 6% MeOH; 220 nm; 5.0 mL/min)



**3-50**

**(5-Fluoropyridin-2-yl)methanol (3-50).**<sup>239</sup> To a solution of 5-fluoro-2-formylpyridine (0.79 mL, 7.67 mmol, 1 equiv) in MeOH (35 mL, 0.2 M) was added sodium borohydride (0.871 g, 23.0 mmol, 3 equiv). The mixture was stirred at rt for 21 h, quenched with water (15 mL), and the organic layer was extracted with EtOAc (3 x 15 mL), dried (MgSO<sub>4</sub>), filtered, and concentrated under reduced pressure to afford **3-50** (0.970 g, 7.62 mmol, quant) as a colorless liquid: IR (ATR, neat) 3279, 2865, 2859, 1586, 1485, 1389, 1238, 1060, 1022, 832, 715 cm<sup>-1</sup>; <sup>1</sup>H NMR (500 MHz, CDCl<sub>3</sub>) δ 8.43 (s, 1H), 7.46-7.42 (m, 1H), 7.31-7.29 (m, 1H), 4.76 (s, 2H), 2.71 (brd s, 1H); <sup>13</sup>C NMR (100 MHz, CDCl<sub>3</sub>) δ 155.0, 136.8, 136.5, 124.0, 123.7, 121.4, 63.9; <sup>19</sup>F NMR (470 MHz, CDCl<sub>3</sub>) δ -129.1.



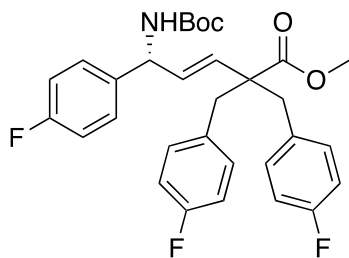
**3-51**

**2-(Bromomethyl)-5-fluoropyridine (3-51).**<sup>239</sup> To a solution of **3-50** (1.00 mL, 7.87 mmol, 1 equiv) in anhydrous CH<sub>2</sub>Cl<sub>2</sub> (40 mL, 0.2 M) was added dropwise a solution of tribromophosphane (0.757 mL, 7.87 mmol, 1 equiv) in anhydrous CH<sub>2</sub>Cl<sub>2</sub> (5 mL) at 0 °C. The



mixture was stirred for 22 h at rt and diluted with NH<sub>4</sub>Cl. The aqueous layer was extracted with CH<sub>2</sub>Cl<sub>2</sub> (2 x 15 mL), washed with brine, dried (MgSO<sub>4</sub>), filtered, and concentrated under reduced pressure to afford **3-51** (0.996 g, 5.24 mmol, 67%) as a red liquid: <sup>1</sup>H NMR (300 MHz, CDCl<sub>3</sub>) δ 8.44 (s, 1H), 7.50-7.38 (m, 2H), 4.56 (s, 2H); <sup>19</sup>F NMR (282 MHz, CDCl<sub>3</sub>) δ -127.1.

**General procedure F.** For the preparation of bis-alkylated γ,β-unsaturated methyl esters. To a flame-dried round bottom flask containing dry THF (2.0 mL) at -78 °C was added DIPEA (0.184 mL, 1.30 mmol, 3.0 equiv) followed by *n*-BuLi (2.5 M hexanes, 0.520 mL, 1.30 mmol, 3.0 equiv). After 20 min at -78 °C, the solution was warmed to 0 °C for 10 min and then cooled back down to -78 °C. To this solution was added DMPU (0.166 mL, 1.34 mmol, 3.1 equiv). After 10 min, the β,α-unsaturated methyl ester (0.165 g, 0.306 mmol, 1 equiv) in THF (2.0 mL) was added dropwise over 15 min. After 20 min, the alkyl bromide (0.172 mL, 1.34 mmol, 3.1 equiv) was added dropwise and the solution was allowed to warm slowly to rt over 21 h. After 21 h, the solution was treated with satd. NH<sub>4</sub>Cl (3 mL) and extracted with EtOAc (3 x 5 mL). The combined organic layers were washed with brine, dried (MgSO<sub>4</sub>), filtered, and concentrated under reduced pressure. The crude product was purified by chromatography on SiO<sub>2</sub> (5:1, hexanes:EtOAc) to afford the desired bis-alkylated γ,β-unsaturated methyl ester.

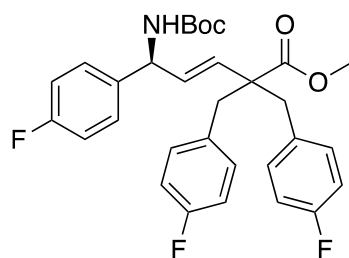


**(R)-3-46**

**Methyl (R,E)-5-((tert-butoxycarbonyl)amino)-2,2-bis(4-**

**fluorobenzyl)-5-(4-fluorophenyl)pent-3-enoate ((R)-3-46).** According to General Procedure F, **(R)-3-45** (0.140 g, 0.433 mmol, 1 equiv), 4-fluorobenzyl bromide (0.172 mL, 1.34 mmol, 3.1 equiv), *n*-BuLi (2.5 M hexanes, 0.520 mL, 1.30 mmol, 3.0 equiv), DIPEA (0.184 mL, 1.30 mmol, 3.0 equiv), and DMPU (0.166 mL, 1.34 mmol, 3.1 equiv) afforded **(R)-3-46** (0.165 g, 0.306 mmol, 71%) as a colorless sticky semi-solid: IR (ATR, neat) 3345, 2979, 1709, 1510, 1451, 1366, 1220,

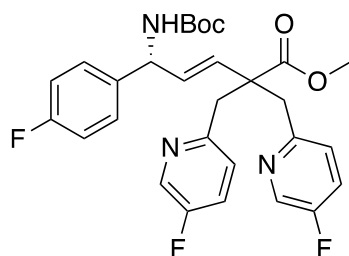
1157, 1101, 1016, 836  $\text{cm}^{-1}$ ;  $[\alpha]_D^{25}$  -9.2 (*c* 0.2,  $\text{CHCl}_3$ );  $^1\text{H}$  NMR (500 MHz,  $\text{CDCl}_3$ )  $\delta$  7.07-7.04 (m, 2H), 7.01-6.96 (m, 6H), 6.92-6.87 (m, 4H), 5.78 (dd, *J* = 16.0, 1.0 Hz, 1H), 5.57 (dd, *J* = 16.0, 6.0 Hz, 1H), 5.25 (brd s, 1H), 4.71 (brd s, 1H), 3.65 (s, 3H), 3.19 (dd, *J* = 14.0, 5.0 Hz, 2H), 2.96-2.91 (m, 2H), 1.45 (s, 9H);  $^{13}\text{C}$  NMR (150 MHz,  $\text{CDCl}_3$ )  $\delta$  174.2, 162.8, 162.5, 161.2, 160.9, 154.8, 132.4, 132.30, 132.28, 131.8, 131.7, 131.61, 131.56, 128.4, 115.4, 115.3, 114.88, 114.86, 114.74, 114.72, 60.4, 54.0, 51.8, 43.8, 43.3, 28.3;  $^{19}\text{F}$  NMR (470 MHz,  $\text{CDCl}_3$ )  $\delta$  -116.20, -114.94; HRMS (LCMS ESI+) *m/z* calcd for  $\text{C}_{31}\text{H}_{32}\text{F}_3\text{NO}_4\text{Na}$  [*M*+*Na*] 562.2176, found 562.2184.



**(S)-3-46**

**Methyl (S,E)-5-((tert-butoxycarbonyl)amino)-2,2-bis(4-**

**fluorobenzyl)-5-(4-fluorophenyl)pent-3-enoate ((S)-3-46).** According to General Procedure F, **(S)-3-45** (0.176 g, 0.544 mmol, 1 equiv), 4-fluorobenzyl bromide (0.217 mL, 1.69 mmol, 3.1 equiv), *n*-BuLi (2.5 M hexanes, 0.653 mL, 1.63 mmol, 3.0 equiv), DIPEA (0.232 mL, 1.63 mmol, 3.0 equiv), and DMPU (0.206 mL, 1.69 mmol, 3.1 equiv) afforded **(S)-3-46** (0.276 g, 0.512 mmol, 94%) as a colorless sticky semi-solid:  $[\alpha]_D^{25}$  +18.9 (*c* 0.2,  $\text{CHCl}_3$ ).

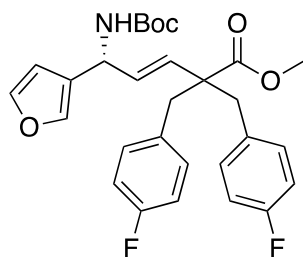


**(R)-3-52**

**Methyl (R,E)-5-((tert-butoxycarbonyl)amino)-5-(4-fluorophenyl)-**

**2,2-bis((5-fluoropyridin-2-yl)methyl)pent-3-enoate ((R)-3-52).** According to General Procedure F, **(R)-3-45** (0.160 g, 0.495 mmol, 1 equiv), **3-51** (0.292 g, 1.53 mmol, 3.1 equiv), *n*-BuLi (2.5 M hexanes, 0.594 mL, 1.48 mmol, 3.0 equiv), DIPEA (0.211 mL, 1.48 mmol, 3.0 equiv), and DMPU (0.189 mL, 1.53 mmol, 3.1 equiv) afforded **(R)-3-52** (0.096 g, 0.160 mmol, 32%, 90% pure) as a colorless sticky semi-solid: IR (ATR, neat) 3351, 2979, 1708, 1602, 1585, 1508, 1482,

1391, 1367, 1209, 1168, 1158, 1045, 1019, 974, 834  $\text{cm}^{-1}$ ;  $[\alpha]_D^{25} +7.7$  ( $c$  0.2,  $\text{CHCl}_3$ );  $^1\text{H}$  NMR (300 MHz,  $\text{CDCl}_3$ )  $\delta$  8.33-8.31 (m, 2H), 7.16-7.03 (m, 3H), 7.01-6.89 (m, 5H), 5.87 (dd,  $J = 16.2$ , 1.2 Hz, 1H), 5.46 (dd,  $J = 16.2$ , 6.0 Hz, 1H), 5.15 (brd s, 1H), 4.82 (brd s, 1H), 3.69 (s, 3H), 3.40-3.22 (m, 4H), 1.42 (s, 9H);  $^{13}\text{C}$  NMR (150 MHz,  $\text{CDCl}_3$ )  $\delta$  174.7, 171.2, 162.8, 161.2, 159.1, 157.42, 157.40, 154.8, 153.7, 153.5, 136.9, 136.7, 130.7, 128.5, 125.6, 125.5, 122.8, 122.7, 115.3, 115.2, 79.7, 60.4, 52.1, 52.0, 42.8, 28.3;  $^{19}\text{F}$  NMR (282 MHz,  $\text{CDCl}_3$ )  $\delta$  -115.18, -130.48; HRMS (LCMS ESI+)  $m/z$  calcd for  $\text{C}_{29}\text{H}_{30}\text{F}_3\text{N}_3\text{O}_4\text{Na}$   $[\text{M}+\text{Na}]$  564.2081, found 564.2090.

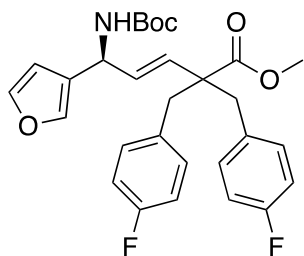


**(*R*)-3-55**

**Methyl**

**(*R,E*)-5-((*tert*-butoxycarbonyl)amino)-2,2-bis(4-**

**fluorobenzyl)-5-(furan-3-yl)pent-3-enoate ((*R*)-3-55).** According to General Procedure F, (*R*)-**3-54** (0.145 g, 0.491 mmol, 1 equiv), 4-fluorobenzyl bromide (0.196 mL, 1.52 mmol, 3.1 equiv), *n*-BuLi (2.5 M hexanes, 0.589 mL, 1.47 mmol, 3.0 equiv), DIPEA (0.209 mL, 1.47 mmol, 3.0 equiv), and DMPU (0.188 mL, 1.52 mmol, 3.1 equiv) afforded (*R*)-**3-55** (0.198 g, 0.387 mmol, 79%) as a colorless solid: Mp 91.3-94.6  $^{\circ}\text{C}$ ; IR (neat) 3344, 2983, 1720, 1687, 1604 1512, 1450, 1366, 1313, 1216, 1160, 1105, 1018, 982, 873, 812, 734  $\text{cm}^{-1}$ ;  $[\alpha]_D^{25} -9.2$  ( $c$  0.1,  $\text{CHCl}_3$ );  $^1\text{H}$  NMR (600 MHz,  $\text{CDCl}_3$ )  $\delta$  7.36 (d,  $J = 1.2$  Hz, 1H), 7.08 (s, 1H), 7.05-7.01 (m, 4H), 6.93 (m, 4H), 6.19 (d,  $J = 1.2$  Hz, 1H), 5.85 (dd,  $J = 16.2$ , 1.2 Hz, 1H), 5.59 (dd,  $J = 16.2$ , 6.6 Hz, 1H), 5.22 (brd s, 1H), 4.66 (brd s, 1H), 3.63 (s, 3H), 3.18 (d,  $J = 13.8$  Hz, 2H), 2.96 (t,  $J = 13.8$  Hz, 2H), 1.47 (s, 9H);  $^{13}\text{C}$  NMR (150 MHz,  $\text{CDCl}_3$ )  $\delta$  174.2, 162.5, 160.9, 154.9, 143.4, 139.4, 132.43, 132.41, 132.38, 132.36, 131.69, 131.66, 131.6, 131.2, 125.9, 114.88, 114.86, 114.74, 114.72, 109.3, 79.8, 53.9, 51.8, 48.7, 43.5, 28.4;  $^{19}\text{F}$  NMR (564 MHz,  $\text{CDCl}_3$ )  $\delta$  -116.28; HRMS (LCMS ESI+)  $m/z$  calcd for  $\text{C}_{29}\text{H}_{31}\text{F}_2\text{NO}_5\text{Na}$   $[\text{M}+\text{Na}]$  534.2063, found 534.2058.

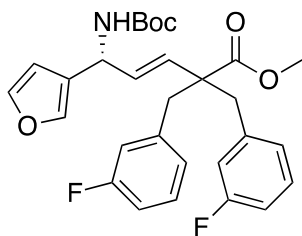


**(S)-3-55**

**Methyl**

**(S,E)-5-((tert-butoxycarbonyl)amino)-2,2-bis(4-**

**fluorobenzyl)-5-(furan-3-yl)pent-3-enoate ((S)-3-55).** According to General Procedure F, (S)-3-54 (0.085 g, 0.288 mmol, 1 equiv), 4-fluorobenzyl bromide (0.115 mL, 0.892 mmol, 3.1 equiv), *n*-BuLi (2.5 M hexanes, 0.345 mL, 0.863 mmol, 3.0 equiv), DIPEA (0.123 mL, 0.863 mmol, 3.0 equiv), and DMPU (0.110 mL, 0.892 mmol, 3.1 equiv) afforded (S)-3-55 (0.122 g, 0.238 mmol, 83%) as a white solid:  $[\alpha]_D^{25} +11.7$  (*c* 0.1, CHCl<sub>3</sub>).



**(R)-3-57**

**Methyl**

**(R,E)-5-((tert-butoxycarbonyl)amino)-2,2-bis(3-**

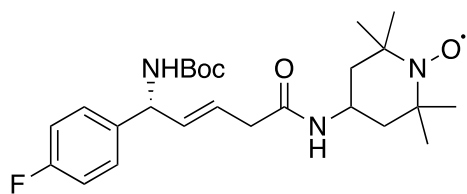
**fluorobenzyl)-5-(furan-3-yl)pent-3-enoate ((R)-3-57).** According to General Procedure F, (R)-3-54 (0.081 g, 0.274 mmol, 1 equiv), 3-fluorobenzyl bromide (0.106 mL, 0.850 mmol, 3.1 equiv), *n*-BuLi (2.5 M hexanes, 0.329 mL, 0.823 mmol, 3.0 equiv), DIPEA (0.117 mL, 0.823 mmol, 3.0 equiv), and DMPU (0.105 mL, 0.850 mmol, 3.1 equiv) afforded (R)-3-57 (0.041 g, 0.080 mmol, 29%) as a colorless oil that was used directly in next step without further purification. Diagnostic peaks: <sup>1</sup>H NMR (300 MHz, CDCl<sub>3</sub>) δ 3.22 (d, *J* = 13.8 Hz, 2H), 3.00 (d, *J* = 13.8, 2H); <sup>19</sup>F NMR (282 MHz, CDCl<sub>3</sub>) δ -113.41; HRMS (LCMS ESI+) *m/z* calcd for C<sub>29</sub>H<sub>31</sub>F<sub>2</sub>NO<sub>5</sub> [M+Na] 534.2063, found 534.2063.

**General procedure G.** For the preparation of JP4-039 analogs. To a solution of  $\gamma,\beta$ -unsaturated methyl ester (0.140 g, 0.246 mmol, 1.0 equiv) in MeOH (2.5 mL) and THF (1.0 mL) was added KOH (2.0 M in H<sub>2</sub>O, 0.62 mL, 1.23 mmol, 5.0 equiv) and the mixture was heated at reflux for 20 h, and acidified with 1 M KHSO<sub>4</sub> (ca. 2 mL) at 0 °C. The aqueous layer was extracted with CH<sub>2</sub>Cl<sub>2</sub>

(3 × 10 mL) and the combined organic layers were dried (MgSO<sub>4</sub>), filtered, concentrated under reduced pressure, and dried under high vacuum to afford the carboxylic acid as colorless oil.

To a solution of crude carboxylic acid in anhydrous CH<sub>2</sub>Cl<sub>2</sub> (3.5 mL, 0.07 M) was added sequentially 4-AT (0.062 g, 0.345 mmol, 1.4 equiv), DMAP (0.036 g, 0.296 mmol, 1.2 equiv), HOBT•H<sub>2</sub>O (0.041 g, 0.296 mmol, 1.2 equiv), and EDC•HCl (0.057 g, 0.296 mmol, 1.2 equiv). The resulting orange solution was stirred at rt for 14.5 h under a N<sub>2</sub> atmosphere. The reaction mixture was diluted with CH<sub>2</sub>Cl<sub>2</sub> (10 mL) and the organic layer was washed with an aqueous solution of saturated NH<sub>4</sub>Cl (2 × 15 mL). The combined organic layers were dried (MgSO<sub>4</sub>), filtered, and concentrated under reduced pressure. The crude product was purified by chromatography on SiO<sub>2</sub> with gradient elution (6:1 to 1:1, hexanes:EtOAc) to afford the desired JP4-039 analog.

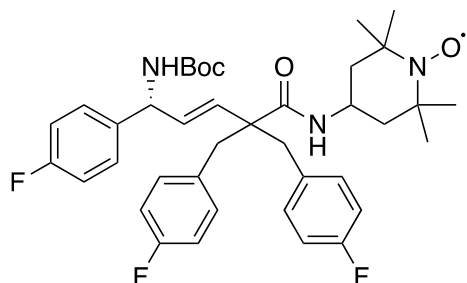
**General procedure H.** For the preparation of JP4-039 hydroxyl amine analogs for <sup>1</sup>H NMR analysis. A sample of the nitroxide (0.0069 g, 0.0149 mmol, 1.0 equiv) was dissolved in MeOH (degassed, 1 mL, 0.1 M) and L-ascorbic acid (0.013 g, 0.0744 mmol, 5.0 equiv) was added. Complete discoloration of the solution occurred within a few seconds. The reaction mixture was stirred for 1 h at rt. The solvent was removed under reduced pressure and the residue was partitioned between CH<sub>2</sub>Cl<sub>2</sub> (3 mL) and H<sub>2</sub>O (1 mL) and the aqueous phase was extracted with CH<sub>2</sub>Cl<sub>2</sub> (2 × 3 mL). The combined organic layers were dried (MgSO<sub>4</sub>), filtered, concentrated under reduced pressure, and dried under high vacuum to afford the desired the JP4-039 hydroxyl amine analogs.



**(R)-3-44**

**4-[[[(3E,5R)-5-[[[(1,1-Dimethylethoxy)carbonyl]amino]-5-(4-fluorophenyl)-1-oxo-3-penten-1-yl]amino]-2,2,6,6-tetramethyl-1-piperidinyloxy ((R)-3-44).** According to General Procedures G and H, **(R)-3-43** (0.045 g, 0.14 mmol, 1 equiv), KOH (1.0 M in H<sub>2</sub>O, 0.70 mL, 0.70 mmol, 5.0 equiv), 4-AT (0.035 g, 0.20 mmol, 1.4 equiv), DMAP (0.020 g, 0.17 mmol, 1.2 equiv), HOBT•H<sub>2</sub>O (0.023 g, 0.17 mmol, 1.2 equiv), and EDC•HCl (0.032 g,

0.17 mmol, 1.2 equiv) afforded **(R)-3-44** (35.4 mg, 0.0765 mmol, 55%) as a peach colored solid: Mp 68.5-70.2 °C; IR (neat) 3294, 2941, 2932, 1647, 1508, 1365, 1222, 1184, 1014, 974, 838 cm<sup>-1</sup>; [ $\alpha$ ]<sub>D</sub><sup>25</sup> +33.4 (c 0.2, CHCl<sub>3</sub>); <sup>1</sup>H NMR (600 MHz, MeOD)  $\delta$  7.31 (dd, *J* = 8.4, 5.4 Hz, 2H), 7.05 (t, *J* = 8.4 Hz, 2H), 5.74 (dd, *J* = 15.6, 6.0 Hz, 1H), 5.70-5.65 (ddt, *J* = 15.0, 6.0, 1.0 Hz, 1H), 5.17 (brd s, 1H), 4.10-4.06 (m, 1H), 2.94 (d, *J* = 6.6 Hz, 2H), 1.74-1.72 (m, 2H), 1.44 (s, 9H), 1.40-1.29 (m, 2H), 1.18-1.16 (m, 12H); <sup>13</sup>C NMR (150 MHz, MeOD)  $\delta$  173.1, 164.2, 162.6, 139.1, 135.1, 129.9, 129.8, 116.2, 116.0, 80.5, 60.2, 54.8, 45.8, 42.2, 40.5, 32.6, 28.8, 20.3; <sup>19</sup>F NMR (564 MHz, MeOD)  $\delta$  -117.9; HRMS (LCMS ESI+) *m/z* calcd for C<sub>25</sub>H<sub>38</sub>FN<sub>3</sub>O<sub>4</sub> [M+H] 463.2841, found 463.2820.

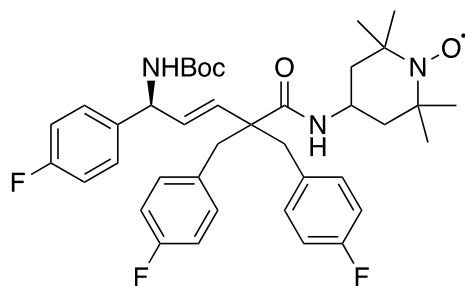


**(R)-3-47**

**4-[[[(3E,5R)-5-[(1,1-Dimethylethoxy)carbonyl]amino]-**

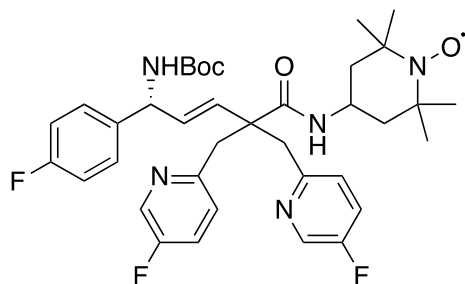
**2,2-di(4-fluorobenzyl)-5-(4-fluorophenyl)-1-oxo-3-penten-1-yl]amino]-2,2,6,6-tetramethyl-**

**1-piperidinyloxy ((R)-3-47).** According to General Procedures G and H, **(R)-3-46** (0.140 g, 0.246 mmol, 1 equiv), KOH (2.0 M in H<sub>2</sub>O, 0.62 mL, 1.2 mmol, 5.0 equiv), 4-AT (0.062 g, 0.35 mmol, 1.4 equiv), DMAP (0.036 g, 0.30 mmol, 1.2 equiv), HOBT•H<sub>2</sub>O (0.041 g, 0.30 mmol, 1.2 equiv), and EDC•HCl (0.057 g, 0.30 mmol, 1.2 equiv) afforded **(R)-3-47** (62.0 mg, 0.0913 mmol, 37%), as a peach colored solid: Mp 112.4-115.5 °C; IR (ATR, neat) 3324, 2976, 2936, 1700, 1646, 1605, 1518, 1365, 1221, 1157, 837, 780 cm<sup>-1</sup>; [ $\alpha$ ]<sub>D</sub><sup>25</sup> +19.6 (c 0.2, CHCl<sub>3</sub>); <sup>1</sup>H NMR (500 MHz, MeOD)  $\delta$  7.24- 7.21 (m, 2H), 7.13-7.11 (m, 2H), 7.09-7.04 (m, 4H), 6.90-6.86 (m, 4H), 6.65 (d, *J* = 7.5 Hz, 1H), 5.76 (dd, *J* = 16.5, 6.0 Hz, 1H) 5.67 (d, *J* = 16.5 Hz, 1H), 5.11 (d, *J* = 6.0 Hz, 1H), 4.03-3.98 (m, 1H), 3.22-3.16 (m, 2H), 2.89 (app t, *J* = 15.0 Hz, 2H), 1.43 (s, 9H), 1.43-1.25 (m, 4H), 1.16-1.11 (m, 12H); <sup>13</sup>C NMR (150 MHz, MeOD)  $\delta$  175.1, 164.3, 163.9, 162.7, 162.3, 157.6, 138.5, 135.1, 134.7, 134.6, 133.4, 133.3, 132.4, 130.1, 116.3, 116.2, 115.57, 115.55, 115.43, 115.41, 80.4, 60.2, 57.9, 55.1, 45.5, 44.5, 44.4, 43.7, 42.7, 32.6, 28.9, 20.3; <sup>19</sup>F NMR (470 MHz, MeOD)  $\delta$  -117.27, -118.82 (2F); HRMS (LCMS ESI+) *m/z* calcd for C<sub>39</sub>H<sub>48</sub>F<sub>3</sub>N<sub>3</sub>O<sub>4</sub> [M+H] 680.3668, found 680.3670.



**(S)-3-47**

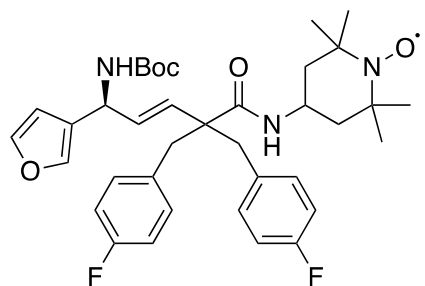
**4-[[[(3E,5S)-5-[[[(1,1-Dimethylethoxy)carbonyl]amino]-2,2-di(4-fluorobenzyl)-5-(4-fluorophenyl)-1-oxo-3-penten-1-yl]amino]-2,2,6,6-tetramethyl-1-piperidinyloxy ((S)-3-47)].** According to General Procedures G and H, (S)-3-46 (0.080 g, 0.15 mmol, 1 equiv), KOH (2.0 M in H<sub>2</sub>O, 0.37 mL, 0.74 mmol, 5.0 equiv), 4-AT (0.037 g, 0.21 mmol, 1.4 equiv), DMAP (0.022 g, 0.18 mmol, 1.2 equiv), HOBT•H<sub>2</sub>O (0.024 g, 0.18 mmol, 1.2 equiv), and EDC•HCl (0.034 g, 0.18 mmol, 1.2 equiv) afforded (S)-3-47 (62.2 mg, 0.0916 mmol, 62%) as a peach colored solid:  $[\alpha]_D^{25}$  -23.5 (*c* 0.1, CHCl<sub>3</sub>).



**(R)-3-53**

**4-[[[(3E,5R)-5-[[[(1,1-Dimethylethoxy)carbonyl]amino]-2,2-di(5-fluoropyridin-2-yl)-5-(4-fluorophenyl)-1-oxo-3-penten-1-yl]amino]-2,2,6,6-tetramethyl-1-piperidinyloxy ((R)-3-53)].** According to General Procedures G and H, (R)-3-52 (0.084 g, 0.14 mmol, 1 equiv), KOH (2.0 M in H<sub>2</sub>O, 0.35 mL, 0.70 mmol, 5.0 equiv), 4-AT (0.035 g, 0.29 mmol, 1.4 equiv), DMAP (0.020 g, 0.17 mmol, 1.2 equiv), HOBT•H<sub>2</sub>O (0.023 g, 0.17 mmol, 1.2 equiv), and EDC•HCl (0.032 g, 0.17 mmol, 1.2 equiv) afforded (R)-3-53 (61.9 mg, 0.0909 mmol, 65%) as a peach colored solid: Mp 79.5-81.7 °C; IR (ATR, neat) 3314, 2978, 2937, 1701, 1650, 1508, 1492, 1390, 1365, 1224, 1158, 1021, 835 cm<sup>-1</sup>;  $[\alpha]_D^{25}$  +41.7 (*c* 0.2, CHCl<sub>3</sub>); <sup>1</sup>H NMR (600 MHz, MeOD)  $\delta$  8.30 (dd, *J* = 5.3, 2.9 Hz, 2H), 7.57 (brd s, 1H), 7.44 (m, 2H), 7.36-7.32 (m, 2H), 7.15 (s, 1H), 7.10 (dd, *J* = 8.7, 5.3 Hz, 2H), 6.99 (t, *J* = 8.7 Hz, 2H), 5.65 (brd s, 2H), 5.03 (brd s, 1H), 4.09-4.05 (m, 1H), 3.28-3.26 (m, 4H), 1.64-1.62 (m, 2H), 1.42 (s, 9H), 1.38-1.34 (m, 2H), 1.17-1.15 (m, 12H); <sup>13</sup>C NMR (150 MHz, MeOD)  $\delta$  175.1, 164.2, 162.6, 160.9,

159.2, 157.5, 155.5, 138.6, 137.4, 137.3, 137.22, 137.16, 133.9, 133.2, 129.9, 127.85, 127.82, 127.78, 124.5, 124.44, 124.38, 124.3, 116.1, 116.0, 80.3, 60.0, 57.4, 54.3, 45.80, 45.75, 44.4, 44.0, 42.8, 32.7, 28.8, 20.3;  $^{19}\text{F}$  NMR (564 MHz, MeOD)  $\delta$  -117.51, -132.28 (2F); HRMS (LCMS ESI+)  $m/z$  calcd for  $\text{C}_{37}\text{H}_{45}\text{F}_3\text{N}_5\text{O}_4\text{Na}$  [M+Na] 703.3316, found 703.3312.



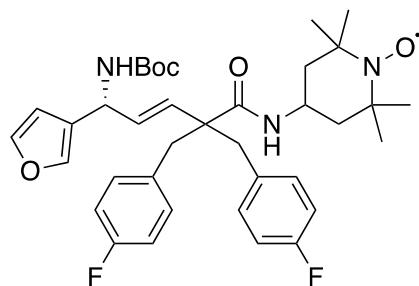
**(S)-3-56**

**4-[(3E,5S)-5-[(1,1-Dimethylethoxy)carbonyl]amino]-2,2-**

**di(4-fluorobenzyl)-5-(furan-3-yl)-1-oxo-3-penten-1-yl]amino]-2,2,6,6-tetramethyl-1-**

**piperidinyloxy ((S)-3-56).** According to General Procedures G and H, **(S)-3-55** (0.115 g, 0.225 mmol, 1 equiv), KOH (2.0 M in  $\text{H}_2\text{O}$ , 0.56 mL, 1.1 mmol, 5.0 equiv), 4-AT (0.057 g, 0.32 mmol, 1.4 equiv), DMAP (0.033 g, 0.27 mmol, 1.2 equiv), HOBT· $\text{H}_2\text{O}$  (0.037 g, 0.27 mmol, 1.2 equiv), and EDC·HCl (0.052 g, 0.27 mmol, 1.2 equiv) afforded **(S)-3-56** (81.0 mg, 0.124 mmol, 55%) as a peach colored solid: Mp 65.9-68.7 °C; IR (ATR, neat) 3329, 2977, 2934, 1698, 1649, 1511, 1365, 1221, 1159, 1018, 874, 846, 825, 780  $\text{cm}^{-1}$ ;  $[\alpha]_D^{25}$  +6.1 ( $c$  0.2,  $\text{CHCl}_3$ );  $^1\text{H}$  NMR (600 MHz, MeOD) 7.47 (s, 1H), 7.30 (s, 1H), 7.14 (ddd,  $J$  = 19.8, 6.0, 2.4 Hz, 4H), 7.06 (brd s, 1H), 6.90 (t,  $J$  = 8.4 Hz, 4H), 6.64 (d,  $J$  = 7.2 Hz, 1H), 6.34 (s, 1H), 5.76 (dd,  $J$  = 15.6, 6.0 Hz, 1H), 5.69 (d,  $J$  = 15.6 Hz, 1H), 5.06 (brd s, 1H), 4.02-4.00 (m, 1H), 3.24-3.16 (m, 2H), 2.93-2.87 (m, 2H), 1.54-1.48 (m, 1H), 1.43 (s, 9H), 1.30-1.23 (m, 3H), 1.16-1.10 (m, 12H);  $^{13}\text{C}$  NMR (150 MHz, MeOD)  $\delta$  175.2, 175.1, 163.93, 163.90, 162.32, 162.29, 157.6, 144.7, 140.7, 134.70, 134.68, 134.6, 133.40, 133.35, 132.1, 126.9, 115.6, 115.4, 110.5, 80.4, 60.0, 55.0, 50.7, 45.60, 45.58, 44.5, 43.6, 42.9, 42.8, 32.7, 28.9, 20.2;  $\delta$   $^{19}\text{F}$  NMR (564 MHz, MeOD)  $\delta$  -118.80, -118.89; HRMS (LCMS ESI+)  $m/z$  calcd for  $\text{C}_{37}\text{H}_{47}\text{F}_2\text{N}_3\text{O}_5$  [M+H] 652.3557, found 652.3540.



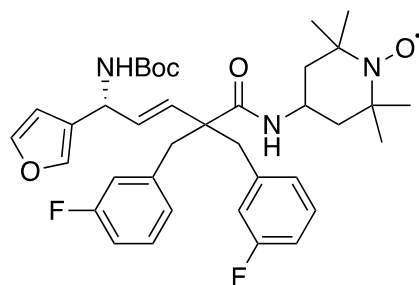


**(R)-3-56**

**4-[[[(3E,5R)-5-[[[(1,1-Dimethylethoxy)carbonyl]amino]-2,2-**

**di(4-fluorobenzyl)-5-(furan-3-yl)-1-oxo-3-penten-1-yl]amino]-2,2,6,6-tetramethyl-1-**

**piperidinyloxy ((R)-3-56).** According to General Procedures G and H, **(R)-3-55** (0.068 g, 0.13 mmol, 1 equiv), KOH (2.0 M in H<sub>2</sub>O, 0.33 mL, 0.66 mmol, 5.0 equiv), 4-AT (0.034 g, 0.19 mmol, 1.4 equiv), DMAP (0.019 g, 0.16 mmol, 1.2 equiv), HOBT•H<sub>2</sub>O (0.022 g, 0.16 mmol, 1.2 equiv), and EDC•HCl (0.031 g, 0.16 mmol, 1.2 equiv) afforded **(R)-3-56** (62.2 mg, 0.0956 mmol, 72%) as a peach colored solid:  $[\alpha]_D^{25}$  -7.0 (*c* 0.2, CHCl<sub>3</sub>).



**(R)-3-58**

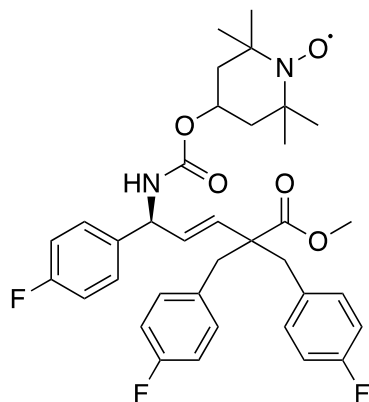
**4-[[[(3E,5R)-5-[[[(1,1-Dimethylethoxy)carbonyl]amino]-2,2-**

**di(3-fluorobenzyl)-5-(furan-3-yl)-1-oxo-3-penten-1-yl]amino]-2,2,6,6-tetramethyl-1-**

**piperidinyloxy ((R)-3-58).** According to General Procedures G and H, **(R)-3-55** (0.035 g, 0.068 mmol, 1 equiv), KOH (2.0 M in H<sub>2</sub>O, 0.17 mL, 0.34 mmol, 5.0 equiv), 4-AT (0.017 g, 0.096 mmol, 1.4 equiv), DMAP (0.010 g, 0.082 mmol, 1.2 equiv), HOBT•H<sub>2</sub>O (0.011 g, 0.082 mmol, 1.2 equiv), and EDC•HCl (0.016 g, 0.082 mmol, 1.2 equiv) afforded **(R)-3-58** (18.0 mg, 0.026 mmol, 38%) as a peach colored solid: Mp 52.7-54.6 °C; IR (ATR, neat) 3327, 2975, 2927, 1697, 1648, 1587, 1517, 1488, 1449, 1366, 1245, 1168, 1020, 874, 782, 693 cm<sup>-1</sup>;  $[\alpha]_D^{25}$  -6.6 (*c* 0.4, CHCl<sub>3</sub>); <sup>1</sup>H NMR (600 MHz, MeOD) δ 7.45 (s, 1H), 7.27 (s, 1H), 7.23-7.19 (m, 2H), 6.98 (d, *J* = 7.2 Hz, 1H), 6.94-6.88 (m, 6H), 6.79 (d, *J* = 7.8 Hz, 1H), 6.32 (s, 1H), 5.81 (dd, *J* = 16.2, 6.0 Hz, 1H), 5.71 (d, *J* = 16.2 Hz, 1H), 5.05 (brd s, 1H), 4.12-4.06 (m, 1H), 3.23 (app d, *J* = 13.2 Hz, 2H), 3.03-2.90 (m, 2H), 1.57-1.54 (m, 1H), 1.42 (s, 9H), 1.38-1.29 (m, 3H), 1.19-1.11 (m, 12H); <sup>13</sup>C NMR

(125 MHz, MeOD)  $\delta$  175.0, 164.9, 162.9, 157.6, 144.7, 141.6, 141.50, 141.46, 141.4, 140.7, 140.5, 134.6, 131.8, 130.6, 130.5, 130.3, 127.7, 118.4, 118.3, 118.19, 118.15, 114.34, 114.32, 114.17, 114.15, 110.5, 80.4, 60.7, 54.8, 50.7, 45.44, 45.40, 45.3, 44.3, 42.7, 32.4, 28.9, 20.3;  $^{19}\text{F}$  NMR (564 MHz, MeOD)  $\delta$  -115.76, -115.86; HRMS (LCMS ESI+)  $m/z$  calcd for  $\text{C}_{37}\text{H}_{47}\text{F}_2\text{N}_3\text{O}_5$  [M+H] 652.3557, found 652.3534.

**General procedure I.** For the preparation of allylic amine nitroxides. To a solution of 4-hydroxy-Tempo (0.015 g, 0.086 mmol, 1.2 equiv) or 4-AT (0.011 g, 0.062 mmol, 1 equiv) in DMF (300  $\mu\text{L}$ ) was added disuccinimidyl carbonate (0.026 g, 0.103 mmol, 1.4 equiv) and pyridine (0.001 mL, 0.017 mmol, 0.25 equiv). The mixture was heated at 40  $^\circ\text{C}$  for 14 h to give the Tempo-mixed carbonate, **3-48** or **3-59**. Separately, trifluoroacetic acid (0.129 mL, 1.72 mmol, 20 equiv) was added to a solution of Boc-protected (*S*)-**3-46** (0.170 g, 0.315 mmol, 1 equiv) or **983-35** (0.055 g, 0.086 mmol, 1 equiv) in  $\text{CH}_2\text{Cl}_2$  (1.2 mL) at 0  $^\circ\text{C}$ . The reaction was stirred 3 h until the starting carbamate was consumed, and the solvent and excess acid were evaporated. The material was dissolved in EtOAc and washed 3x with 10% aqueous  $\text{Na}_2\text{CO}_3$ . The combined aqueous layers were extracted with EtOAc (2 x 5 mL), and the combined organic layers were dried ( $\text{MgSO}_4$ ) and concentrated under reduced pressure. The Tempo-mixed carbonate or carbamate solution, **3-48** or **3-59**, was cooled to rt and transferred to a solution of the above amine and  $\text{K}_3\text{PO}_4$  (0.019 g, 0.086 mmol, 1.1 equiv) in DMF (0.7 mL) and water (80  $\mu\text{L}$ ). The mixture was stirred 17 h, then diluted with water (10 mL) and EtOAc (10 mL). The aqueous layer was extracted with EtOAc (3 x 10 mL). The combined organic layers were washed with 5% aqueous LiCl, dried ( $\text{MgSO}_4$ ), and concentrated under reduced pressure. The residue was purified by chromatography on  $\text{SiO}_2$  with gradient elution (4:1 to 1:1, hexanes:EtOAc) to afford the desired allylic amine nitroxide.

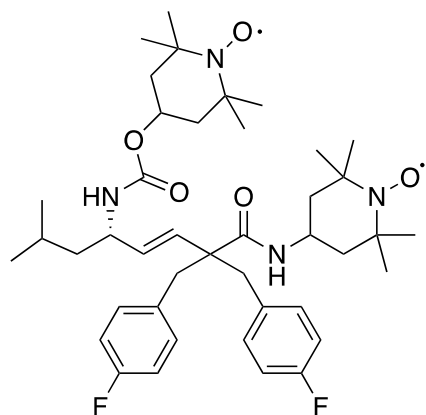


**(S)-3-49**

**Methyl (S,E)-2,2-di(4-fluorobenzyl)-5-(4-fluorophenyl)-5-(((1-**

**oxy-2,2,6,6-tetramethylpiperidin-4-yl)oxy)carbonyl)amino)pent-3-enoate ((S)-3-49).**

According to General Procedures I and H, (S)-3-46 (0.170 g, 0.315 mmol, 1 equiv), 4-hydroxy-Tempo (0.067 g, 0.38 mmol, 1.2 equiv), disuccinimidyl carbonate (0.113 g, 0.441 mmol, 1.4 equiv), pyridine (0.006 mL, 0.08 mmol, 0.25 equiv), TFA (0.47 mL, 6.3 mmol, 20 equiv), and K<sub>3</sub>PO<sub>4</sub> (0.076 g, 0.35 mmol, 1.1 equiv), afforded (S)-3-49 (96.3 mg, 0.151 mmol, 48%) as a peach colored solid: Mp 46.5-48.3 °C; IR (ATR, neat) 3313, 2933, 1719, 1603, 1508, 1449, 1342, 1219, 1177, 1158, 1100, 1047, 976, 836, 774, 739 cm<sup>-1</sup>; [ $\alpha$ ]<sub>D</sub><sup>25</sup> -6.9 (c 0.2, CHCl<sub>3</sub>); <sup>1</sup>H NMR (400 MHz, MeOD)  $\delta$  7.17-7.15 (m, 2H), 7.08-7.06 (m, 6H), 6.91-6.85 (m, 4H), 5.81 (d, *J* = 18.0 Hz, 1H) 5.74 (dd, *J* = 18.0, 6.0 Hz, 1H), 5.22 (d, *J* = 5.4 Hz, 1H), 4.94 (brd s, 1H), 3.63 (s, 3H), 3.22 (dd, *J* = 13.8, 3.6 Hz, 2H), 3.03 (d, *J* = 13.8 Hz, 1H), 2.95 (d, *J* = 13.8 Hz, 1H), 1.48-1.46 (m, 4H), 1.32-1.14 (m, 12H); <sup>13</sup>C NMR (150 MHz, MeOD)  $\delta$  175.8, 164.2, 163.9, 162.6, 162.3, 134.33, 134.31, 134.2, 133.2, 133.1, 133.0, 131.1, 130.2, 129.92, 129.88, 125.9, 125.8, 124.01, 123.99, 116.1, 116.0, 115.61, 115.57, 115.47, 115.42, 60.2, 57.8, 55.6, 52.2, 45.3, 44.7, 28.6; <sup>19</sup>F NMR (564 MHz, MeOD)  $\delta$  -64.09, -64.12, -64.14; HRMS (LCMS ESI+) *m/z* calcd for C<sub>36</sub>H<sub>41</sub>F<sub>3</sub>N<sub>2</sub>O<sub>5</sub> [M+H] 639.3047, found 639.3040.

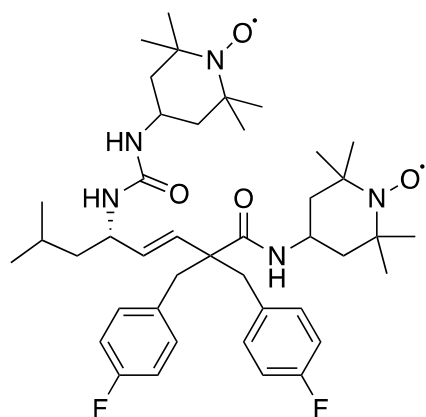


**(S)-3-60**

**(S,E)-N-(2,2,6,6-Tetramethyl-1-oxo-piperidin-4-yl)-2,2-di(4-**

**fluorobenzyl)-5-(2,2,6,6-tetramethyl-1-oxy-piperidin-4-yl)amino-7-methyloct-3-enamide**

**((S)-3-60).** According to General Procedures I and H, **983-35** (0.055 g, 0.086 mmol, 1 equiv), 4-hydroxy-Tempo (0.015 g, 0.086 mmol, 1 equiv), disuccinimidyl carbonate (0.026 g, 0.10 mmol, 1.2 equiv), pyridine (0.001 mL, 0.02 mmol, 0.2 equiv), TFA (0.13 mL, 1.7 mmol, 20 equiv), and K<sub>3</sub>PO<sub>4</sub> (0.019 g, 0.086 mmol, 1 equiv), afforded **(S)-3-60** (17.1 mg, 0.0231 mmol, 27%) as a peach colored solid: Mp 75.6-78.0 °C; IR (ATR, neat) 3328, 2932, 2867, 1703, 1651, 1604, 1512, 1463, 1364, 1314, 1221, 118, 1159, 1018, 992, 848, 825, 780 cm<sup>-1</sup>; [ $\alpha$ ]<sub>D</sub><sup>25</sup> +4.8 (*c* 0.3, CHCl<sub>3</sub>); <sup>1</sup>H NMR (400 MHz, MeOD)  $\delta$  7.16 (brd s, 4H), 6.94-6.91 (m, 4H), 6.42 (brd s, 1H), 5.59 (d, *J* = 14.4 Hz, 1H), 5.50 (dt, *J* = 14.4, 5.6 Hz, 1H), 4.86 (brd s, 1H), 4.01 (s, 2H), 3.26-3.14 (m, 2H), 2.93 (dd, *J* = 14.0, 4.8 Hz, 1H), 2.84 (d, *J* = 14.4 Hz, 1H), 1.84-1.81 (m, 2H), 1.54-1.48 (m, 2H), 1.29 (brd s, 8H), 1.18-1.16 (m, 16H), 1.12-1.10 (m, 6H), 0.93-0.90 (m, 9H); <sup>19</sup>F NMR (376 MHz, MeOD)  $\delta$  -118.81, -118.84; HRMS (LCMS ESI+) *m/z* calcd for C<sub>42</sub>H<sub>60</sub>F<sub>2</sub>N<sub>4</sub>O<sub>5</sub> [M+Na] 761.4424, found 761.4427.



**(S)-3-61**

**(S,E)-N-(2,2,6,6-Tetramethyl-1-oxo-piperidin-4-yl)-2,2-**

**di(4-fluorobenzyl)-5-(3-(2,2,6,6-tetramethyl-1-oxo-piperidin-4-yl)ureido)-7-methyloct-3-enamide ((S)-3-61).** According to General Procedure I, **983-35** (0.040 g, 0.062 mmol, 1 equiv), 4-AT (0.011 g, 0.062 mmol, 1 equiv), disuccinimidyl carbonate (0.019 g, 0.075 mmol, 1.2 equiv), pyridine (0.001 mL, 0.01 mmol, 0.2 equiv), TFA (0.094 mL, 1.3 mmol, 20 equiv), and K<sub>3</sub>PO<sub>4</sub> (0.014 g, 0.062 mmol, 1 equiv), afforded **(S)-3-61** (15.6 mg, 0.021 mmol, 34%) as a peach colored solid: Mp 102.1-105.5 °C; IR (ATR, neat) 3375, 2932, 2870, 1653, 1536, 1505, 1464, 1364, 1303, 1221, 1178, 1158, 1017, 988, 843, 825, 778 cm<sup>-1</sup>; [ $\alpha$ ]<sub>D</sub><sup>25</sup> +8.8 (*c* 0.4, CHCl<sub>3</sub>); HRMS (LCMS ESI+) *m/z* calcd for C<sub>42</sub>H<sub>62</sub>F<sub>2</sub>N<sub>5</sub>O<sub>4</sub> [M+H] 739.4843, found 739.4837.

## 4.0 Appendix A

$^1\text{H}$  NMR,  $^{13}\text{C}$  NMR, and  $^{19}\text{F}$  spectra for compounds **1-6B**, **1-10**, **2-5**, and representative JP4-039 analog sequence originating from sulfone **3-37** and final nitroxide compounds.

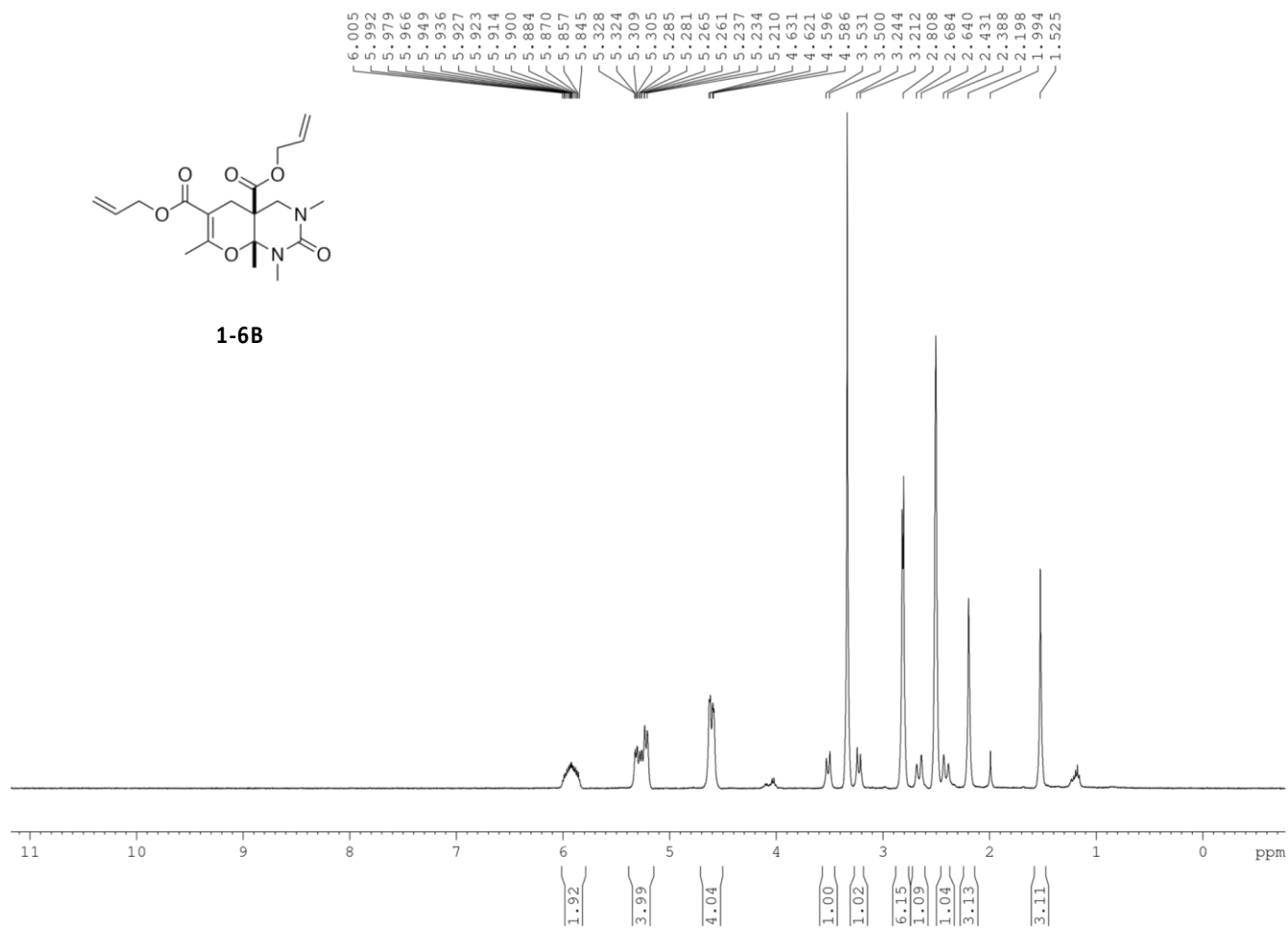


**Figure 4-1 Representative five-component condensation product <sup>1</sup>H spectra (1-6B)**

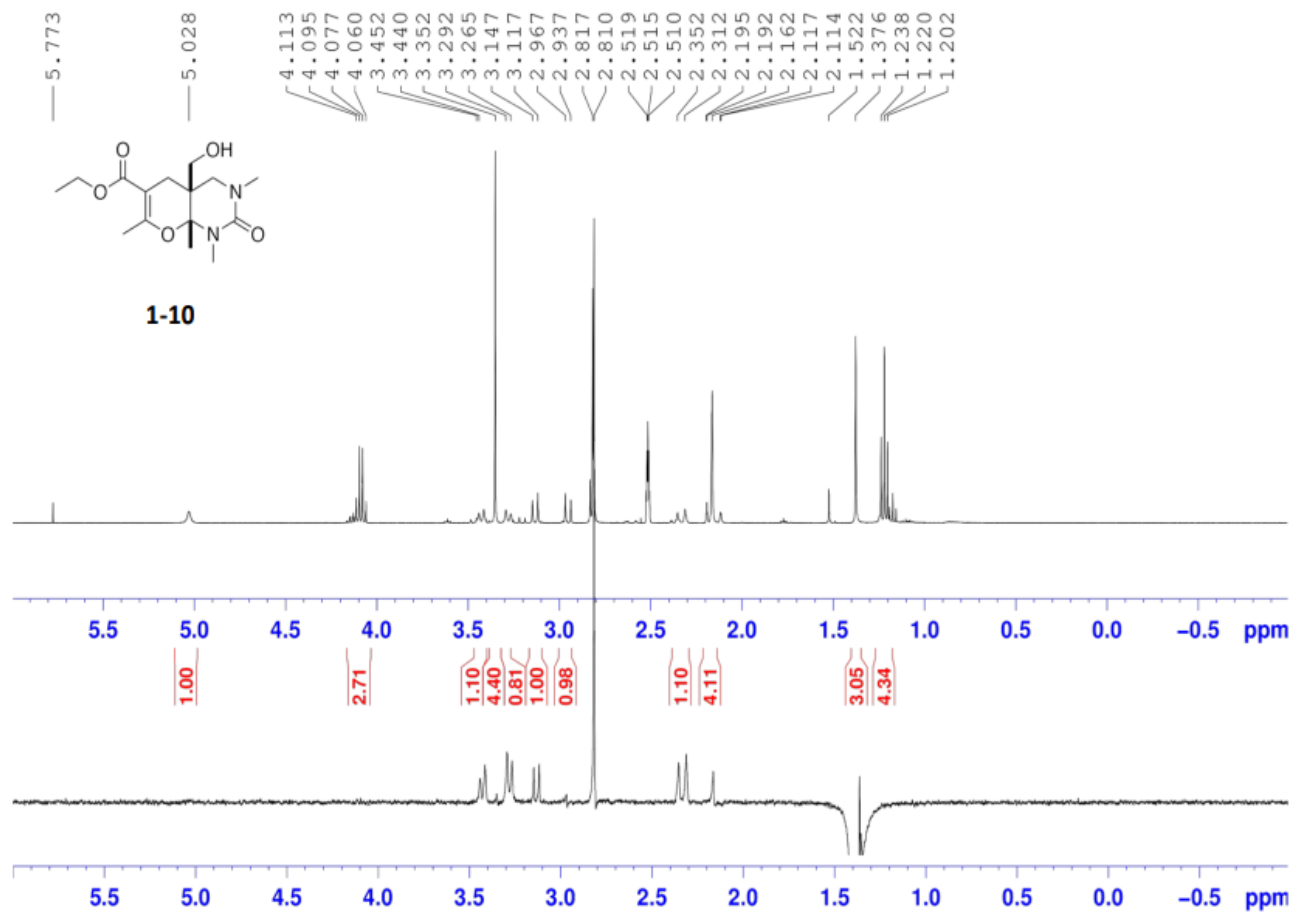


Figure 4-2 Structural confirmation of five-component condensation product by NOE analysis of 1-10



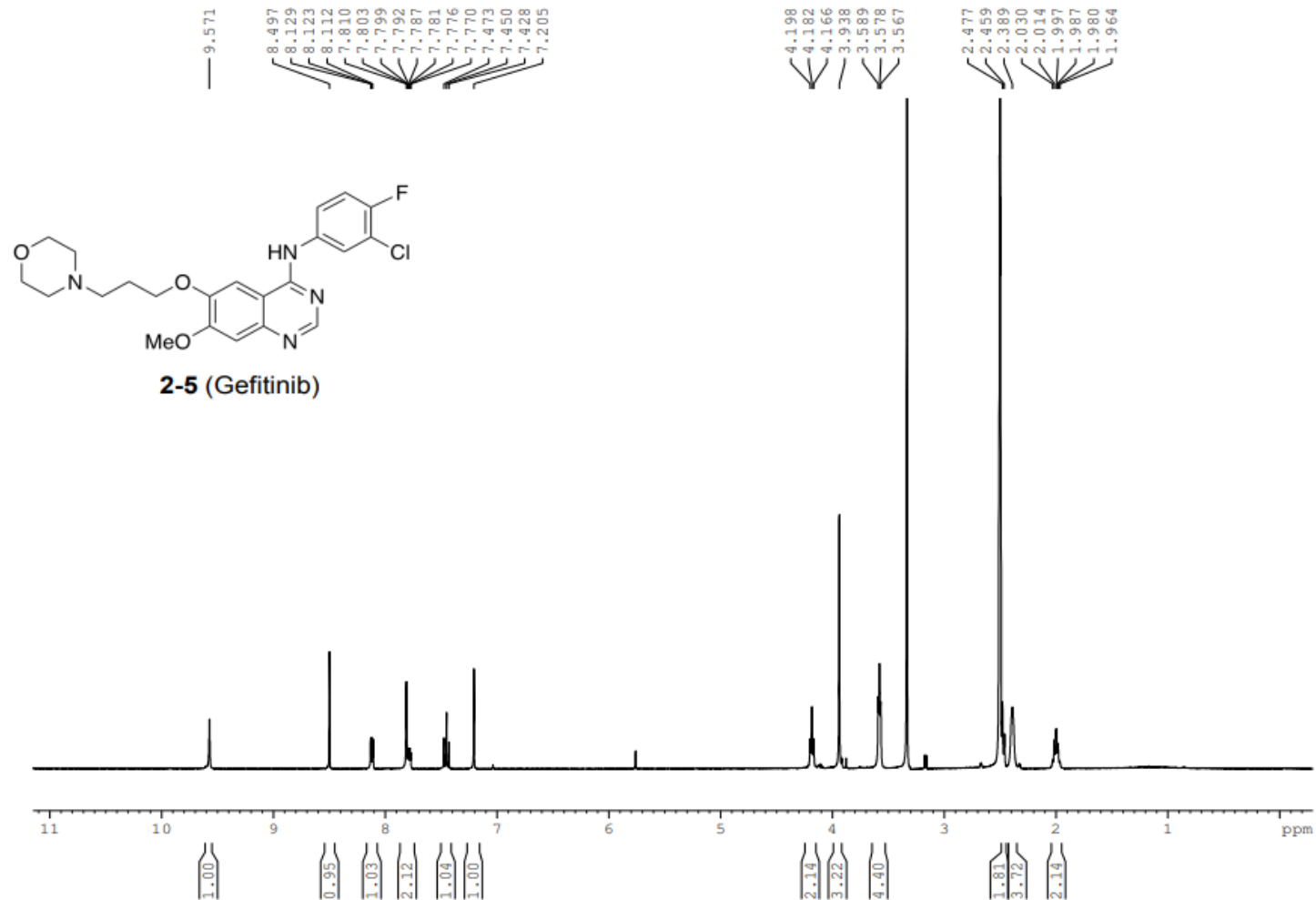


Figure 4-3  $^1\text{H}$  NMR spectra of Gefitinib (2-5) synthesized on pilot-plant scale

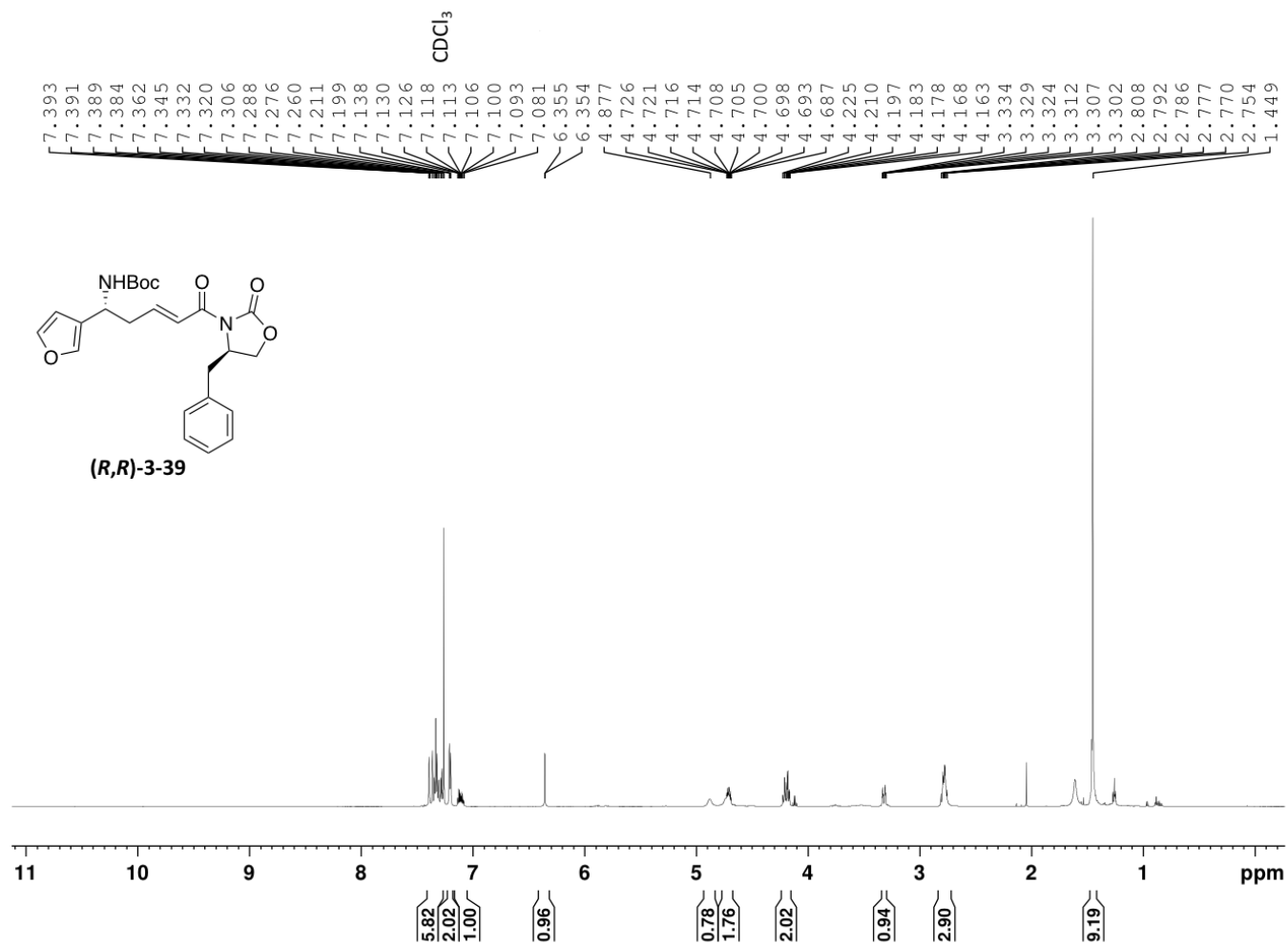


Figure 4-4  $^1\text{H}$  NMR spectra of vinylogous Mannich product (*R,R*)-3-39

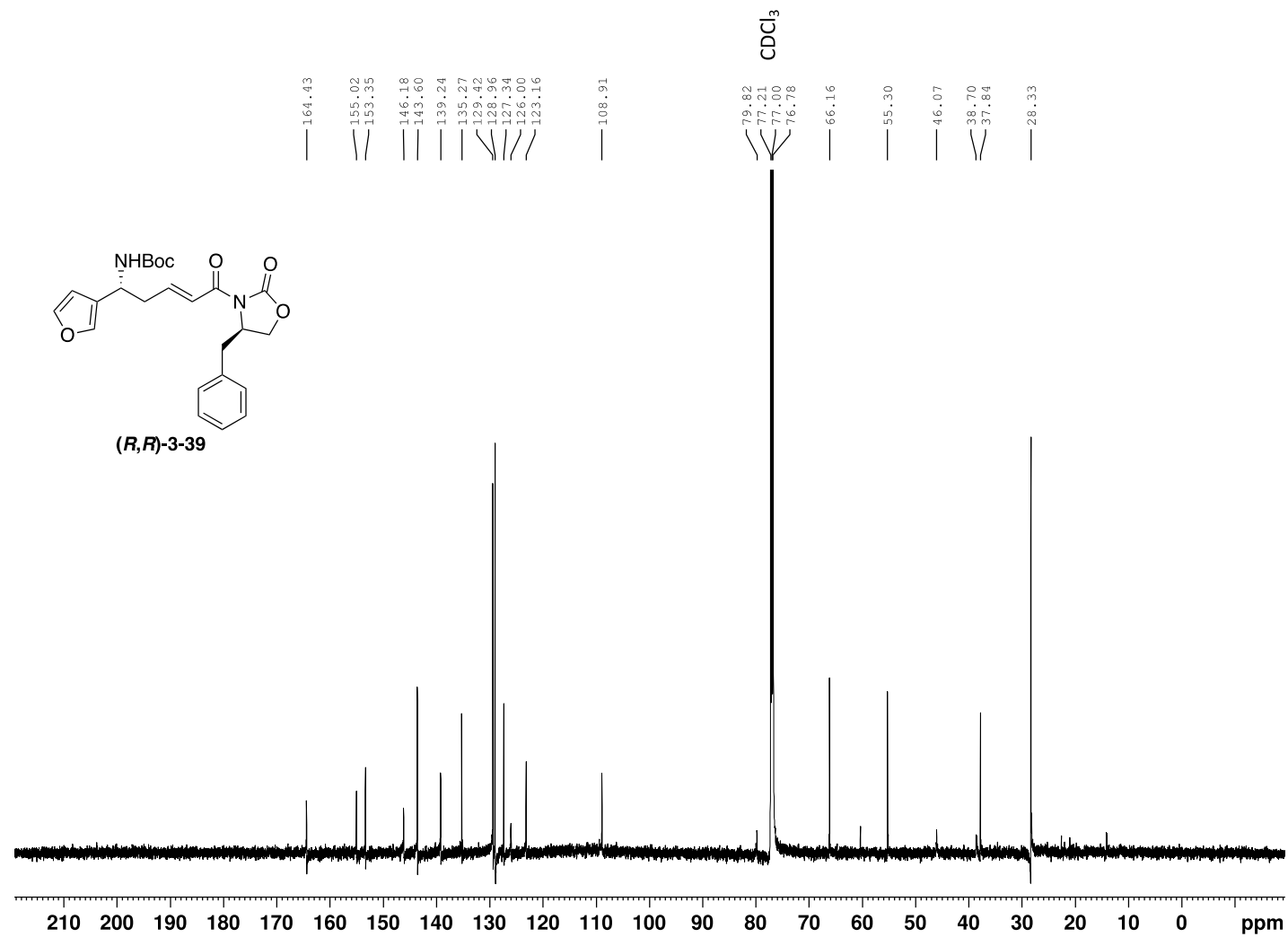


Figure 4-5  $^{13}\text{C}$  NMR spectra of vinylogous Mannich product **(R,R)-3-39**

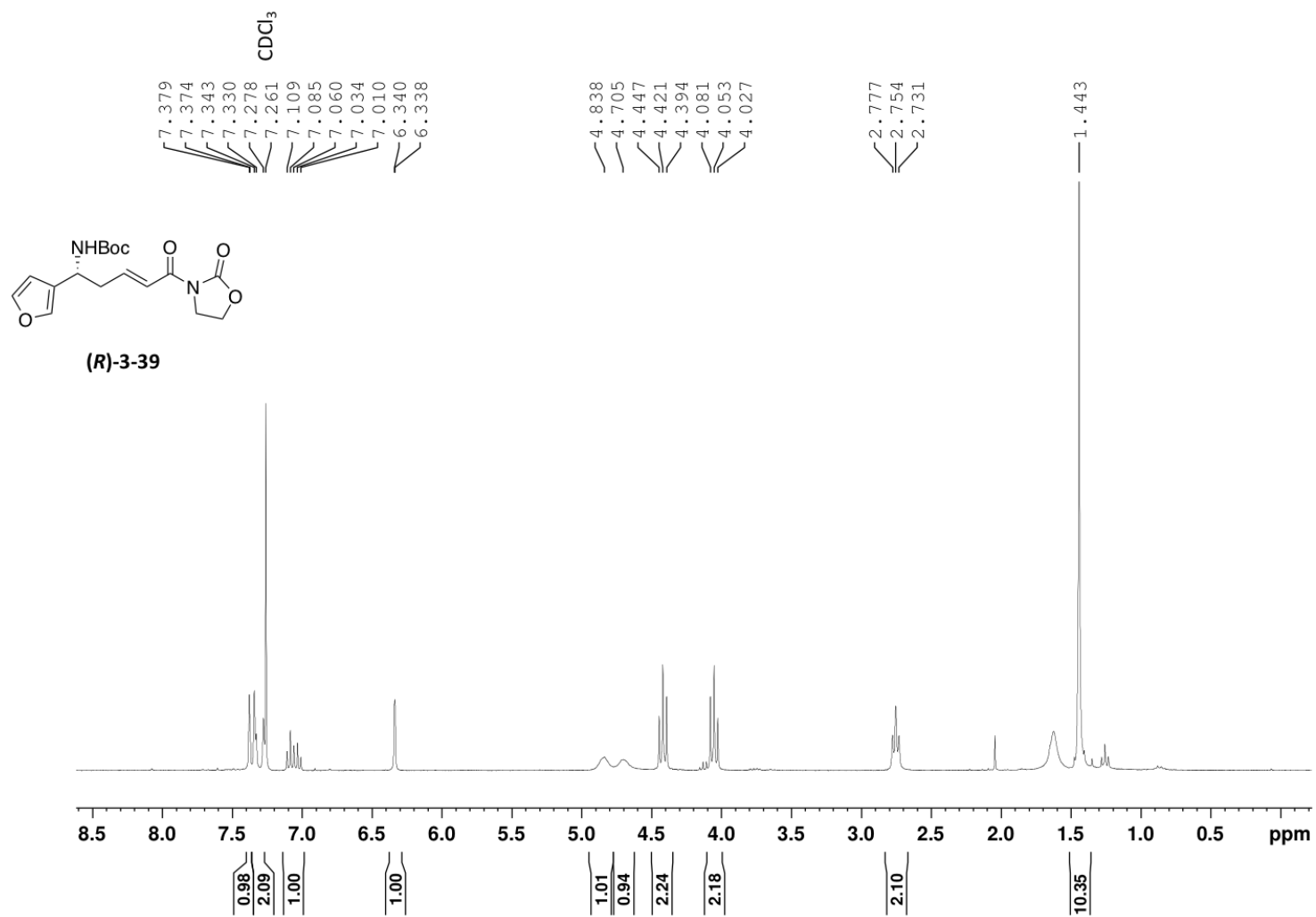


Figure 4-6  $^1\text{H}$  NMR spectra of vinylogous Mannich product (R)-3-39

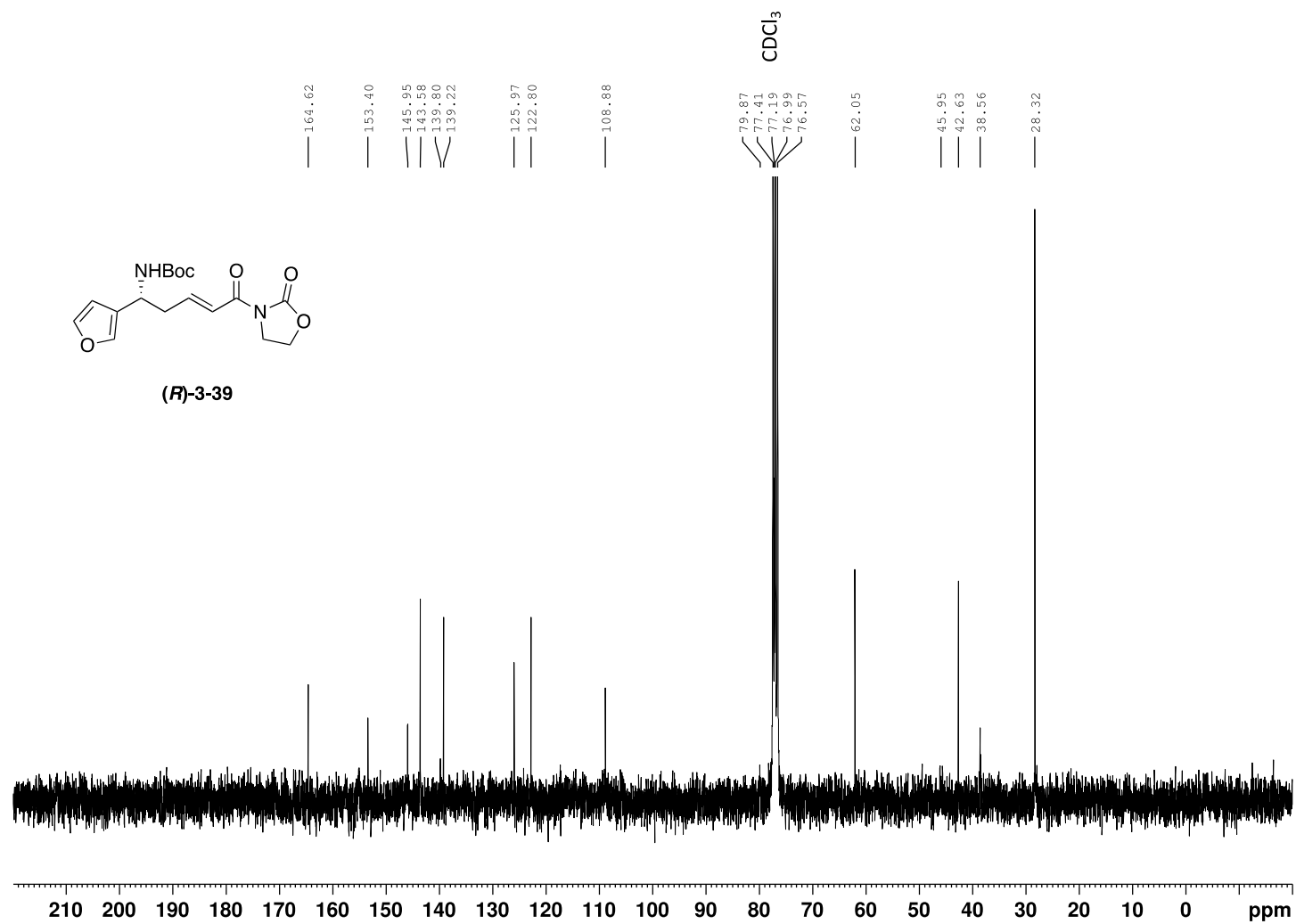


Figure 4-7  $^{13}\text{C}$  NMR spectra of vinylogous Mannich product (R)-3-39

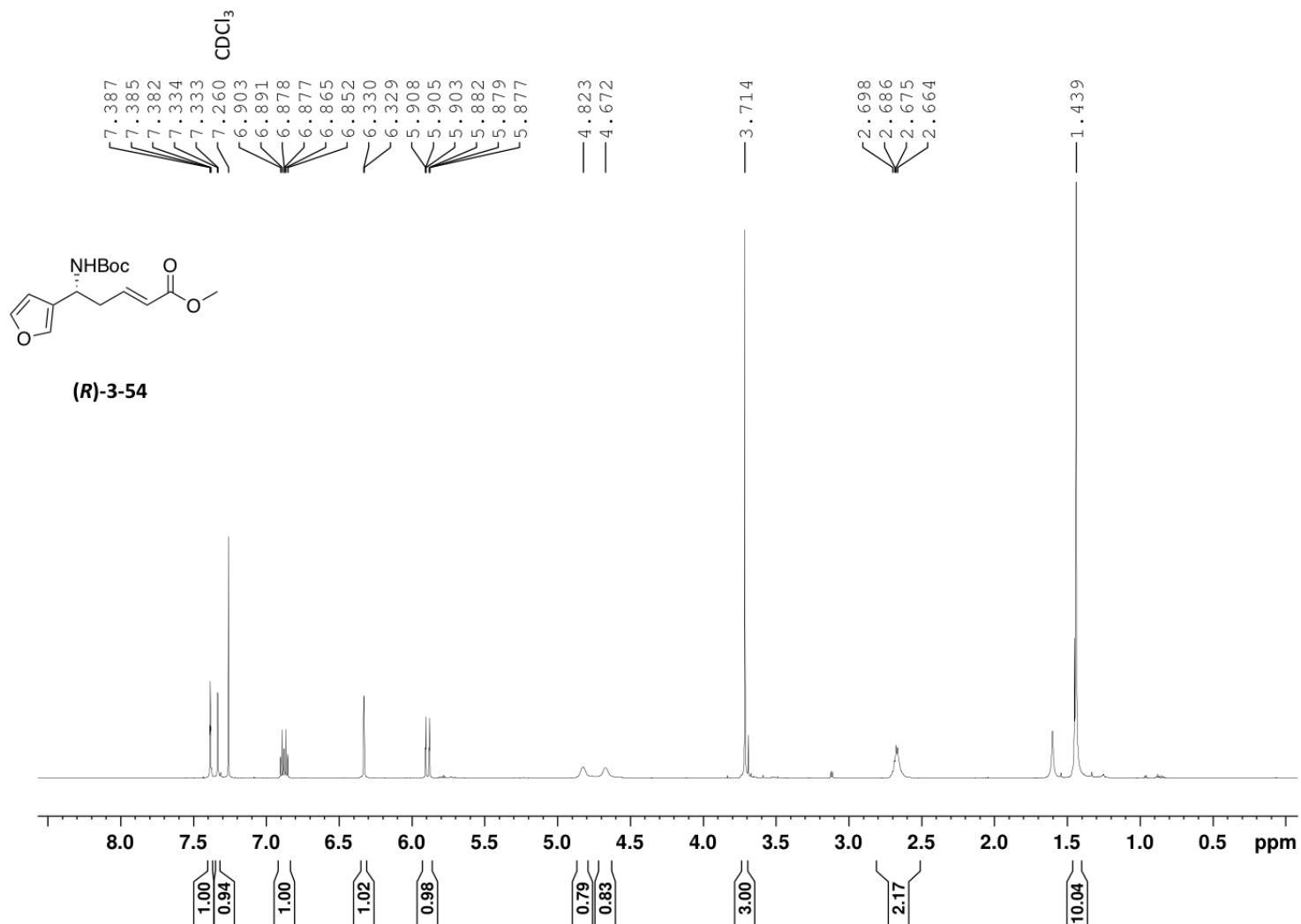


Figure 4-8 <sup>1</sup>H NMR spectra of ester (*R*)-3-54

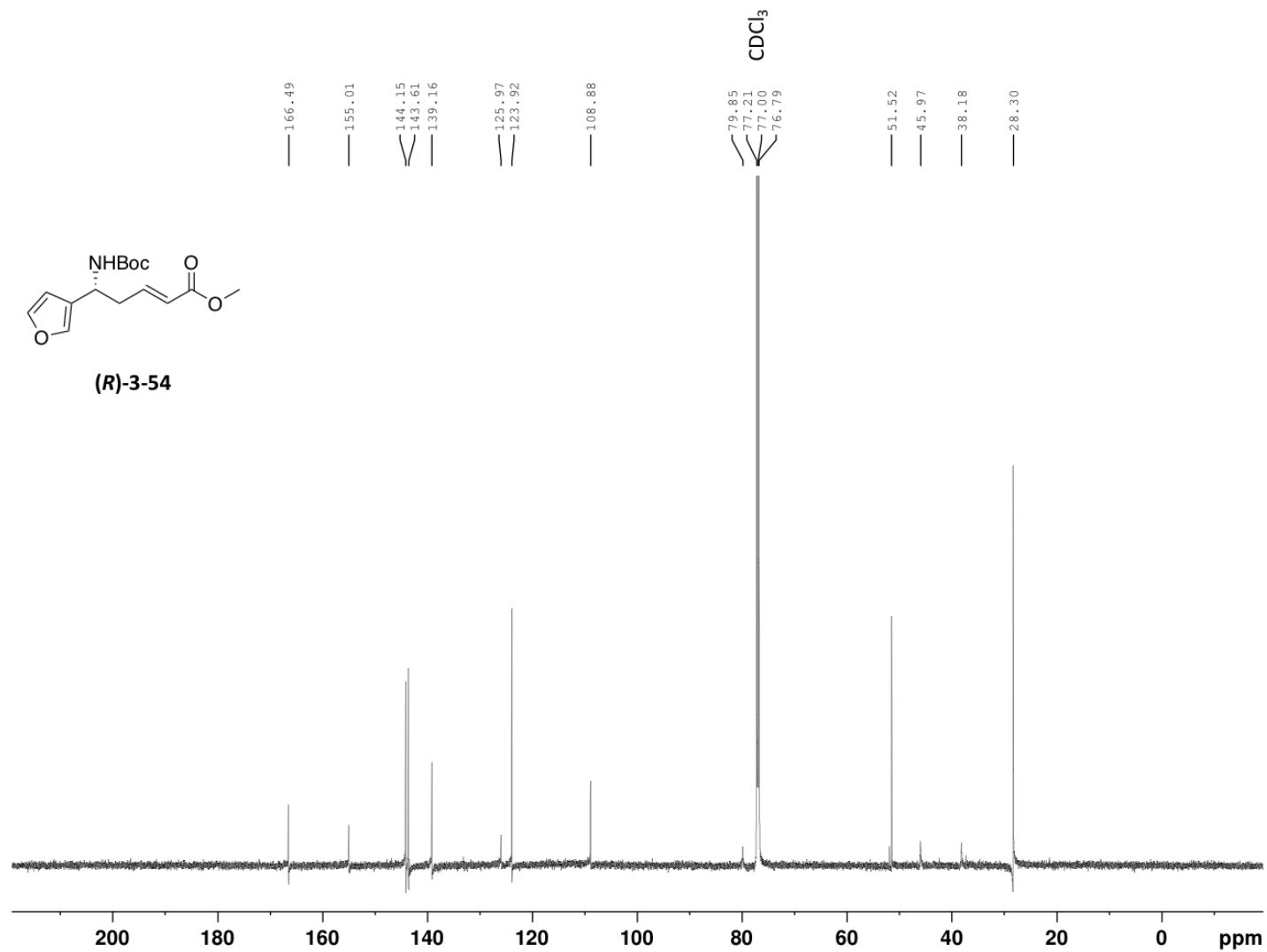
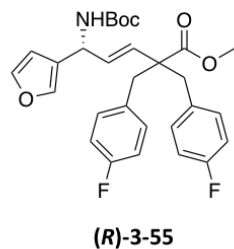


Figure 4-9 <sup>13</sup>C NMR spectra of ester (*R*)-3-54



185



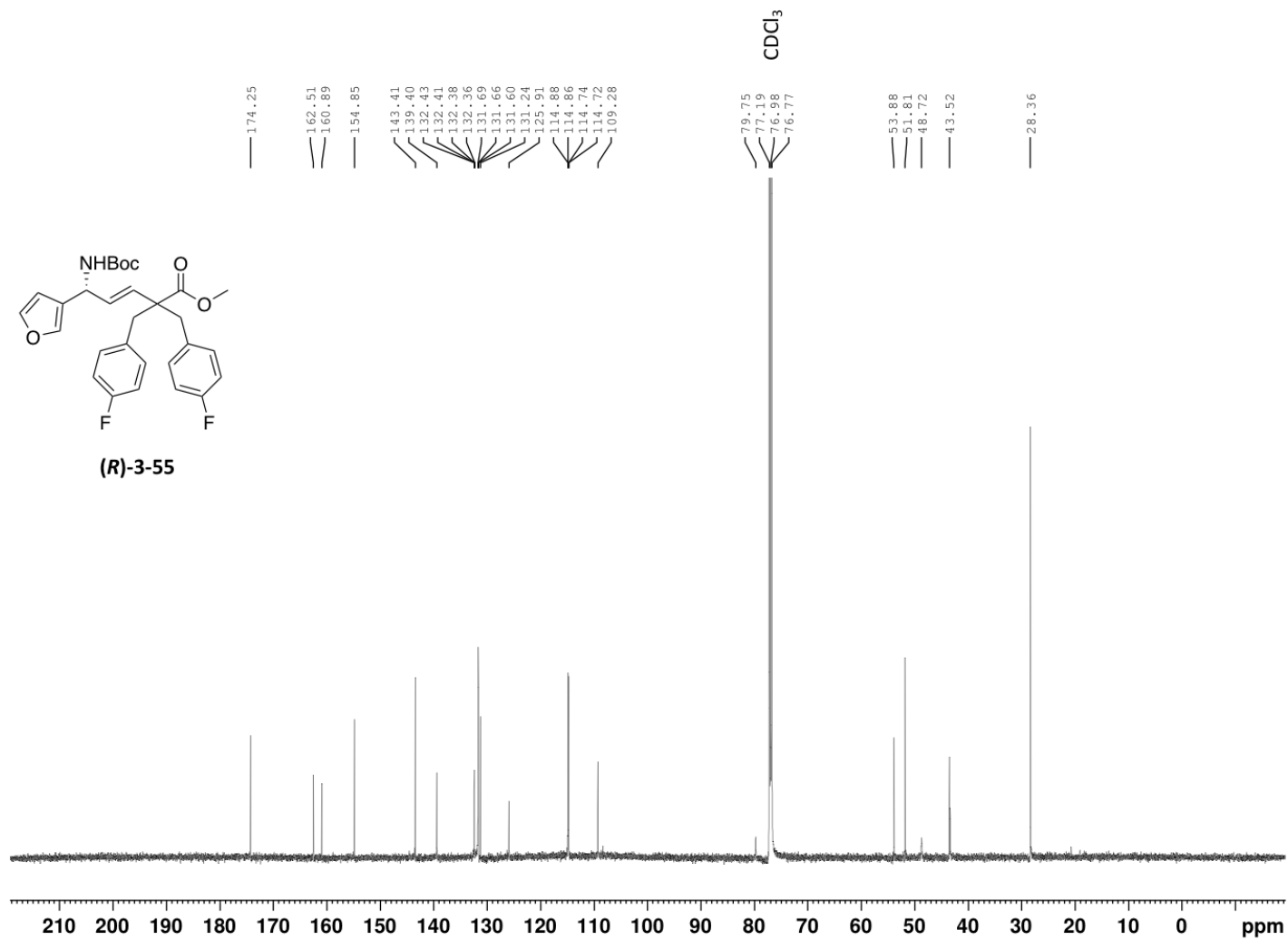


Figure 4-11  $^{13}\text{C}$  NMR spectra of bis-alkylated ester (*R*)-3-55

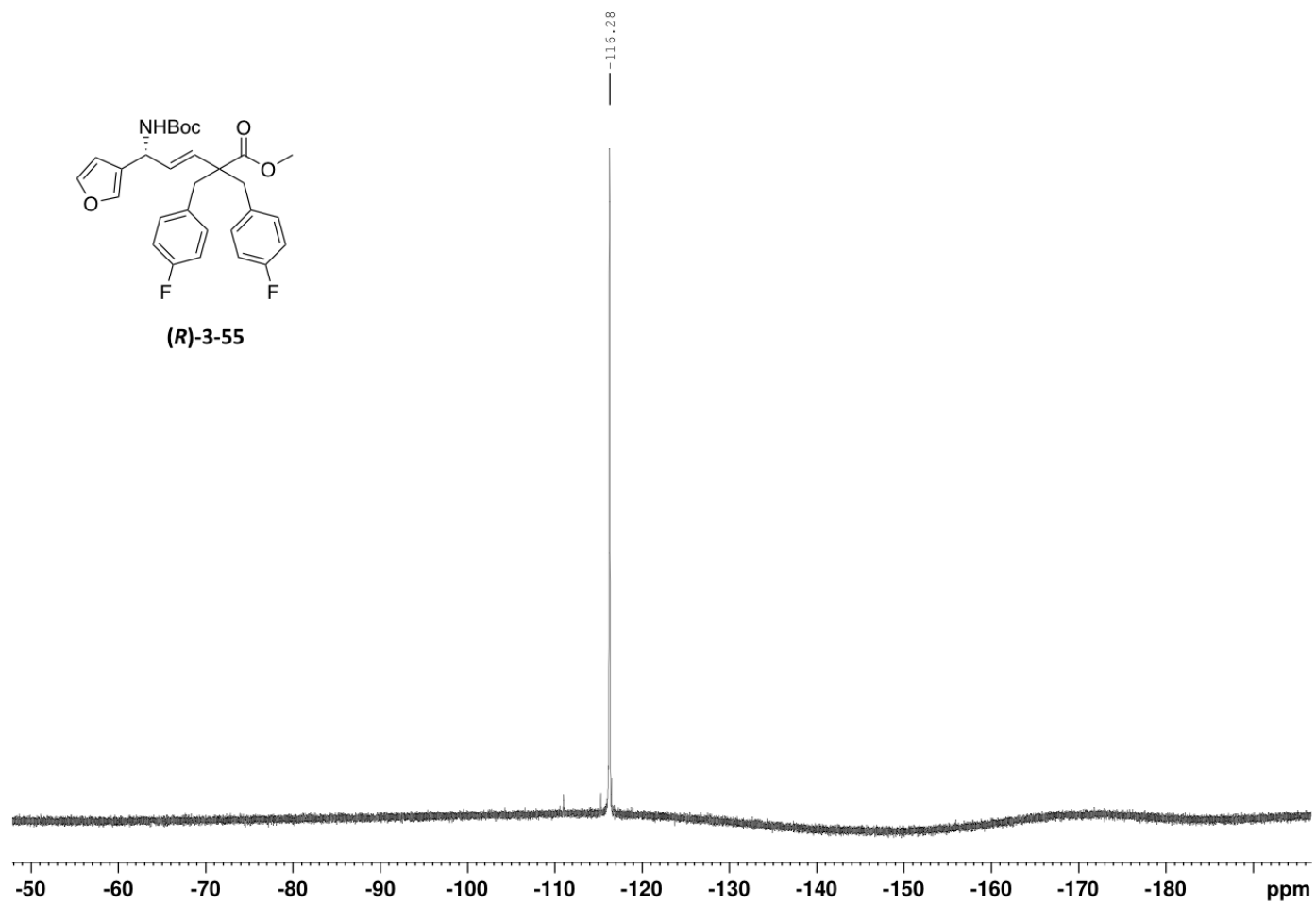


Figure 4-12  $^{19}\text{F}$  NMR spectra of bis-alkylated ester **(R)-3-55**

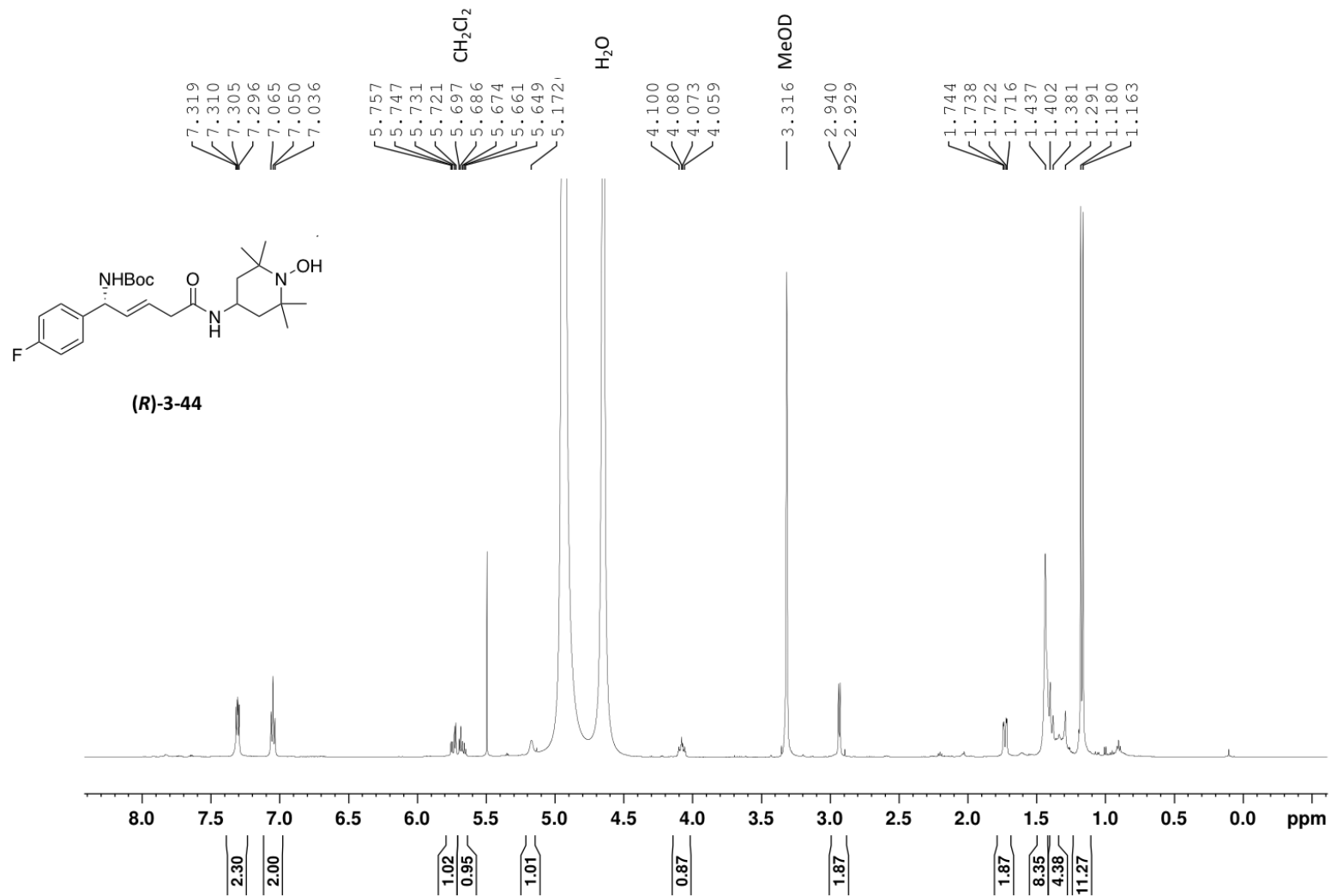


Figure 4-13 <sup>1</sup>H NMR spectra of nitroxide analog (*R*)-3-44

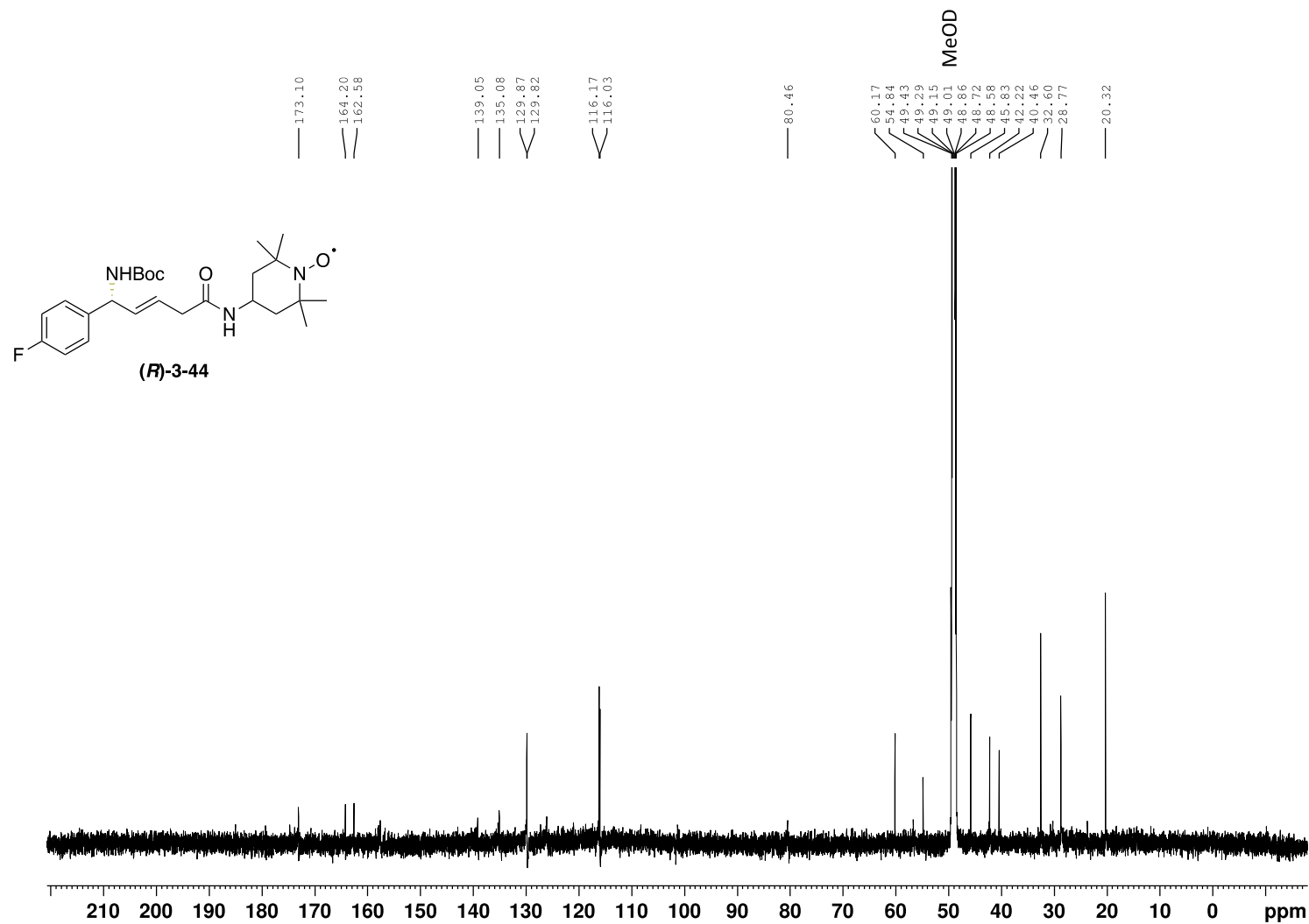
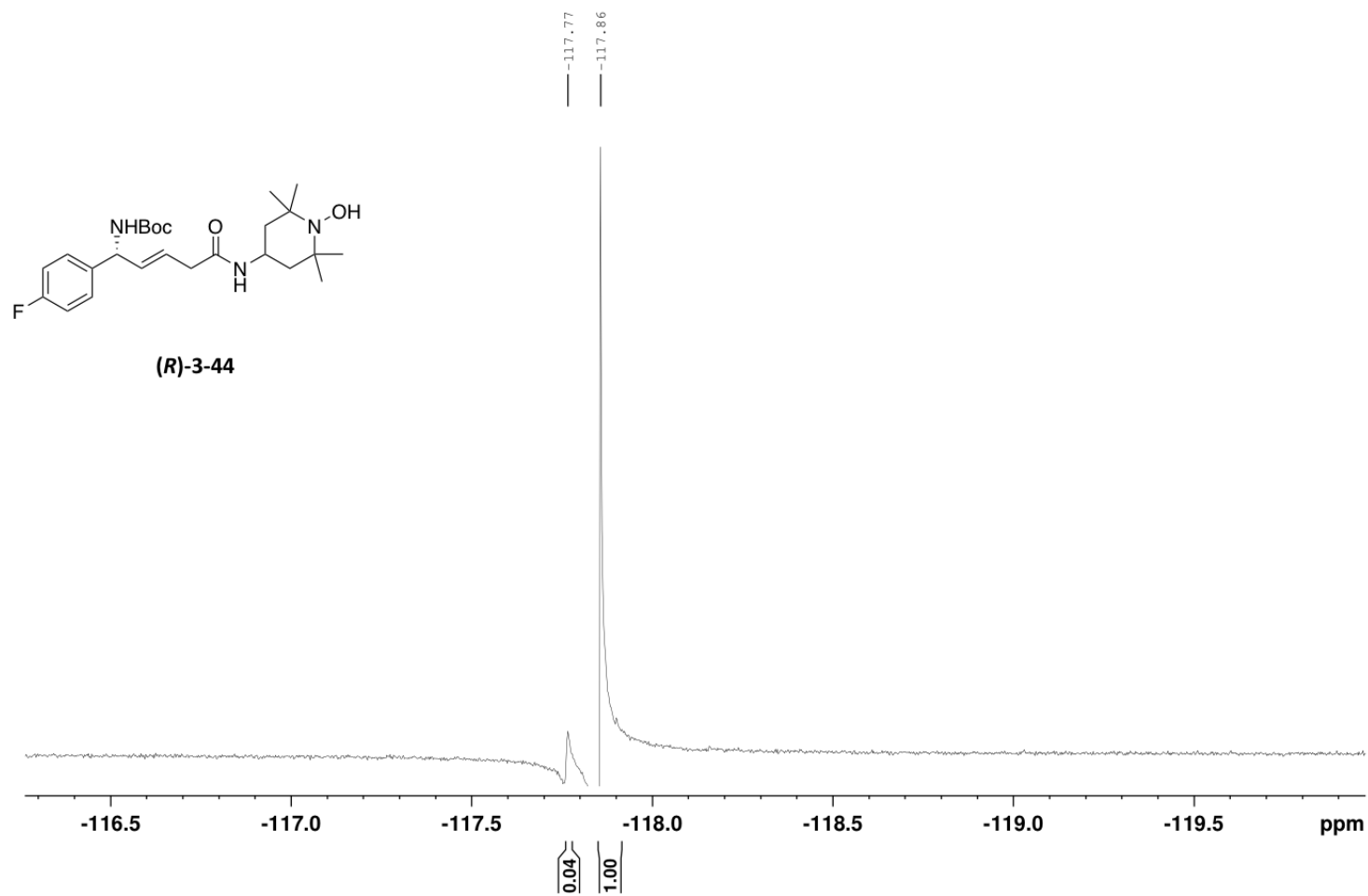


Figure 4-14 <sup>13</sup>C NMR spectra of nitroxide analog (*R*)-3-44



**Figure 4-15**  $^{19}\text{F}$  NMR spectra of nitroxide analog **(R)-3-44**

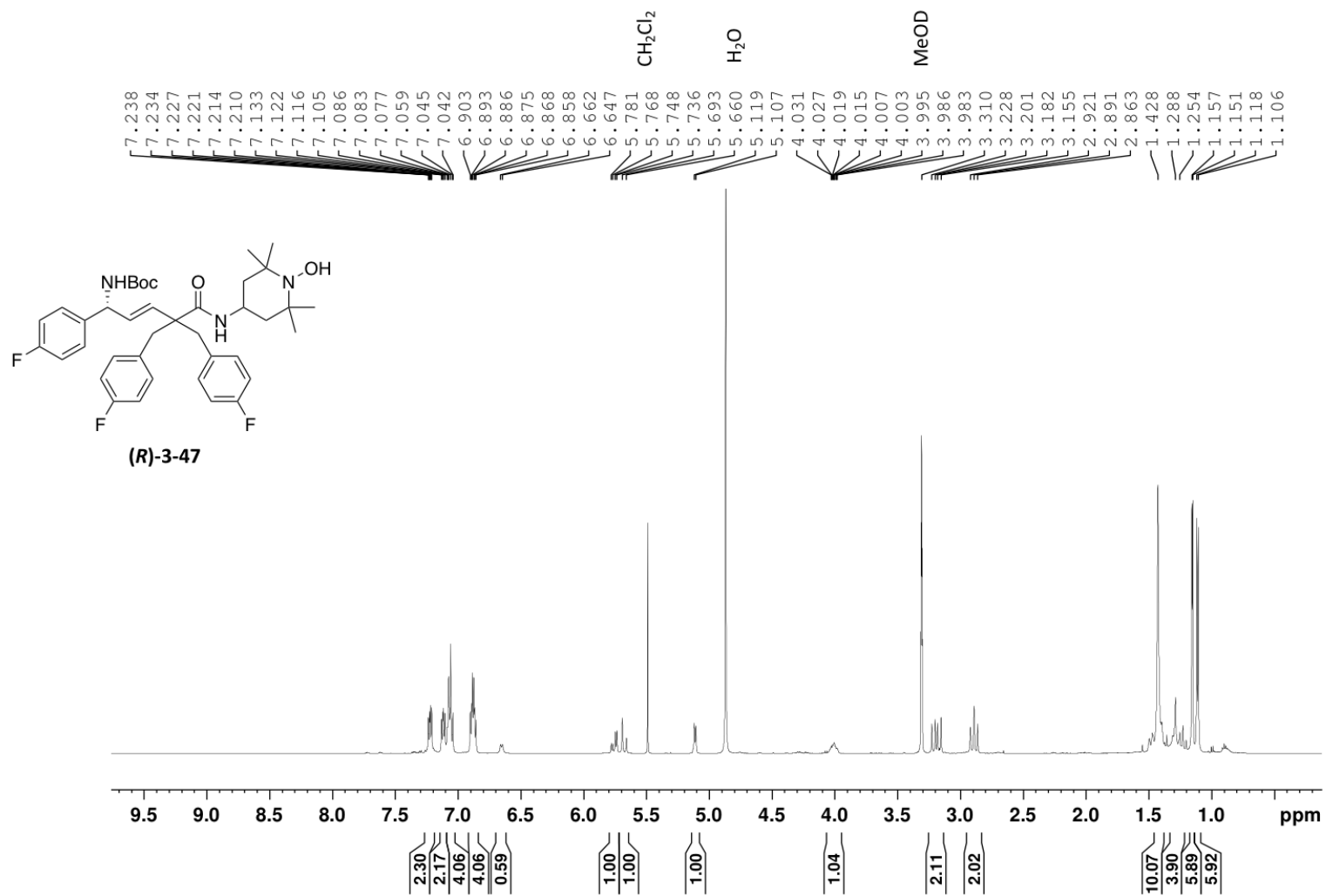


Figure 4-16 <sup>1</sup>H NMR spectra of nitroxide analog (*R*)-3-47

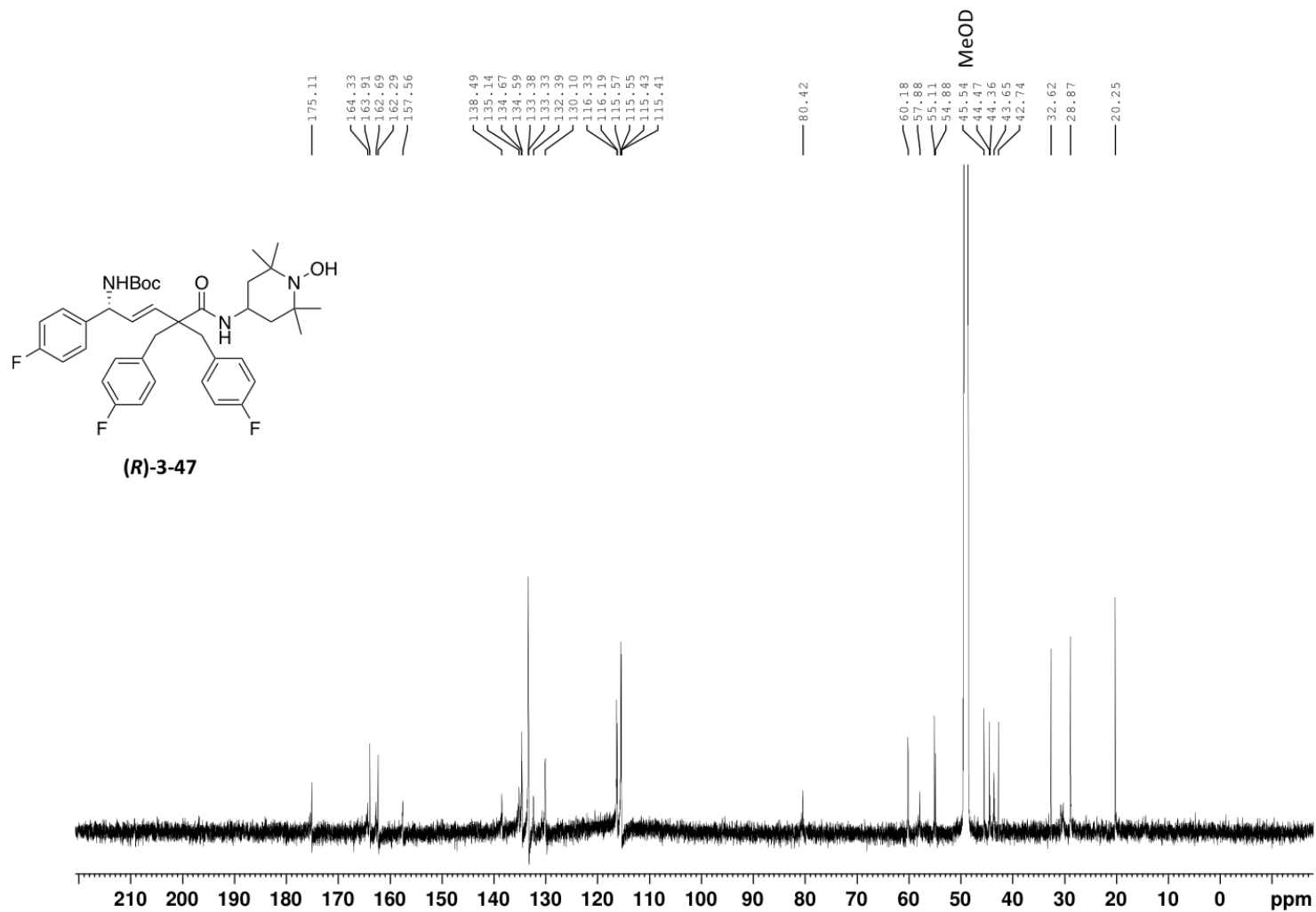


Figure 4-17  $^{13}\text{C}$  NMR spectra of nitroxide analog (R)-3-47





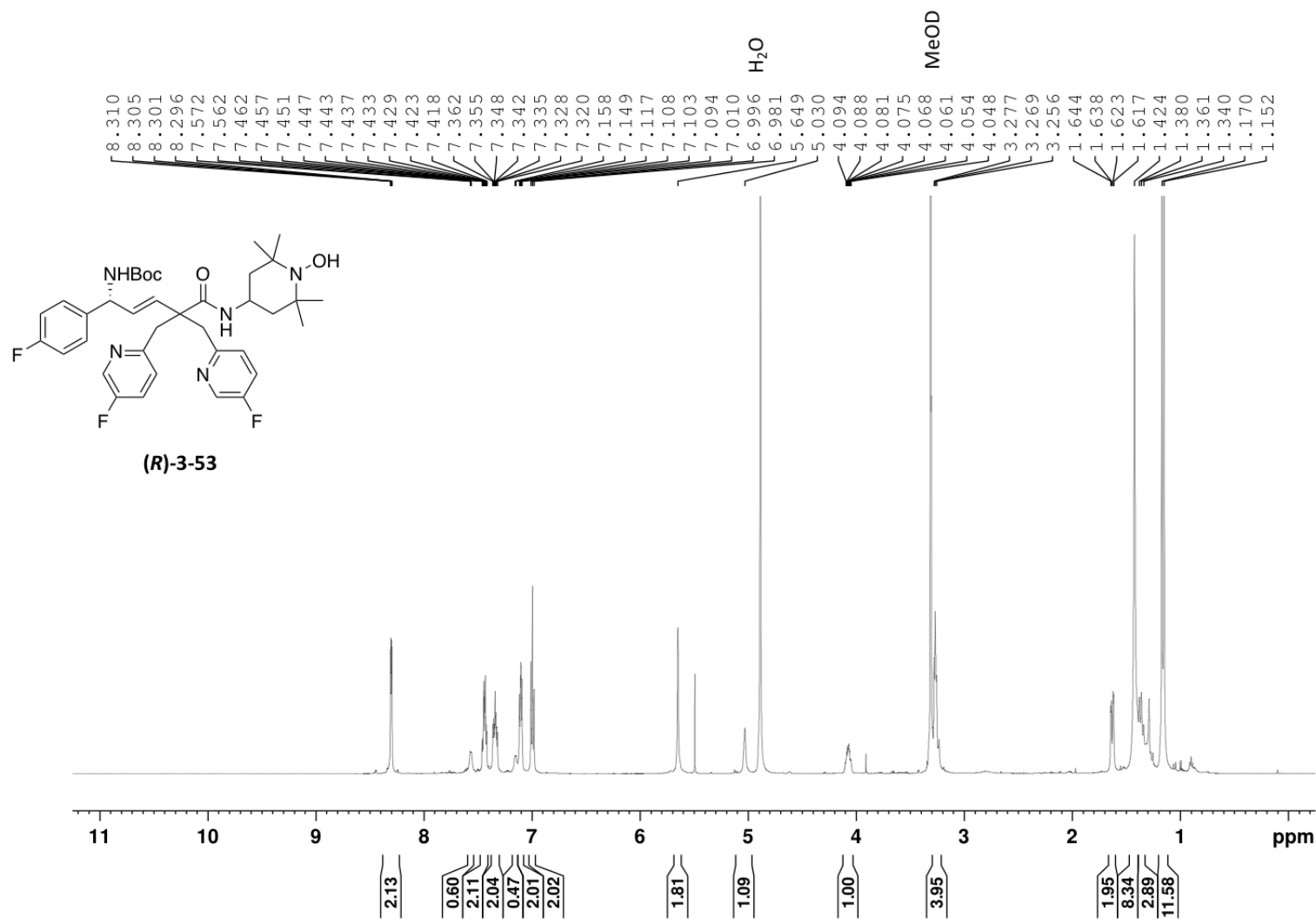


Figure 4-19 <sup>1</sup>H NMR spectra of nitroxide analog (*R*)-3-53

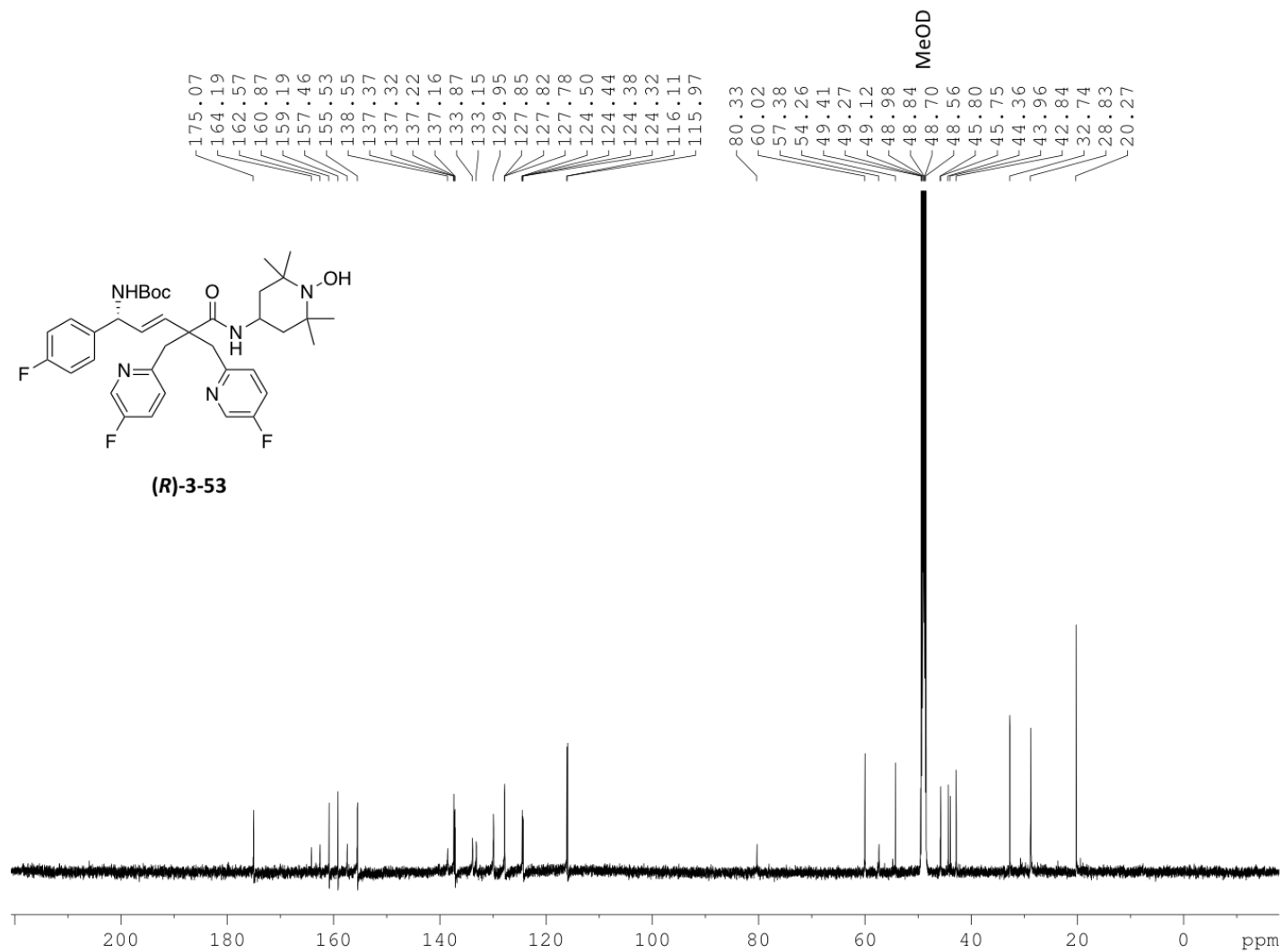


Figure 4-20  $^{13}\text{C}$  NMR spectra of nitroxide analog **(R)-3-53**

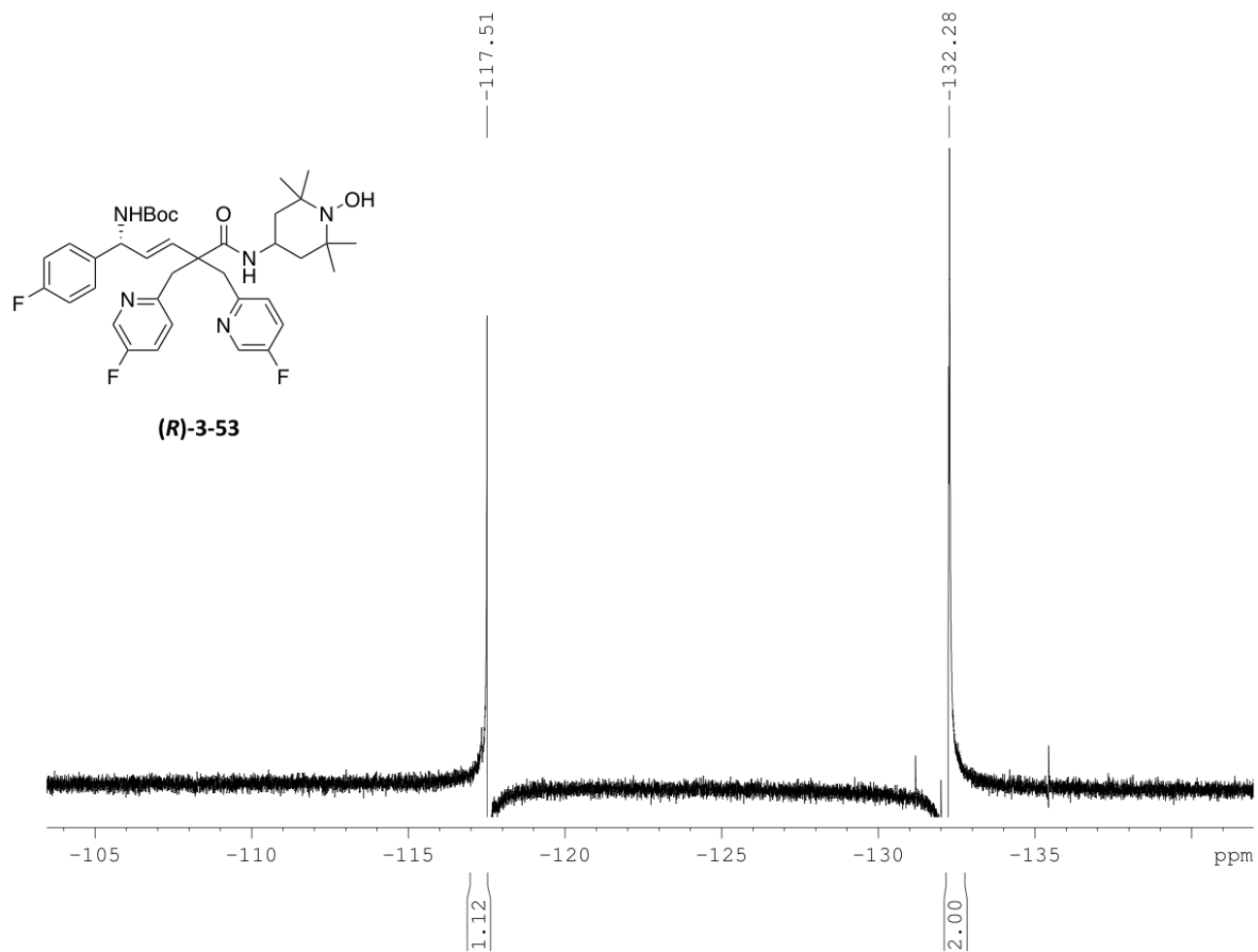


Figure 4-21  $^{19}\text{F}$  NMR spectra of nitroxide analog (*R*)-3-53

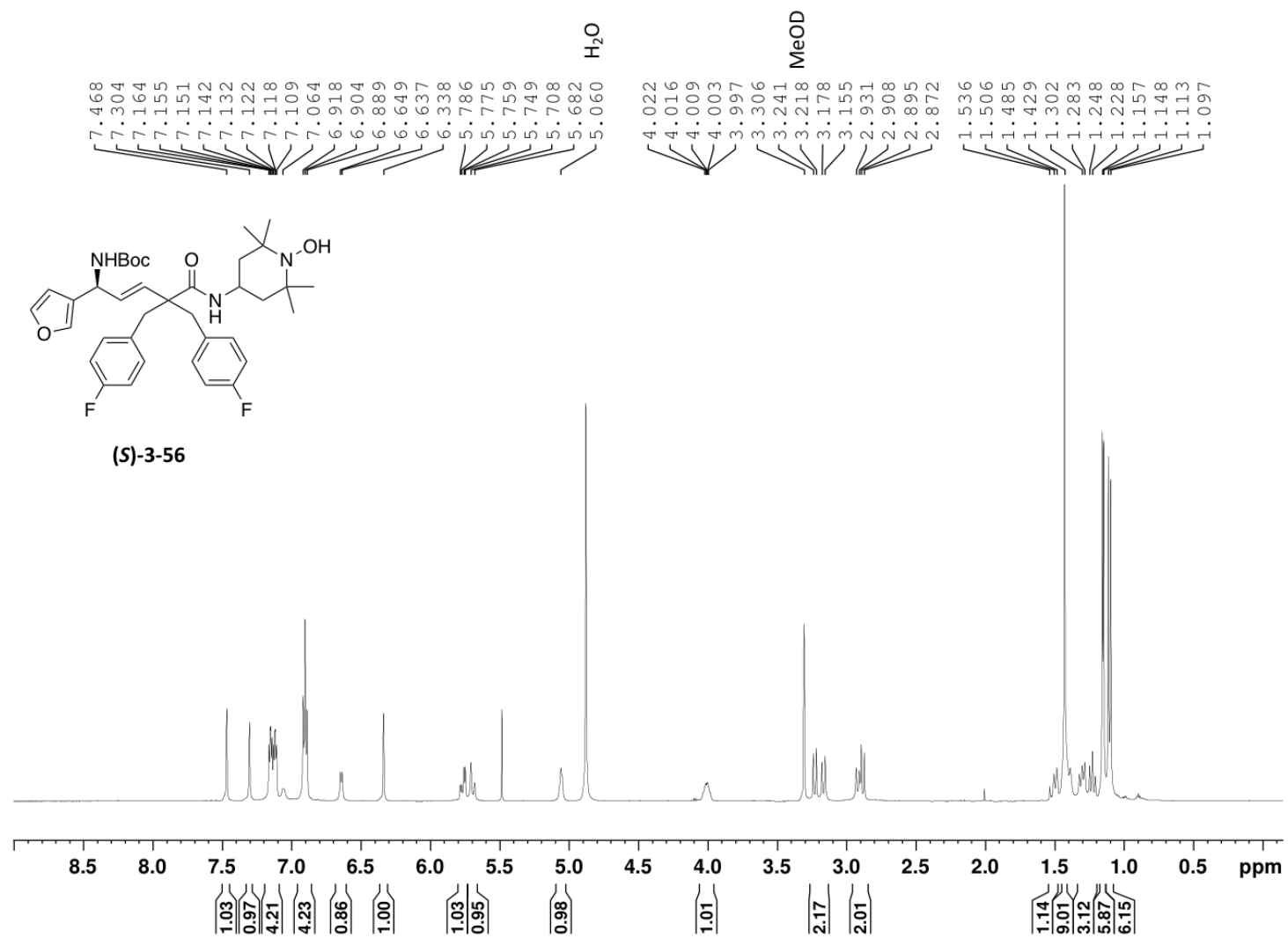


Figure 4-22 <sup>1</sup>H NMR spectra of nitroxide analog (S)-3-56

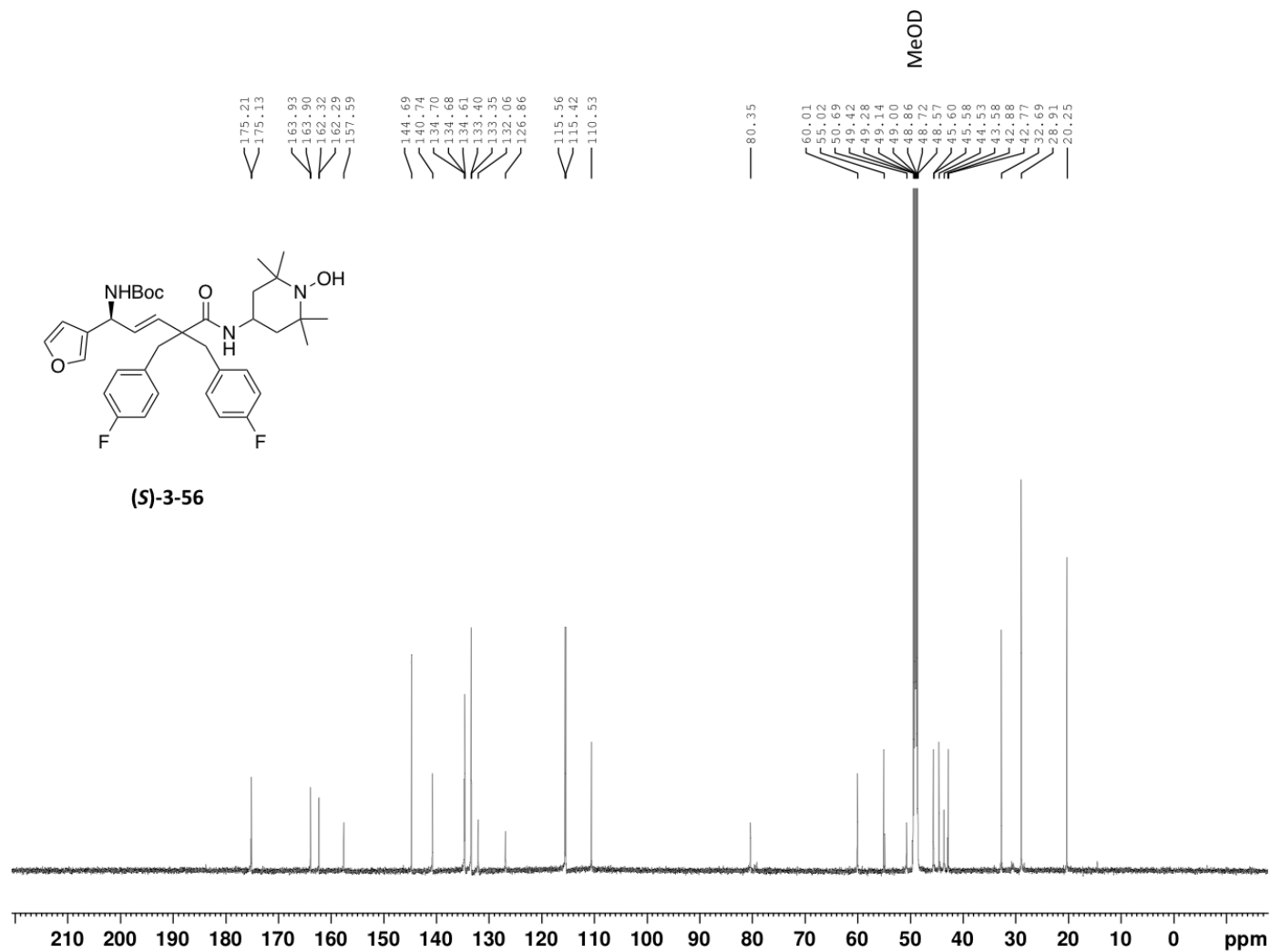


Figure 4-23  $^{13}\text{C}$  NMR spectra of nitroxide analog (S)-3-56

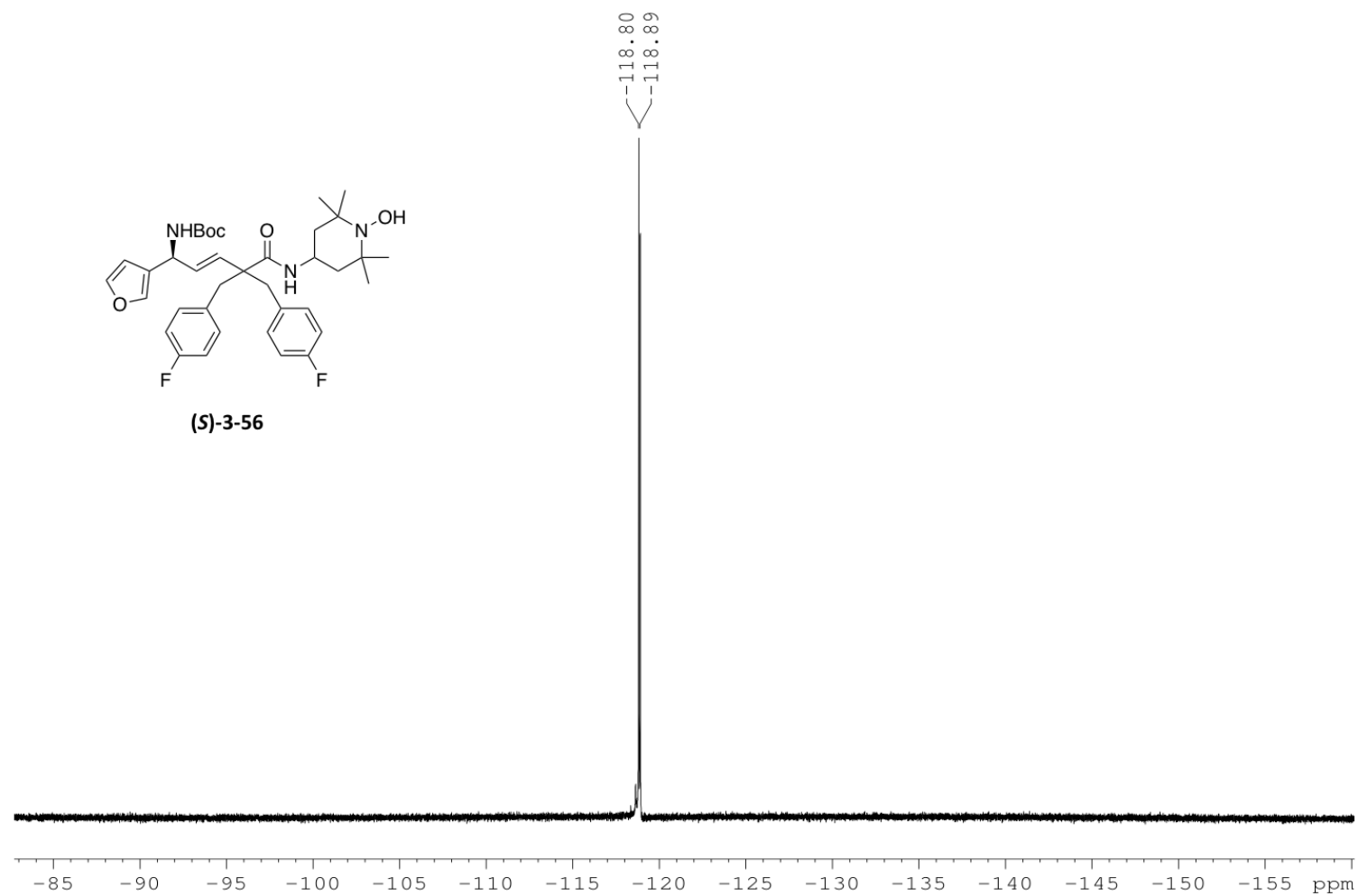


Figure 4-24  $^{19}\text{F}$  NMR spectra of nitroxide analog (S)-3-56

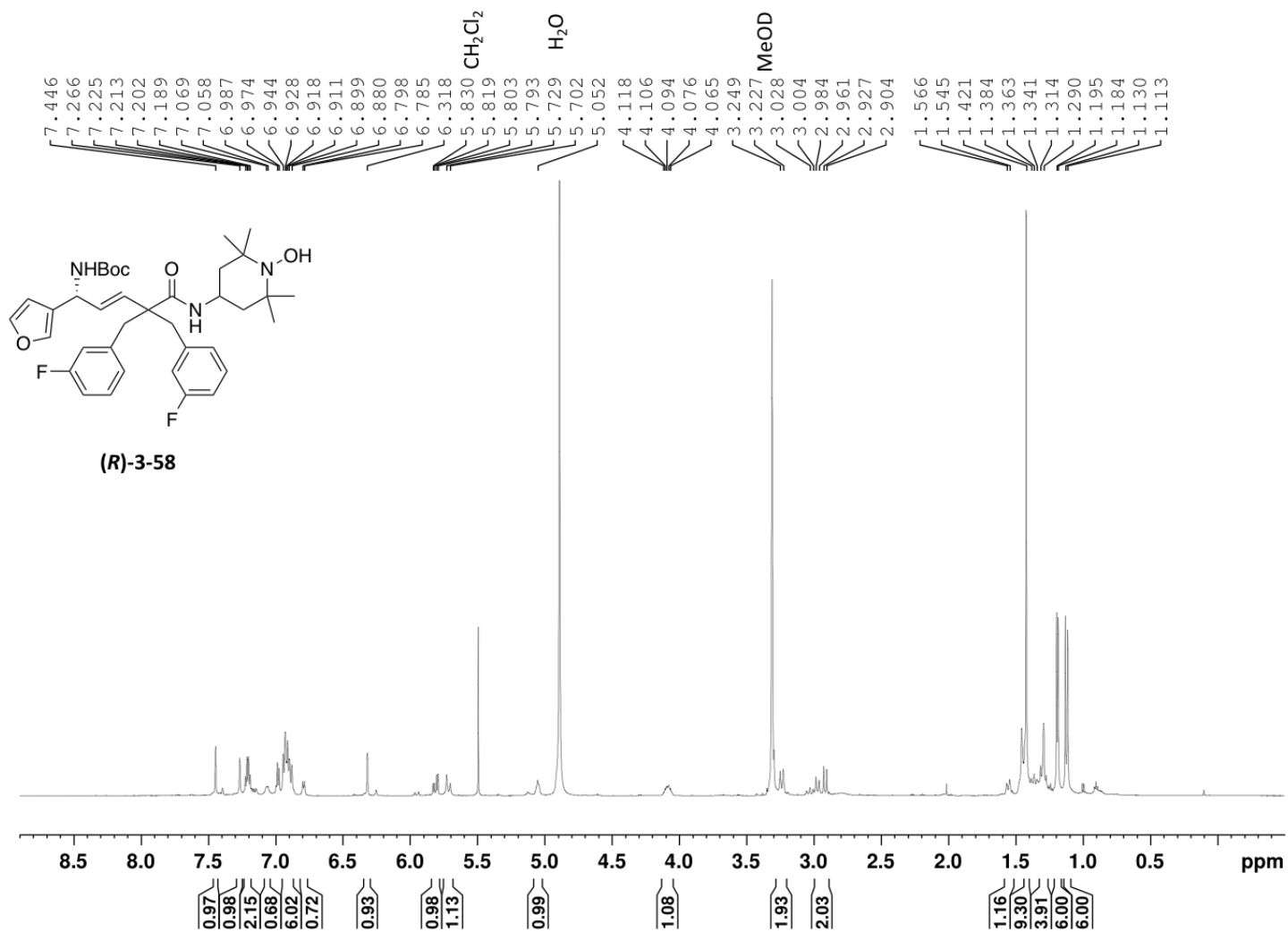


Figure 4-25 <sup>1</sup>H NMR spectra of nitroxide analog (*R*)-3-58

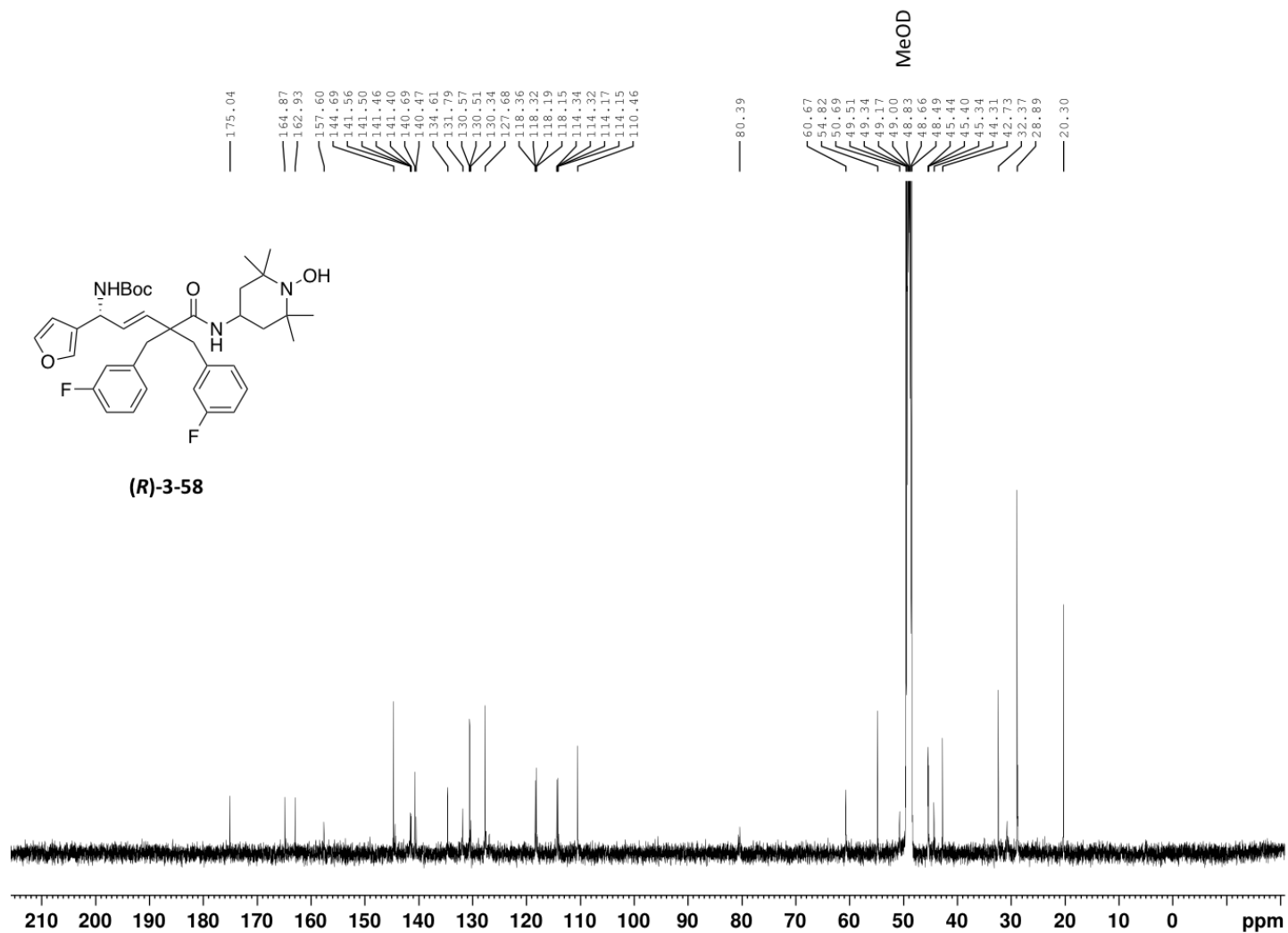


Figure 4-26 <sup>13</sup>C NMR spectra of nitroxide analog (*R*)-3-58



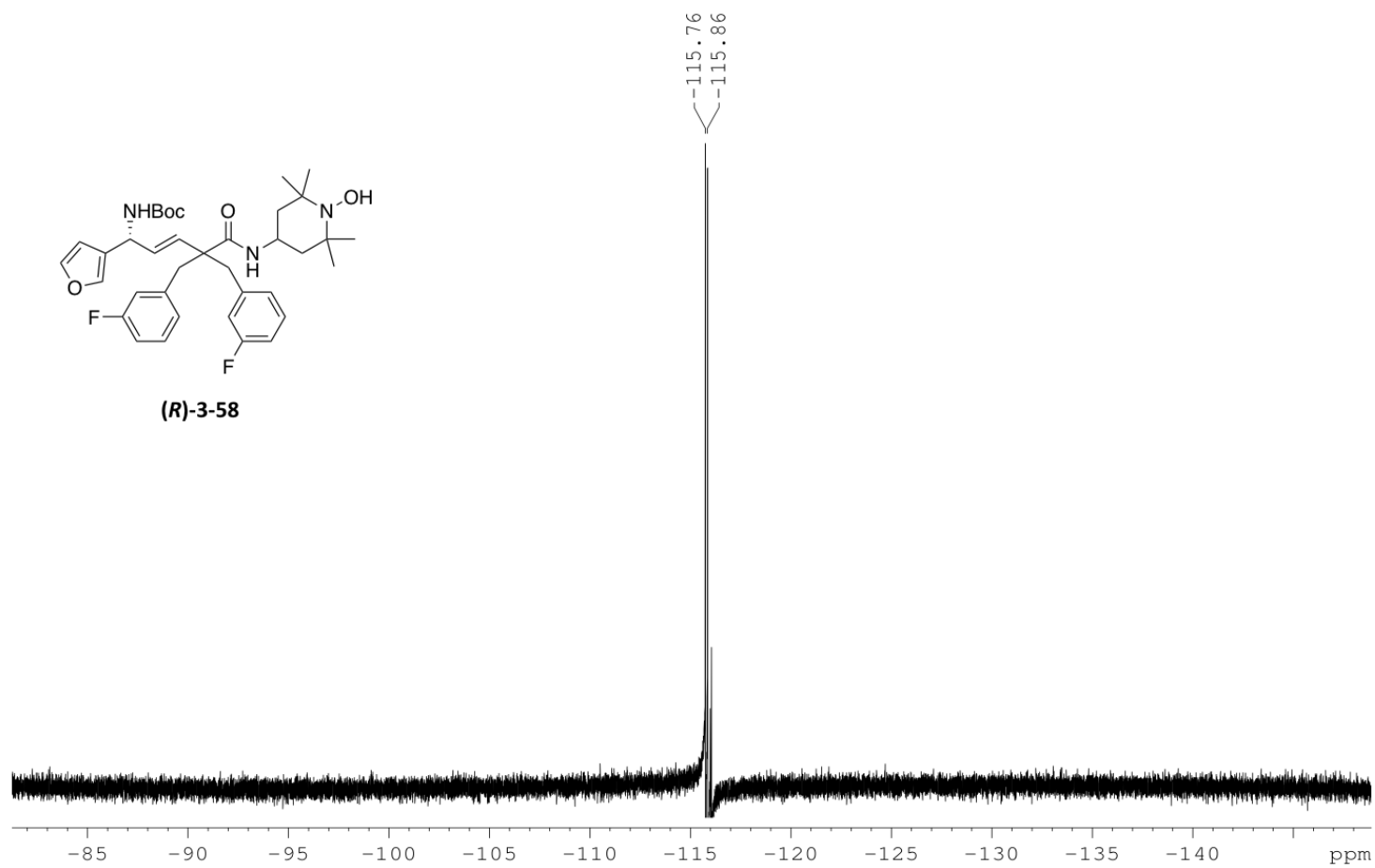


Figure 4-27  $^{19}\text{F}$  NMR spectra of nitroxide analog **(R)-3-58**

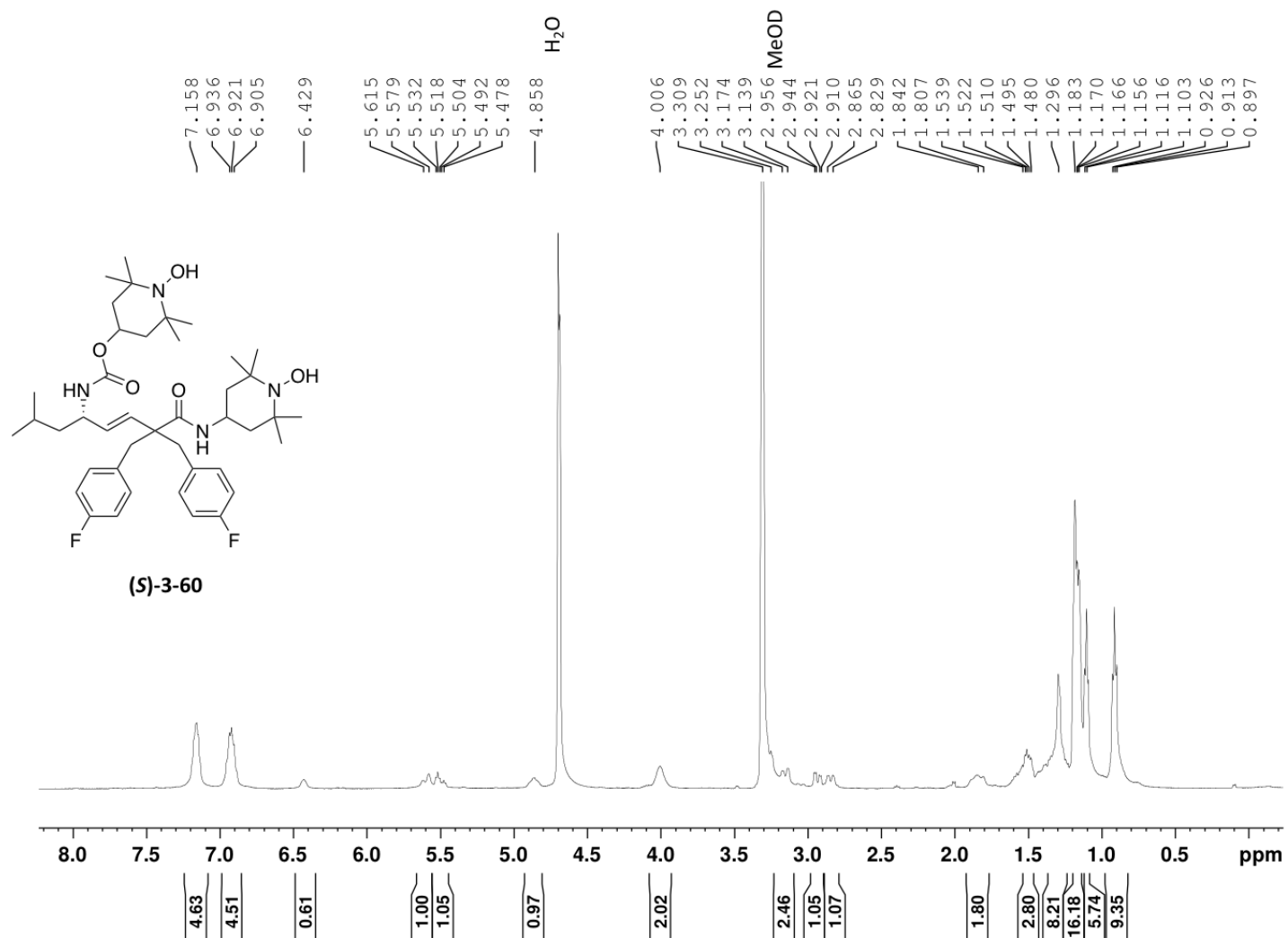


Figure 4-28 <sup>1</sup>H NMR spectra of nitroxide analog (S)-3-60

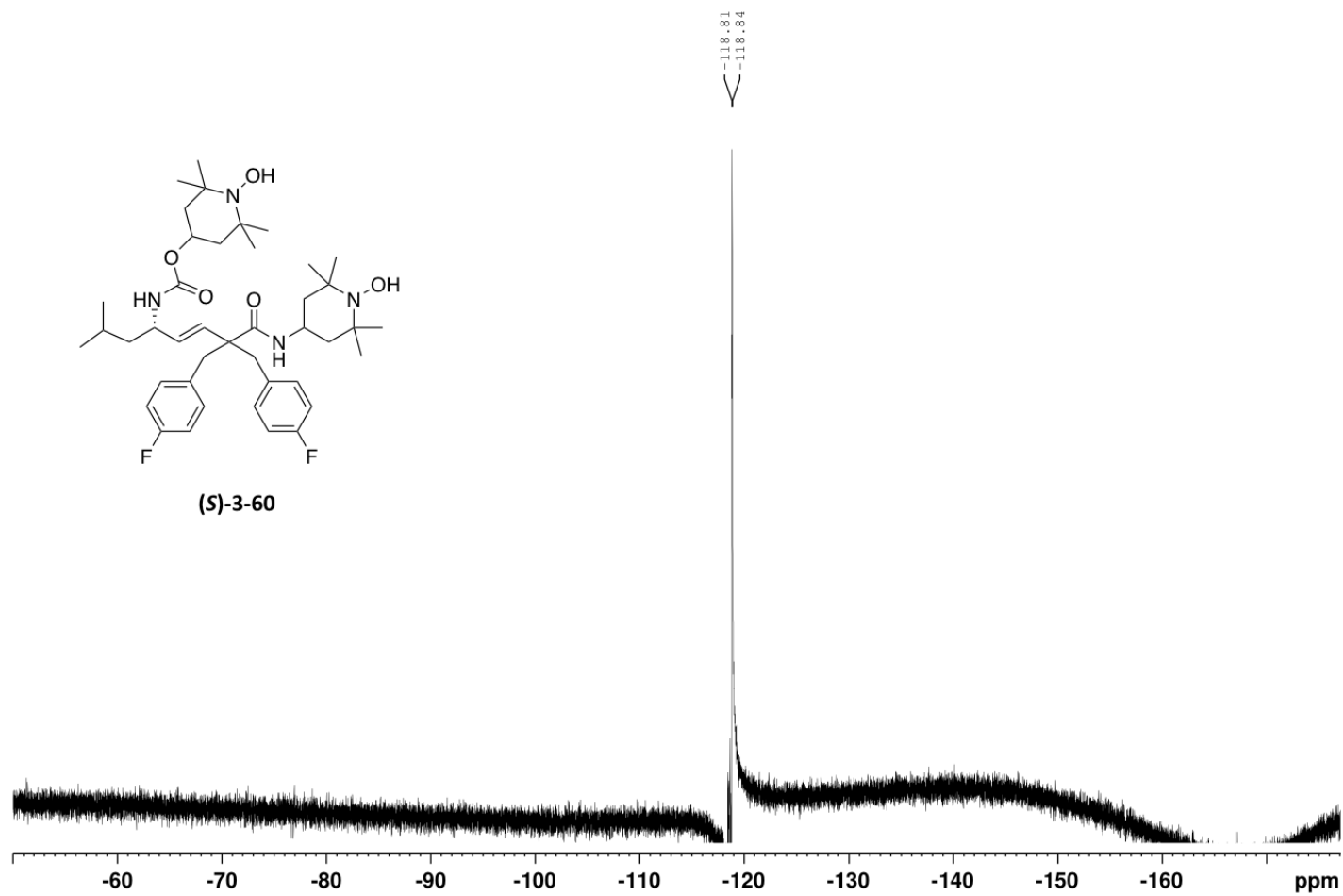


Figure 4-29  $^{19}\text{F}$  NMR spectra of nitroxide analog (*S*)-3-60

## 5.0 Bibliography

1. Biginelli, P. *Ber. Dtsch. Chem. Ges.* **1891**, 24, 1317.
2. Holden, M. S.; Crouch, R. D. *J. Chem. Educ.* **2001**, 78, 1104.
3. Folkers, K.; Johnson, T. B. *J. Am. Chem. Soc.* **1933**, 55, 3784.
4. Sweet, F.; Fissekis, J. D. *J. Am. Chem. Soc.* **1973**, 95, 8741.
5. Kappe, C. O. *J. Org. Chem.* **1997**, 62, 7201.
6. Puripat, M.; Ramozzi, R.; Hatanaka, M.; Parasuk, W.; Parasuk, V.; Morokuma, K. *J. Org. Chem.* **2015**, 80, 6959.
7. Nagarajaiah, H.; Mukhopadhyay, A.; Moorthy, J. N. *Tetrahedron Lett.* **2016**, 57, 5135.
8. Aron, Z. D.; Overman, L. E. *J. Am. Chem. Soc.* **2005**, 127, 3380.
9. de Fátima, Â.; Braga, T. C.; Neto, L. d. S.; Terra, B. S.; Oliveira, B. G. F.; da Silva, D. L.; Modolo, L. V. *J. Adv. Res.* **2015**, 6, 363.
10. Crespo, A.; El Maatougui, A.; Biagini, P.; Azuaje, J.; Coelho, A.; Brea, J.; Loza, M. I.; Cadavid, M. I.; García-Mera, X.; Gutiérrez-de-Terán, H.; Sotelo, E. *ACS Med. Chem. Lett.* **2013**, 4, 1031.
11. Chikhale, R. V.; Bhole, R. P.; Khedekar, P. B.; Bhusari, K. P. *Eur. J. Med. Chem.* **2009**, 44, 3645.
12. Mayer, T. U.; Kapoor, T. M.; Haggarty, S. J.; King, R. W.; Schreiber, S. L.; Mitchison, T. *J. Science* **1999**, 286, 971.
13. Kapoor, T. M.; Mayer, T. U.; Coughlin, M. L.; Mitchison, T. J. *J. Cell Biol.* **2000**, 150, 975.
14. Ragab, F. A. F.; Abou-Seri, S. M.; Abdel-Aziz, S. A.; Alfayomy, A. M.; Aboelmagd, M. *Eur. J. Med. Chem.* **2017**, 138, 140.
15. Kappe, C. *Molecules* **1998**, 3, 1.
16. Atwal, K. S.; Swanson, B. N.; Unger, S. E.; Floyd, D. M.; Moreland, S.; Hedberg, A.; O'Reilly, B. C. *J. Med. Chem.* **1991**, 34, 806.
17. Wipf, P.; Cunningham, A. *Tetrahedron Lett.* **1995**, 36, 7819.

18. Manos-Turvey, A.; Al-Ashtal, H. A.; Needham, P. G.; Hartline, C. B.; Prichard, M. N.; Wipf, P.; Brodsky, J. L. *Bioorg. Med. Chem. Lett.* **2016**, *26*, 5087.
19. Ranu, B. C.; Hajra, A.; Jana, U. *J. Org. Chem.* **2000**, *65*, 6270.
20. Lu, J.; Bai, Y. *Synthesis* **2002**, *2002*, 0466.
21. Hu, E. H.; Sidler, D. R.; Dolling, U.-H. *J. Org. Chem.* **1998**, *63*, 3454.
22. Sun, Q.; Wang, Y.-q.; Ge, Z.-m.; Cheng, T.-m.; Li, R.-t. *Synthesis* **2004**, *2004*, 1047.
23. Yuan, H.; Zhang, K.; Xia, J.; Hu, X.; Yuan, S. *Cogent Chem.* **2017**, *3*, 1318692.
24. Fu, N.-Y.; Yuan, Y.-F.; Cao, Z.; Wang, S.-W.; Wang, J.-T.; Peppe, C. *Tetrahedron* **2002**, *58*, 4801.
25. Russowsky, D.; Lopes, F. A.; Silva, V. S. S. d.; Canto, K. F. S.; D'Oca, M. G. M.; Godoi, M. N. *J. Braz. Chem. Soc.* **2004**, *15*, 165.
26. Peng, J.; Deng, Y. *Tetrahedron Lett.* **2001**, *42*, 5917.
27. Saha, S.; Moorthy, J. N. *J. Org. Chem.* **2011**, *76*, 396.
28. Studer, A.; Jeger, P.; Wipf, P.; Curran, D. P. *J. Org. Chem.* **1997**, *62*, 2917.
29. McDonald, A. I.; Overman, L. E. *J. Org. Chem.* **1999**, *64*, 1520.
30. Strohmeier, G. A.; Kappe, C. O. *Angew. Chem. Int.* **2004**, *43*, 621.
31. Diels, O.; Alder, K. *Justus Liebigs Ann. Chem.* **1928**, *460*, 98.
32. Morell, C.; Ayers, P. W.; Grand, A.; Gutiérrez-Oliva, S.; Toro-Labbé, A. *Phys. Chem. Chem. Phys.* **2008**, *10*, 7239.
33. Fukui, K. *Science* **1982**, *218*, 747.
34. Fukui, K. *Angew. Chem. Int.* **1982**, *21*, 801.
35. García, José I.; Mayoral, José A.; Salvatella, L. *Eur. J. Org. Chem.* **2005**, *2005*, 85.
36. Woodward, R. B.; Sondheimer, F.; Taub, D.; Heusler, K.; McLamore, W. M. *J. Am. Chem. Soc.* **1952**, *74*, 4223.
37. Corey, E. J.; Weinshenker, N. M.; Schaaf, T. K.; Huber, W. *J. Am. Chem. Soc.* **1969**, *91*, 5675.
38. Martin, S. F.; Rueger, H.; Williamson, S. A.; Grzejszczak, S. *J. Am. Chem. Soc.* **1987**, *109*, 6124.

39. Sharma, P.; Kumar, A.; Rane, N.; Gurram, V. *Tetrahedron* **2005**, *61*, 4237.
40. Mannich, C.; Krösche, W. *Arch. Pharm.* **1912**, *250*, 647.
41. Hantzsch, A. *Ber. Dtsch. Chem. Ges.* **1881**, *14*, 1637.
42. Bucherer, H. T. S., W. *J. Prakt. Chem.* **1934**, *140*, 291.
43. Strecker, A. *Justus Liebigs Ann. Chem.* **1850**, *75*, 27.
44. Gewald, K.; Schinke, E.; Böttcher, H. *Chem. Ber.* **1966**, *99*, 94.
45. Passerini, M. S., L. *Gazz. Chim. Ital.* **1921**, *51*, 126.
46. Larsen, S. D.; Grieco, P. A. *J. Am. Chem. Soc.* **1985**, *107*, 1768.
47. Petasis, N. A.; Zavialov, I. A. *J. Am. Chem. Soc.* **1997**, *119*, 445.
48. Ugi, I. M., R.; Fetzer, U.; Steinbruckner, C. *Angew. Chem.* **1959**, *71*, 373.
49. Shaabani, A.; Teimouri, M. B.; Bazgir, A.; Bijanzadeh, H. R. *Mol. Divers.* **2003**, *6*, 199.
50. Shaterian, H. R. Y., H.; Ghashang, M. *ARKIVOC* **2007**, *2007*, 298.
51. Clarke, P. A.; Zaytzev, A. V.; Whitwood, A. C. *Tetrahedron Lett.* **2007**, *48*, 5209.
52. Mousavi Faraz, S.; Rahmati, A.; Mirkhani, V. *Synth. Commun.* **2017**, *47*, 557.
53. Hasaninejad, A.; Mojikhalifeh, S.; Beyrati, M. *Appl. Organomet. Chem.* **2018**, *32*, e4380.
54. Mojikhalifeh, S.; Hasaninejad, A. *Org. Chem. Front.* **2018**, *5*, 1516.
55. Dömling, A.; Ugi, I. *Angew. Chem. Int.* **1993**, *32*, 563.
56. Zhu, J. B., H., *Multicomponent Reactions*. Wiley-VCH: 2005.
57. Maskrey, T. S.; Frischling, M. C.; Rice, M. L.; Wipf, P. *Front. Chem.* **2018**, *6*.
58. Martins, M. A. P.; Teixeira, M. V. M.; Cunico, W.; Scapin, E.; Mayer, R.; Pereira, C. M. P.; Zanatta, N.; Bonacorso, H. G.; Peppe, C.; Yuan, Y.-F. *Tetrahedron Lett.* **2004**, *45*, 8991.
59. Singh, K.; Singh, J.; Deb, P. K.; Singh, H. *Tetrahedron* **1999**, *55*, 12873.
60. Dai, C.; Meschini, F.; Narayanam, J. M. R.; Stephenson, C. R. J. *J. Org. Chem.* **2012**, *77*, 4425.
61. Krapcho, A. P.; Glynn, G. A.; Grenon, B. J. *Tetrahedron Lett.* **1967**, *8*, 215.

62. Gridelli, C.; De Marinis, F.; Di Maio, M.; Cortinovis, D.; Cappuzzo, F.; Mok, T. *Lung Cancer* **2011**, *71*, 249.
63. *Oncology Times* **2015**, *37*, 21.
64. Cohen, M. H.; Williams, G. A.; Sridhara, R.; Chen, G.; Pazdur, R. *Oncologist* **2003**, *8*, 303.
65. Santos, G. d. C.; Shepherd, F. A.; Tsao, M. S. *Annu. Rev. Pathol. Mech. Dis.* **2011**, *6*, 49.
66. Bogdanowicz, B. S.; Hoch, M. A.; Hartranft, M. E. *J. Oncol. Pharm.* **2017**, *23*, 203.
67. Yoneda, K.; Imanishi, N.; Ichiki, Y.; Tanaka, F. *J. UOEH* **2019**, *41*, 153.
68. Gibson, K. H. Quinazoline Derivatives. 5,770,599, 1998.
69. Chandregowda, V.; Venkateswara Rao, G.; Chandrasekara Reddy, G. *Org. Process Res. Dev.* **2007**, *11*, 813.
70. Kang, S. K.; Lee, S. W.; Woo, D.; Sim, J.; Suh, Y.-G. *Synth. Commun.* **2017**, *47*, 1990.
71. Maskrey, T. S.; Kristufek, T.; LaPorte, M. G.; Nyalapatla, P. R.; Wipf, P. *Synlett* **2019**, *30*, 471.
72. Kocienski, P. *Synfacts* **2019**, *15*, 0339.
73. Gerardus J., K.; Theodorus A., R.; Peter W., H. *Eur. J. Org. Chem.* **2003**, *2003*, 1681.
74. J., K. G.; B., T. H.; D., V. d. G.; T., R.; J., B.; R., V. d. E.; J., B. *Eur. J. Org. Chem.* **2006**, *2006*, 3169.
75. Yee, N. K.; Farina, V.; Houpis, I. N.; Haddad, N.; Frutos, R. P.; Gallou, F.; Wang, X.-j.; Wei, X.; Simpson, R. D.; Feng, X.; Fuchs, V.; Xu, Y.; Tan, J.; Zhang, L.; Xu, J.; Smith-Keenan, L. L.; Vitous, J.; Ridges, M. D.; Spinelli, E. M.; Johnson, M.; Donsbach, K.; Nicola, T.; Brenner, M.; Winter, E.; Kreye, P.; Samstag, W. *J. Org. Chem.* **2006**, *71*, 7133.
76. Vilbrandt, F. C. *Ind. Eng. Chem. Res.* **1945**, *37*, 418.
77. Wipf, P.; Xiao, J.; Jiang, J.; Belikova, N. A.; Tyurin, V. A.; Fink, M. P.; Kagan, V. E. *J. Am. Chem. Soc.* **2005**, *127*, 12460.
78. Hoye, A. T.; Davoren, J. E.; Wipf, P.; Fink, M. P.; Kagan, V. E. *Acc. Chem. Res.* **2008**, *41*, 87.
79. Frantz, M.-C.; Pierce, J. G.; Pierce, J. M.; Kangying, L.; Qingwei, W.; Johnson, M.; Wipf, P. *Org. Lett.* **2011**, *13*, 2318.
80. Wipf, P.; Skoda, E. M.; Mann, A., Conformational Restriction and Steric Hindrance in Medicinal Chemistry. In *The Practice of Medicinal Chemistry*, 4 ed.; Academic Press: 2015; pp 279.

81. Vater, J.; Stein, T. H., Structure, Function, and Biosynthesis of Gramicidin S Synthetase. In *Comprehensive Natural Products Chemistry*, Pergamon: 1999; Vol. 4, pp 319.
82. Jenkins, C. L.; Vasbinder, M. M.; Miller, S. J.; Raines, R. T. *Org. Lett.* **2005**, 7, 2619.
83. Lewandowski, M.; Gwozdziński, K. *Int. J. Mol. Sci.* **2017**, 18, 2490.
84. Wilcox, C. S. *Pharmacol. Ther.* **2010**, 126, 119.
85. Krishna, M. C.; Samuni, A., [59] Nitroxides as antioxidants. In *Methods in Enzymology*, Academic Press: 1994; Vol. 234, pp 580.
86. Sardesai, V. M. *Nutr. Clin. Pract.* **1995**, 10, 19.
87. Lobo, V.; Patil, A.; Phatak, A.; Chandra, N. *Pharmacogn. Rev.* **2010**, 4, 118.
88. Pizzino, G.; Irrera, N.; Cucinotta, M.; Pallio, G.; Mannino, F.; Arcoraci, V.; Squadrito, F.; Altavilla, D.; Bitto, A. *Oxid. Med. Cell. Longev.* **2017**, 2017, 8416763.
89. Prescott, C.; Bottle, S. E. *Cell Biochem. Biophys.* **2017**, 75, 227.
90. Birben, E.; Sahiner, U. M.; Sackesen, C.; Erzurum, S.; Kalayci, O. *World Allergy Organ. J.* **2012**, 5, 9.
91. Griesser, M.; Shah, R.; Van Kessel, A. T.; Zilka, O.; Haidasz, E. A.; Pratt, D. A. *J. Am. Chem. Soc.* **2018**, 140, 3798.
92. Zilka, O.; Shah, R.; Li, B.; Friedmann Angeli, J. P.; Griesser, M.; Conrad, M.; Pratt, D. A. *ACS Cent. Sci.* **2017**, 3, 232.
93. Kanai, A.; Zabbarova, I.; Amoscato, A.; Epperly, M.; Xiao, J.; Wipf, P. *Org. Biomol. Chem.* **2007**, 5, 307.
94. Kulkarni, C. A.; Fink, B. D.; Gibbs, B. E.; Chheda, P. R.; Wu, M.; Sivitz, W. I.; Kerns, R. *J. J. Med. Chem.* **2021**, 64, 662.
95. Wipf, P.; Xiao, J.; Fink, M. P.; Kagan, V.; Tyurina, Y. Y.; Kanai, A. Selective Targeting Agents for Mitochondria. US7528174B2, 2006.
96. Bernard, M. E.; Kim, H.; Berhane, H.; Epperly, M. W.; Franicola, D.; Zhang, X.; Houghton, F.; Shields, D.; Wang, H.; Bakkenist, C. J.; Frantz, M.-C.; Forbeck, E. M.; Goff, J. P.; Wipf, P.; Greenberger, J. S. *Radiat. Res.* **2011**, 176, 603.
97. Goff, J. P.; Epperly, M. W.; Dixon, T.; Wang, H.; Franicola, D.; Shields, D.; Wipf, P.; Li, S.; Gao, X.; Greenberger, J. S. *In Vivo* **2011**, 25, 315.
98. Xun, Z.; Rivera-Sanchez, S.; Ayala-Penã, S.; Lim, J.; Budworth, H.; Skoda, E. M.; Robbins, P. D.; Niedernhofer, L. J.; Wipf, P.; McMurray, C. T. *Cell Rep.* **2012**, 2, 1137.



99. Lipinski, C. A.; Lombardo, F.; Dominy, B. W.; Feeney, P. J. *Adv. Drug Deliv. Rev.* **1997**, *23*, 3.
100. Barton, S. A.; Halpin, J. L.; Tomar, P. J. *Energ. Mater.* **1990**, *8*, 336.
101. Young, J. A. *J. Chem. Edu.* **2003**, *80*, 259.
102. Rajagopalan, M. S.; Gupta, K.; Epperly, M. W.; Franicola, D.; Zhang, X.; Wang, H.; Zhao, H.; Tyurin, V. A.; Pierce, J. G.; Kagan, V. E.; Wipf, P.; Kanai, A. J.; Greenberger, J. S. *In Vivo* **2009**, *23*, 717.
103. Epperly, M. W.; Dixon, T. M.; He, S.; Shields, D.; Wipf, P.; Li, S.; Greenberger, J. S. *Blood* **2014**, *124*, 2751.
104. Greenberger, J.; Kagan, V.; Bayir, H.; Wipf, P.; Epperly, M. *Antioxidants* **2015**, *4*.
105. W. Epperly, M.; R. Sacher, J.; Krainz, T.; Zhang, X.; Wipf, P.; Liang, M.; Fisher, R.; Li, S.; Wang, H.; S. Greenberger, J. *In Vivo* **2017**, *31*, 39.
106. Willis, J.; Epperly, M. W.; Fisher, R.; Zhang, X.; Shields, D.; Hou, W.; Wang, H.; Li, S.; Wipf, P.; Parmar, K.; Guinan, E.; Steinman, J.; Greenberger, J. S. *Radiat. Res.* **2018**, *189*, 560.
107. Epperly, M. W.; Sacher, J. R.; Krainz, T.; Zhang, X.; Wipf, P.; Liang, M.; Fisher, R.; Li, S.; Wang, H.; Greenberger, J. S. *In Vivo* **2017**, *31*, 39.
108. Jiang, J.; Kurnikov, I.; Belikova, N. A.; Xiao, J.; Zhao, Q.; Amoscato, A. A.; Braslau, R.; Studer, A.; Fink, M. P.; Greenberger, J. S.; Wipf, P.; Kagan, V. E. *J. Pharmacol. Exp.* **2007**, *320*, 1050.
109. Ji, J.; Kline, A. E.; Amoscato, A.; Samhan-Arias, A. K.; Sparvero, L. J.; Tyurin, V. A.; Tyurina, Y. Y.; Fink, B.; Manole, M. D.; Puccio, A. M.; Okonkwo, D. O.; Cheng, J. P.; Alexander, H.; Clark, R. S.; Kochanek, P. M.; Wipf, P.; Kagan, V. E.; Bayir, H. *Nat. Neurosci.* **2012**, *15*, 1407.
110. Ameisen, J. C. *Cell Death Differ.* **2002**, *9*, 367.
111. Vaux, D. L.; Korsmeyer, S. J. *Cell* **1999**, *96*, 245.
112. Labi, V.; Erlacher, M. *Cell Death Dis.* **2015**, *6*, e1675.
113. Kroemer, G.; Galluzzi, L.; Vandenabeele, P.; Abrams, J.; Alnemri, E. S.; Baehrecke, E. H.; Blagosklonny, M. V.; El-Deiry, W. S.; Golstein, P.; Green, D. R.; Hengartner, M.; Knight, R. A.; Kumar, S.; Lipton, S. A.; Malorni, W.; Nuñez, G.; Peter, M. E.; Tschopp, J.; Yuan, J.; Piacentini, M.; Zhivotovsky, B.; Melino, G. *Cell Death Differ.* **2009**, *16*, 3.
114. Galluzzi, L.; Vitale, I.; Aaronson, S. A.; Abrams, J. M.; Adam, D.; Agostinis, P.; Alnemri, E. S.; Altucci, L.; Amelio, I.; Andrews, D. W.; Annicchiarico-Petruzzelli, M.; Antonov, A.

- V.; Arama, E.; Baehrecke, E. H.; Barlev, N. A.; Bazan, N. G.; Bernassola, F.; Bertrand, M. J. M.; Bianchi, K.; Blagosklonny, M. V.; Blomgren, K.; Borner, C.; Boya, P.; Brenner, C.; Campanella, M.; Candi, E.; Carmona-Gutierrez, D.; Cecconi, F.; Chan, F. K.; Chandel, N. S.; Cheng, E. H.; Chipuk, J. E.; Cidlowski, J. A.; Ciechanover, A.; Cohen, G. M.; Conrad, M.; Cubillos-Ruiz, J. R.; Czabotar, P. E.; D'Angiolella, V.; Dawson, T. M.; Dawson, V. L.; De Laurenzi, V.; De Maria, R.; Debatin, K. M.; DeBerardinis, R. J.; Deshmukh, M.; Di Daniele, N.; Di Virgilio, F.; Dixit, V. M.; Dixon, S. J.; Duckett, C. S.; Dynlacht, B. D.; El-Deiry, W. S.; Elrod, J. W.; Fimia, G. M.; Fulda, S.; García-Sáez, A. J.; Garg, A. D.; Garrido, C.; Gavathiotis, E.; Golstein, P.; Gottlieb, E.; Green, D. R.; Greene, L. A.; Gronemeyer, H.; Gross, A.; Hajnoczky, G.; Hardwick, J. M.; Harris, I. S.; Hengartner, M. O.; Hetz, C.; Ichijo, H.; Jäättelä, M.; Joseph, B.; Jost, P. J.; Juin, P. P.; Kaiser, W. J.; Karin, M.; Kaufmann, T.; Kepp, O.; Kimchi, A.; Kitsis, R. N.; Klionsky, D. J.; Knight, R. A.; Kumar, S.; Lee, S. W.; Lemasters, J. J.; Levine, B.; Linkermann, A.; Lipton, S. A.; Lockshin, R. A.; López-Otín, C.; Lowe, S. W.; Luedde, T.; Lugli, E.; MacFarlane, M.; Madeo, F.; Malewicz, M.; Malorni, W.; Manic, G.; Marine, J. C.; Martin, S. J.; Martinou, J. C.; Medema, J. P.; Mehlen, P.; Meier, P.; Melino, S.; Miao, E. A.; Molkentin, J. D.; Moll, U. M.; Muñoz-Pinedo, C.; Nagata, S.; Nuñez, G.; Oberst, A.; Oren, M.; Overholtzer, M.; Pagano, M.; Panaretakis, T.; Pasparakis, M.; Penninger, J. M.; Pereira, D. M.; Pervaiz, S.; Peter, M. E.; Piacentini, M.; Pinton, P.; Prehn, J. H. M.; Puthalakath, H.; Rabinovich, G. A.; Rehm, M.; Rizzuto, R.; Rodrigues, C. M. P.; Rubinsztein, D. C.; Rudel, T.; Ryan, K. M.; Sayan, E.; Scorrano, L.; Shao, F.; Shi, Y.; Silke, J.; Simon, H. U.; Sistigu, A.; Stockwell, B. R.; Strasser, A.; Szabadkai, G.; Tait, S. W. G.; Tang, D.; Tavernarakis, N.; Thorburn, A.; Tsujimoto, Y.; Turk, B.; Vanden Berghe, T.; Vandenabeele, P.; Vander Heiden, M. G.; Villunger, A.; Virgin, H. W.; Voutsden, K. H.; Vucic, D.; Wagner, E. F.; Walczak, H.; Wallach, D.; Wang, Y.; Wells, J. A.; Wood, W.; Yuan, J.; Zakeri, Z.; Zhivotovsky, B.; Zitvogel, L.; Melino, G.; Kroemer, G. *Cell Death Differ.* **2018**, *25*, 486.
115. Liu, X.; Yang, W.; Guan, Z.; Yu, W.; Fan, B.; Xu, N.; Liao, D. J. *Cell Biosci.* **2018**, *8*, 6.
  116. Dixon, S. J.; Lemberg, K. M.; Lamprecht, M. R.; Skouta, R.; Zaitsev, E. M.; Gleason, C. E.; Patel, D. N.; Bauer, A. J.; Cantley, A. M.; Yang, W. S.; Morrison, B., 3rd; Stockwell, B. R. *Cell* **2012**, *149*, 1060.
  117. McIlwain, D. R.; Berger, T.; Mak, T. W. *Cold Spring Harb. Perspect. Biol.* **2013**, *5*, a008656.
  118. Green, D. R. *Cell* **1998**, *94*, 695.
  119. Elmore, S. *Toxicol. Pathol.* **2007**, *35*, 495.
  120. Hrdinka, M.; Yabal, M. *Genes Immun.* **2019**, *20*, 641.
  121. Mohamad Anuar, N. N.; Nor Hisam, N. S.; Liew, S. L.; Ugusman, A. *Front. Pharmacol.* **2020**, *11*.
  122. Berghe, T. V.; Linkermann, A.; Jouan-Lanhoutet, S.; Walczak, H.; Vandenabeele, P. *Nat. Rev. Mol. Cell Biol.* **2014**, *15*, 135.

123. Wang, X.; Yousefi, S.; Simon, H.-U. *Cell Death Dis.* **2018**, *9*, 111.
124. Choi, M. E.; Price, D. R.; Ryter, S. W.; Choi, A. M. K. *JCI Insight* **2019**, *4*.
125. Vandenabeele, P.; Grootjans, S.; Callewaert, N.; Takahashi, N. *Cell Death Differ.* **2013**, *20*, 185.
126. Fernández-Medarde, A.; Santos, E. *Genes Cancer* **2011**, *2*, 344.
127. Wiernicki, B.; Dubois, H.; Tyurina, Y. Y.; Hassannia, B.; Bayir, H.; Kagan, V. E.; Vandenabeele, P.; Wullaert, A.; Vanden Berghe, T. *Cell Death Dis.* **2020**, *11*, 922.
128. Li, J.; Cao, F.; Yin, H.-l.; Huang, Z.-j.; Lin, Z.-t.; Mao, N.; Sun, B.; Wang, G. *Cell Death Dis.* **2020**, *11*, 88.
129. Mou, Y.; Wang, J.; Wu, J.; He, D.; Zhang, C.; Duan, C.; Li, B. *J. Hematol. Oncol.* **2019**, *12*, 34.
130. Kenny, E. M.; Fidan, E.; Yang, Q.; Anthony-muthu, T. S.; New, L. A.; Meyer, E. A.; Wang, H.; Kochanek, P. M.; Dixon, C. E.; Kagan, V. E.; Bayir, H. *Crit. Care Med.* **2019**, *47*, 410.
131. Jiang, X.; Stockwell, B. R.; Conrad, M. *Nat. Rev. Mol. Cell Biol.* **2021**.
132. Yang, W. S.; Kim, K. J.; Gaschler, M. M.; Patel, M.; Shchepinov, M. S.; Stockwell, B. R. *Proc. Natl. Acad. Sci.* **2016**, *113*, E4966.
133. Conrad, M.; Pratt, D. A. *Nat. Chem. Biol.* **2019**, *15*, 1137.
134. Bateman, L. *Q. Rev. Chem. Soc.* **1954**, *8*, 147.
135. Lei, P.; Bai, T.; Sun, Y. *Front. Psychol.* **2019**, *10*.
136. Winterbourn, C. C. *Toxicol. Lett.* **1995**, 82-83, 969.
137. Nagakannan, P.; Islam, M. I.; Conrad, M.; Eftekharpour, E. *Biochim. Biophys. Acta. Mol. Cell Res.* **2021**, *1868*, 118928.
138. Kajarabille, N.; Latunde-Dada, G. O. *Int. J. Mol. Sci.* **2019**, *20*.
139. Shah, R.; Shchepinov, M. S.; Pratt, D. A. *ACS Cent. Sci.* **2018**, *4*, 387.
140. Conrad, M.; Kagan, V. E.; Bayir, H.; Pagnussat, G. C.; Head, B.; Traber, M. G.; Stockwell, B. R. *Genes Dev.* **2018**, 602.
141. Zou, Y.; Li, H.; Graham, E. T.; Deik, A. A.; Eaton, J. K.; Wang, W.; Sandoval-Gomez, G.; Clish, C. B.; Doench, J. G.; Schreiber, S. L. *Nat. Chem. Biol.* **2020**, *16*, 302.
142. Chen, X.; Yu, C.; Kang, R.; Tang, D. *Front. Cell Dev. Biol.* **2020**, *8*, 590226.

143. Steere, A. N.; Byrne, S. L.; Chasteen, N. D.; Mason, A. B. *Biochim. Biophys. Acta.* **2012**, *1820*, 326.
144. Lu, B.; Chen, X. B.; Ying, M. D.; He, Q. J.; Cao, J.; Yang, B. *Front. Pharmacol.* **2017**, *8*, 992.
145. Yan, N.; Zhang, J. *Front. Neurosci.* **2020**, *13*.
146. Sun, X.; Ou, Z.; Xie, M.; Kang, R.; Fan, Y.; Niu, X.; Wang, H.; Cao, L.; Tang, D. *Oncogene* **2015**, *34*, 5617.
147. Scheerer, P.; Borchert, A.; Krauss, N.; Wessner, H.; Gerth, C.; Höhne, W.; Kuhn, H. *Biochemistry* **2007**, *46*, 9041.
148. Seiler, A.; Schneider, M.; Förster, H.; Roth, S.; Wirth, E. K.; Culmsee, C.; Plesnila, N.; Kremmer, E.; Rådmark, O.; Wurst, W.; Bornkamm, G. W.; Schweizer, U.; Conrad, M. *Cell Metab.* **2008**, *8*, 237.
149. Dixon, S. J.; Patel, D. N.; Welsch, M.; Skouta, R.; Lee, E. D.; Hayano, M.; Thomas, A. G.; Gleason, C. E.; Tatonetti, N. P.; Slusher, B. S.; Stockwell, B. R. *eLife* **2014**, *3*, e02523.
150. Stockwell, B. R.; Friedmann Angeli, J. P.; Bayir, H.; Bush, A. I.; Conrad, M.; Dixon, S. J.; Fulda, S.; Gascón, S.; Hatzios, S. K.; Kagan, V. E.; Noel, K.; Jiang, X.; Linkermann, A.; Murphy, M. E.; Overholtzer, M.; Oyagi, A.; Pagnussat, G. C.; Park, J.; Ran, Q.; Rosenfeld, C. S.; Salnikow, K.; Tang, D.; Torti, F. M.; Torti, S. V.; Toyokuni, S.; Woerpel, K. A.; Zhang, D. D. *Cell* **2017**, *171*, 273.
151. Doll, S.; Freitas, F. P.; Shah, R.; Aldrovandi, M.; da Silva, M. C.; Ingold, I.; Goya Grocin, A.; Xavier da Silva, T. N.; Panzilius, E.; Scheel, C. H.; Mourão, A.; Buday, K.; Sato, M.; Wanninger, J.; Vignane, T.; Mohana, V.; Rehberg, M.; Flatley, A.; Schepers, A.; Kurz, A.; White, D.; Sauer, M.; Sattler, M.; Tate, E. W.; Schmitz, W.; Schulze, A.; O'Donnell, V.; Proneth, B.; Popowicz, G. M.; Pratt, D. A.; Angeli, J. P. F.; Conrad, M. *Nature* **2019**, *575*, 693.
152. Kang, R.; Kroemer, G.; Tang, D. *Free Radic. Biol. Med.* **2019**, *133*, 162.
153. Yang, W.; Liu, X.; Song, C.; Ji, S.; Yang, J.; Liu, Y.; You, J.; Zhang, J.; Huang, S.; Cheng, W.; Shao, Z.; Li, L.; Yang, S. *Eur. J. Med. Chem.* **2021**, *209*, 112842.
154. Manz, D. H.; Blanchette, N. L.; Paul, B. T.; Torti, F. M.; Torti, S. V. *Ann. N. Y. Acad. Sci.* **2016**, *1368*, 149.
155. Tuo, Q. Z.; Lei, P.; Jackman, K. A.; Li, X. L.; Xiong, H.; Li, X. L.; Liuyang, Z. Y.; Roisman, L.; Zhang, S. T.; Ayton, S.; Wang, Q.; Crouch, P. J.; Ganio, K.; Wang, X. C.; Pei, L.; Adlard, P. A.; Lu, Y. M.; Cappai, R.; Wang, J. Z.; Liu, R.; Bush, A. I. *Mol. Psychiatry* **2017**, *22*, 1520.

156. Krainz, T.; Gaschler, M. M.; Lim, C.; Sacher, J. R.; Stockwell, B. R.; Wipf, P. *ACS Cent. Sci.* **2016**, *2*, 653.
157. Shimada, K.; Skouta, R.; Kaplan, A.; Yang, W. S.; Hayano, M.; Dixon, S. J.; Brown, L. M.; Valenzuela, C. A.; Wolpaw, A. J.; Stockwell, B. R. *Nat. Chem. Biol.* **2016**, *12*, 497.
158. Comparison of colorimetric, fluorescence and luminescence analysis. [www.aladdin-e.com](http://www.aladdin-e.com).
159. Zhang, M.-Q.; Wilkinson, B. *Curr. Opin. Biotechnol.* **2007**, *18*, 478.
160. Yagoda, N.; von Rechenberg, M.; Zaganjor, E.; Bauer, A. J.; Yang, W. S.; Fridman, D. J.; Wolpaw, A. J.; Smukste, I.; Peltier, J. M.; Boniface, J. J.; Smith, R.; Lessnick, S. L.; Sahasrabudhe, S.; Stockwell, B. R. *Nature* **2007**, *447*, 864.
161. Zhang, H.-J.; Shi, C.-Y.; Zhong, F.; Yin, L. *J. Am. Chem. Soc.* **2017**, *139*, 2196.
162. Martin, S. F. *Acc. Chem. Res.* **2002**, *35*, 895.
163. Arend, M.; Westermann, B.; Risch, N. *Angew. Chem. Int.* **1998**, *37*, 1044.
164. Yamasaki, S.; Iida, T.; Shibasaki, M. *Tetrahedron Lett.* **1999**, *40*, 307.
165. Juhl, K.; Gathergood, N.; Jørgensen, K. A. *Angew. Chem. Int.* **2001**, *40*, 2995.
166. Trost, B. M.; Terrell, L. R. *J. Am. Chem. Soc.* **2003**, *125*, 338.
167. Casiraghi, G.; Battistini, L.; Curti, C.; Rassu, G.; Zanardi, F. *Chem. Rev.* **2011**, *111*, 3076.
168. Casiraghi, G.; Zanardi, F.; Appendino, G.; Rassu, G. *Chem. Rev.* **2000**, *100*, 1929.
169. Martin, S. F. *Pure Appl. Chem.* **1997**, *69*, 571.
170. Martin, S. F.; Lopez, O. D. *Tetrahedron Lett.* **1999**, *40*, 8949.
171. Carswell, E. L.; Snapper, M. L.; Hoveyda, A. H. *Angew. Chem. Int.* **2006**, *45*, 7230.
172. Liu, T.-Y.; Cui, H.-L.; Long, J.; Li, B.-J.; Wu, Y.; Ding, L.-S.; Chen, Y.-C. *J. Am. Chem. Soc.* **2007**, *129*, 1878.
173. Sickert, M.; Schneider, C. *Angew. Chem. Int.* **2008**, *47*, 3631.
174. Giera, D. S.; Sickert, M.; Schneider, C. *Org. Lett.* **2008**, *10*, 4259.
175. Salvador González, A.; Gómez Arrayás, R.; Rodríguez Rivero, M.; Carretero, J. C. *Org. Lett.* **2008**, *10*, 4335.
176. Sickert, M.; Abels, F.; Lang, M.; Sieler, J.; Birkemeyer, C.; Schneider, C. *Chem. Eur. J.* **2010**, *16*, 2806.

177. Giera, D. S.; Sickert, M.; Schneider, C. *Synthesis* **2009**, 2009, 3797.
178. Abels, F.; Lindemann, C.; Koch, E.; Schneider, C. *Org. Lett.* **2012**, 14, 5972.
179. Abels, F.; Lindemann, C.; Schneider, C. *Chem. Eur. J.* **2014**, 20, 1964.
180. Zhang, Q.; Hui, Y.; Zhou, X.; Lin, L.; Liu, X.; Feng, X. *Adv. Synth. Catal.* **2010**, 352, 976.
181. Wang, Q.; van Gemmeren, M.; List, B. *Angew. Chem. Int.* **2014**, 53, 13592.
182. Bordwell, F. G.; Fried, H. E. *J. Org. Chem.* **1981**, 46, 4327.
183. Gu, C.-L.; Liu, L.; Wang, D.; Chen, Y.-J. *J. Org. Chem.* **2009**, 74, 5754.
184. Yu, J.; Miao, Z.; Chen, R. *Org. Biomol. Chem.* **2011**, 9, 1756.
185. Sasikala, C. H. V. A.; Reddy Padi, P.; Sunkara, V.; Ramayya, P.; Dubey, P. K.; Bhaskar Rao Uppala, V.; Praveen, C. *Org. Process Res. Dev.* **2009**, 13, 907.
186. Barragán, E.; Olivo, H. F.; Romero-Ortega, M.; Sarduy, S. *J. Org. Chem.* **2005**, 70, 4214.
187. Ishikawa, T.; Kawaski-Takasuka, T.; Kubota, T.; Yamazaki, T. *Beilstein J. Org. Chem.* **2017**, 13, 2473.
188. Corey, E. J.; Ensley, H. E. *J. Am. Chem. Soc.* **1975**, 97, 6908.
189. Heravi, M. M.; Zadsirjan, V.; Farajpour, B. *RSC Adv.* **2016**, 6, 30498.
190. Evans, D. A.; Ennis, M. D.; Mathre, D. J. *J. Am. Chem. Soc.* **1982**, 104, 1737.
191. Gage, J. R.; Evans, D. A. *Org. Synth.* **1990**, 68, 77.
192. Evans, D. A.; Chapman, K. T.; Bisaha, J. *J. Am. Chem. Soc.* **1988**, 110, 1238.
193. Hoveyda, A. H.; Evans, D. A.; Fu, G. C. *Chem. Rev.* **1993**, 93, 1307.
194. Mukherjee, S.; Yang, J. W.; Hoffmann, S.; List, B. *Chem. Rev.* **2007**, 107, 5471.
195. Heravi, M. M.; Zadsirjan, V. *Tetrahedron Asymmetry* **2013**, 24, 1149.
196. Cieź, D.; Pałasz, A.; Trzewik, B. *Eur. J. Org. Chem.* **2016**, 2016, 1476.
197. Chen, X.; Dong, S.; Qiao, Z.; Zhu, Y.; Xie, M.; Lin, L.; Liu, X.; Feng, X. *Chem. Eur. J.* **2011**, 17, 2583.
198. Masamune, S.; Choy, W.; Petersen, J. S.; Sita, L. R. *Angew. Chem. Int.* **1985**, 24, 1.
199. Davies, S. G.; Fletcher, A. M.; Hermann, G. J.; Poce, G.; Roberts, P. M.; Smith, A. D.; Sweet, M. J.; Thomson, J. E. *Tetrahedron Asymmetry* **2010**, 21, 1635.

200. Calderón, F.; Doyagüez, E. G.; Cheong, P. H.-Y.; Fernández-Mayoralas, A.; Houk, K. N. *J. Org. Chem.* **2008**, *73*, 7916.
201. Davies, S. G.; Lee, J. A.; Roberts, P. M.; Thomson, J. E.; Yin, J. *Tetrahedron* **2011**, *67*, 6382.
202. Neuvonen, A. J.; Pihko, P. M. *Org. Lett.* **2014**, *16*, 5152.
203. Wenzel, A. G.; Jacobsen, E. N. *J. Am. Chem. Soc.* **2002**, *124*, 12964.
204. Kanazawa, A. M.; Denis, J.-N.; Greene, A. E. *J. Org. Chem.* **1994**, *59*, 1238.
205. Matsunaga, S.; Yoshida, T.; Morimoto, H.; Kumagai, N.; Shibasaki, M. *J. Am. Chem. Soc.* **2004**, *126*, 8777.
206. Vesely, J.; Rios, R. *Chem. Soc. Rev.* **2014**, *43*, 611.
207. Hu, Q.; Nyamekye, G. A.; Rees, R. H.; Mastrup, N. S.; Tihomirov, L.; Pavlakovich, W. N. Composition for filtering and removing particles and/or constituents from a fluid. EP07799552A, 2007.
208. Duhaime, R. M.; Lombardo, D. A.; Skinner, I. A.; Weedon, A. C. *J. Org. Chem.* **1985**, *50*, 873.
209. Valeur, E.; Bradley, M. *Chem. Soc. Rev.* **2009**, *38*, 606.
210. Nguyen, T. B.; Sorres, J.; Tran, M. Q.; Ermolenko, L.; Al-Mourabit, A. *Org. Lett.* **2012**, *14*, 3202.
211. Eldred, S. E.; Stone, D. A.; Gellman, S. H.; Stahl, S. S. *J. Am. Chem. Soc.* **2003**, *125*, 3422.
212. Becerra-Figueroa, L.; Ojeda-Porras, A.; Gamba-Sánchez, D. *J. Org. Chem.* **2014**, *79*, 4544.
213. Bobko, A. A.; Efimova, O. V.; Voinov, M. A.; Khramtsov, V. V. *Free Radic. Res.* **2012**, *46*, 1115.
214. Chan, K. S.; Li, X. Z.; Dzik, W. I.; de Bruin, B. *J. Am. Chem. Soc.* **2008**, *130*, 2051.
215. Yushkova, Y. V.; Chernyak, E. I.; Morozov, S. V.; Grigor'ev, I. A. *Chem. Nat. Compd.* **2014**, *50*, 827.
216. Dobarro, A.; Velasco, D. *Tetrahedron* **1996**, *52*, 13733.
217. N-Methylmorpholine. In *Encyclopedia of Reagents for Organic Synthesis*.
218. Lu, G.; Liu, R. Y.; Yang, Y.; Fang, C.; Lambrecht, D. S.; Buchwald, S. L.; Liu, P. *J. Am. Chem. Soc.* **2017**, *139*, 16548.

219. Thomas, A. A.; Speck, K.; Kevlishvili, I.; Lu, Z.; Liu, P.; Buchwald, S. L. *J. Am. Chem. Soc.* **2018**, *140*, 13976.
220. Gondo, N.; Tanigaki, Y.; Ueda, Y.; Kawabata, T. *Synlett* **2020**, *31*, 398.
221. Bugaenko, D. I.; Karchava, A. V.; Yurovskaya, M. A. *Chem. Heterocycl. Compd.* **2020**, *56*, 128.
222. Selberg, S.; Rodima, T.; Lõkov, M.; Tshepelevitsh, S.; Haljasorg, T.; Chhabra, S.; Kadam, S. A.; Toom, L.; Vahur, S.; Leito, I. *Tetrahedron Lett.* **2017**, *58*, 2098.
223. Nakayama, K. *J. Chem. Educ.* **1990**, *67*, 20.
224. Hatano, M.; Moriyama, K.; Maki, T.; Ishihara, K. *Angew. Chem. Int.* **2010**, *49*, 3823.
225. Raithby, P. R.; Shields, G. P.; Allen, F. H.; Motherwell, W. D. S. *Acta Crystallogr. B* **2000**, *56*, 444.
226. Yue, W.-J.; Zhang, C.-Y.; Yin, L. *iScience* **2019**, *14*, 88.
227. Liu, R. Y.; Yang, Y.; Buchwald, S. L. *Angew. Chem. Int.* **2016**, *55*, 14077.
228. Jang, H.; Romiti, F.; Torker, S.; Hoveyda, A. H. *Nat. Chem.* **2017**, *9*, 1269.
229. Herrmann, J. L.; Kieczkowski, G. R.; Schlessinger, R. H. *Tetrahedron Lett.* **1973**, *14*, 2433.
230. Sun, X.; Collum, D. B. *J. Am. Chem. Soc.* **2000**, *122*, 2452.
231. Mulvey, R. E.; Robertson, S. D. *Angew. Chem. Int.* **2013**, *52*, 11470.
232. Stevens, J. M.; Parra-Rivera, A. C.; Dixon, D. D.; Beutner, G. L.; DelMonte, A. J.; Frantz, D. E.; Janey, J. M.; Paulson, J.; Talley, M. R. *J. Org. Chem.* **2018**, *83*, 14245.
233. Kavrakova, I. K. *J. Chem. Res.* **2005**, *2005*, 682.
234. Hein, J. E.; Zimmerman, J.; Sibi, M. P.; Hultin, P. G. *Org. Lett.* **2005**, *7*, 2755.
235. Park, S. Y.; Liu, Y.; Oh, J. S.; Kweon, Y. K.; Jeong, Y. B.; Duan, M.; Tan, Y.; Lee, J.-W.; Yan, H.; Song, C. E. *Chem. Eur. J.* **2018**, *24*, 1020.
236. Wang, D.; Cao, P.; Wang, B.; Jia, T.; Lou, Y.; Wang, M.; Liao, J. *Org. Lett.* **2015**, *17*, 2420.
237. Mita, T.; Chen, J.; Sugawara, M.; Sato, Y. *Org. Lett.* **2012**, *14*, 6202.
238. Álvarez-Méndez, S. J.; Fariña-Ramos, M.; Villalba, M. L.; Perretti, M. D.; García, C.; Moujir, L. M.; Ramírez, M. A.; Martín, V. S. *J. Org. Chem.* **2018**, *83*, 9039.



239. Estrada, A. A.; Feng, J. A.; Fox, B.; Leslie, C. P.; Lyssikatos, J. P.; Pozzan, A.; Sweeny, Z. K.; De Vicente Fidalgo, J. Inhibitors of Receptor-Interacting Protein Kinase 1. PCT/US2017/016509, 2017.